

Anomalous transport phenomena in Fermi liquids with strong magnetic fluctuations

Hiroshi Kontani

Department of Physics, Nagoya University, Nagoya 464-8602, Japan

E-mail: kon@slab.phys.nagoya-u.ac.jp

Abstract. In this paper, we present a recent developments in the theory of transport phenomena based on the Fermi liquid theory. In conventional metals, various transport coefficients are scaled according to the quasiparticles relaxation time, τ , which implies that the relaxation time approximation (RTA) holds well. However, such a simple scaling does not hold in many strongly correlated electron systems. The most famous example would be high- T_c superconductors (HTSCs), where almost all the transport coefficients exhibit a significant deviation from the RTA results. This issue has been one of the most significant unresolved problems in HTSCs for a long time. Similar anomalous transport phenomena have been observed in metals near their antiferromagnetic (AF) quantum critical point (QCP). The main goal of this study is to demonstrate whether the anomalous transport phenomena in HTSC is the evidence of non-Fermi liquid ground state, or it is just the RTA violation in strongly correlated Fermi liquids. Another goal is to establish a unified theory of anomalous transport phenomena in metals with strong magnetic fluctuations. For these purposes, we develop a method for calculating various transport coefficients beyond the RTA by employing field theoretical techniques.

In a Fermi liquid, an excited quasiparticle induces other excited quasiparticles by collision, and current due to these excitations is called a current vertex correction (CVC). Landau had noticed the existence of CVC first, which is indispensable for calculating transport coefficient in accord with the conservation laws. Here, we develop a transport theory involving resistivity and Hall coefficient on the basis of the microscopic Fermi liquid theory, by considering the CVC. In nearly AF Fermi liquids, we find that the strong backward scattering due to AF fluctuations induces the CVC with prominent momentum dependence. This feature of the CVC can account for the significant enhancements in the Hall coefficient, magnetoresistance, thermoelectric power, and Nernst coefficient in nearly AF metals. According to the present numerical study, aspects of anomalous transport phenomena in HTSC are explained *in a unified way* by considering the CVC, without introducing any fitting parameters; this strongly supports the idea that HTSCs are Fermi liquids with strong AF fluctuations. Further, the present theory also explains very similar anomalous transport phenomena occurring in CeMIn_5 ($M=\text{Co}$ or Rh), which is a heavy-fermion system near the AF QCP, and in the organic superconductor κ -(BEDT-TTF).

In addition, the striking ω -dependence of the AC Hall coefficient and the remarkable effects of impurities on the transport coefficients in HTSCs appear to fit naturally into the present theory. Many aspects of the present theory are in accord with the anomalous transport phenomena in HTSCs, organic superconductors, and heavy-fermion systems near their AF QCPs. We discuss some of the open questions for future work.

Contents

1	Introduction	3
1.1	Relaxation time approximation (RTA) and current vertex correction (CVC)	3
1.2	Non-Fermi-liquid-like transport phenomena in high- T_c cuprates	5
1.3	Non-Fermi liquid transport phenomena in $CeMIn_5$ ($M=Co, Rh,$ or Ir) and κ -(BEDT-TTF)	9
1.4	Fermi liquid or non-Fermi liquid?	10
2	Spin fluctuation theory and model Hamiltonian	12
2.1	Phenomenological spin fluctuation model	12
2.2	Model Hamiltonian and FLEX approximation	13
2.3	Hot/cold-spot structure and T -linear resistivity in nearly AF metals . . .	16
3	Anomalous transport phenomena in nearly AF Fermi liquids	20
3.1	Results by RTA	20
3.2	Physical meaning of the CVC in nearly AF metals	21
3.3	Analysis of the CVC based on the Fermi liquid theory	23
3.4	CVC beyond one loop approximation	32
4	Transport phenomena in HTSCs above T^*	35
4.1	Total current $\vec{J}_{\mathbf{k}}$	35
4.2	Resistivity and Hall coefficient	37
4.3	Magnetoresistance	41
4.4	Thermoelectric power	44
4.5	Summary of this section and comments on other transport coefficients . .	46
5	Transport phenomena in HTSCs below T^*	47
5.1	Mechanism of pseudo-gap phenomena	47
5.2	Enhancement of Nernst coefficient and magnetoresistance	50
5.3	Summary of this section	54
6	AC transport phenomena in HTSCs	55
7	Impurity effects in nearly AF metals	59
7.1	Hall coefficient in the presence of weak local impurities	60
7.2	Effect of strong local impurities near AF QCP	61
8	Anomalous transport behaviors in $CeMIn_5$ ($M=Co$ or Rh) and κ-(BEDT-TTF)	68
8.1	$CeMIn_5$ ($M=Co$ or Rh)	68
8.2	κ -(BEDT-TTF)	73

9 Discussions	76
9.1 Summary of the present study	76
9.2 Applicable scope of the present study and future problems	78
9.3 Fermi arc picture and transport phenomena	80
9.4 Unconventional transport phenomena in multiorbital systems: anomalous Hall effect and grand Kadowaki-Woods relation	83

1. Introduction

1.1. Relaxation time approximation (RTA) and current vertex correction (CVC)

The investigation of transport phenomena in metals is very significant since we can extract a large amount of important information with regard to the electronic states of metals. In conventional metals with weak electron-electron correlation, various transport phenomena are governed by a single parameter, namely, the quasiparticle relaxation time τ . That is, the RTA holds well in such conventional metals [1]. For example, resistivity ρ is proportional to τ^{-1} , which is proportional to T^2 in conventional Fermi liquids. The Hall coefficient R_H is independent of τ , and $1/e|R_H|$ expresses the approximate carrier density n . The magnetoresistance $\Delta\rho/\rho_0$ is proportional to τ^{-2} . The thermoelectric power S is proportional to T for a wide range of temperatures. The signs of R_H and S represent the type of carrier (i.e., electrons or holes). The behaviors of these transport coefficients, which are referred to as Fermi liquid behaviors, are well explained by the RTA.

In strongly correlated electron systems, however, transport coefficients frequently exhibit a prominent deviation from conventional Fermi liquid behaviors. Because of this, it is difficult to obtain information on the electronic states from the transport phenomena. For example, in high- T_c superconductors (HTSCs), both R_H and S/T are very sensitive to temperature; in some compounds, sign changes occur with changes in the temperature [2, 3, 4, 5, 6, 7, 8, 9, 10, 11, 12]. Evidently, a simple RTA does not work well for HTSCs. For example, $1/e|R_H|$ is considerably greater than the electron density in optimally doped or under-doped systems. Prominent “non-Fermi-liquid-like behaviors” are also observed in other strongly correlated systems such as organic superconductors [13, 14, 15, 16, 17, 18] and heavy-fermion systems (f -electron systems) [19, 20, 21, 22]. Although these behaviors reveal essential information about the electronic states, only a little was understood about them for a long time. To obtain a significant amount of information from these wealth of treasures, we had to develop the theory of transport phenomena in strongly correlated Fermi liquids.

The main objective of the present study is to investigate the non-Fermi-liquid-like transport properties in HTSCs, which have been intensively studied as one of the central issues of HTSC. Thus far, two different kinds of theoretical models have been actively investigated: in the first kind of models, non-Fermi-liquid ground states are assumed. For example, Anderson proposed that the elementary excitations are described

by spinons and holons. It is considered that holons, whose density is small in underdoped systems, are responsible for the anomalous transport [5, 23]. In the second kind of models, Fermi-liquid ground states are assumed. For example, transport coefficients were calculated based on the nearly antiferromagnetic (AF) Fermi liquid picture [24]. In the previous studies, the RTA has been frequently used [25, 26, 27]. However, both these models can explain only a limited number of experimental facts involved in HTSC: many other anomalous transport properties remain unsolved. To understand the true ground state of HTSC, it is highly desirable to solve the issue of anomalous transport phenomena in HTSCs in a unified way.

The main aim of the present study is to explain that the *rich variety of anomalous transport phenomena observed in HTSCs can be understood in a unified way in terms of the Fermi liquid picture*. For this purpose, we have to take the CVC into account correctly, which is totally dropped in the RTA. In interacting electron systems, an excited electron induces other particle-hole excitations by collisions. The CVC represents the induced current due to these particle-hole excitations. The CVC is closely related to the momentum conservation law, which is mathematically described using the Ward identity [28, 29, 30, 31]. In fact, Landau proved the existence of the CVC, which is called backflow in the phenomenological Fermi liquid theory, as a natural consequence of the conservation law [28]. The CVC can be significant in strongly correlated Fermi liquids owing to strong electron-electron scattering. However, its effect on the transport phenomena has not been studied well until recently.

In the present study, we discuss the role of CVC in nearly AF Fermi liquids, such as HTSCs, organic metals, and heavy-fermion systems near the magnetic quantum critical point (QCP). For example, the RTA for the highly anisotropic $\tau_{\mathbf{k}}$ model cannot explain the transport anomaly in HTSC. We find that *the RTA is unreliable in the presence of strong AF fluctuations, because the prominently developed CVC entirely modifies the RTA results* [32, 33, 34, 35, 36, 37, 38, 39]. In a Fermi liquid, the transport coefficients are described by the total current $\vec{J}_{\mathbf{k}}$, which is expressed as a sum of quasiparticle velocity $\vec{v}_{\mathbf{k}}$ and CVC [40, 41, 42, 43, 44, 45, 46]. In the present study, we find that *the $\vec{J}_{\mathbf{k}}$ in nearly AF metals shows anomalous \mathbf{k} -dependence due to the CVC*. This is the origin of the transport anomalies in nearly AF metals. Based on the microscopic Fermi liquid theory, we investigate the important role of the CVC in R_{H} , $\Delta\rho/\rho_0$, S , and the Nernst coefficient (ν). Furthermore, we confirm this idea by performing a numerical study based on the FLEX+CVC theory. In this approximation, the Coulomb interaction U is the only fitting parameter.

To demonstrate the physical meaning of CVC, we discuss the scattering processes between quasiparticles in an isotropic model [28]. In the RTA, it is assumed that the conductivity due to a quasiparticle at \mathbf{k} is proportional to the mean free path $v_{\mathbf{k}}\tau_{\mathbf{k}}$. Since $\tau_{\mathbf{k}} \propto T^{-2}$ in a Fermi liquid [28], the resistivity according to the RTA — $\rho^{\text{RTA}} \propto \tau^{-1}$ — is finite. However, this result is *not true* since the momentum conservation law ensures that $\rho = 0$ in a spherical model in the absence of the Umklapp process [42]. The failure of the RTA originates from the assumption that the velocity of the excited quasiparticle

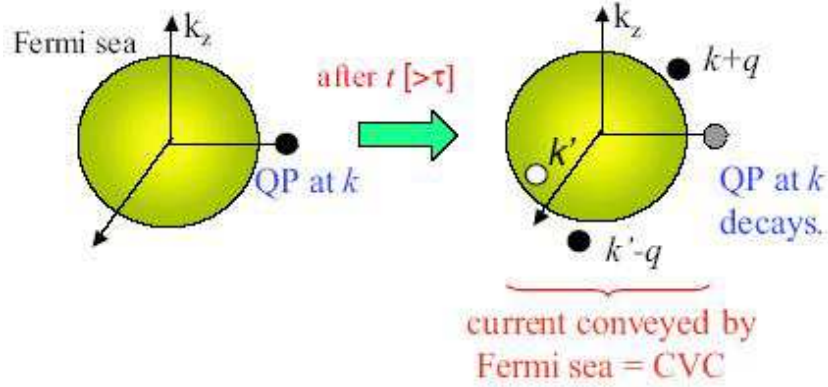


Figure 1. Decay process of a quasiparticle at \mathbf{k} . After the relaxation time τ , the quasiparticle at \mathbf{k} collides with another quasiparticle at \mathbf{k}' in the Fermi sea. As a result of this collision, the two quasiparticles at $\mathbf{k} + \mathbf{q}$ and $\mathbf{k}' - \mathbf{q}$, and a quasi-hole at \mathbf{k}' are created. The total momentum is conserved in this process.

disappears after scattering. Here, we explain that the correct answer (zero resistivity) in the absence of the Umklapp processes is recovered by considering all the relevant normal scattering process as shown in Fig. 1. When a quasiparticle at \mathbf{k} is scattered to $\mathbf{k} + \mathbf{q}$ after the relaxation time $\tau_{\mathbf{k}}$, a particle-hole pair (at $\mathbf{k}' - \mathbf{q}$ and \mathbf{k}') should be created according to the momentum and energy conservation laws. *The CVC represents the current conveyed by the particles at $(\mathbf{k} + \mathbf{q}, \mathbf{k}' - \mathbf{q})$ and a hole at \mathbf{k}' , which emerge during the scattering process.* Therefore, the momentum and energy conservation laws, which are violated in the RTA, are restored by considering the CVC [42]. The CVC is necessary to reproduce the zero-resistivity in the absence of the Umklapp process.

In the RTA, we consider an excited quasiparticle at \mathbf{k} (in Fig. 1) as if it *annihilates* after the relaxation time. Since the RTA allows such an unphysical process, the conservation law $\partial\rho/\partial t + \vec{\nabla} \cdot \vec{j} = 0$ is violated in the RTA. Since the conservation law is a very important constraint on the transport properties, the RTA frequently yields unphysical results [42, 45]. In later sections, we find that the CVC is significant in nearly AF metals: we explain that the CVC is the origin of a variety of anomalous transport phenomena in such metals.

1.2. Non-Fermi-liquid-like transport phenomena in high- T_c cuprates

In HTSCs, almost all the transport phenomena deviate from the conventional Fermi liquid behaviors, which are referred to as the non-Fermi liquid behaviors [47, 48]. These anomalous transport phenomena have been studied intensively as one of the most important issues in HTSCs, since they offer important clues to reveal the true ground state in HTSCs, which has been unsolved until now. To answer this question, many analytical and numerical studies have been performed to determine the ground state of two-dimensional (2D) systems. For example, Anderson et al. considered that the ground state of a square-lattice Hubbard model is the resonating-valence-bond (RVB)

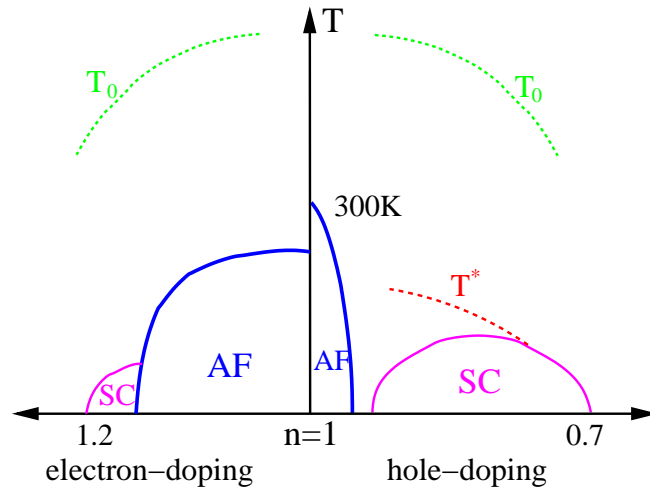


Figure 2. Schematic phase diagram of HTSC. AF spin fluctuations start to increase below T_0 . At the same time, R_H starts to increase. Below T^* (in the pseudo-gap region), the AF fluctuations are suppressed since the strong SC fluctuations reduce the density of states at the Fermi level, which is called the pseudo-gap. In this study, the filling area is $|1 - n| \geq 0.1$.

state, where spin and charge degrees of freedom are separated [23]. In the RVB state, concept of quasiparticle is not valid. According to his philosophy, possibility of the RVB state in the square-lattice t - J model was studied, by using the mean-field theory [49] and the gauge theory [50]. In §1.4, we will introduce significant works performed in the t - J model. Unfortunately, it is difficult to perform quantitative studies of transport coefficients using the t - J model.

On the other hand, the Fermi liquid theory has been developed and applied to analyzing the HTSCs, considering that the Fermi liquid ground state is realized [51, 52]. By using the self-consistent renormalization (SCR) theory, Moriya, Takahashi and Ueda explained that the correct superconducting (SC) order parameter $d_{x^2-y^2}$ as well as T -linear resistivity are derived from the strong AF fluctuations [53, 54, 55]. Based on the phenomenological spin fluctuation model, Monthoux and Pines performed a quantitative analysis for optimally-doped YBCO [56]. Further, Bickers et al. studied the square-lattice Hubbard model according to a self-consistent random-phase-approximation (RPA), which is now called the fluctuation-exchange (FLEX) approximation [57]. These spin fluctuation theories have succeeded in reproducing various non-Fermi-liquid behaviors in the normal state of HTSCs: For example, temperature dependence of nuclear spin-lattice relaxation rate given by NMR/NQR measurements, $1/T_1T \propto \sum_{\mathbf{q}} \text{Im}\chi_{\mathbf{q}}^s(\omega)/\omega|_{\omega=0} \propto T^{-1}$, is reproduced well. Moreover, famous T -linear resistivity in HTSC,

$$\rho \propto 1/\tau \propto T, \quad (1)$$

is also explained. (The Fermi liquid behavior $1/\tau \propto T^2$ will recover at very low T if we suppress the superconductivity.) The FLEX approximation is also useful for the

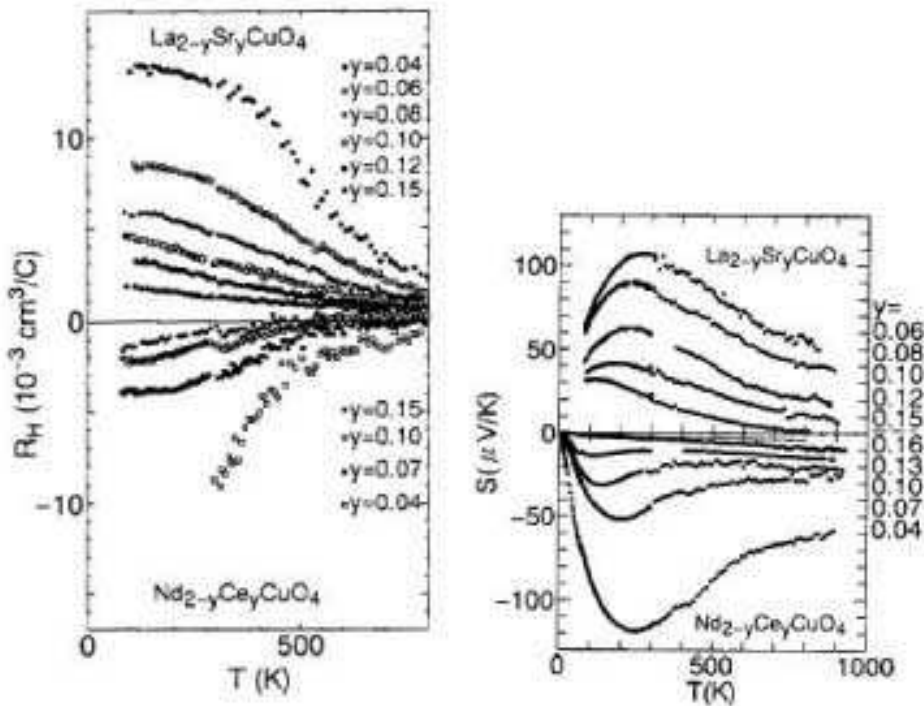


Figure 3. Experimental Hall coefficient and the thermoelectric power for LSCO and NCCO. [Ref. [2]]

study of electron-doped systems [33, 58, 59]. These spin fluctuation theories successfully reproduce various non-Fermi-liquid-like behaviors in HTSCs except for the under-doped region $|1 - n| < 0.1$, where n is the number of electrons per site. A schematic phase diagram of HTSC is shown in Fig. 2. The Fermi liquid description of HTSCs is still in progress [60, 61, 62, 63]. A $d_{x^2-y^2}$ -wave symmetry in the SC state was confirmed by phase-sensitive measurements [64, 65, 66], and tunneling spectroscopy [67]. $d_{x^2-y^2}$ -wave SC state was also derived according to the third-order-perturbation theory with respect to U [68].

Regardless of the remarkable success of the Fermi liquid theory during the 90s, the non-Fermi-liquid-like transport phenomena observed in HTSCs remained unresolved for a long time. The significant deviation from the RTA results in HTSCs was frequently considered as a hallmark of the breakdown of the Fermi liquid state. This issue has remained as one of the most important problems in HTSCs for a long time. In HTSCs, $|R_H|$ increases below $T_0 \sim 600\text{K}$ as

$$R_H \propto 1/T \quad (2)$$

above the pseudo-gap temperature $T^* \sim 200\text{K}$, and $|R_H| \gg 1/ne$ at T^* [2, 69]. The sign of R_H is positive in hole-doped systems such as $\text{La}_{2-\delta}\text{Sr}_\delta\text{CuO}_4$ (LSCO) [2, 3], $\text{YBa}_2\text{Cu}_3\text{O}_{7-\delta}$ (YBCO) [4, 5] and $\text{Tl}_2\text{Ba}_2\text{CuO}_{6+\delta}$ (TBCO) [6]; however, it is negative in electron-doped systems such as $\text{Nd}_{2-\delta}\text{Ce}_\delta\text{CuO}_4$ (NCCO) [7] and $\text{Pr}_{2-\delta}\text{Ce}_\delta\text{CuO}_4$ (PCCO) [8], even though the angle resolved photoemission (ARPES) measurements resolved hole-

like Fermi surfaces [70]. The experimental T -dependences of R_H for LSCO and NCCO are shown in Fig. 3. The magnetoresistance of HTSCs also shows strong temperature dependence as

$$\Delta\rho/\rho_0 \propto T^{-4} \quad (3)$$

for a wide range of temperatures in LSCO [12, 71, 72], YBCO [71] and TBCO [73]. These results completely contradict with Kohler's rule ($R_H \propto \text{const.}$ and $\Delta\rho/\rho_0 \propto \rho_0^{-2}$) which is derived using the RTA for a single-band model. Interestingly, the following "modified Kohler's rule" holds well for optimally-doped LSCO [12, 71], 90K and 60K YBCO [71] and TBCO [73]:

$$\Delta\rho/\rho_0 \propto \tan^2 \Theta_H, \quad (4)$$

where $\Theta_H = \sigma_{xy}/\sigma_{xx}$ is the Hall angle. This experimental fact strongly suggests that the anomalous behaviors of the Hall effect and the magnetoresistance have the same origin. Below T^* , R_H decreases whereas $\Delta\rho/\rho_0$ increases further [74]. Therefore, modified Kohler's rule is not very well applicable for under-doped HTSCs at low temperatures [75, 76, 77].

For a long time, anomalous transport phenomena have been considered as one of the strongest objection against the Fermi liquid description of HTSCs. For example, to explain eqs. (1)-(4), Anderson introduced the Tomonaga-Luttinger model with two types of relaxation times. However, it is not obvious how to describe the crossover from the Tomonaga-Luttinger liquid state in the under-doped region to the Landau-Fermi liquid state with doping. On the other hand, the Fermi liquid description for HTSC, starting from the well-established Fermi liquid state in the over-doped region, appears to account for a wide doping range in HTSCs [52]. Here, we conform to the following principle: before abandoning the Fermi liquid picture in HTSCs, we have to verify whether the RTA is really applicable in HTSCs or not. We stress that the RTA may be unreliable for strongly correlated Fermi liquids since the CVC is not considered, regardless of its importance to satisfy the conservation laws. Due to this inadequacy, the RTA sometimes yields unphysical results in correlated metals [42]. In later sections, we will explain that the non-Fermi liquid-like behaviors in HTSCs can be understood based on the Fermi liquid theory by including the CVC.

Here, we discuss the pseudo-gap phenomena in slightly under-doped systems below $T^* \sim 200\text{K}$, which is also one of the most important issues in HTSC. $1/T_1T$ starts to decrease below T^* , which means that the AF fluctuations are suppressed in the pseudo-gap region [78, 79, 80, 81, 82]. According to ARPES measurements, prominent deep pseudo-gap appears in the density of states (DOS) below T^* [83, 84, 85, 86]. A simple spin fluctuation theory cannot explain the various anomalous phenomena in the pseudo-gap region. Recent theoretical studies using the T -matrix theory [87] and the FLEX+ T -matrix theory [88, 89, 51, 90] have shown that the strong SC amplitude fluctuations, which are induced by the AF fluctuations, are a promising candidate for the origin of pseudo-gap [51, 52, 89]. In §5, we study transport phenomena below T^* using the FLEX+ T -matrix theory by including CVCs, and show that the various anomalous

transport coefficients are well reproduced in a unified way. The present study strongly supports the idea that the pseudo-gap phenomena in under-doped HTSCs are induced by the strong SC amplitude fluctuations with a $d_{x^2-y^2}$ -symmetry [52, 51, 89].

We note that wide and shallow pseudo-gap in the DOS (weak pseudo-gap) is observed by ARPES even above T^* , which is considered to originate from AF fluctuations that appear below $T_0 \sim 600$ K. We will discuss the weak pseudo-gap phenomena in §9.2.

1.3. Non-Fermi liquid transport phenomena in $CeMIn_5$ ($M=Co, Rh, \text{ or } Ir$) and κ -(BEDT-TTF)

During the last decade, it has been found that in strongly correlated materials, including heavy-fermion systems and organic metals, various transport coefficients exhibit striking deviations from the Fermi liquid behaviors. In particular, anomalous transport properties similar to those in HTSCs (eqs. (1)-(4)) have been observed in many systems with strong magnetic fluctuations such as κ -(BEDT-TTF) $_2$ X [X=Cu[N(CN) $_2$]Br [13], X=Cu[N(CN) $_2$]Cl [14, 15], X=Cu(NCS) $_2$ [16, 17]], κ -(BEDT-TTF) $_4$ Hg $_{2.89}$ Br $_8$ [18], and $CeMIn_5$ ($M=Co, Rh$) [19, 20]. BEDT-TTF is an abbreviation of bis(ethylenedithio)tetrathiafulvalene. These experimental facts strongly suggest that the transport anomaly given by eqs. (1)-(4) is not a problem specific to HTSCs, but a universal property in the nearly AF Fermi liquids [20]. The study of these transport phenomena in such systems will serve to resolve the origin of the non-Fermi-liquid-like behaviors in HTSCs.

κ -(BEDT-TTF) is a layered organic compound made of BEDT-TTF molecules. The d -wave superconductivity can be realized in a wide region of the pressure-temperature (P - T) phase diagram, adjacent to the AF insulating states [91]. For example, Cu[N(CN) $_2$]Cl salt at ambient pressure is an AF insulator, with its Néel temperature $T_N = 27$ K. With increasing pressure, T_N decreases and superconductivity appears via a weak first order transition; The maximum T_c is 13 K at 200 bar. An effective theoretical model can be given by the anisotropic triangular lattice Hubbard model at half-filling [92]. According to this model, the phase diagram of κ -(BEDT-TTF) can be well reproduced by using the FLEX approximation, by assuming that $U_{\text{eff}}/W_{\text{band}}$ decreases by pressure [93, 94, 95]. These studies revealed that the $d_{x^2-y^2}$ -wave superconductivity occurs due to the strong AF fluctuations $\mathbf{q} \sim (\pi, \pi)$. In the metallic phase of κ -(BEDT-TTF), the relationships $R_H \propto T^{-1}$ and $\tan \Theta_H \propto T^{-2}$ are observed [13, 14, 15, 16, 17, 18]. Moreover, the magnitude of R_H decreases with increasing the pressure [15, 18, 17]. These behaviors are quantitatively reproduced by the FLEX+CVC theory [96].

$CeMIn_5$ is a quasi two-dimensional (2D) heavy-fermion compound [97, 98, 99]. At ambient pressure, CeCoIn $_5$ is a superconductor with $T_c = 2.3$ K. The electronic specific heat coefficient γ has been measured to be 300 mJ/K 2 mol at $T \gtrsim T_c$. CeIrIn $_5$ is also a superconductor at ambient pressure with $T_c = 0.4$ K and $\gamma = 680$ mJ/K 2 mol. CeRhIn $_5$

is an AF metal with Néel temperature $T_N = 3.8$ K at ambient pressure. Under the pressure, CeRhIn₅ undergoes a SC transition at $P_c = 2$ GPa, indicating that the AF quantum critical point (QCP) is located at or in the vicinity of P_c . The NMR relaxation rate T_1^{-1} measurements indicate the presence of quasi 2D AF spin fluctuations in the normal state [100, 101]. The measurements of the angle resolved thermal conductivity [102, 103] and specific heat [104, 105] revealed that the symmetry of the SC state exhibits *d*-wave symmetry. Furthermore, the Fulde-Ferrell-Larkin-Ovchinnikov (FFLO) SC state has been observed [106].

In CeMIn₅, eqs. (1)-(4) are well satisfied for a wide range of temperatures, and the value of $|R_H/ne|$ reaches ~ 50 in CeRhIn₅ near the AF QCP [19, 20]. Similarly, the Nernst coefficient ν also takes a large positive value at low temperatures [107]. Recently, we studied both R_H and ν in a quasi 2D Hubbard model, and found that they are prominently enhanced, as large as those in pure 2D systems [108]. In CeMIn₅, modified Kohler's rule (4) is well satisfied for $0 < H \lesssim 3$ Tesla, whereas both σ_{xy}/H and $(\Delta\rho/\rho_0)/H^2$ are drastically suppressed by a very weak magnetic field ($H > 0.1$ Tesla) near the AF QCP [19, 20]. This surprising fact can be understood in terms of the field-dependence of the CVC.

1.4. Fermi liquid or non-Fermi liquid?

In the present article, we assume that the Fermi liquid state is realized in a wide range of the phase diagram in HTSCs, and the non-Fermi-liquid-like behaviors are created by strong spin (and SC) fluctuations. According to this idea, we study the anomalous transport phenomena in HTSC, by carefully analyzing the main-body effects that had been overlooked in previous studies. Especially, we intensively study the CVC based on the microscopic Fermi liquid theory. Our final aim is to explain the anomalous transport phenomena in various nearly AF Fermi liquids *in a unified way*, including HTSC, heavy fermions and organic metals.

However, it is a nontrivial question whether the Fermi liquid state is realized in two-dimensional strongly correlated electron systems near the half-filling. In fact, the Fermi liquid state seems to be broken in heavily under-doped HTSCs. In the infinite dimension Hubbard model, the Fermi liquid state with heavy mass is realized next to the Mott insulating state [109, 110]. In 2D Hubbard models [111], it was rigorously proved that the limit value of the interaction U , below which the Fermi liquid state is realized, is finite. However, in strongly correlated 2D systems, an exotic non-Fermi liquid ground state may be realized next to the Mott insulating state due to the strong quantum fluctuations. That is, removal of large tracts of the Hilbert space due to strong correlation effect may lead to a violation of the Fermi liquid state.

To study the strong correlation effect in HTSCs, the *t*-*J* model has been frequently analyzed. The *t*-*J* model is derived from the Hubbard model (or *d*-*p* model) by a canonical transformation, by excluding the double occupancy of holes to represent the

strong Coulomb interaction. It is given by

$$H^{t-J} = \sum_{\langle i,j \rangle, \sigma} P_G(t_{i,j}c_{i\sigma}^\dagger c_{j\sigma} + \text{h.c.})P_G + J \sum_{\langle i,j \rangle}^{\text{n.n.}} \mathbf{S}_i \cdot \mathbf{S}_j \quad (5)$$

where P_G represents the exclusion of the doubly occupied state, $t_{i,j}$ is the hopping integral between (i, j) sites, and J is the superexchange energy between the neighboring spins. $J = 0.10 \sim 0.14$ meV in real HTSCs. In the t - J model, the Hilbert space with high-energy state is eliminated by P_G , which enables us to perform numerical calculations easier or to invent new approximations. Based on the t - J model, various versions of the new fluid have been proposed, with novel kinds of excitation, many involving gauge theories of spin-charge separated spinons and holons [23, 49, 50]. The exact diagonalization technique [112, 113] has been applied to the square-lattice t - J model. The ground state phase diagram of the t - J model has been studied using the variational Monte Carlo method [114, 115], and it was found that the $d_{x^2-y^2}$ -wave SC state is realized in a wide range of the phase diagram. Unfortunately, quantum Monte Carlo (QMC) simulation for t - J model is difficult because of a serious negative sign problem. Instead, QMC simulation for the Hubbard model with moderate value of U [116, 117] have been performed intensively.

On the other hand, many authors have considered non-Fermi liquid ground states due to novel quantum criticalities, other than a conventional (SCR-type) quantum criticality near the spin density wave (SDW) state [61, 118]. For example, Varma et al. proposed that the marginal Fermi liquid state is realized in HTSCs, where the \mathbf{k} -independent self-energy is given by [118]

$$\Sigma(\omega + i\delta) = \lambda(\omega \ln(\omega_c/x) - ix), \quad (6)$$

where $x = \max(|\omega|, \pi T)$, λ is a coupling constant, and ω_c is a cutoff energy. This state is not a Fermi liquid since the quasiparticle renormalization factor $z = (1 - \partial \text{Re}\Sigma / \partial \omega)^{-1} = (1 + \lambda \ln(\omega_c/x))^{-1}$ vanishes logarithmically as $(\omega, T) \rightarrow 0$. The self-energy in eq. (6) can be derived if electrons couple to the following \mathbf{k} -independent charge and spin fluctuations that are singular at $T = 0$:

$$\text{Im}P(\omega + i\delta) \propto \min(|\omega|/T, 1). \quad (7)$$

In this model, $\rho \propto -\text{Im}\Sigma(i\delta) = \lambda\pi T$, $1/T_1 T \propto \text{Im}P(\omega)/\omega|_{\omega=0} \propto 1/T$, and the optical conductivity is $\sigma(\omega) \propto (\omega - i\lambda x)^{-1}$. They are typical non-Fermi liquid behaviors in HTSCs. Now, a microscopic derivation of the \mathbf{k} -independent quantum critical fluctuations is an important issue. Varma proposed [119] that the circulating current phase exists in the under-doped regime, and the current fluctuations near the QCP (\approx at the optimum doping) are the origin of the marginal Fermi liquid state.

In the present article, we will argue that transport anomaly near the AF-QCP can happen even if the Fermi liquid state ($1 \geq z > 0$) remains intact at the QCP. We will show that the CVC in the Landau Fermi liquid theory causes various striking quantum critical behaviors.

2. Spin fluctuation theory and model Hamiltonian

2.1. Phenomenological spin fluctuation model

Here, we discuss the functional form of the dynamical spin susceptibility $\chi_{\mathbf{q}}^s(\omega)$ in nearly AF metals. Hereafter, we use the unit $c = \hbar = k_B = 1$. This is the most important physical quantity in such metals since it is the origin of various non-Fermi liquid behaviors in HTSCs. The phenomenological form of $\chi_{\mathbf{q}}^s(\omega)$, which can be obtained by using NMR/NQR spectroscopy and the neutron diffraction measurement, is given by [53, 56, 120, 25]

$$\chi_{\mathbf{q}}^s(\omega) = \sum_{\mathbf{Q}} \frac{\chi_Q}{1 + \xi_{\text{AF}}^2(\mathbf{q} - \mathbf{Q})^2 - i\omega/\omega_{\text{sf}}}, \quad (8)$$

where $\mathbf{Q} = (\pm\pi, \pm\pi)$ is the antiferromagnetic (AF) wavevector, and ξ_{AF} is the AF correlation length. This is referred to as the Millis-Monien-Pines model [120]. In HTSCs above the pseudo-gap temperature T^* , both χ_Q and $1/\omega_{\text{sf}}$ are scaled by ξ_{AF}^2 as follows [121]:

$$\xi_{\text{AF}}^2 \approx \alpha_0 / (T + \Theta), \quad (9)$$

$$\chi_Q \approx \alpha_1 \cdot \xi_{\text{AF}}^2, \quad 1/\omega_{\text{sf}} \approx \alpha_2 \cdot \xi_{\text{AF}}^2, \quad (10)$$

where Θ , α_0 , α_1 and α_2 are constants. Since $\chi_Q \omega_{\text{sf}} \propto \xi_{\text{AF}}^0$ in eq. (10), the corresponding dynamical exponent z is 2. The coefficient α_0 rapidly increases in the under-doped region: ξ_{AF} reaches $\sim 2a$ in optimally-doped YBCO, and it exceeds $100a$ in slightly under-doped NCCO just above T_c [122]. (a is the unit-cell length; we put $a = 1$ hereafter.) The relationship $\omega_{\text{sf}} \gtrsim T$ ($\omega_{\text{sf}} \lesssim T$) is satisfied in the over-doped (under-doped) YBCO. On the basis of the phenomenological $\chi_{\mathbf{q}}^s(\omega)$ model, the SC transition temperature was successfully reproduced by solving the strong-coupling Eliashberg equation [56].

Theoretically, the relationships in eqs. (9) and (10) can be explained according to the SCR theory, where we consider the renormalization of the dynamical susceptibility due to both self-energy correction and vertex correction. This renormalization effect is referred to as the “mode-mode coupling effect” [123], which represents the destruction of the AF long-range order due to thermal and quantum fluctuations. Relationships (9) and (10) are also reproduced according to the FLEX approximation [57, 124, 125, 126, 127, 128, 129]. In this approximation, only the mode-mode coupling effect due to the self-energy correction is taken into account: Since the large imaginary part of the self-energy reduces the DOS, the spin susceptibility given by the mean-field approximation (which is equivalent to the RPA) is drastically suppressed in the FLEX approximation. As a result, the magnetic long-range order does not occur in pure 2D systems, which means that the Mermin-Wagner theorem is satisfied in the FLEX approximation [130]. In nearly AF metals, the FLEX approximation and the SCR theory yield similar results since the mode-mode coupling effect due to the self-energy is dominant [123]. On the other hand, the mode-mode coupling effect due to the

second-order vertex correction (Aslamazov-Larkin term) can be important in the nearly ferromagnetic metals.

2.2. Model Hamiltonian and FLEX approximation

In the main part of this study, we investigate the transport phenomena in HTSCs based on the Fermi liquid theory, and perform a numerical study using the spin fluctuation theory. In this study, we analyze the following Hubbard model:

$$H = \sum_{\mathbf{k}\sigma} \epsilon_{\mathbf{k}}^0 c_{\mathbf{k}\sigma}^\dagger c_{\mathbf{k}\sigma} + U \sum_{\mathbf{k}\mathbf{k}'\mathbf{q}} c_{\mathbf{k}+\mathbf{q}\uparrow}^\dagger c_{\mathbf{k}'-\mathbf{q}\downarrow}^\dagger c_{\mathbf{k}'\downarrow} c_{\mathbf{k}\uparrow}, \quad (11)$$

where U is the Coulomb interaction, and $\epsilon_{\mathbf{k}}^0$ is the spectrum of the conduction electron. In a square lattice, $\epsilon_{\mathbf{k}}^0$ is given by

$$\epsilon_{\mathbf{k}}^0 = 2t_0(\cos k_x + \cos k_y) + 4t_1 \cos k_x \cos k_y + 2t_2(\cos 2k_x + \cos 2k_y), \quad (12)$$

where $c_{\mathbf{k}\sigma}^\dagger$ is the creation operator of an electron with momentum \mathbf{k} and spin σ , and U is the on-site Coulomb repulsion. We represent the electron filling by n , and $n = 1$ corresponds to the half-filling. To fit the band structures given by the local density approximation (LDA) band calculations for YBCO [131], NCCO [132], and LSCO [133, 134] and by the angle resolved photoemission (ARPES) experiments for YBCO [135], NCCO [70] and LSCO [136], we select the following set of parameters [137, 33]. (I) YBCO (hole-doping) and NCCO (electron-doping): $t_0 = -1$, $t_1 = 1/6$, and $t_2 = -1/5$. (II) LSCO (hole-doping): $t_0 = -1$, $t_1 = 1/10$, and $t_2 = -1/10$. Here, n is smaller (larger) than unity in YBCO and LSCO (NCCO). The Fermi surfaces for YBCO and NCCO without interaction are shown in Fig. 4 (i). The deformation of the Fermi surface in the presence of U has been discussed in Ref. [33]. Note that the Fermi surface in $\text{Bi}_2\text{Sr}_2\text{CaCu}_2\text{O}_8$ (BSCCO) is similar to that in YBCO [138]. Since $|t_0| \sim 4000\text{K}$ in HTSCs, $T = 0.1$ in the present study corresponds to 400K.

Here, we study the self-energy, dynamical spin susceptibility and the CVC using the FLEX approximation [57]. The FLEX approximation is classified as a conserving approximation whose framework was constructed by Baym and Kadanoff [139] and by Baym [140]. For this reason, we can calculate the CVC without ambiguity, by following the Ward identity $\Gamma^I = \delta\Sigma/\delta G$. Here, the Green function and the self-energy are given by

$$G_{\mathbf{k}}(\epsilon_n) = (i\epsilon_n + \mu - \epsilon_{\mathbf{k}}^0 - \Sigma_{\mathbf{k}}(\epsilon_n))^{-1}, \quad (13)$$

$$\Sigma_{\mathbf{k}}(\epsilon_n) = T \sum_{\mathbf{q}, l} G_{\mathbf{k}-\mathbf{q}}(\epsilon_n - \omega_l) \cdot V_{\mathbf{q}}(\omega_l), \quad (14)$$

$$V_{\mathbf{q}}(\omega_l) = U^2 \left(\frac{3}{2} \chi_{\mathbf{q}}^s(\omega_l) + \frac{1}{2} \chi_{\mathbf{q}}^c(\omega_l) - \chi_{\mathbf{q}}^0(\omega_l) \right) + U, \quad (15)$$

$$\chi_{\mathbf{q}}^{s(c)}(\omega_l) = \chi_{\mathbf{q}}^0 \cdot \{1 - (+)U\chi_{\mathbf{q}}^0(\omega_l)\}^{-1}, \quad (16)$$

$$\chi_{\mathbf{q}}^0(\omega_l) = -T \sum_{\mathbf{k}, n} G_{\mathbf{q}+\mathbf{k}}(\omega_l + \epsilon_n) G_{\mathbf{k}}(\epsilon_n), \quad (17)$$

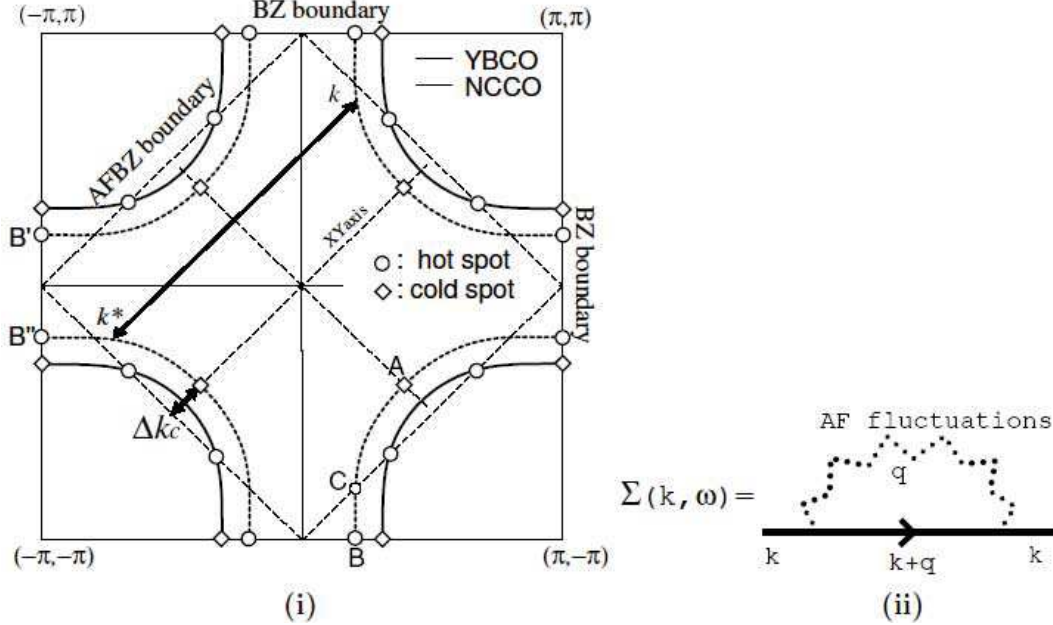


Figure 4. (i) The Fermi surfaces for YBCO ($n < 1$) and NCCO ($n > 1$). The location of the hot spots and the cold spots are shown. According to the FLEX approximation, the hot spot in YBCO shifts to point B, by reflecting the large DOS at $(\pi, 0)$. (ii) Diagrammatic representation of the self-energy in the one-loop (FLEX) approximation.

where $\epsilon_n = (2n + 1)\pi T$ and $\omega_l = 2l\pi T$, respectively. The self-energy in eq. (14) is schematically shown by Fig. 4 (ii). We solve the eqs. (14)-(17) self-consistently, choosing μ so as to satisfy $n = T \sum_{k,n} G_{\mathbf{k}}(\epsilon_n) \cdot e^{-i\epsilon_n \delta}$.

The FLEX approximation is suitable for the analysis of nearly AF Fermi liquids. Many authors have applied this approximation to the square-lattice Hubbard model [57, 124, 125, 126]. Although it is an approximation, the imaginary-time Green function obtained from the FLEX approximation is in good agreement with the results obtained from the quantum Monte Carlo simulations for a moderate value of U [57]. It has also been applied to the SC ladder compound, $\text{Sr}_{14-x}\text{Ca}_x\text{Cu}_{24}\text{O}_{41}$ [127], and the organic SC κ -(BEDT-TTF) compounds [93, 94, 95, 141]. Using the FLEX approximation, T_c was studied in various types of tight-binding models [142]. The FLEX approximation predicts that the AF fluctuations are predominant in a square-lattice Hubbard model near half-filling. This result has been confirmed by renormalization group analyses, which considers both spin and charge fluctuations on the same footing by solving the parquet equation [143, 144, 145].

The FLEX approximation can not reproduce the pseudo-gap behaviors below $T^* \sim 200\text{K}$ in slightly under-doped systems. However, they are well explained by the FLEX+ T -matrix approximation [88, 51, 89], where the self-energy correction due to strong SC fluctuations, which are induced by AF fluctuations, are considered self-consistently. We will explain about the FLEX+ T -matrix approximation in §5. In the present study, we perform numerical studies from the over-doped region to

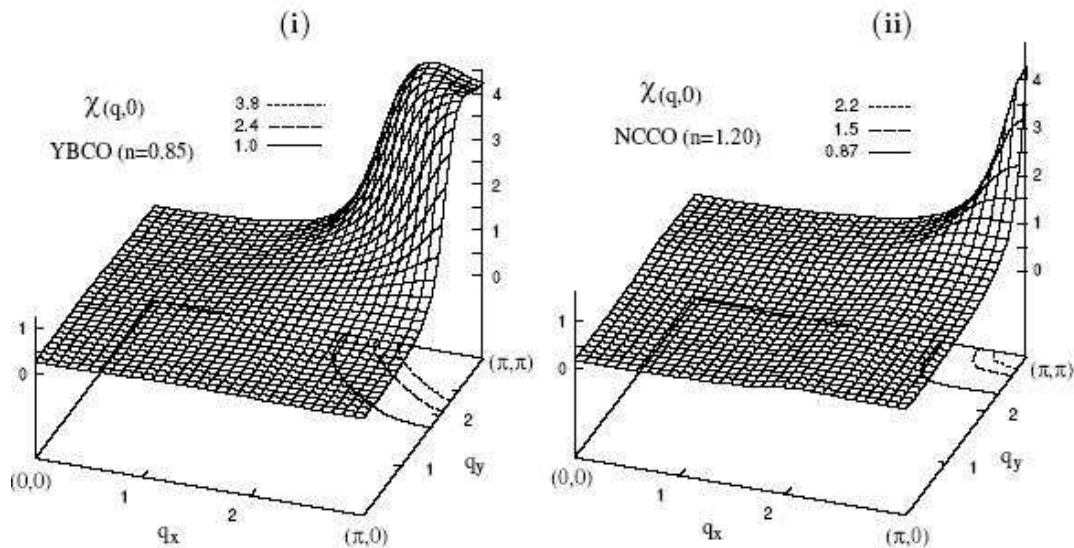


Figure 5. $\chi(\mathbf{q}, \omega = 0)$ for (i) YBCO ($n = 0.85$) at $T = 0.02$ and (ii) for NCCO ($n = 1.20$) at $T = 0.04$, given by the FLEX approximation. In YBCO, $\xi_{\text{AF}} = 2a \sim 3a$, whereas ξ_{AF} for NCCO exceeds $\sim 10a$ at $T = 0.02$. a is the lattice spacing. [Ref. [33]]

the slightly under-doped region (i.e., $n \leq 0.9$ or $n \geq 1.1$), where the FLEX(+ T -matrix) approximation yields reasonable results. Note that the FLEX approximation is inappropriate to describe the “Mott physics” in the heavily under-doped region.

Figure 5 shows the spin susceptibility $\chi_{\mathbf{q}}^s(\omega = 0)$ given by the FLEX approximation, both for YBCO ($n = 0.85$; optimum doping) at $T = 0.02$ and for NCCO ($n = 1.20$, slightly over-doping) at $T = 0.04$, respectively [33]. Since the nesting of the Fermi surface is not good as shown in Fig. 4, $\xi_{\text{AF}} \propto \sqrt{\chi_{\mathbf{Q}}}$ is moderate even at low temperatures. In optimum YBCO, the Stoner factor $U\chi_{\mathbf{Q}}^0(0) \sim 0.98$ at $T = 0.02$, and the AF correlation length ξ_{AF} is approximately $2 \sim 3 a$ (a denotes the lattice spacing). On the other hand, ξ_{AF} in NCCO ($n = 1.20$) exceeds $10 a$ at $T = 0.02$. It should be noted that $\chi_{\mathbf{q}}^s(\omega = 0)$ given by the RPA shows an incommensurate structure, which is inconsistent with the experimental results. I verified that $1/T_1 T$ of the Cu nuclei under $\mathbf{H} \perp \hat{c}$ given by the FLEX approximation for $n = 0.85$ is $1 \sim 2$ [1/K msec] at 200K, which is consistent with the experimental results [146].

One of the advantages of the FLEX approximation is that the Mermin-Wagner theorem with respect to the magnetic instability is satisfied: its analytic proof is given in the appendix A of Ref. [130]. Hence, the critical region ($U\chi_{\mathbf{Q}}^0(0) \gtrsim 0.99$) is stable in 2D systems since the SDW order ($U\chi_{\mathbf{Q}}^0(0) = 1$) is prevented by the Mermin-Wagner theorem. That is, $U_{\text{cr}} = \infty$ in 2D systems. As a result, the U dependence on R_{H} (and $\chi_{\mathbf{Q}}^s$) given by the FLEX+CVC approximation is rather moderate, as shown in Refs. [33, 96].

In the next stage, we derive the two-particle Green function $L(k, k')$ which is indispensable for the study of transport phenomena. According to the microscopic Fermi liquid theory [30, 31], $L(k, k')$ can be obtained by the solution of the following

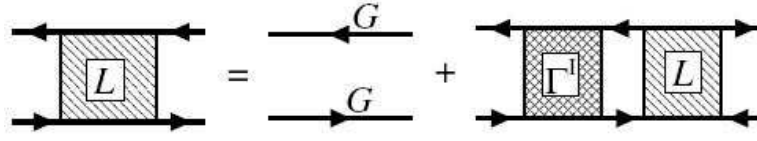


Figure 6. Bethe-Salpeter equation for two-particle Green function $L(k, k')$. $\Gamma^I(k, k')$ is the irreducible four point vertex with respect to the particle-hole channel $G_{k''+q}G_{k''}$.

Bethe-Salpeter equation:

$$\begin{aligned}
 L(k, k'; q) &= -G_{k+q}G_k\delta_{k,k'}/T - G_{k+q}G_k\Gamma(k, k'; q)G_{k'+q}G_{k'} \\
 &= -G_{k+q}G_k\delta_{k,k'}/T \\
 &\quad - T \sum_{k''} G_{k+q}G_k\Gamma^I(k, k''; q)G_{k''+q}G_{k''}L(k'', k'; q), \quad (18)
 \end{aligned}$$

where $k = (\mathbf{k}, \epsilon_n)$ and $\Gamma(k, k'; q)$ is the full four-point vertex. $\Gamma^I(k, k'; q)$ is the irreducible four-point vertex, which is given by the Fourier transformation of the Ward identity in real space; $\hat{\Gamma}^I = \delta\hat{\Sigma}/\delta\hat{G}$. The Bethe-Salpeter equation is expressed by Fig. 6. In later sections, we show that various linear transport coefficients are described in terms of L . (e.g., see. eq. (51).) In the conserving approximation, transport coefficient obtained by $L(k, k')$ in eq. (18) automatically satisfies conservation laws [139, 140]. This is the reason why we refer to it as the conserving approximation. This is a great advantage of the FLEX approximation for the study of transport phenomena. In the FLEX approximation, irreducible four-point vertex will be given in eq. (89) in §4.1.

2.3. Hot/cold-spot structure and T -linear resistivity in nearly AF metals

As we have explained, important advance in HTSCs has been achieved by using the Fermi liquid theory with strong AF fluctuations [54, 56, 57, 52, 25, 24]. One of the most important predictions given by these theories is the “hot/cold-spot structure” of the quasiparticle damping rate, $\gamma_{\mathbf{k}} = \text{Im}\Sigma_{\mathbf{k}}(-i\delta)$ ($\tau_{\mathbf{k}} = 1/2\gamma_{\mathbf{k}}$). That is, $\gamma_{\mathbf{k}}$ becomes anisotropic in the presence of AF fluctuations. This fact is very important to understand the transport phenomena in HTSCs. The portions of the Fermi surface at which $\gamma_{\mathbf{k}}$ takes the maximum and minimum values are referred to as *hot spots* and (*cold spots*), respectively [25, 24]. According to the spin fluctuation theory, the hot spots usually exist around the crossing points with the AF Brillouin zone (AFBZ)-boundary, whereas the cold spot is at the points where the distance from the AFBZ-boundary is the largest. Their positions are shown in Fig. 4 (i). The electronic states around the cold spots play the major role for various transport phenomena. Note that the hot spot in YBCO shifts to the Brillouin zone boundary (point B), by reflecting the large DOS at $(\pi, 0)$.

Figure 7 shows the \mathbf{k} -dependence of $\gamma_{\mathbf{k}}$ on the Fermi surface given by the FLEX approximation [33]. In YBCO, the hot spot shifts from point C in Fig. 4 (i) to the BZ-boundary [point B], by reflecting the large DOS at the van-Hove singularity point $(\pi, 0)$. Therefore, the spectral weight at the Fermi energy is strongly reduced around

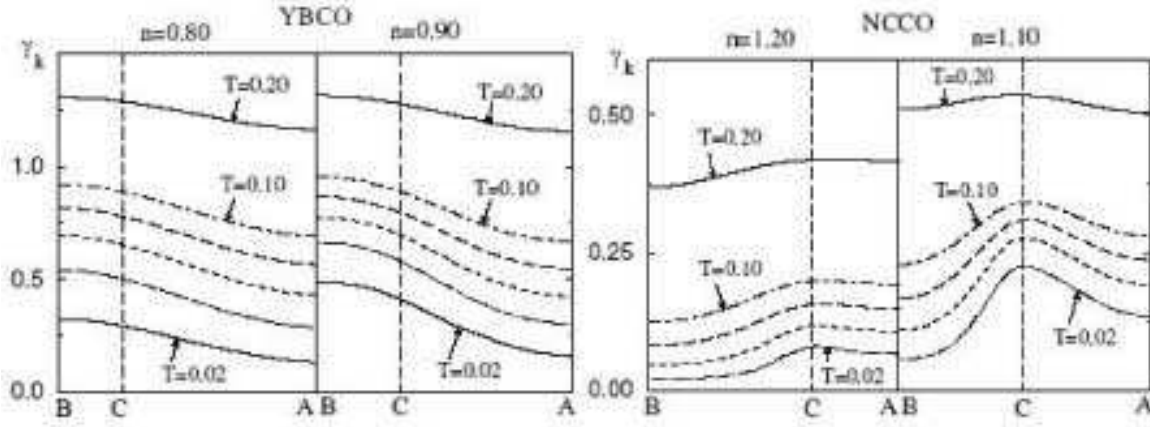


Figure 7. The \mathbf{k} -dependence of $\gamma_{\mathbf{k}}$ on the Fermi surface at various temperatures. The cold spot in YBCO (NCCO) is point A (B).

$(\pi, 0)$ due to large γ_{hot} , which is consistent with the ARPES experiments [86]. In NCCO, in contrast, the hot spot and the cold spot are located at point C and point B, respectively. We emphasize that the location of the cold spot in NCCO was first predicted by the FLEX approximation in 1999 [33], and it was later confirmed by ARPES [70]. According to the spin fluctuation theories [25], $\gamma_{\text{hot}} \propto \sqrt{T}$, and $\gamma_{\text{cold}} \propto T$ except that $\xi_{\text{AF}} \gg (\Delta k_c)^{-1}$; Δk_c is shown in Fig. 4 (i).

The critical value of U for a spin density wave (SDW) transition in the RPA (i.e., the mean-field approximation) is $U_{\text{cr}}^{\text{RTA}} \sim 2.3$ in LSCO ($n = 0.9$). In YBCO and NCCO, $U_{\text{cr}}^{\text{RTA}}$ takes a much larger value, $U_{\text{cr}}^{\text{RTA}} \sim 3.5$ for both YBCO ($n = 0.9$) and NCCO ($n = 1.1$), since the nesting is not good due to the large next-nearest and third-nearest hopping integrals (t_1 and t_2). Here, we consider to put the same U for both YBCO and NCCO. In YBCO, the dimensionless coupling constant $UN(0)$ is large, since the saddle point is close to the Fermi level. Here, $N(0)$ is the DOS at the Fermi level. Therefore, $\text{Im}\Sigma_{\mathbf{k}}(0)$ takes a large value, which significantly reduces the interacting DOS and $\chi_{\mathbf{q}}^s(0)$ at $\mathbf{q} = (\pi, \pi)$ [33]. In fact, the obtained $N_{\text{FLEX}}(0)/N_{U=0}(0)$ is considerably smaller than unity in YBCO. On the other hand, the reduction in $\chi_{\mathbf{q}}^s(0)$ due to $\text{Im}\Sigma_{\mathbf{k}}(0)$ is small in NCCO since the saddle point is far below the Fermi level. For this reason, ξ_{AF} for NCCO is much larger than that for YBCO in the FLEX approximation. This result is consistent with experiments.

The real-frequency Green function $G_{\mathbf{k}}(\epsilon)$ is given by the analytic continuation of $G_{\mathbf{k}}(\epsilon_n)$ in eq. (13). In a Fermi liquid, the advanced Green function $G_{\mathbf{k}}^A(\epsilon) = G_{\mathbf{k}}(\epsilon - i\delta)$ in the vicinity of $\epsilon \sim 0$ and $|\mathbf{k}| \sim k_F$ can be represented as

$$G_{\mathbf{k}}^A(\epsilon) = z_{\mathbf{k}}/(\epsilon - E_{\mathbf{k}}^* - i\gamma_{\mathbf{k}}^*), \quad (19)$$

$$E_{\mathbf{k}} = \epsilon_{\mathbf{k}}^0 + \Sigma_{\mathbf{k}}(0) - \mu, \quad E_{\mathbf{k}}^* = z_{\mathbf{k}}E_{\mathbf{k}}, \quad (20)$$

$$\gamma_{\mathbf{k}} = \text{Im}\Sigma_{\mathbf{k}}^A(0), \quad \gamma_{\mathbf{k}}^* = z_{\mathbf{k}}\gamma_{\mathbf{k}}, \quad (21)$$

where $z_{\mathbf{k}}$ is the renormalization factor given by $z_{\mathbf{k}} = 1/(1 - \partial \text{Re}\Sigma_{\mathbf{k}}(\epsilon)/\partial \epsilon)_{\epsilon=0}$, and $E_{\mathbf{k}}^*$ is the renormalized quasi-particle spectrum, which is the solution of $\text{Re}G_{\mathbf{k}}^{-1}(E_{\mathbf{k}}^*) = 0$. The

quasiparticle weight is given by

$$\rho_{\mathbf{k}}(\epsilon) = \frac{1}{\pi} \text{Im} G_{\mathbf{k}}^A(\epsilon). \quad (22)$$

The DOS is expressed as $N(\epsilon) = \sum_{\mathbf{k}} \rho_{\mathbf{k}}(\epsilon)$. In the case of $z_{\mathbf{k}} \gamma_{\mathbf{k}} \ll \mu$,

$$\rho_{\mathbf{k}}(\epsilon) = z_{\mathbf{k}} \delta(\epsilon - E_{\mathbf{k}}^*) \quad (23)$$

for $\epsilon \approx 0$.

In the FLEX approximation, $\gamma_{\mathbf{k}}$ is obtained by the analytic continuation of eq. (14):

$$\gamma_{\mathbf{k}} = \frac{1}{2} \sum_{\mathbf{q}} \int d\epsilon \left[\text{cth} \frac{\epsilon}{2T} - \text{th} \frac{\epsilon}{2T} \right] \text{Im} V_{\mathbf{q}}(\epsilon + i\delta) \rho_{\mathbf{k}+\mathbf{q}}(\epsilon) \quad (24)$$

where $V_{\mathbf{q}}(\omega + i\delta)$ is given by the analytic continuation of eq. (15). In the spin fluctuation model (Millis-Monien-Pines model in eq. (8)), $\text{Im} V_{\mathbf{q}}(0)$ in eq. (24) is replaced with $(3U^2/2) \text{Im} \chi_{\mathbf{q}}^s(0) = (3U^2/2) \omega \chi_Q \omega_{\text{sf}} / (\omega_{\mathbf{q}}^2 + \omega^2)$, where $\omega_{\mathbf{q}} = \omega_{\text{sf}} + \omega_{\text{sf}} \xi_{\text{AF}}^2 (\mathbf{q} - \mathbf{Q})^2$. According to Refs. [25, 33], eq. (24) is approximately transformed to

$$\gamma_{\mathbf{k}} \approx \frac{3U^2}{4\pi} \int_{\text{FS}} \frac{dk'_{\parallel}}{v_{\mathbf{k}'}} \chi_Q \omega_{\text{sf}} \frac{(\pi T)^2}{4\omega_{\mathbf{k}-\mathbf{k}'} (\omega_{\mathbf{k}-\mathbf{k}'} + \pi T/2)} \quad (25)$$

According to eq. (25), γ_{hot} ($\gamma_{\mathbf{k}}$ at the hot spot) in 2D systems is given by [25]:

$$\gamma_{\text{hot}} \propto T \xi_{\text{AF}} \quad \text{for } \pi T/2\omega_{\text{sf}} \gg 1 \quad (26)$$

$$\gamma_{\text{hot}} \propto T^2 \xi_{\text{AF}}^3 \quad \text{for } \pi T/2\omega_{\text{sf}} \ll 1. \quad (27)$$

Since $\xi_{\text{AF}}^2 \propto T^{-1}$, $\gamma_{\text{hot}} \propto \sqrt{T}$ for any value of ω_{sf}/T : This result is recognized in the numerical study in Fig. 7. Also, γ_{cold} in 2D systems is obtained as [25]:

$$\gamma_{\text{cold}} \propto T \quad \text{for } \pi T/2\omega_{\text{sf}} \sim (\xi_{\text{AF}} \Delta k_c)^2, \quad (28)$$

$$\gamma_{\text{cold}} \propto T^2 \quad \text{for } \pi T/2\omega_{\text{sf}} \ll (\xi_{\text{AF}} \Delta k_c)^2. \quad (29)$$

According to eqs. (9) and (10), $\pi T/2\omega_{\text{sf}}$ is constant if $\Theta \approx 0$, and it is of the order of $O(1)$ in optimally-doped HTSCs. Therefore, $\gamma_{\text{cold}} \propto T$ when $\xi_{\text{AF}} \Delta k_c \sim O(1)$, and $\gamma_{\text{cold}} \propto T^2$ when $\xi_{\text{AF}} \Delta k_c \gg 1$. [Here, Δk_c represents the ‘‘deviation from the nesting condition at the cold spot’’; see Fig. 4.] We comment that the almost all part of the Fermi surface becomes the cold spot in the case of $\xi_{\text{AF}} \Delta k_c \gg 1$.

Now, we discuss the temperature dependence of resistivity according to the SCR theory [54], by dropping the CVC. In the SCR theory, the resistivity is derived from the Born approximation $\rho \propto \langle \gamma_{\mathbf{k}} \rangle_{\text{FS}} \equiv \sum_{\mathbf{k}} \gamma_{\mathbf{k}} \rho_{\mathbf{k}}(0)$. In the case of $\omega_{\text{sf}} \gg T$, eq. (25) is simplified as

$$\gamma_{\mathbf{k}} \approx \sum_{\mathbf{q}} \frac{(\pi T)^2}{2} \text{Im} \dot{V}_{\mathbf{q}}(0) \rho_{\mathbf{k}+\mathbf{q}}(0), \quad (30)$$

where $\dot{V}_{\mathbf{q}}(0) = dV_{\mathbf{q}}(\omega + i\delta)/d\omega|_{\omega=0}$. It can also be derived directly from eq. (24) by using the relation $\int_{-\infty}^{\infty} d\epsilon [\text{cth}(\epsilon/2T) - \text{th}(\epsilon/2T)] \epsilon = (\pi T)^2$. Using eqs. (8) and (30), the temperature dependence of the resistivity is given by [54, 147]

$$\rho_{\text{SCR}} \propto \langle \gamma_{\mathbf{k}} \rangle_{\text{FS}} \propto T^2 \xi_{\text{AF}}^{4-d}, \quad (31)$$

where d is the dimension of the system. In deriving eq. (31), we utilized the fact that the \mathbf{q} -dependence of $\text{Im}\chi_{\mathbf{q}}^0(0) = (\pi/2) \sum_{\mathbf{k}} \rho_{\mathbf{k}}(0)\rho_{\mathbf{k}+\mathbf{q}}(0)$ is moderate. Since $\xi_{\text{AF}} \propto T^{-0.5}$ near the AF-QCP [54], ρ_{SCR} is proportional to $T^{d/2}$ ($d = 2, 3$). We stress that the Fermi liquid behavior $\rho_{\text{SCR}} \propto T^2$ is recovered when $\xi_{\text{AF}} = \text{constant}$ away from the AF-QCP, like in over-doped systems at low temperatures.

In §4.2, we will calculate the resistivity using the FLEX approximation (and FLEX+ T -matrix approximation), based on the linear response theory. In Fig. 18, ‘‘FLEX’’ represents the resistivity obtained by dropping the CVC, and ‘‘FLEX+CVC’’ represents ρ given by the FLEX+CVC approximation; the latter gives the correct result. Consistently with eq. (31), the obtained ρ follows an approximate T -linear behavior in under-doped LSCO and NCCO, and it shows a T^2 -like behavior in the over-doped NCCO. As for the resistivity, the CVC is quantitatively important. In later sections, we explain that the CVC completely changes the T -dependence of R_{H} , $\Delta\rho/\rho_0$ and ν .

However, the Born approximation (eq. (31)) gives overestimated values when $\gamma_{\mathbf{k}}$ is highly anisotropic, as pointed out by Refs. [24, 148]: According to the linear response theory, the correct resistivity is give by

$$\rho \propto 1/\langle \gamma_{\mathbf{k}}^{-1} v_{\mathbf{k}x}^2 \rangle_{\text{FS}} \sim \gamma_{\text{cold}}. \quad (32)$$

According to eqs. (28) and (29), ρ shows the T -linear behavior in the case of $\xi_{\text{AF}}\Delta k_c \sim O(1)$, whereas $\rho \propto T^2$ in the case of $\xi_{\text{AF}}\Delta k_c \gg 1$.

In optimally doped or slightly under-doped YBCO and LSCO, ρ shows an approximate T -linear behavior, which means that the relation $\xi_{\text{AF}}\Delta k_c \sim O(1)$ is satisfied in these compounds above T_c . In fact, if $\xi_{\text{AF}}\Delta k_c \gg 1$, the dominant part of the Fermi surface should be the cold spot. However, this result is inconsistent with the ARPES measurements [86]. In electron-doped systems, on the other hand, $\xi_{\text{AF}}\Delta k_c \gg 1$ seems to be realized at low temperatures even in optimally-doped systems, since ξ_{AF} reaches 100 just above T_c in NCCO [122]. The relationship $\xi_{\text{AF}}\Delta k_c \gg 1$ is also satisfied in the present numerical study. In this case, $\gamma_{\mathbf{k}}$ becomes highly anisotropic and $\rho \sim \gamma_{\text{cold}} \sim T^2$ is realized [25].

According to eq. (32), the relationship $\rho \propto T^2$ holds in the close vicinity of the AF-QCP; $\xi_{\text{AF}}\Delta k_c \gg 1$. However, Rosch [148] pointed out that the relationship $\rho = a + bT$ ($a, b > 0$) holds even at the AF-QCP when the quasiparticle damping rate due to impurities γ_{imp} is finite: In fact, at sufficiently low temperatures where elastic scattering is dominant ($\gamma_{\text{imp}} \gg \gamma_{\mathbf{k}}$), then eq. (32) becomes

$$\rho \propto 1/\langle (\gamma_{\mathbf{k}} + \gamma_{\text{imp}})^{-1} \rangle_{\text{FS}} \propto \gamma_{\text{imp}} + \langle \gamma_{\mathbf{k}} \rangle_{\text{FS}}. \quad (33)$$

Therefore, according to eq. (31), $\rho - \rho_0 \propto T^{d/2}$ ($d = 2, 3$) holds near the AF-QCP in the presence of impurities.

Here, we explained the T -linear resistivity in HTSCs based on the spin fluctuation theory. There are other theories which accounts for the T -linear resistivity. As discussed in §1.4, the marginal Fermi liquid hypothesis was proposed by Varma et al. [118, 119]. Also, the Tomonaga-Luttinger model with two types of relaxation times was proposed by Anderson [23]. Unfortunately, based on these theories, it is difficult to calculate other

transport coefficients such as R_H and $\Delta\rho/\rho_0$. In later sections, we will explain various anomalous transport phenomena in HTSCs in a unified way based on the Fermi liquid theory.

3. Anomalous transport phenomena in nearly AF Fermi liquids

3.1. Results by RTA

Before investigating the transport coefficients using the microscopic Fermi liquid theory, we briefly review the relaxation time approximation (RTA) based on the Bloch-Boltzmann theory [1]. The CVC provides correction for the RTA. In later sections, we will see that the CVC becomes crucial near the AF QCP. The Boltzmann equation in a nonequilibrium steady state is expressed as [1]

$$\left(\frac{\partial f_{\mathbf{k}}}{\partial t}\right)_{\text{scatt.}} = -e(\mathbf{E} + \vec{v}_{\mathbf{k}} \times \mathbf{H}) \cdot \vec{\nabla}_{\mathbf{k}} f_{\mathbf{k}}, \quad (34)$$

where we put $c = \hbar = 1$, and $-e$ ($e > 0$) is the charge of electron. $f_{\mathbf{k}}$ is the distribution function in a nonequilibrium steady state, and \mathbf{E} and \mathbf{H} are the electric and magnetic fields, respectively. $(\partial f_{\mathbf{k}}/\partial t)_{\text{scatt.}}$ represents the rate of change in $f_{\mathbf{k}}$ due to scattering between quasiparticles, which is called the collision integral. Using the scattering amplitude $I(\mathbf{k}, \mathbf{k}; \mathbf{q})$ for $(\mathbf{k}, \mathbf{k}') \leftrightarrow (\mathbf{k} + \mathbf{q}, \mathbf{k}' - \mathbf{q})$, it is given by [1]

$$\begin{aligned} \left(\frac{\partial f_{\mathbf{k}}}{\partial t}\right)_{\text{scatt.}} = & - \sum_{\mathbf{k}'\mathbf{q}} I(\mathbf{k}, \mathbf{k}; \mathbf{q}) [f_{\mathbf{k}} f_{\mathbf{k}'} (1 - f_{\mathbf{k}+\mathbf{q}}) (1 - f_{\mathbf{k}'-\mathbf{q}}) \\ & - (1 - f_{\mathbf{k}}) (1 - f_{\mathbf{k}'}) f_{\mathbf{k}+\mathbf{q}} f_{\mathbf{k}'-\mathbf{q}}] \end{aligned} \quad (35)$$

where the first (second) term represents the outgoing (incoming) scattering process. To derive the conductivity, we have to linearize the Boltzmann equations (34) and (35) with respect to \mathbf{E} .

In solving these equations, we frequently apply the RTA; $(\partial f_{\mathbf{k}}/\partial t)_{\text{scatt.}} = -g_{\mathbf{k}}/\tau_{\mathbf{k}}$, where $g_{\mathbf{k}} = f_{\mathbf{k}} - f_{\mathbf{k}}^0$ and $f_{\mathbf{k}}^0 = (e^{(\epsilon_{\mathbf{k}} - \mu)/k_B T} + 1)^{-1}$ is the equilibrium distribution function. Then, the linearized Boltzmann equation is simplified as

$$\frac{g_{\mathbf{k}}}{\tau_{\mathbf{k}}} = -e\mathbf{E} \cdot \vec{v} \left(-\frac{\partial f_{\mathbf{k}}^0}{\partial \epsilon_{\mathbf{k}}}\right) + e(\vec{v}_{\mathbf{k}} \times \mathbf{H}) \cdot \vec{\nabla}_{\mathbf{k}} g_{\mathbf{k}}. \quad (36)$$

The solution of eq. (36) is given by

$$g_{\mathbf{k}} = - \left(1 - e\tau_{\mathbf{k}}(\vec{v} \times \mathbf{H}) \cdot \vec{\nabla}_{\mathbf{k}}\right)^{-1} e\mathbf{E} \cdot \tau_{\mathbf{k}} \vec{v}_{\mathbf{k}} \left(-\frac{\partial f_{\mathbf{k}}^0}{\partial \epsilon_{\mathbf{k}}}\right). \quad (37)$$

Although it is a crude approximation, the RTA can successfully explain the various transport phenomena in metals with weak correlation.

In the RTA, the conductivity is given by $\sigma_{\mu\nu}^{\text{RTA}} = -2e \sum v_{\mathbf{k}\mu} g_{\mathbf{k}}/E_{\nu}$, where the factor 2 is attributed to the spin degeneracy. When the \mathbf{k} -dependence of $\tau_{\mathbf{k}}$ is moderate, the functional form of $\sigma_{\mu\nu}$ under the magnetic field is $\sigma_{\mu\nu} = \tau F_{\mu\nu}(\tau H)$. Here, we assume

$\mathbf{H} \parallel \hat{\mathbf{z}}$. Then, $(\vec{v} \times \mathbf{H}) \cdot \vec{\nabla}_{\mathbf{k}} = -H_z(\vec{v}_{\mathbf{k}} \times \vec{\nabla}_{\mathbf{k}})_z$. In the RTA, the longitudinal conductivity, Hall conductivity, and magnetoconductivity are given by

$$\sigma_{xx}^{\text{RTA}} = 2e^2 \sum_{\mathbf{k}} \left(-\frac{df^0}{d\epsilon_{\mathbf{k}}} \right) v_{\mathbf{k}x} \cdot \tau_{\mathbf{k}} v_{\mathbf{k}x}, \quad (38)$$

$$\sigma_{xy}^{\text{RTA}} = -2e^3 H_z \sum_{\mathbf{k}} \left(-\frac{df^0}{d\epsilon_{\mathbf{k}}} \right) v_{\mathbf{k}x} (\tau_{\mathbf{k}} \vec{v}_{\mathbf{k}} \times \vec{\nabla}_{\mathbf{k}})_z \tau_{\mathbf{k}} v_{\mathbf{k}y}, \quad (39)$$

$$\Delta\sigma_{xx}^{\text{RTA}} = 2e^4 H_z^2 \sum_{\mathbf{k}} \left(-\frac{df^0}{d\epsilon_{\mathbf{k}}} \right) v_{\mathbf{k}x} (\tau_{\mathbf{k}} \vec{v}_{\mathbf{k}} \times \vec{\nabla}_{\mathbf{k}})_z^2 \tau_{\mathbf{k}} v_{\mathbf{k}x}, \quad (40)$$

where $(\tau_{\mathbf{k}} \vec{v}_{\mathbf{k}} \times \vec{\nabla}_{\mathbf{k}})_z = \tau_{\mathbf{k}}(v_x \partial_y - v_y \partial_x)$. When the \mathbf{k} -dependence of $\tau_{\mathbf{k}}$ is moderate,

$$\sigma_{xx} \propto \tau, \quad \sigma_{xy} \propto \tau^2 H_z, \quad \Delta\sigma_{xx}^{\text{RTA}} \propto \tau^3 H_z^2, \quad (41)$$

which is called the Kohler's rule.

Based on the RTA, Hussey et al. studied transport coefficients in heavily over-doped Tl2201 [149] and LSCO [150]. They determined the anisotropy of $\tau_{\mathbf{k}}$ in Tl2201 by measuring the Angle-dependent Magnetoresistance Oscillation (AMRO) along c -axis [151], and calculated transport coefficients using eqs. (38)-(40). The derived $R_{\text{H}}^{\text{RTA}}$ agrees with the experimental Hall coefficient $R_{\text{H}}^{\text{exp}}$ in heavily over-doped samples ($T_c \approx 10$ K), where the Hall coefficient is small and its temperature dependence is tiny. As the doping decreases, $R_{\text{H}}^{\text{exp}}$ increases quickly and its temperature dependence becomes prominent, whereas the doping dependence of $R_{\text{H}}^{\text{RTA}}$ is more moderate.

In optimally doped HTSCs, however, the RTA does not work: Stojkovic and Pines [25] attempted to explain the violation of Kohler's rule in HTSCs based on the RTA. They assumed the highly anisotropic $\tau_{\mathbf{k}}$ model (hot/cold-spot model), where only the quasiparticles near the cold spot contribute toward the transport phenomena. In this model, R_{H} can take a large value since the "effective carrier density for the transport phenomena" is reduced. They calculated $\tau_{\mathbf{k}}$ based on the Millis-Monien-Pines model; the anisotropy of $\tau_{\mathbf{k}}$ reaches 100 in the optimally doped YBCO, which is too large to be consistent with the ARPES measurements. The reason for this overestimation is that self-consistency is not imposed in their calculations. In spite of the large anisotropy of $\tau_{\mathbf{k}}$, the obtained enhancement ratio of R_{H} is about two according to Ref. [27]. Therefore, this scenario cannot account for the large R_{H} in under-doped systems. It should be stressed that the magnetoresistance becomes 100 times greater than the experimental value when the anisotropy of $\tau_{\mathbf{k}}$ is of the order of 100 [26]. Therefore, the highly anisotropic $\tau_{\mathbf{k}}$ model is not applicable for optimally-doped HTSCs. In the next section, we explain the various anomalous transport phenomena in HTSCs "all together", by considering the CVC.

3.2. Physical meaning of the CVC in nearly AF metals

In the RTA where $\dot{g}_{\mathbf{k}} = -g_{\mathbf{k}}/\tau_{\mathbf{k}}$ is assumed, the deviation from the equilibrium distribution function $g_{\mathbf{k}}$ dissipates with time since $g_{\mathbf{k}} \propto e^{-t/\tau_{\mathbf{k}}}$. This oversimplification

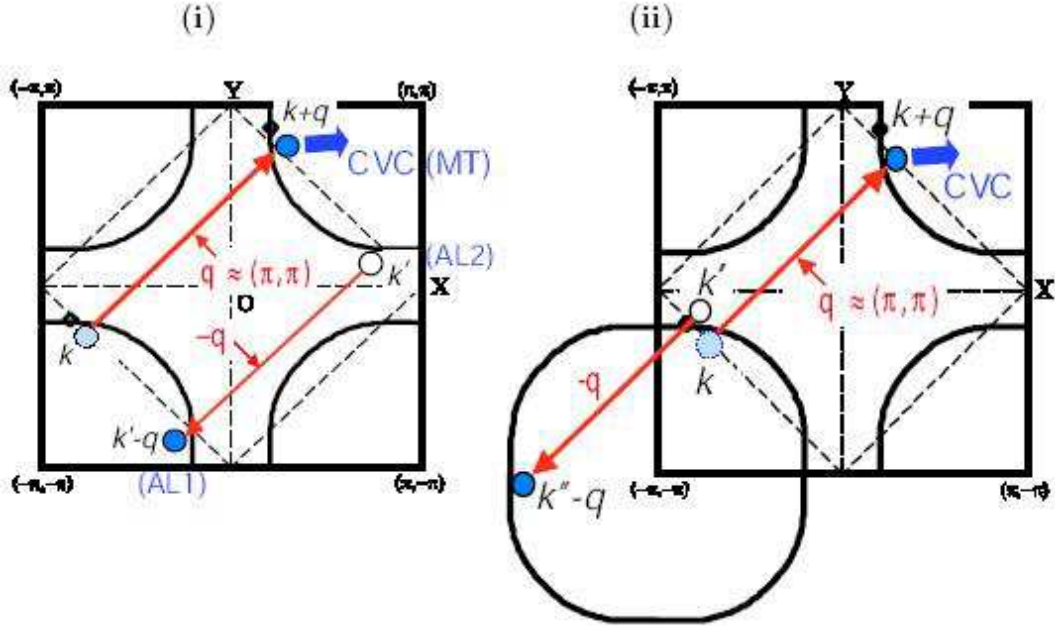


Figure 8. Decay process of a quasiparticle at \mathbf{k} in HTSCs. (i) Due to strong AF fluctuations, this quasiparticle at \mathbf{k} is scattered to $\mathbf{k} + \mathbf{q}$ ($\mathbf{q} \sim \mathbf{Q}$), creating a particle-hole pair (\mathbf{k}' , $\mathbf{k}' - \mathbf{q}$). (ii) The current of the particle-hole excitation in (i) is almost canceled by another particle-hole excitation (\mathbf{k}'' , $\mathbf{k}'' - \mathbf{q}$) for $\mathbf{k}'' = -\mathbf{k}'$. Therefore, the CVC is given by the quasiparticle at $\mathbf{k} + \mathbf{Q}$ alone. The process (ii) is the Umklapp scattering.

frequently leads to serious unphysical results. For example, in the absence of electric field, the RTA predicts that $g_{\mathbf{k}}$ always vanishes when $t \rightarrow \infty$ since $\tau_{\mathbf{k}} > 0$ at finite temperatures. However, $g_{\mathbf{k}}$ should remain finite when the Umklapp scattering process is absent, because of the momentum conservation laws [1, 42]. Therefore, the RTA violates the conservation laws. To satisfy the conservation laws, the incoming scattering from the other states to \mathbf{k} has to be taken into account by solving eq. (35). This scattering process is represented by the CVC in the microscopic Fermi liquid theory. Here, we intuitively discuss the CVC in nearly AF metals, where the quasiparticles are scattered by strong AF fluctuations with $\mathbf{q} \sim \mathbf{Q} = (\pi, \pi)$. Then, the momentum transfer \mathbf{q} in the scattering process is restricted to $\sim \mathbf{Q}$, as shown in Fig. 8. According to the momentum conservation law, the quasiparticle at \mathbf{k}' is scattered to $\mathbf{k}' - \mathbf{q}$ as shown in Fig. 8 (i). The current due to the quasiparticle at $\mathbf{k}' - \mathbf{q}$ and the hole at \mathbf{k}' is given by $\vec{v}_{\mathbf{k}' - \mathbf{q}} - \vec{v}_{\mathbf{k}'}$. This current almost cancels after performing the \mathbf{k}' -summation: In fact, the current of the particle-hole pair ($\mathbf{k}'' - \mathbf{q}$, \mathbf{k}'') for $\mathbf{k}'' = -\mathbf{k}'$, which is shown in Fig. 8 (ii), is $\vec{v}_{\mathbf{k}'' - \mathbf{q}} - \vec{v}_{\mathbf{k}''} \approx -\vec{v}_{\mathbf{k}' - \mathbf{q}} + \vec{v}_{\mathbf{k}'}$ since $2\mathbf{q} \approx 2\mathbf{Q}$ is a reciprocal lattice vector. Therefore, the CVC is given only by the quasiparticle at $\mathbf{k} + \mathbf{q}$; $\vec{v}_{\mathbf{k} + \mathbf{q}}$. In this case, the conductivity does not diverge because of the existence of the Umklapp processes, e.g., the process in Fig. 8 (ii).

In nearly AF metals, the total current $\vec{J}_{\mathbf{k}}$ is approximately parallel to $\vec{v}_{\mathbf{k}} + \vec{v}_{\mathbf{k} + \mathbf{Q}}$,

which implies that $\vec{J}_{\mathbf{k}}$ is not perpendicular to the Fermi surface. This fact is the origin of the enhancement of R_{H} [33]. The anomalous \mathbf{k} -dependence of $\vec{J}_{\mathbf{k}}$ becomes much more prominent near the AF QCP due to the multiple backscattering of the quasiparticle between that at \mathbf{k} and that at $\mathbf{k} + \mathbf{Q}$. [The schematic behavior of $\vec{J}_{\mathbf{k}}$ is shown in Fig. 14.] Thus far, we discussed only the two-body scattering process, and ignored the higher-order processes. This simplicity is justified in good metals where $\gamma/E_{\text{F}} \ll 1$, which is satisfied in HTSCs except for heavily under-doped compounds [28].

3.3. Analysis of the CVC based on the Fermi liquid theory

Here, we calculate the CVC based on the microscopic Fermi liquid theory. In principle, we can also calculate the CVC based on the Bloch-Boltzmann theory, by analyzing eq. (35) using the variational principle [1]. However, a systematic calculation of the CVC is very difficult, particularly in the presence of a magnetic field. Therefore, we analyze the CVC based on the linear response theory since we can utilize the powerful field theoretical techniques. In the linear response theory [152, 153, 154], the conductivity is given by

$$\sigma_{\mu\nu}(\omega) = \frac{1}{i\omega} [K_{\mu\nu}^R(\omega) - K_{\mu\nu}^R(0)], \quad (42)$$

where $K_{\mu\nu}^R(\omega)$ is the retarded current-current correlation function.

Here, we consider the conductivities in the presence of the uniform magnetic field. Then, the hopping integral between site i and j exhibits the Peierls phase:

$$t_{m,j} = t_{m,j}^0 \exp[-ie(\mathbf{A}_m + \mathbf{A}_j) \cdot (\mathbf{r}_m - \mathbf{r}_j)/2], \quad (43)$$

where $t_{m,j}^0$ is the original hopping integral, and \mathbf{A}_m is the vector potential at site m . Then, the Hamiltonian and the velocity operator under the magnetic field, H_A and j_{μ}^A respectively, are given by

$$H_A = \sum_{(m,j),\sigma} t_{m,j} c_{m\sigma}^{\dagger} c_{j\sigma} + \frac{U}{2} \sum_m n_{m\uparrow} n_{m\downarrow}, \quad (44)$$

$$j_{\mu}^A(\mathbf{r}_m) = \sum_{\sigma} i[H_A, \mathbf{r}_m c_{m\sigma}^{\dagger} c_{m\sigma}] \quad (45)$$

Here, we assume that the vector potential is given by $\mathbf{A}_j = \mathbf{A}e^{i\mathbf{q}\cdot\mathbf{r}_j}$, and take the limit $\mathbf{q} \rightarrow 0$ at the final stage of the calculation [44]. (The magnetic field is $\mathbf{H} = i\mathbf{q} \times \mathbf{A}$.) Then, eq. (43) can be expanded as $t_{m,j} = t_{m,j}^0 [1 - i(e/2)\mathbf{A} \cdot (\mathbf{r}_m - \mathbf{r}_j)(e^{i\mathbf{q}\cdot\mathbf{r}_m} + e^{i\mathbf{q}\cdot\mathbf{r}_j})] + O(A^2)$. After the Fourier transformation, both the Hamiltonian and the velocity operator of the order of $O(A)$ are given by [38]

$$H_A = H - \mathbf{A} \cdot \mathbf{j}(-\mathbf{q}) + O(A^2), \quad (46)$$

$$j_{\mu}^A(\mathbf{q}') = j_{\mu}(\mathbf{q}') - \sum_{\alpha}^{x,y} A_{\alpha} j_{\alpha\mu}(\mathbf{q}' - \mathbf{q}) + O(A^2), \quad (47)$$

where $j_{\mu}(\mathbf{q}) = -e \sum_{\mathbf{k},\sigma} \partial_{\mu} \epsilon_{\mathbf{k}}^0 \cdot c_{\mathbf{k}-\mathbf{q}/2,\sigma}^{\dagger} c_{\mathbf{k}+\mathbf{q}/2,\sigma}$, and $j_{\alpha\mu}(\mathbf{q}) = e^2 \sum_{\mathbf{k}} \partial_{\alpha\mu} \epsilon_{\mathbf{k}}^0 \cdot c_{\mathbf{k}-\mathbf{q}/2,\sigma}^{\dagger} c_{\mathbf{k}+\mathbf{q}/2,\sigma}$. Here, $\partial_{\mu} = \partial/\partial k_{\mu}$, $\partial_{\mu\alpha} = \partial^2/\partial k_{\mu} \partial k_{\alpha}$, and $-e$ ($e > 0$) is the electron charge. Therefore,

$K_{\mu\nu}^R(\omega)$ is given by the analytic continuation of the following function for $\omega_l \geq 0$ [43, 44, 38]:

$$K_{\mu\nu}(i\omega_l) = \sum_{m=0,1,\dots} \int_0^{1/T} d\tau e^{-i\omega_l\tau} \langle T_\tau j_\mu^A(m\mathbf{q}, 0) j_\nu^A(0, \tau) \rangle_A \quad (48)$$

$$= \int_0^{1/T} d\tau e^{-i\omega_l\tau} \langle T_\tau j_\mu(0, 0) j_\nu(0, \tau) \rangle \quad (49)$$

$$\begin{aligned} &+ \sum_{\alpha}^{x,y} A_\alpha \int \int_0^{1/T} d\tau d\tau' e^{-i\omega_l\tau} \{-T \cdot \langle T_\tau j_\mu(\mathbf{q}, 0) j_{\alpha\nu}(-\mathbf{q}, \tau) \rangle \\ &\quad + \langle T_\tau j_\mu(\mathbf{q}, 0) j_\nu(0, \tau) j_\alpha(-\mathbf{q}, \tau') \rangle\} \\ &+ O(A^2), \end{aligned} \quad (50)$$

where $\omega_l \equiv 2\pi Tl$ is the Matsubara frequency; here we promise l represents an integer and n is a half-integer, respectively.

Hereafter, we ignore the spin indices to simplify expressions. According to eq. (49), $K_{xx}(i\omega_l)$ without the magnetic field is given by [40]

$$\begin{aligned} K_{xx}(i\omega_l) &= -2e^2T \sum_{n,m,\mathbf{k},\mathbf{k}'} v_{\mathbf{k}x}^0 v_{\mathbf{k}'x}^0 L(\mathbf{k}n, \mathbf{k}'m; i\omega_l) \\ &= -2e^2T \sum_{n,\mathbf{k}} v_{\mathbf{k}x}^0 g_{\mathbf{k}}^{n;l} \Lambda_{\mathbf{k}x}^{n;l}, \end{aligned} \quad (51)$$

where $g_{\mathbf{k}}^{n;l} \equiv G_{\mathbf{k}}^n G_{\mathbf{k}}^{n+l}$. $G_{\mathbf{k}}^n \equiv G_{\mathbf{k}}(\epsilon_n)$ is the Green function where n is a half-integer, and $L(\mathbf{k}n, \mathbf{k}'m; i\omega_l)$ is the two-particle Green function in eq. (18). $v_{\mathbf{k}\mu}^0 \equiv \partial\epsilon_{\mathbf{k}}^0/\partial k_\mu$ is the velocity of the free electron, and

$$\Lambda_{\mathbf{k}}^{n;l} = \mathbf{v}_{\mathbf{k}}^0 + T \sum_{\mathbf{k}',m} L(\mathbf{k}n, \mathbf{k}'m; i\omega_l) g_{\mathbf{k}'}^{m;l} \mathbf{v}_{\mathbf{k}'}^0 \quad (52)$$

is the three-point vertex.

In the same way, Kohno and Yamada [43] derived the H -linear term of $K_{xy}(i\omega_l)$ from eq. (50) as

$$\begin{aligned} K_{xy}(i\omega_l) &= i \cdot e^3 HT \sum_{n,\mathbf{k}} \sum_{\mu,\nu}^{x,y} [\partial_\mu G_{\mathbf{k}}^{n+l} \cdot G_{\mathbf{k}}^n - G_{\mathbf{k}}^{n+l} \cdot \partial_\mu G_{\mathbf{k}}^n] \left[\Lambda_{\mathbf{k}x}^{n;l} \cdot \partial_\nu \Lambda_{\mathbf{k}y}^{n;l} \right] \cdot \epsilon_{\mu\nu z} \\ &\quad + [6 \text{ point VC term}], \end{aligned} \quad (53)$$

where $\epsilon_{\mu\nu\lambda}$ is an antisymmetric tensor with $\epsilon_{xyz} = 1$. In deriving eq. (53), we used the relation $H_z = i(q_x A_y - q_y A_x)$ and took the limit $\mathbf{q} \rightarrow 0$ at the final stage of calculation [44]. Several kinds of Ward identities have to be correctly applied to maintain the gauge invariance [43].

In order to derive the conductivity $\sigma_{\mu\nu}(\omega)$, we have to perform the analytic continuations of eqs. (51) and (53); ω_l ($l > 0$) $\rightarrow \omega + i\delta$. Then, the ϵ_n summation is replaced with the integrations along the three cut lines in the complex plane in Fig. 9, together with the thermal factor $(4\pi iT)^{-1} \text{th}(\epsilon/2T)$. In region 1, $g_{\mathbf{k}}^{n;l}$ becomes $g_{\mathbf{k}}^{(1)}(\epsilon; \omega) \equiv G_{\mathbf{k}}^R(\epsilon) G_{\mathbf{k}}^R(\epsilon + \omega)$. In the same way, it becomes $g_{\mathbf{k}}^{(2)}(\epsilon; \omega) \equiv G_{\mathbf{k}}^A(\epsilon) G_{\mathbf{k}}^R(\epsilon + \omega)$

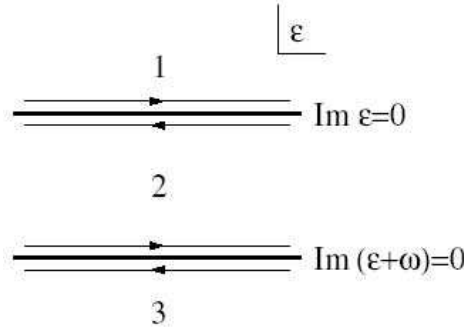


Figure 9. The analytic regions 1-3 as a function of a complex variable ϵ (or ϵ'). Here, we put $\text{Im } \omega > 0$. From each region, $g_{\mathbf{k}}^{n;l}$ and $\Lambda_{\mathbf{k}x}^{n;l}$ are analytically continued to become $g_{\mathbf{k}}^{(i)}(\epsilon; \omega)$ and $J_{\mathbf{k}x}^{(i)}(\epsilon; \omega)$ ($i=1-3$), respectively.

and $g_{\mathbf{k}}^{(3)}(\epsilon; \omega) \equiv G_{\mathbf{k}}^A(\epsilon)G_{\mathbf{k}}^A(\epsilon + \omega)$ in region 2 and 3, respectively. Here, we stress the relation $g^{(2)}(\epsilon; 0) = \pi\rho_{\mathbf{k}}(\epsilon)/\gamma_{\mathbf{k}}^* \approx \pi\delta(E_{\mathbf{k}})/\gamma_{\mathbf{k}}$, see eqs. (19)-(21). As a result, $K_{xx}(\omega + i\delta)$ is given by [40]

$$K_{xx}(\omega + i\delta) = -2e^2 \int_{-\infty}^{\infty} \frac{d\epsilon}{4\pi i} \left[\text{th} \frac{\epsilon}{2T} K_{xx}^{(1)}(\epsilon; \omega) + \left(\text{th} \frac{\epsilon + \omega}{2T} - \text{th} \frac{\epsilon}{2T} \right) K_{xx}^{(2)}(\epsilon; \omega) - \text{th} \frac{\epsilon + \omega}{2T} K_{xx}^{(3)}(\epsilon; \omega) \right] \quad (54)$$

$$K_{xx}^{(i)}(\epsilon; \omega) = \sum_{\mathbf{k}} v_{\mathbf{k}x}^0 g_{\mathbf{k}}^{(i)}(\epsilon; \omega) J_{\mathbf{k}x}^{(i)}(\epsilon; \omega), \quad (55)$$

where $i = 1, 2, 3$. $J_{\mathbf{k}x}^{(i)}(\epsilon; \omega)$ is given by the analytic continuation of $\Lambda_{\mathbf{k}x}^{n;l}$ from region i . It is expressed as

$$J_{\mathbf{k}x}^{(i)}(\epsilon, \omega) = v_{\mathbf{k}x}^0 + \sum_{\mathbf{k}', j=1,2,3} \int_{-\infty}^{\infty} \frac{d\epsilon'}{4\pi i} \mathcal{T}_{\mathbf{k}, \mathbf{k}'}^{i,j}(\epsilon, \epsilon'; \omega) g_{\mathbf{k}'}^{(j)}(\epsilon'; \omega) v_{\mathbf{k}'x}^0, \quad (56)$$

where $\mathcal{T}_{\mathbf{k}, \mathbf{k}'}^{i,j}(\epsilon, \epsilon'; \omega)$ is given by the analytic continuation of the full four-point vertex Γ in eq. (18) from region (i, j) for (ϵ, ϵ') . Thermal factors [such as $(4\pi i)^{-1} \text{th}(x/2T)$ and $(4\pi i)^{-1} \text{ch}(x/2T)$] are included in the definition of $\mathcal{T}_{\mathbf{k}, \mathbf{k}'}^{i,j}$. The explicit expression for $\mathcal{T}_{\mathbf{k}, \mathbf{k}'}^{i,j}$ is given in eq. (12) of Ref. [40].

The DC-conductivity σ_{xx} is given by $\partial \text{Im} K_{xx} / \partial \omega|_{\omega=0}$. For example, if we take the ω -derivative of the thermal factor $(\text{th} \frac{\epsilon + \omega}{2T} - \text{th} \frac{\epsilon}{2T})$ associated with $g^{(2)}$ in eq. (54), we obtain

$$(e^2/\pi) \sum_{\mathbf{k}} z_{\mathbf{k}} (-\partial f^0 / \partial \epsilon)_{E_{\mathbf{k}}^*} v_{\mathbf{k}x}^0 J_{\mathbf{k}x}^{(2)}(0; 0) / \gamma_{\mathbf{k}}, \quad (57)$$

where $f^0(\epsilon) = (e^{\epsilon/T} + 1)^{-1}$; note that $z_{\mathbf{k}} (-\partial f^0 / \partial \epsilon)_{E_{\mathbf{k}}^*} = (-\partial f^0 / \partial \epsilon)_{E_{\mathbf{k}}} = \delta(E_{\mathbf{k}})$ at sufficiently low temperatures. Since $J_{\mathbf{k}x}^{(2)}(\epsilon; 0)$ is not singular with respect to γ^{-1} , eq. (57) is proportional to γ^{-1} , which diverges when $\gamma \rightarrow 0$. On the other hand, if we take the ω -derivative of the thermal factor in front of $g^{(1,3)}$ in eq. (54), the obtained term is (γ^0) . To derive the exact expression for σ_{xx} with respect to $O(\gamma^{-1})$, we also have to take

the ω -derivative of the thermal factor in front of $g^{(2)}$ in $K_{xx}^{(1,3)}(\epsilon; \omega)$. As a result, the exact expression for σ_{xx} is given by eq. (57) by replacing $v_{\mathbf{k}x}^0$ with $v_{\mathbf{k}x} \equiv v_{\mathbf{k}x}^0 + \partial \text{Re} \Sigma_{\mathbf{k}}(0) / \partial k_x$ [40].

$J_{\mathbf{k}x}^{(2)}$ is called the total current since it contains the CVC discussed in previous sections. Hereafter, we denote $J_{\mathbf{k}x}^{(2)}(\epsilon, 0)$ and $\mathcal{T}_{\mathbf{k}, \mathbf{k}'}^{2,2}(\epsilon, \epsilon'; 0)$ as $J_{\mathbf{k}x}(\epsilon)$ and $\mathcal{T}_{\mathbf{k}, \mathbf{k}'}(\epsilon, \epsilon')$. The analytic continuation of $K_{xy}(i\omega_l)$ had been performed in Refs. [43, 44]. To summarize, the general expressions for σ_{xx} and σ_{xy} , which are exact within the most divergent term with respect to $O(\gamma^{-1})$, are given by

$$\sigma_{xx} = e^2 \sum_{\mathbf{k}} z_{\mathbf{k}} \left(-\frac{\partial f^0}{\partial \epsilon} \right)_{E_{\mathbf{k}}^*} v_{\mathbf{k}x} \frac{J_{\mathbf{k}x}}{\gamma_{\mathbf{k}}}, \quad (58)$$

$$\sigma_{xy} = -\frac{e^3}{2} H \sum_{\mathbf{k}} z_{\mathbf{k}} \left(-\frac{\partial f^0}{\partial \epsilon} \right)_{E_{\mathbf{k}}^*} \frac{J_{\mathbf{k}x}}{\gamma_{\mathbf{k}}} (\vec{v}_{\mathbf{k}} \times \vec{\nabla}_{\mathbf{k}})_z \frac{J_{\mathbf{k}y}}{\gamma_{\mathbf{k}}}. \quad (59)$$

Equation (58) was derived by Eliashberg [40]. Equation (59) was derived by Fukuyama et al within the Born approximation [44], and it was proved to be correct in Fermi liquids [43]. Note that we dropped the [6 point VC term] in eq. (53) since they are less singular with respect to $\gamma_{\mathbf{k}}^{-1}$ [43]. In particular, its contribution to σ_{xy} vanishes in the FLEX approximation. In the same way, the present author has derived the exact expressions for the magneto-conductivity $\Delta\sigma_{xx} \equiv \sigma_{xx}(H_z) - \sigma_{xx}(0)$ [38] and the Peltier coefficient $\alpha_{xy} = E_y / (-\nabla_x T)$ in the presence of H_z [39].

Apparently, eqs. (58) and (59) become equal to the RTA results given in eqs. (38) and (39) if we replace the total current $\vec{J}_{\mathbf{k}}$ with the quasiparticle velocity $\vec{v}_{\mathbf{k}}$, that is, if we drop the CVC. The RTA had been frequently used in analyzing transport anomaly in high- T_c cuprates. However, we will explain that the neglect of the CVC frequently causes various unphysical results.

According to Eliashberg, the total current $J_{\mathbf{k}x}$ can be rewritten as [40]

$$J_{\mathbf{k}x}(0) = v_{\mathbf{k}x} + \sum_{\mathbf{k}'} \int_{-\infty}^{\infty} \frac{d\epsilon'}{4\pi i} \mathcal{T}_{\mathbf{k}, \mathbf{k}'}^{(0)}(0, \epsilon') g_{\mathbf{k}'}^{(2)}(\epsilon'; 0) J_{\mathbf{k}'x}(0), \quad (60)$$

where $v_{\mathbf{k}x} = v_{\mathbf{k}x}^0 + \partial \text{Re} \Sigma_{\mathbf{k}}(0) / \partial k_x$, and we put $\epsilon = 0$ in $J_{\mathbf{k}x}(\epsilon)$ for simplicity. $\mathcal{T}_{\mathbf{k}, \mathbf{k}'}^{(0)}(0, \epsilon')$ is the ‘‘irreducible’’ vertex with respect to $g^{(i)}$, which is given by

$$\mathcal{T}_{\mathbf{k}, \mathbf{k}'}^{(0)}(0, \epsilon') = i \left(\text{cth} \frac{\epsilon'}{2T} - \text{th} \frac{\epsilon'}{2T} \right) 2 \text{Im} \Gamma_{\mathbf{k}, \mathbf{k}'}^I(0, \epsilon' - i\delta). \quad (61)$$

Equation (60) is expressed in Fig. 10 (i). The CVC in the microscopic Fermi liquid theory is also called the backflow in the phenomenological Fermi liquid theory.

Here, we analyze the Bethe-Salpeter equation (60): The solution of eq. (60) is real since $\mathcal{T}_{\mathbf{k}, \mathbf{k}'}^{(0)}(0, \epsilon')$ in eq. (61) is pure imaginary. Since $\text{Im} \Gamma_{\mathbf{k}, \mathbf{k}'}^I(0, 0) = 0$, we have to extract the ϵ' -linear term of $\text{Im} \Gamma_{\mathbf{k}, \mathbf{k}'}^I(0, \epsilon')$, which is derived from the cut of the particle-hole pair or that of the particle-particle pair in $\Gamma_{\mathbf{k}, \mathbf{k}'}^I(0, \epsilon')$ [31]. By this procedure, Γ^I is divided into two Γ 's. Therefore, ϵ' -linear term of $\text{Im} \Gamma(0, \epsilon')$ is given by [42]

$$\text{Im} \Gamma_{\mathbf{k}, \mathbf{k}'}^I(0, \epsilon' - i\delta) = \pi \epsilon' \sum_{\mathbf{q}} \Gamma^2(\mathbf{k}, \mathbf{k}'; \mathbf{k}' - \mathbf{q}, \mathbf{k} + \mathbf{q})$$

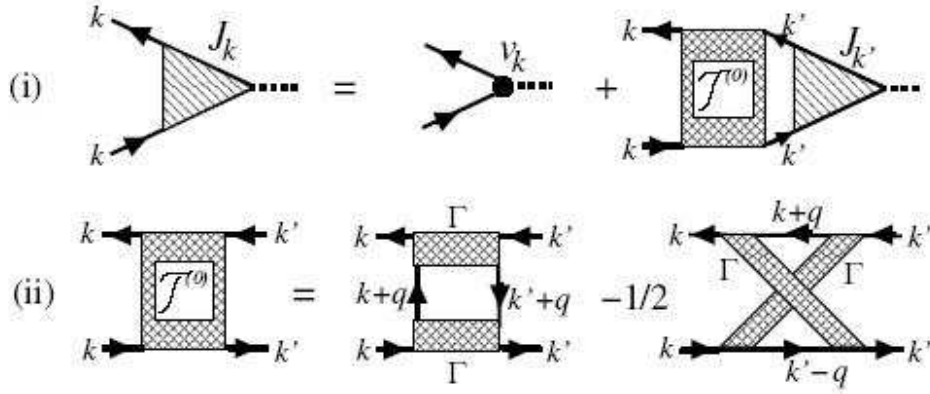


Figure 10. (i) Bethe-Salpeter equation (eq. (60)) for the total current \vec{J}_k . (ii) Expression for $\mathcal{T}_{\mathbf{k},\mathbf{k}'}^{(0)}(0, \epsilon')$ in the microscopic Fermi liquid theory. The factor $-1/2$ is necessary to avoid double counting.

$$\times \left(\rho_{\mathbf{k}+\mathbf{q}}(0)\rho_{\mathbf{k}'+\mathbf{q}}(0) - \frac{1}{2}\rho_{\mathbf{k}+\mathbf{q}}(0)\rho_{\mathbf{k}'-\mathbf{q}}(0) \right), \quad (62)$$

where $\Gamma(\mathbf{k}, \mathbf{k}'; \mathbf{k}' - \mathbf{q}, \mathbf{k} + \mathbf{q})$ is the full four-point vertex at the Fermi level, which is a real function of $(\mathbf{k}, \mathbf{k}', \mathbf{q})$. The factor $\frac{1}{2}$ in front of the second term in the curly bracket in eq. (62) is necessary to avoid double counting. Then, $\mathcal{T}_{\mathbf{k},\mathbf{k}'}^{(0)}(0, \epsilon')$ is given by $i[\text{cth}(\epsilon/2T) - \text{th}(\epsilon/2T)]2\text{Im}\Gamma(0, \epsilon' - i\delta)$; it is schematically shown in Fig. 10 (ii).

After changing momentum variables, the Bethe-Salpeter equation (60) is transformed into [42]

$$\begin{aligned} \vec{J}_k &= \vec{v}_k + \Delta \vec{J}_k, \\ \Delta \vec{J}_k &= \sum_{\mathbf{k}'\mathbf{q}} \bar{\mathcal{T}}_{\mathbf{k},\mathbf{k}+\mathbf{q}}^{(0a)} \frac{\rho_{\mathbf{k}+\mathbf{q}}(0)}{2\gamma_{\mathbf{k}+\mathbf{q}}} \vec{J}_{\mathbf{k}+\mathbf{q}} + \sum_{\mathbf{k}'\mathbf{q}} \bar{\mathcal{T}}_{\mathbf{k},\mathbf{k}'-\mathbf{q}}^{(0b)} \frac{\rho_{\mathbf{k}'-\mathbf{q}}(0)}{2\gamma_{\mathbf{k}'-\mathbf{q}}} \vec{J}_{\mathbf{k}'-\mathbf{q}} \\ &\quad + \sum_{\mathbf{k}'\mathbf{q}} \bar{\mathcal{T}}_{\mathbf{k},\mathbf{k}'}^{(0c)} \frac{\rho_{\mathbf{k}'}(0)}{2\gamma_{\mathbf{k}'}} \vec{J}_{\mathbf{k}'}, \end{aligned} \quad (63)$$

$$(64)$$

where we used the relation $\int_{-\infty}^{\infty} d\epsilon [\text{cth}(\epsilon/2T) - \text{th}(\epsilon/2T)]\epsilon = (\pi T)^2$. $\bar{\mathcal{T}}^{(0\alpha)}$ ($\alpha = a, b, c$) are functions of $(\mathbf{k}, \mathbf{k}', \mathbf{q})$, and they represent the forward scattering amplitude [31, 40]. The expressions for $\bar{\mathcal{T}}^{(0\alpha)}$ ($\alpha = a, b, c$) at sufficiently low temperatures are given by [42]

$$\bar{\mathcal{T}}_{\mathbf{k},\mathbf{k}+\mathbf{q}}^{(0a)} = \frac{\pi(\pi T)^2}{2} \frac{1}{2} \Gamma^2(\mathbf{k}, \mathbf{k}'; \mathbf{k}' - \mathbf{q}, \mathbf{k} + \mathbf{q}) \rho_{\mathbf{k}'}(0) \rho_{\mathbf{k}'-\mathbf{q}}(0), \quad (65)$$

$$\bar{\mathcal{T}}_{\mathbf{k},\mathbf{k}'-\mathbf{q}}^{(0b)} = \frac{\pi(\pi T)^2}{2} \frac{1}{2} \Gamma^2(\mathbf{k}, \mathbf{k}'; \mathbf{k}' - \mathbf{q}, \mathbf{k} + \mathbf{q}) \rho_{\mathbf{k}'}(0) \rho_{\mathbf{k}+\mathbf{q}}(0), \quad (66)$$

$$\bar{\mathcal{T}}_{\mathbf{k},\mathbf{k}'}^{(0c)} = -\frac{\pi(\pi T)^2}{2} \frac{1}{2} \Gamma^2(\mathbf{k}, \mathbf{k}'; \mathbf{k}' - \mathbf{q}, \mathbf{k} + \mathbf{q}) \rho_{\mathbf{k}+\mathbf{q}}(0) \rho_{\mathbf{k}'-\mathbf{q}}(0). \quad (67)$$

Since the CVC due to $\bar{\mathcal{T}}^{(0c)}$ represents the hole current, the minus sign appears in eq. (67). In eqs. (65)-(67), we dropped spin indices in Γ to simplify equations: If spin indices are taken into account, $\frac{1}{2}\Gamma^2$ in each equation is replaced with $\frac{1}{2}\Gamma_{\uparrow,\uparrow;\uparrow,\uparrow}^2 + \Gamma_{\uparrow,\downarrow;\downarrow,\uparrow}^2 + \Gamma_{\downarrow,\downarrow;\downarrow,\downarrow}^2$ as explained in Ref. [42]. Equations (65)-(67) are expressed in Fig. 11 (i). Note that

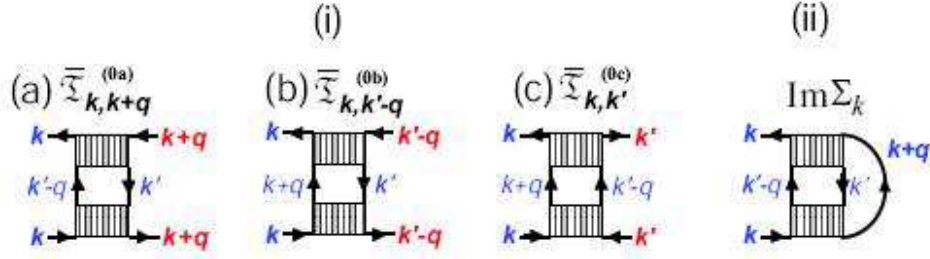


Figure 11. (i) Diagrammatic representation of eqs. (65)-(67). Each hatched part represents the real part of the full antisymmetrized four point vertex $\Gamma(\mathbf{k}, \mathbf{k}'; \mathbf{k} + \mathbf{q}, \mathbf{k}' - \mathbf{q})$. Each line with arrow represents the imaginary part of the Green function. Note that (a) becomes different from (b) if we violate the antisymmetric nature of $\Gamma(\mathbf{k}, \mathbf{k}'; \mathbf{k} + \mathbf{q}, \mathbf{k}' - \mathbf{q})$ in the course of approximation. (ii) Diagrammatic representation of eq. (68).

eqs. (65) and (66) are equivalent since $\Gamma(\mathbf{k}, \mathbf{k}'; \mathbf{k}' - \mathbf{q}, \mathbf{k} + \mathbf{q})$ is full antisymmetrized as a consequence of the Pauli principle.

In the same way, $\text{Im}\Sigma_{\mathbf{k}}(-i\delta) = \gamma_{\mathbf{k}}$ at sufficiently low temperatures can be expressed as [31, 42]

$$\begin{aligned} \gamma_{\mathbf{k}} &= \frac{1}{2} \sum_{\mathbf{k}'} \int \frac{d\epsilon'}{4\pi i} \mathcal{T}_{\mathbf{k}, \mathbf{k}'}^{(0)}(0, \epsilon') \cdot \pi \rho_{\mathbf{k}'}(\epsilon') \\ &= \frac{1}{2} \sum_{\mathbf{k}'\mathbf{q}} \bar{\mathcal{T}}_{\mathbf{k}, \mathbf{k}+\mathbf{q}}^{(0a)} \rho_{\mathbf{k}+\mathbf{q}}(0), \end{aligned} \quad (68)$$

which is proportional to T^2 at the zero-temperature limit, if the dimension is slightly higher than two. [In pure 2D systems, $\gamma_{\mathbf{k}} \propto -T^2 \ln T$.] Equation (68) is shown in Fig. 11 (ii). We note that $\gamma_{\mathbf{k}}$ is also given by $\gamma_{\mathbf{k}} = \frac{1}{2} \sum_{\mathbf{k}'\mathbf{q}} \bar{\mathcal{T}}_{\mathbf{k}, \mathbf{k}'-\mathbf{q}}^{(0b)} \rho_{\mathbf{k}'-\mathbf{q}}(0) = -\frac{1}{2} \sum_{\mathbf{k}'\mathbf{q}} \bar{\mathcal{T}}_{\mathbf{k}, \mathbf{k}'}^{(0c)} \rho_{\mathbf{k}'}(0)$.

Here, we calculate the CVC in a free dispersion model in the absence of Umklapp scattering according to Yamada and Yosida [42]. In this case, both $\gamma_{\mathbf{k}}$ and $\vec{J}_{\mathbf{k}}$ on the Fermi surface are isotropic, that is, $\gamma_{\mathbf{k}} = \gamma_{k_F}$ and $\vec{J}_{\mathbf{k}} = J \cdot \mathbf{k}/k_F$. By noticing the relationship $\vec{J}_{\mathbf{k}+\mathbf{q}} + \vec{J}_{\mathbf{k}'-\mathbf{q}} - \vec{J}_{\mathbf{k}'} = \vec{J}_{\mathbf{k}}$ and using eqs. (65)-(68), it is easy to verify that the CVC in eq. (64) is exactly given by

$$\Delta \vec{J}_{\mathbf{k}} = \vec{J}_{\mathbf{k}}, \quad (69)$$

in a free dispersion model. If we put $\Delta \vec{J}_{\mathbf{k}} = c \vec{J}_{\mathbf{k}}$ (c is a constant), the solution of eq. (63) is given by $\vec{J}_{\mathbf{k}} = \vec{v}_{\mathbf{k}}/(1-c)$, which diverges when $c \rightarrow 1$. Therefore, the conductivity given by eq. (58) diverges, which is a natural consequence of the momentum conservation of the system [42]. Yamada and Yosida also showed that $\vec{J}_{\mathbf{k}}$ remains finite in the presence of the Umklapp processes [42].

Next, we discuss the case where $\epsilon_{\mathbf{k}}^0$ is anisotropic. Then, the formal solution of eq. (60) is given by

$$\vec{J}_{\mathbf{k}} = \sum_{\mathbf{k}'} (\hat{1} - \hat{C})_{\mathbf{k}, \mathbf{k}'}^{-1} \vec{v}_{\mathbf{k}'}, \quad (70)$$

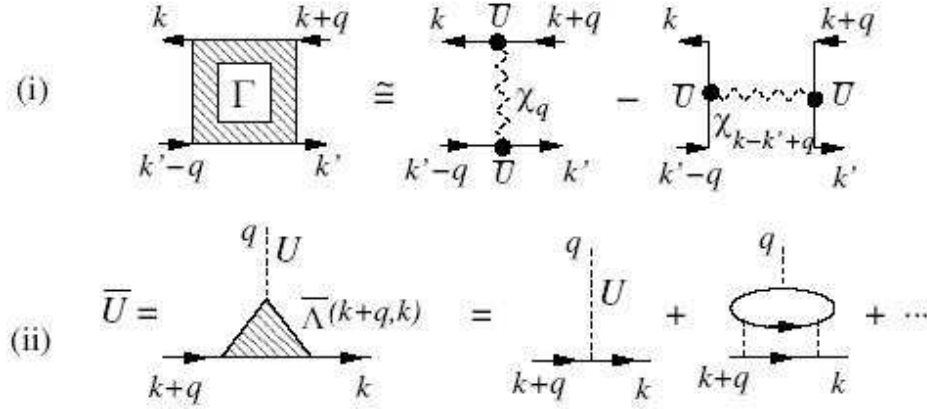


Figure 12. (i) Diagrammatic representation of eq. (71). The wavy lines represent the spin fluctuations, $\chi_{\mathbf{q}}^s(0)$. (ii) Diagrammatic representation of \bar{U} in eq. (71). U is the bare Coulomb interaction in the Hubbard model and $\bar{\Lambda}(\mathbf{k}+\mathbf{q}, \mathbf{q})$ is the three-point vertex that is irreducible with respect to U .

where $C_{\mathbf{k}, \mathbf{k}'} = \int \frac{d\epsilon'}{4\pi i} \mathcal{T}_{\mathbf{k}, \mathbf{k}'}^{(0)}(0, \epsilon') \cdot \rho_{\mathbf{k}'}(0) / 2\gamma_{\mathbf{k}'}$. When $\epsilon_{\mathbf{k}}^0$ is anisotropic, quasiparticle current is not conserved in the normal scattering process; $\mathbf{v}_{\mathbf{k}} + \mathbf{v}_{\mathbf{k}'} \neq \mathbf{v}_{\mathbf{k}+\mathbf{q}} + \mathbf{v}_{\mathbf{k}'-\mathbf{q}}$. Nonetheless of the fact, one can show that $\det\{\hat{1} - \hat{C}\} = 0$ as a result of the momentum conservation [46, 155]. Therefore, $\vec{J}_{\mathbf{k}}$ given in eq. (70) and σ_{xx} diverge in any anisotropic model if the Umklapp processes are absent. [Exactly speaking, $\rho_{xx} = 1/\sigma_{xx}$ is proportional to T^{2N-2} when the N -particle Umklapp scattering processes are present [155].]

We stress that the FLEX approximation can reproduce the divergence of the conductivity in the absence of the Umklapp scatterings, if one consider the CVC correctly. This result is assured by the fact that the Ward identity $\Gamma^I = \delta\Sigma/\delta G$ is consistently satisfied in the FLEX approximation [139, 140]. Therefore, the FLEX approximation will be appropriate for the study of transport phenomena in correlated electron systems.

Next, we consider the role of the CVC in nearly AF Fermi liquids in the presence of Umklapp scatterings, where the electron-electron scatterings are mainly given by the strong AF fluctuations with $\mathbf{q} \sim \mathbf{Q}$. In this case, we can approximate the full four-point vertex in eqs. (65)-(67) as

$$\Gamma_{s_1, s_2; s_3, s_4}(\mathbf{k}, \mathbf{k}'; \mathbf{k}' - \mathbf{q}, \mathbf{k} + \mathbf{q}) \approx \frac{\bar{U}^2}{2} \left\{ \chi_{\mathbf{q}}^s(0) \vec{\sigma}_{s_1, s_4} \cdot \vec{\sigma}_{s_2, s_3} - \chi_{\mathbf{k}-\mathbf{k}'+\mathbf{q}}^s(0) \vec{\sigma}_{s_1, s_3} \cdot \vec{\sigma}_{s_2, s_4} \right\}, \quad (71)$$

which satisfies the antisymmetric nature of Γ that is the consequence of the Pauli principle. The diagrammatic representation of eq. (71) is shown in Fig. 12 (i). Here, s_i ($i = 1 \sim 4$) represents the spin index and $\vec{\sigma}$ is the Pauli matrix vector. \bar{U} in eq. (71) is the effective interaction between the electrons and spin fluctuations, which is the renormalized Coulomb interaction due to the irreducible three-point vertex shown in Fig. 12 (ii).

In the present subsection, however, we analyze the CVC using the following more

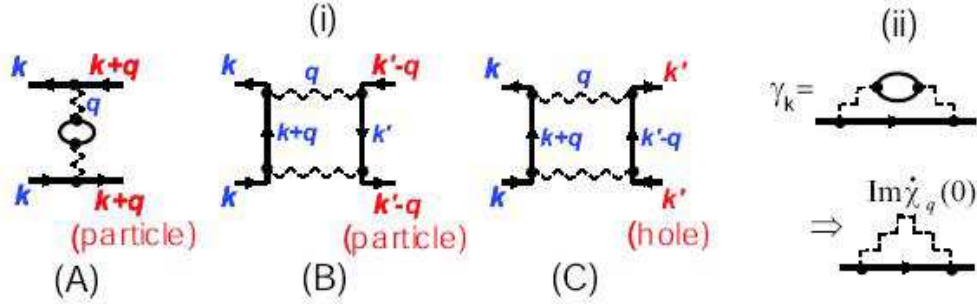


Figure 13. (i) According to the approximation in eq. (72), $\bar{T}_{\mathbf{k},\mathbf{k}+\mathbf{q}}^{(0a)}$, $\bar{T}_{\mathbf{k},\mathbf{k}'-\mathbf{q}}^{(0b)}$, and $\bar{T}_{\mathbf{k},\mathbf{k}'}^{(0c)}$ in eqs. (65)-(67) are approximated as (A)-(C), respectively. (A) corresponds to the Maki-Thompson term in the FLEX approximation, which represents the CVC (MT) in Fig. 8. (B) and (C) correspond to the Aslamazov-Larkin terms, which represent the (AL1) and (AL2) in Fig. 8. (ii) The expression for $\gamma_{\mathbf{k}}$ according to the approximation in eq. (72).

simplified approximation for Γ :

$$\Gamma_{s_1, s_2; s_3, s_4}(\mathbf{k}, \mathbf{k}'; \mathbf{k}' - \mathbf{q}, \mathbf{k} + \mathbf{q}) \approx \frac{\bar{U}^2}{2} \chi_{\mathbf{q}}^s(0) \vec{\sigma}_{s_1, s_4} \cdot \vec{\sigma}_{s_2, s_3}. \quad (72)$$

Although eq. (72) violates the Pauli principle, this approximation produces the dominant CVC (Maki-Thompson term) near AF-QCP. In §3.4, we will analyze the CVC using eq. (71), and show that the analysis based on eq. (72) is justified. According to the present approximation, $\bar{T}^{(0\alpha)}$ ($\alpha = a, b, c$) in eqs. (65)-(67) are expressed by (A)-(C) in Fig. 13 (i), respectively, where wavy lines represent the spin fluctuations. The CVCs expressed in (A) and (B) correspond to the current due to the quasiparticles at $\mathbf{k} + \mathbf{q}$ and $\mathbf{k}' - \mathbf{q}$, respectively, and the CVC in (C) corresponds to the current due to the quasi-hole at \mathbf{k}' in Fig. 8. In the field theory, (A) is called the Maki-Thompson term, and (B) and (C) are called the Aslamazov-Larkin terms. As explained in Fig. 8, the Aslamazov-Larkin terms approximately disappears [33] whereas the Maki-Thompson term plays an important role when $\xi_{\text{AF}} \gg 1$ and $\mathbf{Q} \approx (\pi, \pi)$.

According to eq. (72), $\frac{1}{2}\Gamma^2$ in $\bar{T}^{(0a)}$ becomes $(3U^4/4)[\chi_{\mathbf{q}}^s(0)]^2$ after taking the summation of spin indices. However, we replace $\frac{1}{2}\Gamma^2$ with $(3U^4/2)[\chi_{\mathbf{q}}^s(0)]^2$ since the term (A) in Fig. 13 appears twice if we use eq. (71). Then, the CVC in eq. (64) and $\gamma_{\mathbf{k}}$ given in eq. (68) near the AF QCP are obtained as

$$\Delta \vec{J}_{\mathbf{k}} = \sum_{\mathbf{q}} (\pi T)^2 \frac{3\bar{U}^4}{2} [\chi_{\mathbf{q}}^s(0)]^2 \text{Im} \dot{\chi}_{\mathbf{q}}^0(0) \frac{\rho_{\mathbf{k}+\mathbf{q}}(0)}{\gamma_{\mathbf{k}+\mathbf{q}}} \vec{J}_{\mathbf{k}+\mathbf{q}}, \quad (73)$$

$$\gamma_{\mathbf{k}} = \sum_{\mathbf{q}} (\pi T)^2 \frac{3\bar{U}^4}{2} [\chi_{\mathbf{q}}^s(0)]^2 \text{Im} \dot{\chi}_{\mathbf{q}}^0(0) \rho_{\mathbf{k}+\mathbf{q}}(0), \quad (74)$$

where we used the relation $\text{Im} \dot{\chi}_{\mathbf{q}}^0(0) = (\pi/2) \sum_{\mathbf{k}} \rho_{\mathbf{k}}(0) \rho_{\mathbf{k}+\mathbf{q}}(0)$. Since $\text{Im} \dot{\chi}_{\mathbf{q}}^s(0) = \text{Im} \dot{\chi}_{\mathbf{q}}^0(0) [\bar{U} \chi_{\mathbf{q}}^s(0)]^2$, the Bethe-Salpeter equation (73) and $\gamma_{\mathbf{k}}$ in eq. (74) in a nearly

AF Fermi liquid are given by

$$\vec{J}_{\mathbf{k}} = \vec{v}_{\mathbf{k}} + \sum_{\mathbf{q}} \frac{3\bar{U}^2}{4} (\pi T)^2 \text{Im} \dot{\chi}_{\mathbf{q}}^s(0) \frac{\rho_{\mathbf{k}+\mathbf{q}}(0)}{\gamma_{\mathbf{k}+\mathbf{q}}} \vec{J}_{\mathbf{k}+\mathbf{q}}. \quad (75)$$

$$\gamma_{\mathbf{k}} = \sum_{\mathbf{q}} \frac{3\bar{U}^2}{4} (\pi T)^2 \text{Im} \dot{\chi}_{\mathbf{q}}^s(0) \rho_{\mathbf{k}+\mathbf{q}}(0). \quad (76)$$

Note that eq. (76) is equivalent to $\gamma_{\mathbf{k}}$ in the spin fluctuation theory in eq. (30).

In this subsection, we have neglected the energy-dependence of the four-point vertices [in eqs. (65)-(67)] and that of the spin susceptibilities [in eqs. (73)-(76)] to simplify the discussion. For this reason, eqs. (75) and (76) are appropriate only for $\omega_{\text{sf}} \gtrsim T$ where ω -dependence of $\chi_{\mathbf{q}}^s(\omega)$ can be ignored. In the case of $\omega_{\text{sf}} \ll T$, $(\pi T)^2$ in eqs. (75) and (76) should be replaced with $\int_{-\omega_{\text{sf}}}^{\omega_{\text{sf}}} [\text{cth}(\epsilon/2T) - \text{th}(\epsilon/2T)] \epsilon d\epsilon = 4T\omega_{\text{sf}}$. For any value of ω_{sf}/T , they are expressed by eqs. (36) and (33) in Ref. [33], respectively.

Here, we approximately solve eq. (75) in the case of $\xi_{\text{AF}} \gg 1$ and $\xi_{\text{AF}} \Delta k_c \sim O(1)$. Here, we assume \mathbf{k} is close to point A in Fig. 4 (i). Because $\chi_{\mathbf{q}}^s(0)$ takes a large value only when $|\mathbf{q} - \mathbf{Q}| \lesssim \xi_{\text{AF}}^{-1}$, the CVC term in eq. (75) can be expressed as $\Delta \vec{J}_{\mathbf{k}} \approx (\vec{J}_{\mathbf{k}^*}/\gamma_{\mathbf{k}^*}) \sum_{\mathbf{q}} (3\bar{U}^2/4) (\pi T)^2 \text{Im} \dot{\chi}_{\mathbf{q}}^s(0)$, where $(k_x^*, k_y^*) = (-k_y, -k_x)$ for $k_x k_y > 0$, and $(k_x^*, k_y^*) = (k_y, k_x)$ for $k_x k_y < 0$ as shown in Fig. 4 (i). Considering eq. (76), $\Delta \vec{J}_{\mathbf{k}} \approx \vec{J}_{\mathbf{k}^*}$ in the case of $\xi_{\text{AF}} \gg 1$. The more detailed expression for the CVC term $\Delta \vec{J}_{\mathbf{k}}$ is given by [33]

$$\begin{aligned} \Delta \vec{J}_{\mathbf{k}} &\approx \langle \vec{J}_{\mathbf{k}'} \rangle_{|\mathbf{k}' - \mathbf{k}^*| < 1/\xi_{\text{AF}}} \\ &\approx \vec{J}_{\mathbf{k}^*} \cdot \langle \cos(\theta_{\mathbf{k}'}^J - \theta_{\mathbf{k}^*}^J) \rangle_{|\mathbf{k}' - \mathbf{k}^*| < 1/\xi_{\text{AF}}} \approx \alpha_{\mathbf{k}} \vec{J}_{\mathbf{k}^*}, \end{aligned} \quad (77)$$

where $\alpha_{\mathbf{k}} \approx (1 - c/\xi_{\text{AF}}^2) < 1$ and $c \sim O(1)$ is a constant. The \mathbf{k} -dependence of $\alpha_{\mathbf{k}}$ will be moderate if $\xi_{\text{AF}} \Delta k_c \gtrsim 1$. By this simplification, eq. (75) becomes

$$\vec{J}_{\mathbf{k}} = \vec{v}_{\mathbf{k}} + \alpha_{\mathbf{k}} \vec{J}_{\mathbf{k}^*}, \quad (78)$$

and the solution is given by [33]

$$\vec{J}_{\mathbf{k}} = \frac{1}{1 - \alpha_{\mathbf{k}}^2} (\vec{v}_{\mathbf{k}} + \alpha_{\mathbf{k}} \vec{v}_{\mathbf{k}^*}). \quad (79)$$

Here, we examine the \mathbf{k} -dependence of $\vec{J}_{\mathbf{k}}$ given in eq. (79): (a) near points A and B, $\vec{J}_{\mathbf{k}}$ is parallel to $\vec{v}_{\mathbf{k}}$ by symmetry. At point A, $\vec{J}_{\mathbf{k}} = \vec{v}_{\mathbf{k}}/(1 + \alpha_{\mathbf{k}}) \sim \frac{1}{2}\vec{v}_{\mathbf{k}}$ since $\vec{v}_{\mathbf{k}} = -\vec{v}_{\mathbf{k}^*}$. (b) Near point C, $\vec{J}_{\mathbf{k}} \approx (\xi_{\text{AF}}^2/2c)(\vec{v}_{\mathbf{k}} + \vec{v}_{\mathbf{k}^*})$, which is nearly parallel to the AFBZ. These behaviors of $\vec{J}_{\mathbf{k}}$ together with $\vec{v}_{\mathbf{k}}$ are schematically shown in Fig. 14 (i). In the present discussion, we assumed that $\xi_{\text{AF}} \Delta k_c \sim O(1)$, where Δk_c represents the deviation from the nesting condition at the cold spot in Fig. 4 (i). This condition seems to be satisfied in slightly under-doped YBCO and LSCO above T_c , as discussed in §2.3. In Fig. 4 (ii), we show an “effective Fermi surface” obtained by bending the true Fermi surface such that it is orthogonal to $\vec{J}_{\mathbf{k}}$ around the cold spot [20]. we discuss the role of the CVC in the Hall coefficient based on the concept of the effective Fermi surface in §4.2.

When $\xi_{\text{AF}} \Delta k_c \gg 1$, one may think that the CVC is small around the cold spot, and therefore the increment in R_{H} due to the CVC is also small. However, this expectation

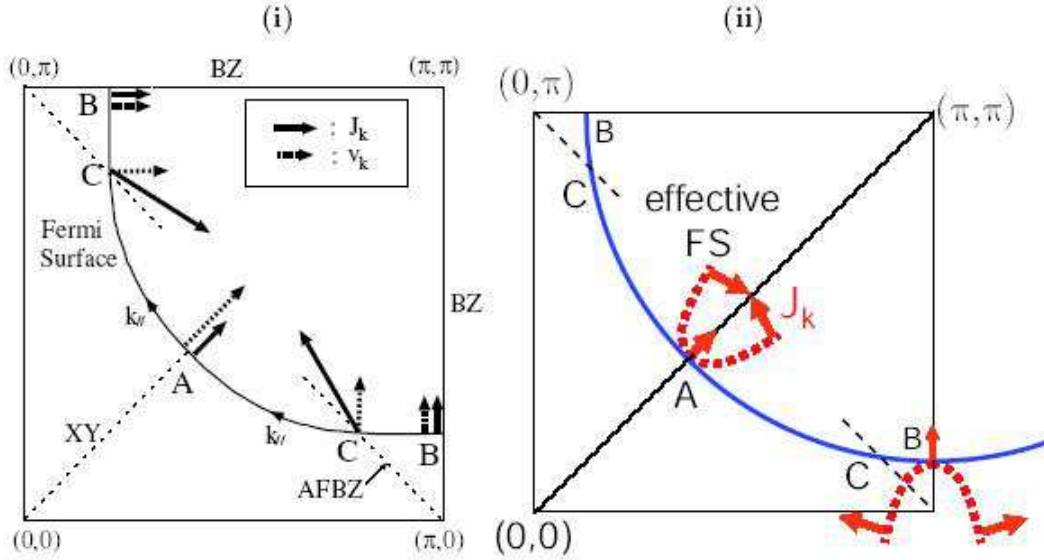


Figure 14. (i) Schematic behavior of the total current \vec{J}_k and the quasiparticle velocity \vec{v}_k on the Fermi surface. The cold spot is located around the point A (B) in hole-doped (electron-doped) HTSCs. (ii) Effective Fermi surface for σ_{xy} . The large curvature of the effective Fermi surface around the cold spot is the origin of the enhancement (and the sign-change) of R_H .

is not true unless $\chi_q^s(\omega)$ is a step function like $\theta(1 - |\mathbf{Q} - \mathbf{q}|\xi_{AF})$. In fact, we verified that the CVC around the cold spot is significant even if $\xi_{AF}\Delta k_c$ is much larger than unity, by assuming a phenomenological $\chi_q^s(\omega)$ model given in eq. (8) [34]. In later sections, we demonstrate that R_H is prominently enhanced by the CVC using the FLEX approximation, which yields a realistic functional form of $\chi_q^s(\omega)$. We will show that the CVC is important in NCCO, although $\xi_{AF}\Delta k_c \gg 1$ is realized at low temperatures.

Finally, we comment that the Aslamazov-Larkin terms ((B) and (C) in Fig. 13) become important when the AF fluctuations are weak. In the FLEX approximation, one can reproduce the divergence of the conductivity in the absence of the Umklapp scatterings, only if all the CVCs ((A)-(C) in Fig. 13) are taken into consideration.

3.4. CVC beyond one loop approximation

In the previous subsection, we analyzed the CVC by assuming eq. (72), which corresponds to the one-loop approximation for the self-energy like the FLEX approximation. In this approximation, eq. (73) and eq. (74) contain the same Kernel function $[\chi_q^s(0)]^2 \text{Im}\dot{\chi}_q^s(0)\rho_{\mathbf{k}+\mathbf{q}}(0)$ as a consequence of the Ward identity between the CVC and the imaginary part of the self-energy. For this reason, the factor α_k in eq. (79) approaches unity near AF-QCP, which assures the anomalous \mathbf{k} -dependence of \vec{J}_k near AF-QCP that shown in Fig. 14. However, one may be afraid that this result is an artifact due to the violation of the Pauli principle. In this subsection, we analyze the self-energy and the CVC beyond the one-loop approximation by assuming eq. (71).

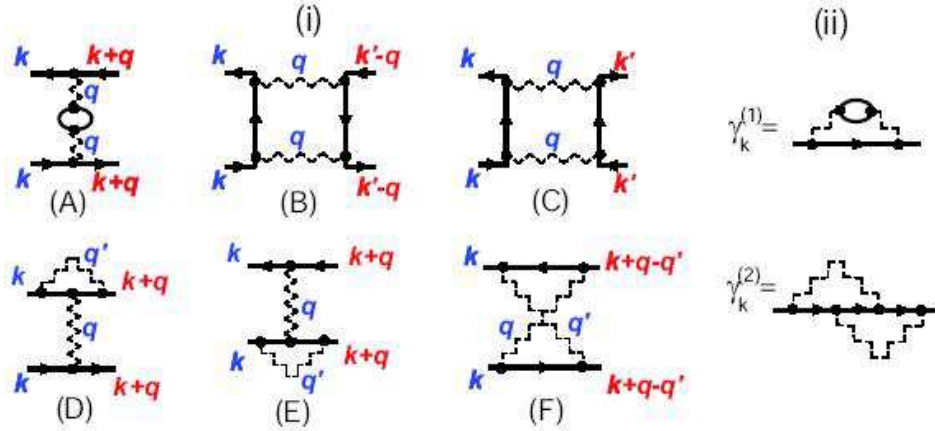


Figure 15. (i) According to the approximation in eq. (71), $\bar{\mathcal{T}}_{\mathbf{k},\mathbf{k}+\mathbf{q}}^{(0a)}$, $\bar{\mathcal{T}}_{\mathbf{k},\mathbf{k}'-\mathbf{q}}^{(0b)}$, and $\bar{\mathcal{T}}_{\mathbf{k},\mathbf{k}'}^{(0c)}$ in eqs. (65)-(67) are approximated as (A)-(F), respectively. (A), (B), (D), and (E) come from $\bar{\mathcal{T}}^{(0a)}$ and $\bar{\mathcal{T}}^{(0b)}$. (C) and (F) come from $\bar{\mathcal{T}}^{(0c)}$. (ii) The expression for $\gamma_{\mathbf{k}}$ according to the approximation in eq. (71).

Here, we confirm that the CVC near the AF QCP is important even if the higher-loop diagrams are taken into account.

According to eq. (71), $\gamma_{\mathbf{k}}$ in eq. (68) is approximately given by

$$\gamma_{\mathbf{k}} = \gamma_{\mathbf{k}}^{(1)} + \gamma_{\mathbf{k}}^{(2)}, \quad (80)$$

$$\gamma_{\mathbf{k}}^{(1)} = \text{eq. (74)},$$

$$\gamma_{\mathbf{k}}^{(2)} = - \sum_{\mathbf{q},\mathbf{q}'} \frac{\pi(\pi T)^2}{2} \frac{5\bar{U}^4}{8} \chi_{\mathbf{q}}^s(0) \chi_{\mathbf{q}'}^s(0) \rho_{\mathbf{k}+\mathbf{q}}(0) \rho_{\mathbf{k}-\mathbf{q}'}(0) \rho_{\mathbf{k}+\mathbf{q}-\mathbf{q}'}(0), \quad (81)$$

where $\gamma_{\mathbf{k}}^{(1)} (> 0)$ and $\gamma_{\mathbf{k}}^{(2)} (< 0)$ are shown in Fig. 15 (ii). The integrand in eq. (81) takes a large value when $|\mathbf{q} - \mathbf{Q}|, |\mathbf{q}' - \mathbf{Q}| \lesssim \xi_{\text{AF}}^{-1}$, under the condition that $\epsilon_{\mathbf{k}+\mathbf{q}} = \epsilon_{\mathbf{k}-\mathbf{q}'} = \epsilon_{\mathbf{k}+\mathbf{q}-\mathbf{q}'} = \mu$. When $\mathbf{Q} = (\pi, \pi)$, $\gamma_{\mathbf{k}}^{(2)}$ can be significant at the hot spot since $\mathbf{k} + \mathbf{q} \approx \mathbf{k} - \mathbf{q}' \approx \mathbf{k}^*$ and $\mathbf{k} + \mathbf{q} - \mathbf{q}' \approx \mathbf{k}$ in modulo $(2\pi, 2\pi)$.

In the same way, the CVC in eq. (64) is given by the six diagrams shown in Fig. 15. As discussed in §3.3, terms (B) and (C) are negligible in nearly AF Fermi liquids. Other terms are given by

$$(A) = \text{eq. (73)},$$

$$(D, E) = - \sum_{\mathbf{q},\mathbf{q}'} \frac{\pi(\pi T)^2}{2} \frac{5\bar{U}^4}{8} \chi_{\mathbf{q}}^s(0) \chi_{\mathbf{q}'}^s(0) \rho_{\mathbf{k}-\mathbf{q}'}(0) \rho_{\mathbf{k}+\mathbf{q}-\mathbf{q}'}(0) \times \frac{\rho_{\mathbf{k}+\mathbf{q}}(0)}{\gamma_{\mathbf{k}+\mathbf{q}}} \vec{J}_{\mathbf{k}+\mathbf{q}}, \quad (82)$$

$$(F) = \sum_{\mathbf{q},\mathbf{q}'} \frac{\pi(\pi T)^2}{2} \frac{5\bar{U}^4}{8} \chi_{\mathbf{q}}^s(0) \chi_{\mathbf{q}'}^s(0) \rho_{\mathbf{k}-\mathbf{q}'}(0) \rho_{\mathbf{k}+\mathbf{q}}(0) \times \frac{\rho_{\mathbf{k}+\mathbf{q}-\mathbf{q}'}(0)}{\gamma_{\mathbf{k}+\mathbf{q}-\mathbf{q}'}} \vec{J}_{\mathbf{k}+\mathbf{q}-\mathbf{q}'}. \quad (83)$$

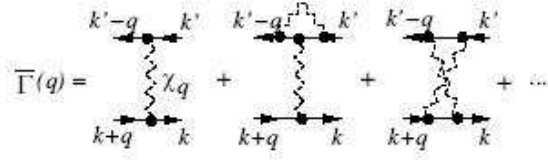


Figure 16. Diagrammatic representation of $\bar{\Gamma}(q)$ in eq. (87).

Here, $\chi_{\mathbf{q}}^s(0)\chi_{\mathbf{q}'}^s(0)$ takes a large value only when $|\mathbf{q} - \mathbf{Q}|, |\mathbf{q}' - \mathbf{Q}| \lesssim \xi_{\text{AF}}^{-1}$. In (D)-(F), the set of momenta $(\mathbf{k}, \mathbf{k}', \mathbf{q})$ is changed to $(\mathbf{k}, \mathbf{q}, \mathbf{q}')$ due to the transformation of variables. Applying the same approximation that was used in eq. (77), the total CVC is given by

$$\Delta \vec{J}_{\mathbf{k}} = \alpha_{\mathbf{k}} \frac{\gamma_{\mathbf{k}}^{(1)}}{\gamma_{\mathbf{k}}} \vec{J}_{\mathbf{k}^*} + 2\alpha'_{\mathbf{k}} \frac{\gamma_{\mathbf{k}}^{(2)}}{\gamma_{\mathbf{k}}} \vec{J}_{\mathbf{k}^*} - \alpha''_{\mathbf{k}} \frac{\gamma_{\mathbf{k}}^{(2)}}{\gamma_{\mathbf{k}}} \vec{J}_{\mathbf{k}}, \quad (84)$$

where $(1 - \alpha_{\mathbf{k}})$, $(1 - \alpha'_{\mathbf{k}})$ and $(1 - \alpha''_{\mathbf{k}})$ are positive, and they approach zero in proportion to ξ_{AF}^{-2} near the AF-QCP. Then, the solution of the Bethe-Salpeter equation $\vec{J}_{\mathbf{k}} = \vec{v}_{\mathbf{k}} + \Delta \vec{J}_{\mathbf{k}}$ is given by

$$\begin{aligned} \vec{J}_{\mathbf{k}} &= \frac{\gamma_{\mathbf{k}}(\gamma_{\mathbf{k}} + \alpha''_{\mathbf{k}}\gamma_{\mathbf{k}}^{(2)})}{[\gamma_{\mathbf{k}} - \alpha_{\mathbf{k}}\gamma_{\mathbf{k}}^{(1)} - (2\alpha'_{\mathbf{k}} - \alpha''_{\mathbf{k}})\gamma_{\mathbf{k}}^{(2)}][\gamma_{\mathbf{k}} + \alpha_{\mathbf{k}}\gamma_{\mathbf{k}}^{(1)} + (2\alpha'_{\mathbf{k}} + \alpha''_{\mathbf{k}})\gamma_{\mathbf{k}}^{(2)}]} \\ &\times \left\{ \vec{v}_{\mathbf{k}} + \frac{\alpha_{\mathbf{k}}\gamma_{\mathbf{k}}^{(1)} + 2\alpha'_{\mathbf{k}}\gamma_{\mathbf{k}}^{(2)}}{\gamma_{\mathbf{k}} + \alpha''_{\mathbf{k}}\gamma_{\mathbf{k}}^{(2)}} \vec{v}_{\mathbf{k}^*} \right\}. \end{aligned} \quad (85)$$

When $\xi_{\text{AF}} \gg 1$, eq. (85) is approximately given by

$$\vec{J}_{\mathbf{k}} = \frac{\gamma_{\mathbf{k}}}{2[\gamma_{\mathbf{k}} - \alpha_{\mathbf{k}}\gamma_{\mathbf{k}}^{(1)} - (2\alpha'_{\mathbf{k}} - \alpha''_{\mathbf{k}})\gamma_{\mathbf{k}}^{(2)}]} \{ \vec{v}_{\mathbf{k}} + \vec{v}_{\mathbf{k}^*} \}. \quad (86)$$

Near the AF-QCP, $\gamma_{\mathbf{k}} - \alpha_{\mathbf{k}}\gamma_{\mathbf{k}}^{(1)} - (2\alpha'_{\mathbf{k}} - \alpha''_{\mathbf{k}})\gamma_{\mathbf{k}}^{(2)} \propto \gamma_{\mathbf{k}}\xi_{\text{AF}}^{-2}$ since $\gamma_{\mathbf{k}} = \gamma_{\mathbf{k}}^{(1)} + \gamma_{\mathbf{k}}^{(2)}$. Therefore, $\vec{J}_{\mathbf{k}}$ in eq.(86) shows a similar behavior to that given in eq. (79). As a result, the significance of the CVC in nearly AF Fermi liquid is confirmed even if we assume eq. (71), which satisfy the Pauli principle.

Finally, we discuss the CVC composed of the higher loop terms with respect to $\chi_{\mathbf{q}}^s(0)$, by considering the following approximation for the full four-point vertex:

$$\begin{aligned} \Gamma_{s_1, s_2; s_3, s_4}(\mathbf{k}, \mathbf{k}'; \mathbf{k}' - \mathbf{q}, \mathbf{k} + \mathbf{q}) &\approx \bar{\Gamma}(\mathbf{q}) \vec{\sigma}_{s_1, s_4} \cdot \vec{\sigma}_{s_2, s_3} \\ &\quad - \bar{\Gamma}(\mathbf{k} - \mathbf{k}' + \mathbf{q}) \vec{\sigma}_{s_1, s_3} \cdot \vec{\sigma}_{s_2, s_4}, \end{aligned} \quad (87)$$

by considering that Γ mainly depends on the momentum transfer in the electron-electron scattering. $\bar{\Gamma}(\mathbf{q})$ is given by Fig. 16. Using the full four-point vertex, the spin susceptibility is given by $\chi_{\mathbf{q}}^s(0) = \chi_{\mathbf{q}}^0(0) + T^2 \sum_{\mathbf{k}, \mathbf{k}', \epsilon, \epsilon'} G_{\mathbf{k}}(\epsilon) G_{\mathbf{k}+\mathbf{q}}(\epsilon) \bar{\Gamma}(\mathbf{k}, \mathbf{k}'; \mathbf{k}' - \mathbf{q}, \mathbf{k} + \mathbf{q}) G_{\mathbf{k}'}(\epsilon') G_{\mathbf{k}'-\mathbf{q}}(\epsilon')$, where $\chi_{\mathbf{q}}^0(0) = -T \sum_{\mathbf{k}, \epsilon} G_{\mathbf{k}}(\epsilon) G_{\mathbf{k}+\mathbf{q}}(\epsilon)$. According to the approximation in eq. (87), $\chi_{\mathbf{q}}^s(0)$ is given by

$$\begin{aligned} &\chi_{\mathbf{q}}^0(0) + 2[\chi_{\mathbf{q}}^0(0)]^2 \bar{\Gamma}(\mathbf{q}) \\ &- 2T^2 \sum_{\mathbf{k}, \mathbf{k}', \epsilon, \epsilon'} G_{\mathbf{k}}(\epsilon) G_{\mathbf{k}+\mathbf{q}}(\epsilon) \bar{\Gamma}(\mathbf{k} - \mathbf{k}') G_{\mathbf{k}'+\mathbf{q}}(\epsilon') G_{\mathbf{k}'}(\epsilon'). \end{aligned} \quad (88)$$

The third term of eq. (88) is expected to be smaller than the second term since the integrand takes large values only when $\mathbf{k} - \mathbf{k}' \sim \mathbf{Q}$. Since the \mathbf{q} -dependence of $\chi_{\mathbf{q}}^0(0)$ is moderate, the present analysis suggests that the approximate relation $\chi_{\mathbf{q}}^s(0) \propto \bar{\Gamma}(\mathbf{q})$ holds for $\mathbf{q} \sim \mathbf{Q}$. For this reason, the solution of $\vec{J}_{\mathbf{k}}$ obtained in this subsection, eq. (85) or (86), will be valid even in higher-loop approximations.

As a result, the anomalous \mathbf{k} -dependence of $\vec{J}_{\mathbf{k}}$ in Fig. 14, which is derived in the previous section within the one-loop approximation, is expected to be realized even in the close vicinity of the AF QCP where the higher-loop diagrams becomes important. In later sections, we present a numerical study of the transport phenomena based on the FLEX+CVC approximation. Although it is a one-loop approximation with respect to the spin fluctuation, the obtained numerical results will be qualitatively reliable even in the under-doped region, since the CVC due to the higher-loop diagrams do not alter the one-loop approximation results qualitatively.

4. Transport phenomena in HTSCs above T^*

4.1. Total current $\vec{J}_{\mathbf{k}}$

Here, we discuss the transport phenomena in HTSCs above the pseudo-gap temperature T^* where the SC fluctuations are negligibly small. In the FLEX+CVC approximation, the self-energy is given by eq. (14), and the vertex function in the Bethe-Salpeter equation, $\mathcal{T}_{\mathbf{k},\mathbf{k}'}^{(0)}$, is given by eq. (61). The total current $\vec{J}_{\mathbf{k}}$ is obtained by solving the Bethe-Salpeter equation [33]. According to the Ward identity, the irreducible four-point vertex is given by $\Gamma^I = \delta\Sigma/\delta G$. In the FLEX approximation, the self-energy is given by the convolution of G and V as in eq. (14). Then, Γ^I contains one Maki-Thompson term that is given by taking derivative of G , and two Aslamazov-Larkin terms that are given by taking derivative of V , which is composed of infinite G 's. These three terms corresponds to (A)-(C) in Fig. 13 [33, 57].

Considering the relation $\delta\chi_{\mathbf{q}}^0/\delta G_{\mathbf{k}'} = -(G_{\mathbf{k}'+\mathbf{q}} + G_{\mathbf{k}'-\mathbf{q}})$, we can derive $\Gamma_{\mathbf{k},\mathbf{k}'}^I = \delta\Sigma_{\mathbf{k}}/\delta G_{\mathbf{k}'}$ in the FLEX approximation as

$$\begin{aligned} \Gamma_{\mathbf{k},\mathbf{k}'}^I(\epsilon_n, \epsilon_{n'}) &= V_{\mathbf{k}-\mathbf{k}'}(\epsilon_n - \epsilon_{n'}) \\ &\quad - T \sum_{\mathbf{q},l} U^2 \left[\frac{3}{2}(U\chi_{\mathbf{q}}^s(\omega_l) + 1)^2 + \frac{1}{2}(U\chi_{\mathbf{q}}^c(\omega_l) - 1)^2 - 1 \right] \\ &\quad \times G_{\mathbf{k}'-\mathbf{q}}(\epsilon_{n'} - \omega_l) G_{\mathbf{k}-\mathbf{q}}(\epsilon_n - \omega_l) \\ &\quad - T \sum_{\mathbf{q},l} U^2 \left[\frac{3}{2}(U\chi_{\mathbf{q}}^s(\omega_l) + 1)^2 + \frac{1}{2}(U\chi_{\mathbf{q}}^c(\omega_l) - 1)^2 - 1 \right] \\ &\quad \times G_{\mathbf{k}'+\mathbf{q}}(\epsilon_{n'} + \omega_l) G_{\mathbf{k}-\mathbf{q}}(\epsilon_n - \omega_l). \end{aligned} \quad (89)$$

The first term $V_{\mathbf{q}}(\omega_l)$ corresponds to the Maki-Thompson vertex correction. The last two terms in eq. (89), both of which contain $[\chi_{\mathbf{q}}^s]^2$, are the Aslamazov-Larkin vertex corrections. Hereafter, we drop the Aslamazov-Larkin terms since they are negligible in nearly AF Fermi liquids ($\chi_Q^s \gg \chi_Q^c, \chi_Q^0$), as we have discussed in previous sections.

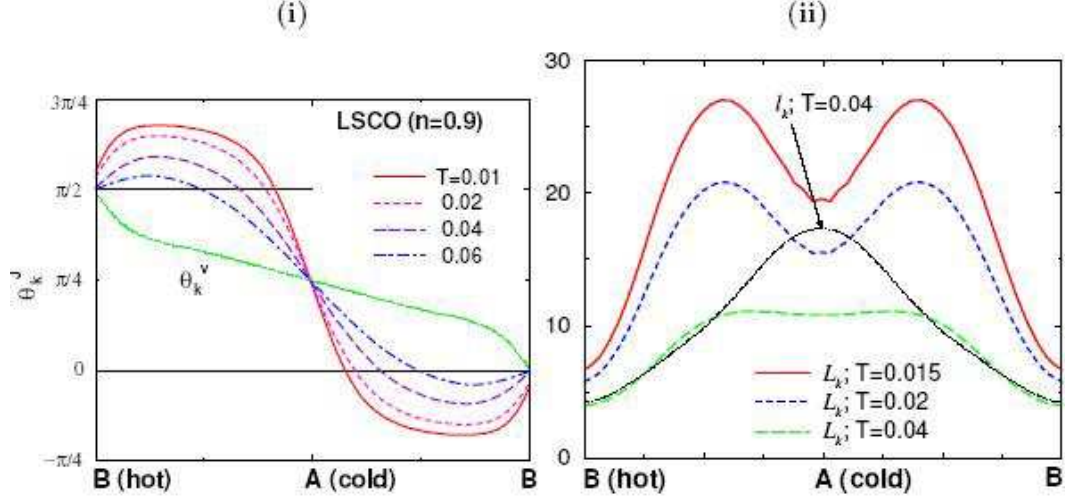


Figure 17. (i) $\theta_{\mathbf{k}}^J = \tan^{-1}(J_{\mathbf{k}x}/J_{\mathbf{k}y})$ and (ii) mean free path with CVC obtained by eq. (90); $|\vec{L}_{\mathbf{k}}| = |\vec{J}_{\mathbf{k}}/\gamma_{\mathbf{k}}|$. $-d\theta_{\mathbf{k}}^J/dk_{\parallel}$ at the cold spot (A) increases as T decreases. $|\vec{L}_{\mathbf{k}}|$ attains its local minimum at the cold spot for $T \leq 0.02$, which induces increases in the Nernst coefficient and magnetoresistance. We also plot the mean free path without CVC; $|\vec{l}_{\mathbf{k}}^v| = |\vec{v}_{\mathbf{k}}/\gamma_{\mathbf{k}}|$.

After the analytic continuation of the Maki-Thompson term $i\omega_l \rightarrow \omega + i\delta$ from the region $\epsilon_n, \epsilon_{n'} < 0$ and $\epsilon_n + \omega_l, \epsilon_{n'} + \omega_l > 0$, the Bethe-Salpeter equation in the FLEX+CVC theory for $\omega = 0$ is given by [33],

$$\begin{aligned} \vec{J}_{\mathbf{k}}(\epsilon) &= \vec{v}_{\mathbf{k}}(\epsilon) + \sum_{\mathbf{q}} \int \frac{d\epsilon'}{2\pi} \left[\text{cth} \frac{\epsilon' - \epsilon}{2T} - \text{th} \frac{\epsilon'}{2T} \right] \\ &\quad \times \text{Im} V_{\mathbf{q}}(\epsilon' + i\delta) \cdot |G_{\mathbf{k}+\mathbf{q}}(\epsilon + \epsilon' + i\delta)|^2 \cdot \vec{J}_{\mathbf{k}+\mathbf{q}}(\epsilon + \epsilon') \\ &\approx \vec{v}_{\mathbf{k}} + \sum_{\mathbf{q}} \frac{(\pi T)^2}{2} \text{Im} \dot{V}_{\mathbf{q}}(0) \frac{\rho_{\mathbf{k}+\mathbf{q}}(0)}{\gamma_{\mathbf{k}+\mathbf{q}}} \vec{J}_{\mathbf{k}+\mathbf{q}}, \end{aligned} \quad (90)$$

where $\vec{v}_{\mathbf{k}}(\epsilon) = \vec{\nabla}_{\mathbf{k}}(\epsilon_{\mathbf{k}}^0 + \text{Re}\Sigma_{\mathbf{k}}(\epsilon))$. In deriving eq. (90), we used the relation $\int [\text{cth}(\epsilon/2T) - \text{th}(\epsilon/2T)] \epsilon d\epsilon = (\pi T)^2$, and assumed the relation $\omega_{\text{sf}} \gg T$. If we approximate $V_{\mathbf{q}} \approx 3U^2\chi_{\mathbf{q}}^s/2$, eq. (90) is equivalent to eq. (75). [Note that $\bar{U} = U$ in the FLEX approximation.] The numerical solution of eq. (90) is shown in Fig. 17, whose schematic behavior is shown in Fig. 14 (i). This singular \mathbf{k} -dependence of $\mathbf{J}_{\mathbf{k}}$ is realized because $\alpha_{\mathbf{k}}$ in eq. (77) approaches unity for $\xi_{\text{AF}} \rightarrow \infty$. As discussed in §3.4, this result is not specific to the FLEX approximation since the same vertex function $[\mathcal{T}_{\mathbf{k},\mathbf{k}'}^{(0)}]$ appears in both (60) and (68) in the microscopic Fermi liquid theory, which is one of the Ward identity. For this reason, singular \mathbf{k} -dependence of $\mathbf{J}_{\mathbf{k}}$ in the case of $\xi_{\text{AF}} \gg 1$, which is shown in Fig. 17, is not specific to the FLEX approximation, but is a universal behavior in Fermi liquids near the AF QCP.

In hole-doped systems, $\gamma_{\mathbf{k}}$ attains its minimum (maximum) at point A (point B) as shown in Fig. 7 [24, 25]. At low T , the local minimum of $|\vec{J}_{\mathbf{k}}|$ is located at points A and

B, and its maximum is located at point C: this is schematically shown in Fig. 14 (i). Further, Fig. 17 (ii) shows that the mean free path with CVC, $|\vec{L}_{\mathbf{k}}| = |\vec{J}_{\mathbf{k}}/\gamma_{\mathbf{k}}|$, attains its local minimum at point A for $T \leq 0.02$, since $|\vec{J}_{\mathbf{k}}|$ rapidly increases as \mathbf{k} deviates from the point A. In fact, eq. (79) suggests that $|\vec{J}_{\mathbf{k}}| \propto \xi_{\text{AF}}^2 |\vec{v}_{\mathbf{k}} + \vec{v}_{\mathbf{k}^*}|$. Therefore, $|\vec{J}_{\mathbf{k}}|$ takes a large value near the AF QCP except for point A and B. In later sections, we explain that the a local minimum structure of $|\vec{L}_{\mathbf{k}}|$ at point A becomes prominent below T^* , which causes the significant increases in the Nernst coefficient and magnetoresistance.

In Ref. [33], we solved the Bethe-Salpeter equation by considering both Maki-Thompson term and the Aslamazov-Larkin terms, and calculated both ρ and R_{H} . As a result, we verified numerically that the Aslamazov-Larkin terms are negligible in nearly AF metals.

4.2. Resistivity and Hall coefficient

First, we analyze the conductivity σ_{xx} using eq. (58). According to the approximate expression for $\vec{J}_{\mathbf{k}}$ given in eq. (79),

$$[v_{\mathbf{k}x} J_{\mathbf{k}x}]_{\text{cold}} = \left[\frac{v_{\mathbf{k}x}^2}{1 + \alpha_{\mathbf{k}}} \right]_{\text{cold}} \quad (91)$$

at the cold spot of YBCO [point A]. We have used the relationship $\mathbf{k} = -\mathbf{k}^*$ at the cold spot. Since $1/(1 + \alpha_{\mathbf{k}}) \sim 1/2$ when $\xi_{\text{AF}} \gg 1$, then $\sigma_{xx} \sim \sigma_{xx}^{\text{RTA}}/2$. Therefore, the resistivity ρ is slightly increased by the CVC [33]. Since the effect of the CVC on ρ is not large, the RTA result for ρ can be qualitatively justified.

Figure 18 (i) shows the numerical results of ρ for LSCO ($n = 0.92$ and $U = 4.5$) obtained from the FLEX approximation and the FLEX+ T -matrix approximation. In the FLEX approximation without CVC, ρ shows an approximate T -linear behavior for $T \geq 0.02$ (~ 80 K). Because of the CVC, ρ is slightly enhanced for a wide range of temperatures. Moreover, ρ obtained by the FLEX+CVC approximation shows a tiny “kink” structure at $\sim T_0$, below which AF fluctuations grows prominently. This result is consistent with the experimental results [167]. The kink becomes more prominent in the FLEX+ T -matrix approximation, which will be discussed in §5.2. In optimally-doped YBCO and LSCO, the resistivity at 300 K is 200 – 300 $\mu\Omega\text{cm}$, and it increases to 400 – 600 $\mu\Omega\text{cm}$ in slightly under-doped compounds ($n \sim 0.1$) [156]. In Fig. 18 (i), $\rho = 1 \sim 250$ $\mu\Omega\text{cm}$ at $T = 0.08 \sim 320$ K: The resistivity increases with U , and $\rho \sim 450$ $\mu\Omega\text{cm}$ for YBCO with $U = 8$ and $n = 0.9$ [33], which is consistent with experimental values. However, the FLEX+CVC method cannot reproduce the huge resistivity in heavily under-doped compounds, since the self-consistency condition in the FLEX approximation tends to suppress $\gamma_{\mathbf{k}}$ too strongly; see §9.2. In under-doped compounds, one has to take account of the effect of residual disorder since the residual resistivity grows prominently. We will explain the reason in §7.2 based on the Fermi liquid theory with strong AF fluctuations.

Figure 18 (ii) shows the ρ for NCCO ($U = 5.5$) obtained from the FLEX approximation (within the RTA) and the FLEX+CVC approximation. In the case

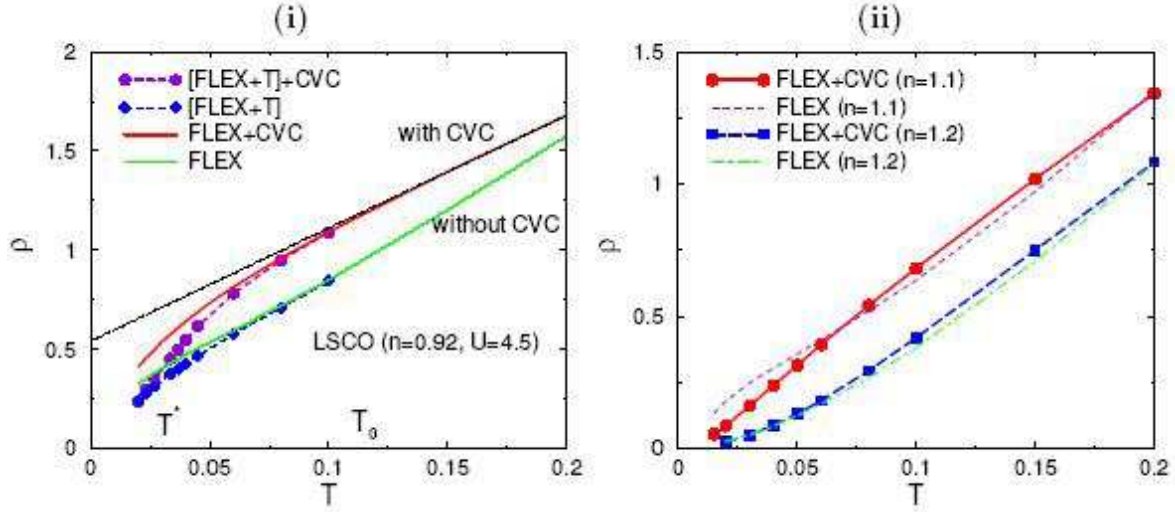


Figure 18. (i) ρ for LSCO obtained by the FLEX (without CVC) and FLEX+CVC approximations. ρ is slightly enhanced because of the CVC. We also plot ρ obtained by the FLEX+ T -matrix (without CVC) and [FLEX+ T -matrix]+CVC approximations. The FLEX+ T -matrix approximation coincides with the FLEX approximation for $T \gg T^*$, where SC fluctuations disappear. $T = 0.2$ corresponds to 800 K. (ii) ρ for NCCO obtained by the FLEX (without CVC) and FLEX+CVC approximations.

of $n = 1.20$ (over-doped), ρ shows a T^2 -like behavior below $T = 0.1 \sim 400$ K, which is consistent with experiments. In the case of $n = 1.10$ (under-doped), ρ shows an approximate T -linear behavior when the CVC is included in the calculation. Interestingly, $\rho_{\text{FLEX+CVC}} < \rho_{\text{FLEX(RTA)}}$ for $n = 1.10$ below $T = 0.06$, since $|\vec{J}_{\mathbf{k}}| \gg |\vec{v}_{\mathbf{k}}|$ due to the CVC in NCCO at low temperatures.

Next, we discuss the Hall coefficient. Using the Onsager's relation $\sigma_{xy} = -\sigma_{yx}$, the general expression for σ_{xy} in eq. (59) and σ_{xy}^{RTA} in eq. (39) in 2D systems can be rewritten as [33]

$$\begin{aligned} \sigma_{xy}/H_z &= \frac{e^3}{4} \oint_{\text{FS}} \frac{dk_{\parallel}}{(2\pi)^2} \left(\vec{L}_{\mathbf{k}} \times \frac{\partial \vec{L}_{\mathbf{k}}}{\partial k_{\parallel}} \right)_z \\ &= \frac{e^3}{4} \oint_{\text{FS}} \frac{dk_{\parallel}}{(2\pi)^2} |\vec{J}_{\mathbf{k}}|^2 \left(\frac{-d\theta_{\mathbf{k}}^J}{dk_{\parallel}} \right) \cdot \frac{1}{\gamma_{\mathbf{k}}^2}, \end{aligned} \quad (92)$$

$$\sigma_{xy}^{\text{RTA}}/H_z = \frac{e^3}{4} \oint_{\text{FS}} \frac{dk_{\parallel}}{(2\pi)^2} |\vec{v}_{\mathbf{k}}|^2 \left(\frac{-d\theta_{\mathbf{k}}^v}{dk_{\parallel}} \right) \cdot \frac{1}{\gamma_{\mathbf{k}}^2}, \quad (93)$$

where $\vec{L}_{\mathbf{k}} = \vec{J}_{\mathbf{k}}/\gamma_{\mathbf{k}}$, $\theta_{\mathbf{k}}^J = \tan^{-1}(J_{kx}/J_{ky})$ and $\theta_{\mathbf{k}}^v = \tan^{-1}(v_{kx}/v_{ky})$. dk_{\parallel} is the momentum tangent to the Fermi surface, which is depicted in Fig. 14 (i). Note that $|\vec{L}_{\mathbf{k}}| = |\vec{J}_{\mathbf{k}}/\gamma_{\mathbf{k}}|$ represents the mean free path by considering the CVC. In deriving above equations, we used the relation $|v_{\mathbf{k}}|\partial/\partial k_{\parallel} = (\hat{z} \times \vec{v}_{\mathbf{k}}) \cdot \vec{\nabla}_{\mathbf{k}} = (\vec{v}_{\mathbf{k}} \times \vec{\nabla}_{\mathbf{k}})_z$ in 2D systems. Using the

relation $\sqrt{v_{\mathbf{k}x}^2 + v_{\mathbf{k}y}^2} \partial/\partial k_{\parallel} = (\vec{v}_{\mathbf{k}} \times \vec{\nabla}_{\mathbf{k}})_z$, σ_{xy} in a 3D system is given by

$$\sigma_{xy}/H_z = \frac{e^3}{4} \int_{\text{FS}} \frac{dS_{\mathbf{k}}}{(2\pi)^3} \frac{\sqrt{v_{\mathbf{k}x}^2 + v_{\mathbf{k}y}^2}}{|\vec{v}_{\mathbf{k}}|} |\vec{J}_{\mathbf{k}}|^2 \left(\frac{-d\theta_{\mathbf{k}}^J}{dk_{\parallel}} \right) \cdot \frac{1}{\gamma_{\mathbf{k}}^2}, \quad (94)$$

where $dS_{\mathbf{k}}$ represents the Fermi surface element, and dk_{\parallel} is the momentum tangent to the Fermi surface and parallel to the xy -plane. We stress that the k -derivative of $\gamma_{\mathbf{k}}$ does not enter into the expression of σ_{xy} , while it exists in expressions of $\Delta\sigma_{xx}$ and α_{xy} .

In the expression of σ_{xy}^{RTA} , $(-d\theta_{\mathbf{k}}^v/dk_{\parallel})$ represents the curvature of the Fermi surface [168, 169]; in both hole-doped and electron-doped HTSCs, $(-d\theta_{\mathbf{k}}^v/dk_{\parallel}) \sim 1/k_{\text{F}} (> 0)$ on the Fermi surface. On the other hand, $(-d\theta_{\mathbf{k}}^J/dk_{\parallel})$ exhibits strong \mathbf{k} -dependence in nearly AF metals, as shown in Fig. 14 (i); $(-d\theta_{\mathbf{k}}^J/dk_{\parallel})$ is positive around point A, whereas it is negative around point B. Since the cold spot is located around point A in hole-doped systems [33], the present study predicts that $R_{\text{H}} > 0$ in hole-doped systems when the AF fluctuations are strong. [Note that the charge of electron is $-e$ ($e > 0$) in the present study.] On the other hand, $R_{\text{H}} < 0$ in electron-doped systems since the cold spot in electron-doped systems is B [33].

For an intuitive understanding of the CVC, we introduce an ‘‘effective Fermi surface’’ obtained by bending the true Fermi surface such that it is orthogonal to $\vec{J}_{\mathbf{k}}$ around the cold spot [20]. The effective Fermi surface in HTSCs is shown in Fig. 14 (ii). It can be seen that the curvature of the effective Fermi surface, which is equal to $(-d\theta_{\mathbf{k}}^J/dk_{\parallel})$ by definition, takes a large positive (negative) value around the cold spot in hole-doped (electron-doped) systems. Therefore, R_{H} in hole-doped (electron-doped) systems exhibits a large positive (negative) value at low temperatures [33].

Figures 19 (i), (iii), and (iv) show the numerical results for R_{H} obtained from the FLEX approximation by including the CVC. In hole-doped systems ($n < 1$), R_{H} increases as the doping $\delta = |1 - n|$ decreases. On the other hand, R_{H} for electron-doped systems ($n > 1$) becomes negative below $T = 0.09 \sim 400$ K. These results are consistent with the experimental results. Previously, negative R_{H} in electron-doped systems had been considered to be strong evidence of the breakdown of the Fermi liquid state since the curvature of the Fermi surface in HTSCs is positive everywhere. However, it is naturally explained in terms of the Fermi liquid picture since the curvature of the effective Fermi surface becomes negative around point B, as shown in Fig. 14 (ii) [33].

As shown in Fig. 19 (i), (iii), and (iv), R_{H} given by the RTA (without CVC) decreases with decreasing T , since the curvature of the true interacting Fermi surface becomes smaller in the FLEX approximation at low temperatures [33]: The deformation of the Fermi surface is caused by the strong \mathbf{k} -dependence of the self-energy, which becomes prominent when AF fluctuations are strong. A tiny increment in $R_{\text{H}}^{\text{RTA}}$ in YBCO below $T = 0.02$ is caused by the strong anisotropy of $\gamma_{\mathbf{k}}$. In the present calculation, $\gamma_{\text{hot}}/\gamma_{\text{cold}}$ is approximately 3 at $T = 0.02$

Figure 19 (ii) shows the k_{\parallel} -dependence of $\Delta\sigma_{xx}(k_{\parallel}) = \vec{v}_{\mathbf{k}} \cdot \vec{L}_{\mathbf{k}}/|\vec{v}_{\mathbf{k}}|$ and $\Delta\sigma_{xy}(k_{\parallel}) = |\vec{L}_{\mathbf{k}}|^2(-\partial\theta_{\mathbf{k}}^J/\partial k_{\parallel})$, where $\sigma_{xx} = \oint_{\text{FS}} dk_{\parallel} \Delta\sigma_{xx}(k_{\parallel})$ and $\sigma_{xy} = \oint_{\text{FS}} dk_{\parallel} \Delta\sigma_{xy}(k_{\parallel})$. In both σ_{xx} and σ_{xy} , the quasiparticles around the cold spot gives the dominant contributions.

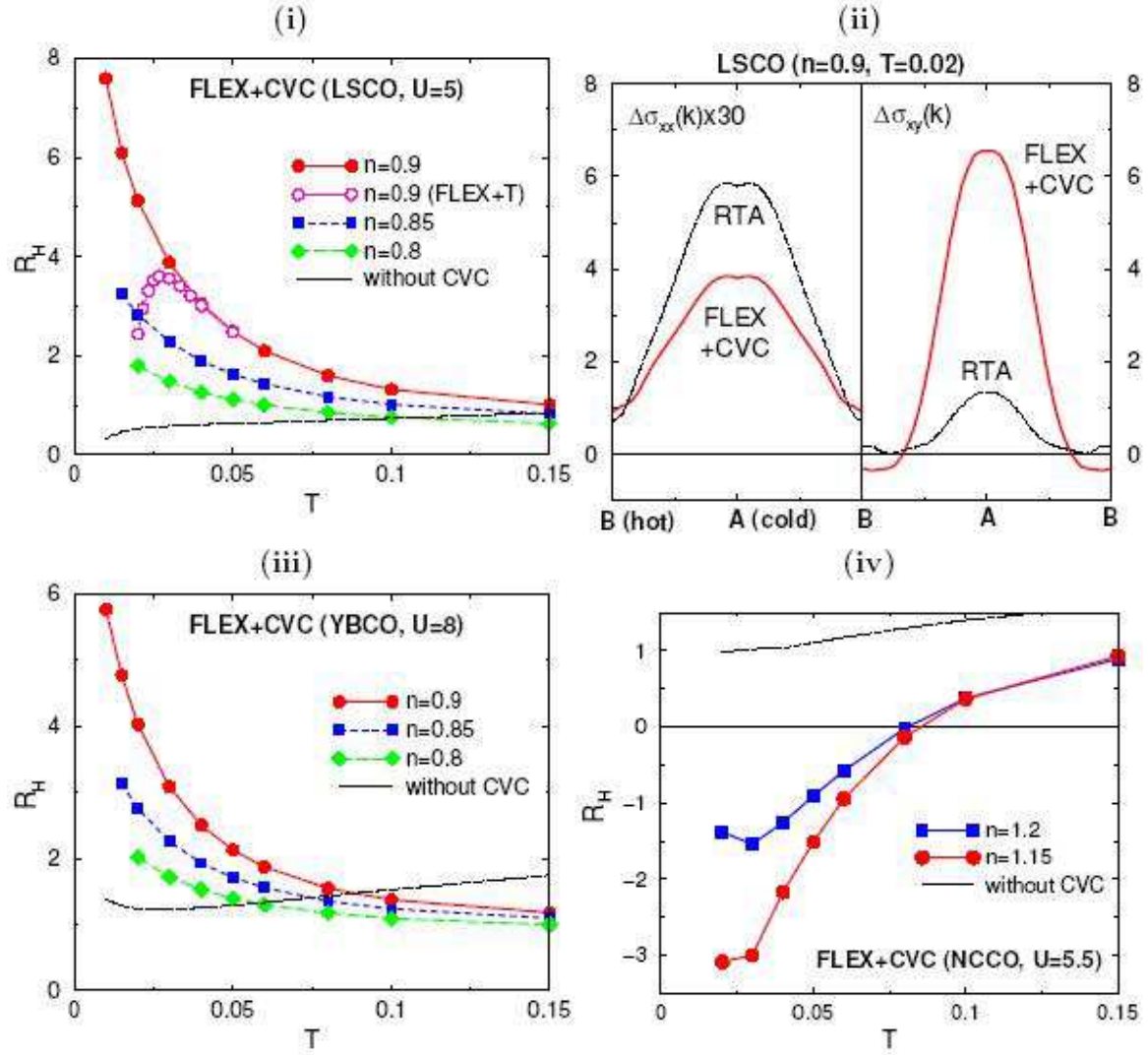


Figure 19. (i) R_H for LSCO obtained by the FLEX+CVC approximation. In contrast to its prominent T -dependence, R_H^{RTA} given by the RTA (without CVC) shows only a weak T -dependence. R_H obtained using the FLEX+ T -matrix approximation is also shown; it starts to decrease below $T^* \sim 0.04$ (~ 160) K (pseudo-gap behavior). (ii) k_{\parallel} -dependence of $\Delta\sigma_{xx}(k_{\parallel})$ and $\Delta\sigma_{xy}(k_{\parallel})$ at $T = 0.02$. Note that $\sigma_{\mu\nu} = \int_{\text{FS}} dk_{\parallel} \Delta\sigma_{\mu\nu}(k_{\parallel})$. (iii) R_H for YBCO obtained using the FLEX+CVC method. (iv) R_H for NCCO obtained using the FLEX+CVC method.

We can see that σ_{xx} is slightly reduced by including the CVC. On the other hand, σ_{xy} obtained from the FLEX+CVC theory is considerably larger than σ_{xy}^{RTA} , since $|d\theta_{\mathbf{k}}^J/dk_{\parallel}| \gg |d\theta_{\mathbf{k}}^v/dk_{\parallel}|$ at the cold spot. $\Delta\sigma_{xy}(k_{\parallel})$ is large only around the cold spot, and it becomes negative around the hot spot.

Here, we discuss the temperature dependence of R_H in detail using the approximate expression for $\vec{J}_{\mathbf{k}}$ in eq. (79). Since $\partial\alpha_{\mathbf{k}}/\partial k_{\parallel} = 0$ at the cold spot [point A] because of

the symmetry,

$$\frac{\partial \vec{J}_{\mathbf{k}}}{dk_{\parallel}} = \frac{1}{1 - \alpha_{\mathbf{k}}^2} \left(\frac{d\vec{v}_{\mathbf{k}}}{dk_{\parallel}} + \alpha_{\mathbf{k}} \frac{d\vec{v}_{\mathbf{k}^*}}{dk_{\parallel}} \right) \quad (95)$$

at the cold spot. By noticing the relationships $(\vec{v}_{\mathbf{k}^*} \times d\vec{v}_{\mathbf{k}^*}/dk_{\parallel})_z = -(\vec{v}_{\mathbf{k}} \times d\vec{v}_{\mathbf{k}}/dk_{\parallel})_z$ and $(\vec{v}_{\mathbf{k}^*} \times d\vec{v}_{\mathbf{k}}/dk_{\parallel})_z = -(\vec{v}_{\mathbf{k}} \times d\vec{v}_{\mathbf{k}^*}/dk_{\parallel})_z$, we obtain that

$$\begin{aligned} \left(\vec{J}_{\mathbf{k}} \times \frac{d\vec{J}_{\mathbf{k}}}{dk_{\parallel}} \right)_z &= |\vec{J}_{\mathbf{k}}|^2 \left(\frac{-d\theta_{\mathbf{k}}^J}{dk_{\parallel}} \right)_{\text{cold}} \\ &= \frac{1}{1 - \alpha_{\mathbf{k}}^2} |\vec{v}_{\mathbf{k}}|^2 \left(\frac{-d\theta_{\mathbf{k}}^v}{dk_{\parallel}} \right)_{\text{cold}}, \end{aligned} \quad (96)$$

which is proportional to $(1 - \alpha_{\mathbf{k}})^{-1} \propto \xi_{\text{AF}}^2$ [33]. In fact, Fig. 17 (i) shows that eq. (96) increases as the temperature decreases. As a result, R_{H} behaves as [33]

$$|R_{\text{H}}| \propto \xi_{\text{AF}}^2. \quad (97)$$

Therefore, both the sign and the T -dependence of R_{H} in hole-doped HTSC are successfully reproduced in the present approach.

Finally, we discuss electron-doped systems. At the point B in Fig. 4 (i), $|\mathbf{k}_{\text{B}} - \mathbf{k}_{\text{B}'} - \mathbf{Q}|$ is equal to $|\mathbf{k}_{\text{B}} - \mathbf{k}_{\text{B}''} - \mathbf{Q}|$ for $\mathbf{Q} = (\pi, -\pi)$. Then, the CVC at \mathbf{k}_{B} , which is given by the second term of eq. (75), is approximately proportional to $\vec{J}_{\text{B}'} + \vec{J}_{\text{B}''} = 0$. Therefore, $\alpha_{\mathbf{k}} = 0$ in the simplified Bethe-Salpeter equation (78) and $\vec{J}_{\mathbf{k}} \approx \vec{v}_{\mathbf{k}}$ at point B. Since $\alpha_{\mathbf{k}}$ rapidly increases if \mathbf{k} deviates from point B, $(-d\theta_{\mathbf{k}}^J/dk_{\parallel})$ attains a large negative value around the cold spot of NCCO. Therefore, the negative sign of R_{H} is realized by considering the CVC.

Finally, we stress that we have also studied the CVC by using a widely used phenomenological AF fluctuation model given in eq. (8). Assuming a reasonable set of parameters, we find that R_{H} is prominently enhanced due to the CVC [34]. Thus, the enhancement of R_{H} in nearly AF metals is not an artifact in the FLEX approximation, but a universal phenomena near the AF QCP.

4.3. Magnetoresistance

Next, we study the orbital magnetoresistance $\Delta\rho/\rho_0$ in HTSCs by considering the CVC. According to the linear response theory [1], the magnetoresistance is give by

$$\Delta\rho/\rho_0 \equiv -\Delta\sigma_{xx}/\sigma_{xx}^0 - (\sigma_{xy}/\sigma_{xx}^0)^2, \quad (98)$$

where σ_{xx}^0 denotes the conductivity without a magnetic field, and $\Delta\sigma_{xx} \equiv \sigma_{xx}(H_z) - \sigma_{xx}^0$ is the magneto-conductivity, which is always negative.

To derive the magnetoresistance, we have to calculate the magneto-conductivity, which is given in eq. (40) in the RTA. By performing the partial integration, eq. (40) for 2D system is rewritten as

$$\Delta\sigma_{xx}^{\text{RTA}} = -H_z^2 \cdot \frac{e^4}{8} \oint_{\text{FS}} \frac{dk_{\parallel}}{(2\pi)^2} |\vec{v}_{\mathbf{k}}| \left[|\vec{l}_{\mathbf{k}}|^2 \left(\frac{\partial\theta_{\mathbf{k}}^v}{\partial k_{\parallel}} \right)^2 + \left(\frac{\partial|\vec{l}_{\mathbf{k}}|}{\partial k_{\parallel}} \right)^2 \right] \frac{1}{\gamma_{\mathbf{k}}}, \quad (99)$$

where $\vec{l}_{\mathbf{k}} = \vec{v}_{\mathbf{k}}/\gamma_{\mathbf{k}}$. Here, we used the relation $|v_{\mathbf{k}}|\partial/\partial k_{\parallel} = (\hat{z} \times \vec{v}_{\mathbf{k}}) \cdot \vec{\nabla}_{\mathbf{k}} = (\vec{v}_{\mathbf{k}} \times \vec{\nabla}_{\mathbf{k}})_z$ in 2D systems. When the Fermi surface is spherical, the second term in the bracket in eq. (99) vanishes identically. In this case, $\sigma_{xx}^0 = e^2 k_F v_F / 4\pi\gamma$, $\sigma_{xy} = (ev_F/2\gamma)\sigma_{xx}^0$ and $\Delta\sigma_{xx} = -(ev_F/2\gamma)^2\sigma_{xx}^0$ according to the RTA, where k_F and v_F are the Fermi momentum and the Fermi velocity, respectively. Therefore, $\Delta\rho/\rho_0$ given in eq. (98) becomes zero. Except for this special case, the orbital magnetoresistance is always positive [1].

The general expression for the magneto-conductivity in Fermi liquids are derived in Ref. [38], which is exact of order $O(\gamma^{-3})$. It is derived by performing the analytic continuation of eq. (48) for $m = 2$. This work had enabled us to calculate the magneto-conductivity along with satisfying the conservation laws. At low temperatures, the magneto-conductivity can be expressed by a simple form: $\Delta\sigma_{xx} = \Delta\sigma_{xx}^a + \Delta\sigma_{xx}^b$;

$$\Delta\sigma_{xx}^a = -H_z^2 \cdot \frac{e^4}{4} \sum_{\mathbf{k}} z_{\mathbf{k}} \left(-\frac{\partial f^0}{\partial \epsilon} \right)_{E_{\mathbf{k}}^*} \{d_{\mathbf{k}x}\}^2 \frac{1}{\gamma_{\mathbf{k}}}, \quad (100)$$

$$\Delta\sigma_{xx}^b = -H_z^2 \cdot \frac{e^4}{4} \sum_{\mathbf{k}} z_{\mathbf{k}} \left(-\frac{\partial f^0}{\partial \epsilon} \right)_{E_{\mathbf{k}}^*} d_{\mathbf{k}x} D_{\mathbf{k}x} \frac{1}{\gamma_{\mathbf{k}}}, \quad (101)$$

$$d_{\mathbf{k}x} = |v_{\mathbf{k}}| \frac{\partial L_{\mathbf{k}x}}{\partial k_{\parallel}}, \quad (102)$$

$$D_{\mathbf{k}x} = \sum_{\mathbf{k}'} \int_{-\infty}^{\infty} \frac{d\epsilon'}{4\pi i} \mathcal{T}_{\mathbf{k},\mathbf{k}'}^{(0)}(0, \epsilon') \rho_{\mathbf{k}'}(0) d_{\mathbf{k}'x} / \gamma_{\mathbf{k}'}, \quad (103)$$

where $\vec{L}_{\mathbf{k}} = \vec{J}_{\mathbf{k}}/\gamma_{\mathbf{k}}$ and $\mathcal{T}_{\mathbf{k},\mathbf{k}'}^{(0)}(0, \epsilon')$ is the irreducible four-point vertex in the particle-hole channel introduced in eq. (60) [40]. $\Delta\sigma_{xx}^{\text{RTA}}$ in eq. (40) is given by eqs. (100) and (102), by replacing $\vec{J}_{\mathbf{k}}$ with $\vec{v}_{\mathbf{k}}$. In the FLEX approximation, $\int \frac{d\epsilon'}{4\pi i} \mathcal{T}_{\mathbf{k},\mathbf{k}'}^{(0)}(0, \epsilon') \approx (3U^2/2)(\pi T)^2 \text{Im} \partial \chi_{\mathbf{k}-\mathbf{k}'}^s(\omega) / \partial \omega|_{\omega=0}$, as shown in eq. (75).

Here, we can rewrite $\Delta\sigma_{xx}^a$ as

$$\Delta\sigma_{xx}^a = -H_z^2 \cdot \frac{e^4}{8} \oint_{\text{FS}} \frac{dk_{\parallel}}{(2\pi)^2} |\vec{v}_{\mathbf{k}}| \left[|\vec{L}_{\mathbf{k}}|^2 \left(\frac{\partial \theta_{\mathbf{k}}^J}{\partial k_{\parallel}} \right)^2 + \left(\frac{\partial |\vec{L}_{\mathbf{k}}|}{\partial k_{\parallel}} \right)^2 \right] \frac{1}{\gamma_{\mathbf{k}}}, \quad (104)$$

where $\vec{L}_{\mathbf{k}} = \vec{J}_{\mathbf{k}}/\gamma_{\mathbf{k}}$. According to eq. (96), the first term in the bracket in eq. (104) is proportional to $(d\theta_{\mathbf{k}}^J/dk_{\parallel})_{\text{cold}}^2 \gamma_{\text{cold}}^{-3} \propto \xi_{\text{AF}}^4 \gamma_{\text{cold}}^{-3}$ [35]. Further, remaining terms (the second term in eq. (104) and $\Delta\sigma_{xx}^b$) are also proportional to $\xi_{\text{AF}}^4 \gamma_{\text{cold}}^{-3}$ for a wide range of temperatures, since the k_{\parallel} -derivative of $\vec{\mathcal{T}}_{\mathbf{k},\mathbf{k}'}^{(0)}$ yields a factor proportional to ξ_{AF}^2 [33, 35]. In §5.2, we will explain that $|\vec{L}_{\mathbf{k}}|$ becomes highly anisotropic below T^* due to AF+SC fluctuations. For this reason, due to the second term in eq. (104), $\Delta\rho/\rho_0$ is prominently enhanced below T^* in under-doped HTSCs.

Therefore, the magnetoresistance in nearly AF metals behaves as

$$\Delta\rho/\rho_0 \propto \xi_{\text{AF}}^4 \cdot \rho_0^{-2} \propto T^{-4} \quad (105)$$

above T^* due to the CVC since $\rho_0 \propto T$ and $\xi_{\text{AF}}^2 \propto T^{-1}$. Equation (105) is consistent with experimental results in LSCO [12, 71, 72], YBCO [71] and TBCO [73]. On the other hand, in a conventional Fermi liquid where ξ_{AF} is constant, eq. (105) gives Kohler's rule

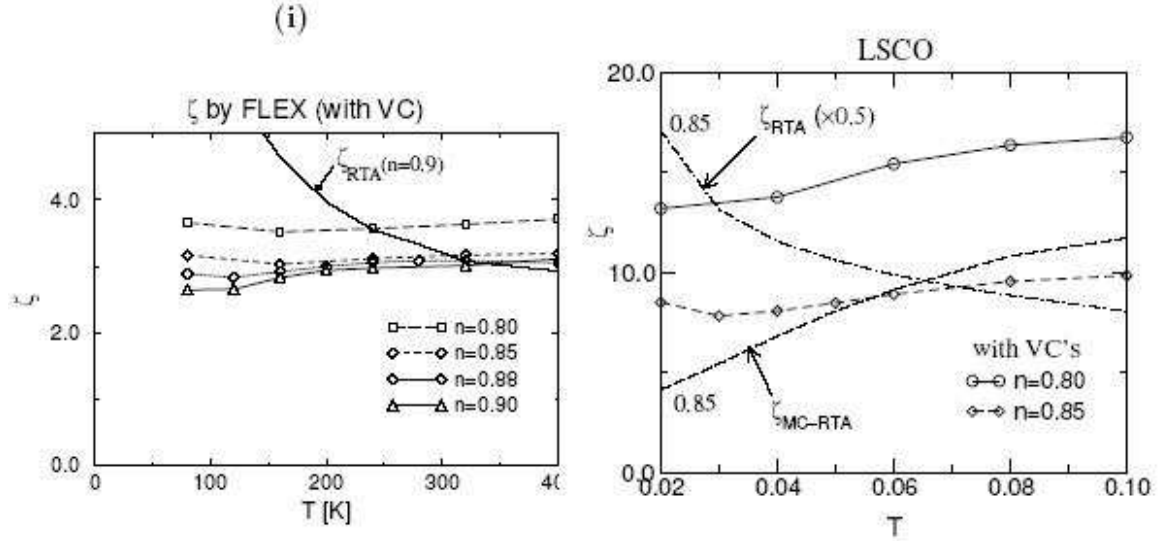


Figure 20. $\zeta = (\Delta\rho/\rho_0) \cot^2 \theta_H$ for (i) YBCO and (ii) LSCO calculated by the FLEX+CVC method for $0.02 \leq T \leq 0.1$ (80K \sim 400K). The modified Kohler's rule ($\zeta = \text{const.}$) holds well by considering the CVC. On the other hand, ζ_{RTA} obtained by the RTA exhibits a strong T -dependence. [Ref. [35]]

$\Delta\rho/\rho_0 \propto \rho_0^{-2}$. Equations (97) and (105) directly imply the “modified Kohler's rule” [35]

$$\Delta\rho/\rho_0 \propto \tan^2 \theta_H, \quad (106)$$

where $\tan \theta_H = \sigma_{xy}/\sigma_{xx}^0 = R_H/\rho_0$. Experimentally, the modified Kohler's rule is well satisfied in various HTSC compounds [12, 71, 73] and in CeMIn_5 ($M=\text{Co}$ or Rh) [19, 20], whereas the conventional Kohler's rule is completely broken. This long-standing problem had been naturally explained in terms of the Fermi liquid theory. The modified Kohler's rule implies that the enhancements of R_H and $\Delta\rho/\rho_0$ are induced by the same origin; the CVC due to AF fluctuations.

Figure 20 shows the numerical results for (i) YBCO and (ii) LSCO by using the FLEX+CVC method. The coefficient

$$\zeta = (\Delta\rho/\rho_0) \cot^2 \theta_H \quad (107)$$

takes an almost constant value for a wide range of temperatures, only when the CVCs are correctly considered: In Fig. 20, we show that $\zeta_{RTA} \equiv (\Delta\rho/\rho_0)_{RTA} (\cot^2 \theta_H)_{RTA}$ and $\zeta_{MC-RTA} \equiv (\Delta\rho/\rho_0)_{RTA} \cot^2 \theta_H$: ζ_{RTA} increases as T decreases, since the anisotropy of $|\vec{l}_k| = |\vec{v}_k/\gamma_k|$ increases at low temperatures. In contrast, ζ_{MC-RTA} decreases at low temperatures since the R_H is strikingly enhanced by the CVC. Only when both σ_{xy} and $\Delta\sigma_{xx}$ are calculated using the FLEX+CVC method, the modified Kohler's rule $\zeta \approx \text{const.}$ is satisfied. In YBCO, the dominant contribution to the total magnetoconductivity is given by $\Delta\sigma_{xx}^a$, particularly by the first term in the bracket in eq. (104) that includes $(\partial\theta_{\mathbf{k}}^J/\partial k_{\parallel})^2$. In the case of LSCO, the second term in eq. (104) is very important. Further, $|\Delta\sigma_{xx}^a| \sim |\Delta\sigma_{xx}^b|$. In both these systems, the modified Kohler's rule (106) is well reproduced by the FLEX+CVC method.

The experimental value is $\zeta \approx 1.5 \sim 1.7$ for YBCO [71] and $\zeta \approx 2 \sim 3$ for $\text{Tl}_2\text{Ba}_2\text{CuO}_{6+\delta}$ [73]. In contrast, ζ takes much larger value in LSCO: $\zeta \approx 13.6$ for a slightly over-doped sample ($x = 0.17$) [72], and it increases (decreases) as the doping increases (decreases) [12]. These experimental results are reproduced by the present study and they are shown in Fig. 20. In LSCO, the Fermi surface is very close to the van-Hove singularity point $(\pi, 0)$ since both $|t'/t|$ and $|t''/t|$ in eq. (12) are smaller than those in other systems. Since $\vec{v}_{\mathbf{k}} = 0$ at $(\pi, 0)$, the anisotropy of the velocity $|\vec{v}_{\mathbf{k}}|$ on the Fermi surface is larger in LSCO. Hence, the second term in eq. (104) [or eq. (99)] takes a large value in LSCO. In heavily over-doped LSCO at $\delta = 0.225$, where CVC is expected to be unimportant, ζ exceeds 100 [12]. This result is consistent with recent ARPES measurement [136], which shows that the Fermi surface in LSCO passes through $(\pi, 0)$ in the over-doped region $\delta = 0.2 \sim 0.22$.

Therefore, experimental value of ζ gives us a useful measure of the anisotropy of $\vec{L}_{\mathbf{k}} = \vec{J}_{\mathbf{k}}/\gamma_{\mathbf{k}}$ ($\vec{l}_{\mathbf{k}} = \vec{v}_{\mathbf{k}}/\gamma_{\mathbf{k}}$ in weakly correlated systems). In CeMIn_5 ($M=\text{Rh,Co}$), ζ is of order $O(100)$ [20], which indicates that the anisotropy of $\vec{L}_{\mathbf{k}}$ is large in the main Fermi surface.

4.4. Thermoelectric power

We also discuss the thermoelectric power, S . In HTSCs, S takes a large value in under-doped systems, and it increases as T decreases from the room temperature. Except for over-doped compounds, $S > 0$ in hole-doped systems [2, 157, 158, 159, 160, 161, 162] whereas $S < 0$ in electron-doped systems [7, 163] below the room temperature. Interestingly, the peak temperature of S is nearly equal to the pseudo-gap temperature T^* in many hole-doped compounds; in $\text{HgBa}_2\text{CuO}_{4+\delta}$ [159, 160], LSCO, YBCO [161] and $\text{Bi}_2\text{Sr}_2\text{RCu}_2\text{O}_8$ ($R = \text{Ca, Y, Pr, Dy or Er}$) [162]. By neglecting the CVC, Hildebrand et al. calculated the thermoelectric power for YBCO using the FLEX approximation [164]. Here, we study the thermoelectric power both for hole-doped and electron-doped systems using the FLEX+CVC method.

According to the linear response theory [165, 166, 39], the thermoelectric power in a Fermi liquid system is given by

$$S = \alpha_{xx}/\sigma_{xx}, \quad (108)$$

where α_{xx} is the diagonal Peltier conductivity; $j_x = \alpha_{xx}(-\nabla_x T)$. It is given by [165, 166, 39],

$$\alpha_{xx} = K_{xx}^\alpha(\omega + i0)/i\omega|_{\omega \rightarrow 0}, \quad (109)$$

where $K_{xx}^\alpha(\omega + i0)$ is given by the analytic continuation of [39]

$$K_{xx}^\alpha(i\omega_\lambda) = \frac{1}{T} \int_0^\beta d\tau e^{-\omega_\lambda \tau} \langle T_\tau j_x^Q(0) j_x(\tau) \rangle, \quad (110)$$

where \vec{j} and \vec{j}^Q are charge current operator and heat current one, respectively. The heat current is defined by the following energy conservation law; $\partial_t(h(\mathbf{r}) - \mu n(\mathbf{r})) + \vec{\nabla} \cdot \vec{j}^Q(\mathbf{r}) = 0$. Then, \vec{j}^Q contains complex two-body terms in the presence of electron-electron

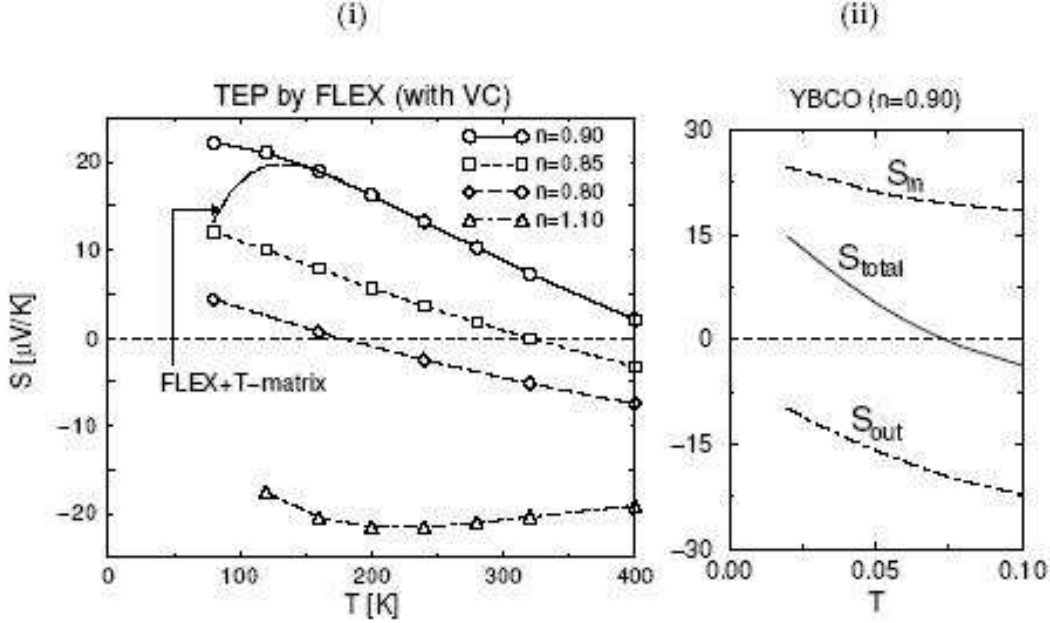


Figure 21. (i) S for YBCO and NCCO given by the FLEX+CVC approximation, by including the CVC for $\vec{J}_{\mathbf{k}}$. Reflecting the reduction in AF fluctuations, S starts to decrease below $T^* \approx 0.04$ (~ 160) K in the FLEX+ T -matrix method, which is consistent with the experimental pseudo-gap behavior in S . (ii) S_{in} (S_{out}) denotes the thermoelectric power given by the inside (outside) of the AFBZ. $S_{\text{total}} = S_{\text{in}} + S_{\text{out}}$. [Ref. [36]]

correlation. Fortunately, the Ward identity allows us to rewrite the heat current as $\vec{j}_{\mathbf{k}}^Q(\epsilon) = \epsilon \vec{v}_{\mathbf{k}}$, where $\vec{v}_{\mathbf{k}} = \vec{\nabla}_{\mathbf{k}}(\epsilon_{\mathbf{k}}^0 + \text{Re}\Sigma_{\mathbf{k}})$ [39]. By performing the analytic continuation of eq. (110), we can derive the exact expression of α_{xx} of order $O(E_F/\gamma)$ as [39]

$$\alpha_{xx} = \frac{-e}{T} \sum_{\mathbf{k}} \int \frac{d\epsilon}{\pi} \left(-\frac{\partial f^0}{\partial \epsilon} \right) \epsilon v_{\mathbf{k}x}(\epsilon) \times (J_{\mathbf{k}x}(\epsilon) |G_{\mathbf{k}}(\epsilon)|^2 - 2v_{\mathbf{k}x}(\epsilon) \text{Re}G_{\mathbf{k}}(\epsilon)^2), \quad (111)$$

where $J_{\mathbf{k}x}(\epsilon)$ is the total current given in eq. (60). At sufficiently low temperatures, α_{xx} is approximately simplified as

$$\alpha_{xx} = -e \frac{\pi^2 T}{3} \int_{\text{FS}} \frac{dk_{\parallel}}{(2\pi)^2} \frac{1}{z_{\mathbf{k}} |v_{\mathbf{k}}(E_{\mathbf{k}}^*)|} \frac{\partial}{\partial k_{\perp}} \left(\frac{v_{\mathbf{k}x}(E_{\mathbf{k}}^*) J_{\mathbf{k}x}(E_{\mathbf{k}}^*)}{|v_{\mathbf{k}}(E_{\mathbf{k}}^*)| \gamma_{\mathbf{k}}(E_{\mathbf{k}}^*)} \right), \quad (112)$$

where $-e$ ($e > 0$) is the electron charge. dk_{\perp} represents the momentum vertical to the Fermi surface. When γ is energy-independent, eq. (112) yields $S = -e\pi T/6z\gamma\sigma_{xx} = -\pi T m^*/3en$ ($m^* = m/z$ is the effective mass) in the 2D isotropic system with $E_{\mathbf{k}} = k^2/2m - \mu$.

In Fig. 21 (i), we show the numerical results for S of YBCO and NCCO given by the FLEX+CVC method. In LSCO, $S > 0$ in the optimally-doped case ($n = 0.85$) below the room temperature, and it increases in the under-doped case. In NCCO ($n = 1.10$), $S < 0$ and it takes a peak around 200K. These results are consistent with the experimental

results [2, 157, 158, 159, 160, 161]. The origin of the non-Fermi-liquid-like behavior is the prominent \mathbf{k} - and ϵ -dependences of $\gamma_{\mathbf{k}}(\epsilon)$ due to strong AF fluctuations. According to the spin fluctuation theory, $\partial\gamma_{\mathbf{k}}(E_{\mathbf{k}}^*)/\partial k_{\perp} > 0$ at point A in Fig. 4 (i) because $\gamma_{\mathbf{k}}$ becomes large near the AFBZ. Since point A is the cold spot of YBCO, eq. (112) becomes positive in YBCO. Therefore, $S > 0$ in under-doped YBCO and LSCO. On the other hand, $S < 0$ in NCCO because $\partial\gamma_{\mathbf{k}}(E_{\mathbf{k}}^*)/\partial k_{\perp} < 0$ at point B. In YBCO, S slightly decreases if the CVC is included, since $|\vec{J}_{\mathbf{k}}| < |\vec{v}_{\mathbf{k}}|$ around the cold spot. In NCCO, in contrast, absolute value of S is enhanced by the CVC. In both cases, the effect of the CVC on S is smaller than that on R_{H} . Figure 21 (ii) shows the S for YBCO ($n = 0.90$), together with S_{in} (S_{out}) which denotes the contribution from the inside (outside) of the AFBZ. S_{in} is positive and it deviates from a conventional behavior ($S \propto T$) since the ϵ -dependence of $\gamma_{\mathbf{k}}(\epsilon)$ becomes large inside of the AFBZ at lower temperatures. On the other hand, S_{out} is negative and it approaches zero as T decreases. Therefore, the sign of $S = S_{\text{in}} + S_{\text{out}}$ becomes positive below $T = 0.075$ (~ 300 K).

4.5. Summary of this section and comments on other transport coefficients

In HTSCs, anomalous transport phenomena (such as the violation of Kohler's rule) had been frequently considered as strong evidence for the breakdown of the quasiparticle picture. For example, the RTA for the highly anisotropic $\tau_{\mathbf{k}}$ model cannot reproduce relationships (1)-(4) for hole-doped systems *at the same time for a wide range of temperatures*. Furthermore, the RTA cannot explain the negative Hall coefficient in electron-doped systems, since the curvature of the true Fermi surface is positive everywhere. The explanation for the nearly symmetric behavior of R_{H} and S with respect to the type of carrier doping (shown in Fig. 3) was desirable for a long time. These highly nontrivial transport phenomena had been one of the central issues in HTSCs, which should serve to elucidate the actual electric ground state of HTSCs.

To resolve this long-standing problem, we developed a method to calculate various transport coefficients based on the microscopic Fermi liquid theory. In the RTA, the momentum and energy transfers between the quasiparticles by scattering are not treated correctly. Therefore, the RTA results frequently yield erroneous results. To overcome this defect, we study the role of the CVC in nearly AF Fermi liquids. We find that the total current $\vec{J}_{\mathbf{k}}$ shows an anomalous \mathbf{k} -dependence because of the CVC in nearly AF metals, which gives rise to the non-Fermi liquid behaviors such as $R_{\text{H}} \propto \xi_{\text{AF}}^2 \propto T^{-1}$ and $\Delta\rho/\rho_0 \propto \rho_0^{-2} \xi_{\text{AF}}^4 \propto T^{-4}$. Consequently, the modified Kohler's rule $\Delta\rho/\rho_0 \propto (R_{\text{H}}/\rho)^2 \propto T^{-4}$ is realized in HTSCs. We also studied the S for HTSCs, which increases as the temperature decreases above T^* . This experimental fact is reproduced by considering the strong \mathbf{k} - and ϵ -dependences of $\tau_{\mathbf{k}}(\epsilon)$ [36]. Therefore, various anomalous transport phenomena in HTSCs above T^* can be well explained by the FLEX+CVC method.

Recently, Tsukada et al. measured the R_{H} in clean heavily over-doped LSCO samples [170], and found that R_{H} becomes almost temperature-independent for $\delta \gtrsim 0.24$;

further, its sign smoothly changes from positive to negative between $\delta = 0.28$ and 0.32 , corresponding to the change in the curvature of the Fermi surface. Hussey et al. also showed that the RTA analysis is successful in heavily over-doped Tl2201 [149] and LSCO [150]. These experimental results are consistent with the present theory: According to the present analysis, the RTA works well in heavily over-doped systems since the CVC is unimportant when the AF fluctuations are very weak. This fact is well explained in Ref. [167].

Finally, we comment on other important theoretical study involving the CVC in strongly correlated systems. In the interacting electron gas model, the electron cyclotron frequency ω_c is given by eH/mc , where m is the bare electron mass. In 1961, Kohn proved that ω_c is unchanged by electron-electron interaction due to the consequence of the angular momentum conservation law, which is called the ‘‘Kohn’s theorem’’ [171]. The Kohn’s theorem is also proved by the phenomenological Fermi liquid theory, by correctly considering the CVC [172]. Kanki and Yamada studied this problem based on the microscopic Fermi liquid theory, and found that ω_c is influenced by the electron-electron correlation if the Umklapp processes are present [173]. The Umklapp processes also reduces the Drude weight in $\sigma(\omega)$ [174] and the penetration depth in the SC state [175]. Moreover, the effect of the vertex correction on the Raman spectroscopy in HTSC was studied [176].

5. Transport phenomena in HTSCs below T^*

5.1. Mechanism of pseudo-gap phenomena

In under-doped HTSCs, a deep pseudo-gap in the DOS emerges at the chemical potential below $T^* \sim 200$ K. The origin of the pseudo-gap has been a central issue with regard to HTSCs. The pseudo-gap does not originate from the spin fluctuations since the strength of the spin fluctuations decrease below T^* [78, 79, 80, 81, 82]. According to recent ARPES measurements [83, 84, 85, 86], the \mathbf{k} -dependence of the pseudo-gap coincides with that of the $d_{x^2-y^2}$ -wave SC gap function. This pseudo-gap structure in the quasiparticle spectrum $\rho(\mathbf{k}, \omega) = \text{Im}G(\mathbf{k}, \omega - i\delta)/\pi$ starts to appear around $\omega = 0$ below T^* . Below T_c , the quasiparticle spectrum shows sharp peaks at the edge of the SC gap ($\omega \sim \Delta$) since the inelastic scattering is reduced by the SC gap. At the same time, a dip-hump structure is induced around $\omega_d (\gtrsim \Delta)$ by the strong resonance peak in $\text{Im}\chi^s(\omega)$ at $\omega_r \sim 40$ meV in YBCO and $\text{Bi}_2\text{Sr}_2\text{CaCu}_2\text{O}_8$ (BSCCO). We note that $\omega_d \approx \Delta + \omega_r$ and $\omega_r < 2\Delta$. However, the overall gap-like structure in the quasiparticle spectrum remains unchanged around T_c .

Motivated by these experimental facts, various strong-coupling theories of SC fluctuations have been studied to reproduce the pseudo-gap phenomena [87, 89, 51, 88]. Several groups developed the ‘‘FLEX+ T -matrix theory’’, where the normal self-energy correction induced by the strong SC fluctuations, $\Sigma_{\mathbf{k}}^{\text{SCF}}(\epsilon)$, has been self-consistently included into the FLEX approximation. The SC ‘‘amplitude’’ fluctuations are given by

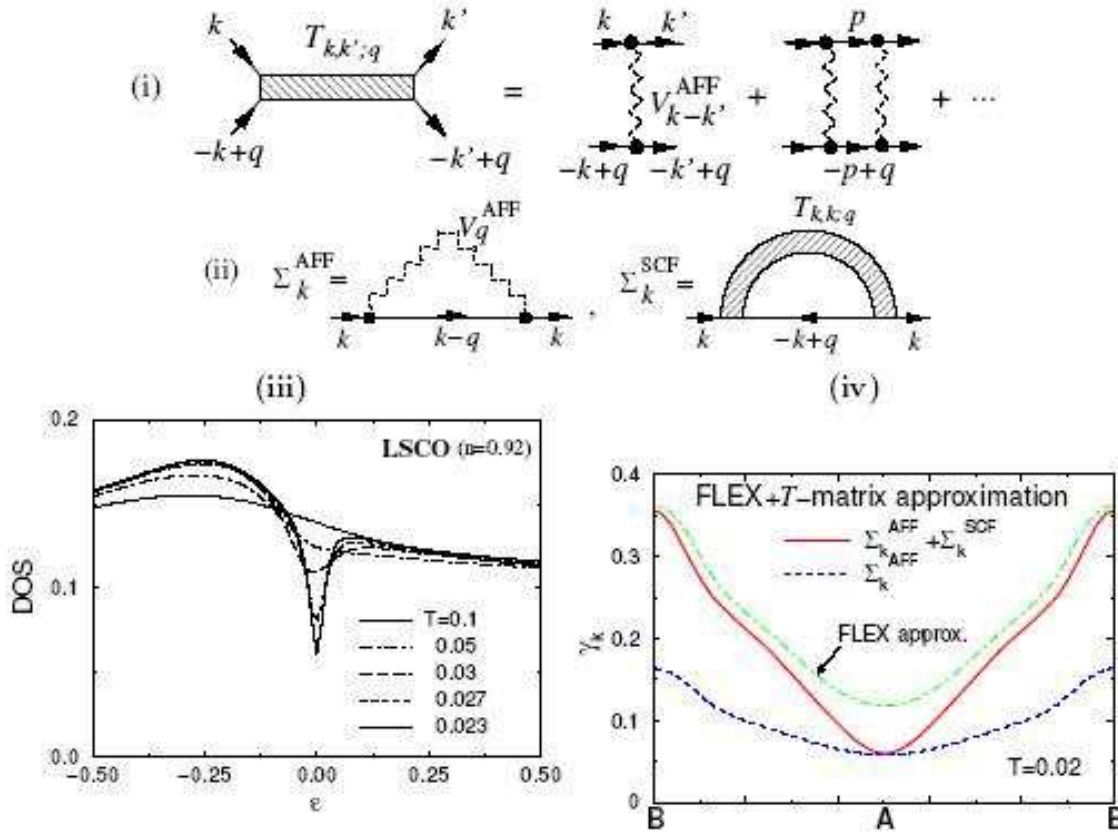


Figure 22. (i) T -matrix induced by the AF fluctuations. (ii) Self-energy $\Sigma_{\mathbf{k}}(\omega)$ in the FLEX+ T -matrix approximation. (iii) DOS given by the FLEX+ T -matrix approximation. The pseudo-gap appears below $T^* \sim 0.04$ due to the strong SC fluctuations. (iv) $\text{Im}\Sigma_{\mathbf{k}}^{\text{AFF}}(-i\delta)$ and $\text{Im}\Sigma_{\mathbf{k}}^{\text{SCF}}(-i\delta)$ given by the FLEX+ T -matrix approximation at $T = 0.02$. For comparison, $\text{Im}\Sigma_{\mathbf{k}}(-i\delta)$ given by the FLEX approximation at $T = 0.02$ is also shown.

the T -matrix (particle-particle scattering amplitude) induced by the AF fluctuations, which prominently increase below T^* [51, 52, 88, 89, 37]. The T -matrix with respect to the AF fluctuations, which is responsible for the Thouless instability for the $d_{x^2-y^2}$ -channel, is given by

$$T_{\mathbf{k},\mathbf{k}';\mathbf{q}}(\epsilon_n, \epsilon_{n'}; \omega_l) = V_{\mathbf{k}-\mathbf{p}}^{\text{AFF}}(\epsilon_n - \epsilon_{n'}) + T \sum_{m,\mathbf{p}} V_{\mathbf{k}-\mathbf{k}'}^{\text{AFF}}(\epsilon_n - \epsilon_m) \times G_{\mathbf{p}}(\epsilon_m) G_{-\mathbf{p}+\mathbf{q}}(-\epsilon_m + \omega_l) T_{\mathbf{p},\mathbf{k}';\mathbf{q}}(\epsilon_m, \epsilon_{n'}; \omega_l), \quad (113)$$

which is shown in Fig. 22 (i). $V_{\mathbf{k}}^{\text{AFF}}$ is given in eq. (15). In the FLEX+ T -matrix approximation, the Green function and the self-energy are given by

$$G_{\mathbf{k}}(\epsilon_n) = [i\epsilon_n + \mu - \epsilon_{\mathbf{k}}^0 - \Sigma_{\mathbf{k}}^{\text{AFF}}(\epsilon_n) - \Sigma_{\mathbf{k}}^{\text{SCF}}(\epsilon_n)]^{-1}, \quad (114)$$

$$\Sigma_{\mathbf{k}}^{\text{AFF}}(\epsilon_n) = \text{eq. (14)},$$

$$\Sigma_{\mathbf{k}}^{\text{SCF}}(\epsilon_n) = T \sum_{\mathbf{q},l} G_{-\mathbf{k}+\mathbf{q}}(-\epsilon_n + \omega_l) T_{\mathbf{k},\mathbf{k};\mathbf{q}}(\epsilon_n, \epsilon_n; \omega_l), \quad (115)$$

where $\Sigma_{\mathbf{k}}^{\text{AFF}}$ and $\Sigma_{\mathbf{k}}^{\text{SCF}}$ are shown in Fig. 22 (ii). In the self-consistent FLEX+ T -matrix approximation, we have to solve eqs. (14), (15), and (113)-(115) self-consistently. Unfortunately, it is very difficult to calculate the T -matrix in eq. (113) since a lot of memory in computer is required. Fortunately, eq. (113) can be simplified by considering only the $d_{x^2-y^2}$ -channel and drop other pairing channels as $T_{\mathbf{k},\mathbf{k}';\mathbf{q}}(\epsilon_n, \epsilon_{n'}; \omega_l) \approx \psi_{\mathbf{k}}(\epsilon_n)\psi_{\mathbf{k}'}(\epsilon_{n'})t_{\mathbf{q}}(\omega_l)$, where $\psi_{\mathbf{k}} \propto \cos k_x - \cos k_y$ [51, 52, 88, 89, 37]. This approximation is expected to be reasonable when the temperature is close to T_c in HTSCs. Then, the \mathbf{k} -dependence of $\Sigma_{\mathbf{k}}^{\text{SCF}}$ becomes $\Sigma_{\mathbf{k}}^{\text{SCF}} \propto T_{\mathbf{k},\mathbf{k};\mathbf{q}} \propto \psi_{\mathbf{k}}^2$.

In the present approximation, T^* is defined as the temperature below which $\Sigma_{\mathbf{k}}^{\text{SCF}}$ takes considerable values. T^* is slightly greater than the T_c^{FLEX} in the FLEX approximation. In a pure 2D system, $T_c = 0$ since the FLEX+ T -matrix theory satisfies the Mermin-Wagner-Hohenberg theorem. T_c becomes finite when weak three-dimensionality is assumed. Sufficiently above T^* , where $\Sigma_{\mathbf{k}}^{\text{SCF}} \approx 0$, the FLEX+ T -matrix theory is equivalent to the FLEX approximation. The obtained DOS and the self-energy are shown in Fig. 22 (iii) and (iv), respectively. Below $T^* \sim 0.04$, a large pseudo-gap structure appears in the FLEX+ T -matrix approximation, due to the cooperation of the real part and the imaginary part of $\Sigma_{\mathbf{k}}^{\text{SCF}}$ [37]. The AF fluctuations are suppressed below T^* in accordance with the pseudo-gap in the DOS [88, 52, 51, 89]. For this reason, $\text{Im}\Sigma_{\mathbf{k}}^{\text{AFF}}(0)$ in the FLEX+ T -matrix approximation is much smaller than $\text{Im}\Sigma_{\mathbf{k}}(0)$ in the FLEX approximation, as recognized in Fig. 22 (iv). Below T_c , the pseudo-gap in the FLEX+ T -matrix approximation smoothly changes to the SC gap [87].

Here, we discuss transport phenomena in the pseudo-gap region. In YBCO [9, 74], Bi2201 and Bi2212 [177], R_H shows a maximum around the pseudo-gap temperature T^* , at which $1/T_1T$ shows the maximum value. Also, the peak temperature of S is nearly equal to T^* in HgBa₂CuO_{4+ δ} [159, 160], LSCO, YBCO [161] and Bi₂Sr₂RCu₂O₈ (R = Ca, Y, Pr, Dy and Er) [162]. As discussed in Ref. [33], these behaviors are naturally understood since both of them are strikingly enhanced by the AF fluctuations above T^* . Therefore, *both R_H and S should decrease below T^* in accordance with the reduction in the AF fluctuation.* This behavior is easily reproduced by the FLEX+ T -matrix method [33, 51]. The obtained ρ , R_H and S for hole-doped systems by using the [FLEX+ T -matrix]+CVC method are shown in Figs. 18 (i), 19 (i), and 21 (i), respectively. In this approximation, $\mathcal{T}_{\mathbf{k},\mathbf{k}'}^{(0)}(\epsilon, \epsilon')$ in eq. (60) is given by $i [\text{cth}\frac{\epsilon'-\epsilon}{2T} + \text{th}\frac{\epsilon'}{2T}] \text{Im}\{V_{\mathbf{k}-\mathbf{k}'}(\epsilon - \epsilon') - T_{\mathbf{k},\mathbf{k};\mathbf{k}-\mathbf{k}'}(\epsilon, \epsilon; \epsilon - \epsilon')\}$, where $T_{\mathbf{k},\mathbf{k};\mathbf{k}-\mathbf{k}'}$ represents the T -matrix in eq. (113). The detailed method of calculation is explained in Ref. [37].

As shown in Figs. 19 (i) and 21 (i), both R_H and S start to decrease below $T^* \sim 0.04$ (~ 160 K) in the FLEX+ T -matrix approximation. These results are consistent with experiments [159, 160, 161]. Figure 18 (i) shows the resistivity given by the FLEX approximation and the FLEX+ T -matrix approximation, both of which are given by including CVCs. As pointed out in Ref. [167], ρ given by the FLEX+CVC method shows a tiny “kink” structure at $\sim T_0$ because of the CVC. This kink structure at $T_0 \sim 0.12$ is experimentally observed in LSCO [185] and YBCO [186]. The kink becomes more prominent in the [FLEX+ T -matrix]+CVC method since the inelastic scattering

is reduced by the formation of the pseudo-gap. As shown in Fig. 22 (iv), $\text{Im}\Sigma_{\mathbf{k}}^{\text{AFF}}(0)$ decreases prominently below T^* , in accordance with the emergence of $\text{Im}\Sigma_{\mathbf{k}}^{\text{SCF}}(0)$. As a result, ρ is approximately proportional to T^2 below T^* . To summarize, ρ , R_{H} and S are suppressed in the pseudo-gap region in the [FLEX+ T -matrix]+CVC method.

According to the FLEX+ T -matrix theory, the SC “amplitude” fluctuations is the origin of the pseudo-gap formation. Other than this scenario, various mechanisms of pseudo-gap formation have been proposed. For example, Kivelson and Emery proposed the SC “phase” fluctuation scenario [178]: they considered that the amplitude of the SC order-parameter develops in the pseudo-gap region, whereas the global phase coherence is absent. Moreover, several hidden-order scenarios, such as d -density wave formation [179], have been proposed. To elucidate the correct scenario, anomalous transport phenomena in the pseudo-gap region are significant and they severely constrain the theories. In the following, we show that the scenario involving SC “amplitude” fluctuations enables us to understand the anomalous transport phenomena below T^* in a unified way.

5.2. Enhancement of Nernst coefficient and magnetoresistance

In contrast to R_{H} and S , the Nernst coefficient ν ($\nu \equiv S_{yx}/H_z = -E_y/H_z \nabla_x T$; off-diagonal thermoelectric power under a magnetic field) prominently increases in the pseudo-gap region by approximately 100 times than that in conventional metals [180, 181, 182]. Moreover, in the pseudo-gap region, the magnetoresistance $\Delta\rho/\rho_0$ increases faster than T^{-4} [75, 76]. Therefore, the modified Kohler’s rule in eq. (106) violates below T^* . Such nontrivial behaviors of ν and $\Delta\rho/\rho_0$ have attracted considerable attention as a key phenomenon closely related to the origin of the pseudo-gap.

Here, we study the Nernst coefficient. According to the linear response theory [165, 166, 39], ν is given by

$$\nu = [\alpha_{xy}/\sigma_{xx} - S\sigma_{xy}/\sigma_{xx}]/H_z, \quad (116)$$

where $\alpha_{xx} = j_x/(-\nabla_x T)$, and $\alpha_{xy} = j_x/(-\nabla_y T)$ is the off-diagonal Peltier conductivity under the magnetic field H_z . In conventional metals with simple Fermi surfaces, ν is small because of an approximate cancellation between the first and the second terms in Eq.(116), which is known as the Sondheimer cancellation. (Sondheimer cancellation is exact only when $\epsilon_{\mathbf{k}}^0 = k^2/2m$.) In HTSCs, however, Sondheimer cancellation is totally violated since α_{xy} is considerably enhanced. That is, α_{xy} is the origin of giant Nernst coefficient in LSCO below T^* and in NCCO below T_0 [180, 181].

In this study, we investigate α_{xy} due to the quasiparticle transport, and find that α_{xy} is prominently enhanced below T^* if we include the CVC caused by SC and AF fluctuations. As a result, $\nu \approx \alpha_{xy}/\sigma_{xx}$ takes a large value below T^* . Moreover, we show that all the transport anomalies below T^* are understood as the quasiparticle transport phenomena in a unified way. Note that Yip showed that the Maki-Thompson-type CVC due to SC fluctuations disappears in d -wave superconductors when the inelastic scatterings are negligible [184]. However, this is inappropriate for HTSC since inelastic

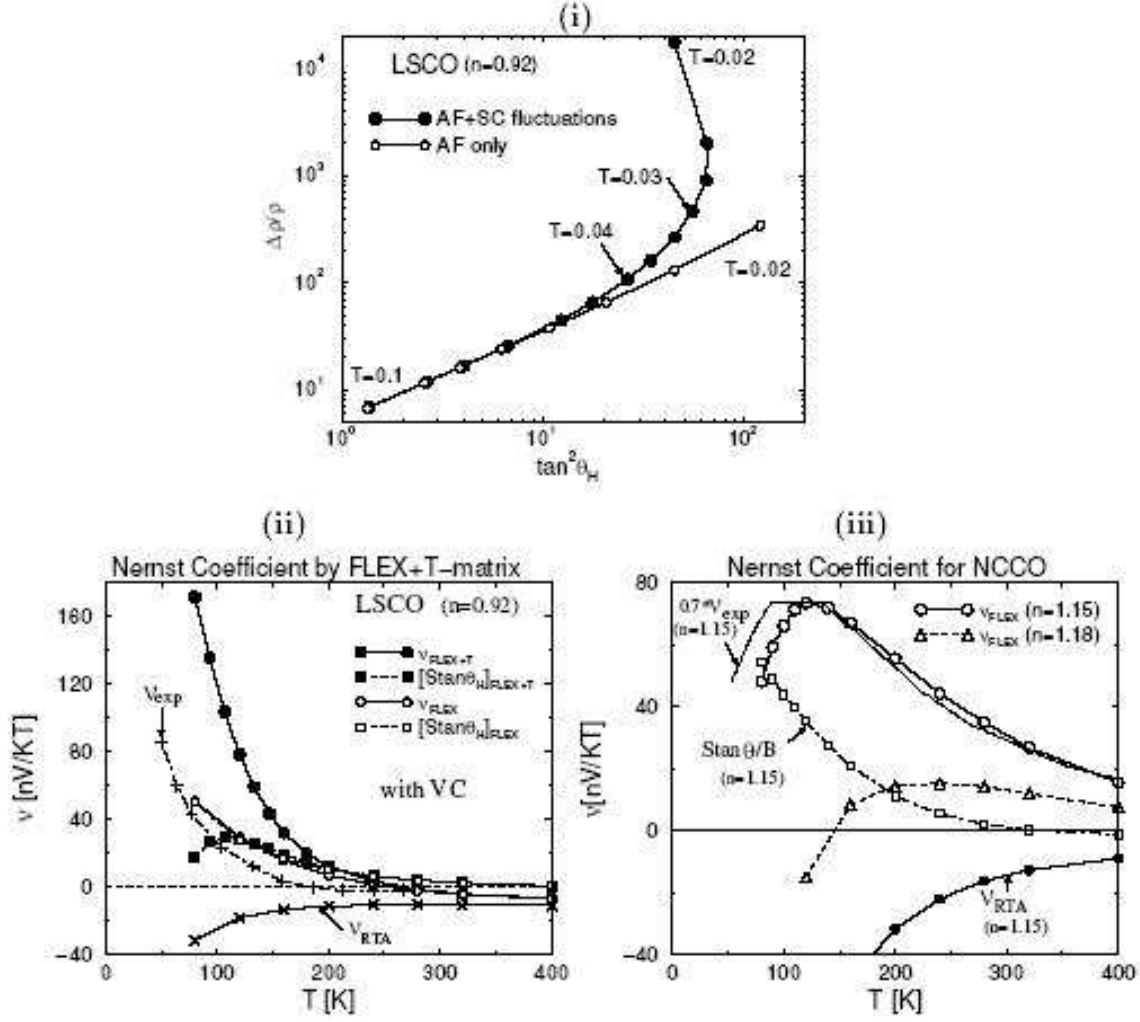


Figure 23. (i) $\Delta\rho/\rho_0$ for LSCO obtained by the [FLEX+ T -matrix]+CVC; The modified Kohler's rule $\Delta\rho/\rho_0 \propto \tan^2\theta_H$ holds above T^* . Below $T^* \sim 0.04$ (~ 160) K, modified Kohler's rule is violated since $\Delta\rho/\rho_0$ increases quite drastically that is caused by the CVC due to AF+SC fluctuations. (ii) ν for LSCO obtained by the [FLEX+ T -matrix]+CVC; the abrupt increase in ν below T^* is caused by the CVC due to AF+SC fluctuations. Experimental data ν_{exp} is cited from [180]. (iii) ν for NCCO is obtained by using the FLEX+CVC approximation. Experimental data ν_{exp} is cited from [7]. [Ref. [32]]

scatterings are much larger than elastic scatterings. We find that the Maki-Thompson type CVC is significant in HTSC.

We note that Ussishkin et al. studied ν induced by short-lived Cooper pairs, which is independent of the quasiparticle lifetime and order $O(\gamma^0)$ [183]. It will be observed in the close vicinity of T_c . However, quasiparticle transport is dominant in good metals where $k_F l \sim E_F/\gamma \gg 1$. (Here, $l = v_{k_F}\tau$ is the mean free path.) In HTSCs, $k_F l = 1$ corresponds to $1700 \mu\Omega\text{cm}$ if we omit the \mathbf{k} -dependence of $l_{\mathbf{k}}$. Therefore, quasiparticle transport will be dominant in slightly under-doped HTSC ($\rho \lesssim 200 \mu\Omega\text{cm}$ above T_c)

for a wide range of temperatures. Hereafter, we show that α_{xy} due to quasiparticle transport is strongly enhanced by the CVC.

According to the microscopic Fermi liquid theory, α_{xy} is given by the correlation function between the heat current and the charge current in the presence of $H_z \neq 0$. Therefore, α_{xy} is given by eq. (50) by replacing j_μ with j_μ^Q . After the analytic continuation, the exact expression for α_{xy} of the order γ^{-1} is given by [39]

$$\alpha_{xy} = H_z \cdot \frac{e^2}{T} \sum_{\mathbf{k}} \int \frac{d\epsilon}{2\pi} \left(-\frac{\partial f^0}{\partial \epsilon} \right) |\text{Im}G_{\mathbf{k}}^R(\epsilon)| |G_{\mathbf{k}}^R(\epsilon)|^2 \times |\vec{v}_{\mathbf{k}}(\epsilon)| \gamma_{\mathbf{k}}(\epsilon) A_{\mathbf{k}}(\epsilon), \quad (117)$$

$$A_{\mathbf{k}}(\epsilon) = \left(\vec{Q}_{\mathbf{k}}(\epsilon) \times \frac{\partial \vec{L}_{\mathbf{k}}(\epsilon)}{\partial k_{\parallel}} \right)_z, \quad (118)$$

$$\vec{Q}_{\mathbf{k}}(\epsilon) = \vec{q}_{\mathbf{k}}(\epsilon) + \sum_{\mathbf{k}'} \int \frac{d\epsilon'}{4\pi i} \mathcal{T}_{\mathbf{k},\mathbf{k}'}^{(0)}(\epsilon, \epsilon') |G_{\mathbf{k}'}^R(\epsilon')|^2 \vec{Q}_{\mathbf{k}'}(\epsilon'), \quad (119)$$

where $\vec{L}_{\mathbf{k}}(\epsilon) = \vec{J}_{\mathbf{k}}(\epsilon)/\gamma_{\mathbf{k}}(\epsilon)$, $\vec{q}_{\mathbf{k}}(\epsilon) = \epsilon \cdot \vec{v}_{\mathbf{k}}$ is the quasiparticle heat velocity, and $\vec{Q}_{\mathbf{k}}(\epsilon)$ is the total heat current [39, 37]. We stress that the CVC term in eq. (119) vanishes if we omit the energy dependence of $\mathcal{T}_{\mathbf{k},\mathbf{k}'}^{(0)}(\epsilon, \epsilon')$. This fact means that the heat CVC is small and thus $\vec{Q}_{\mathbf{k}}(\epsilon) \sim \vec{q}_{\mathbf{k}}(\epsilon)$ in general cases [39, 37]. In the FLEX+ T -matrix approximation, $\mathcal{T}_{\mathbf{k},\mathbf{k}'}^{(0)}(\epsilon, \epsilon')$ is given by $i [\text{cth} \frac{\epsilon' - \epsilon}{2T} + \text{th} \frac{\epsilon'}{2T}] \text{Im}\{V_{\mathbf{k}-\mathbf{k}'}(\epsilon - \epsilon') - T_{\mathbf{k},\mathbf{k};\mathbf{k}-\mathbf{k}'}(\epsilon, \epsilon; \epsilon - \epsilon')\}$.

In contrast to R_H and S , the Nernst coefficient ν [180, 181] and $\Delta\rho/\rho_0$ [75, 76, 12] in LSCO rapidly increase below T^* . These experimental facts are also reproduced by the [FLEX+ T -matrix]+CVC method as shown in Fig. 23 (i) and (ii). Since R_H decreases whereas $\Delta\rho/\rho_0$ increases drastically below T^* , the plot of $\Delta\rho/\rho_0$ as a function of $\tan^2 \theta_H$ forms an ‘‘inverse S-shape’’. Therefore, the modified Kohler’s rule is completely violated below T^* . This result is very similar to the experimental results provided in Ref. [12]. Next, we discuss ν in NCCO using the FLEX (not the FLEX+ T -matrix) approximation since SC fluctuations is considered to be absent in NCCO. The obtained ν is shown in Fig. 23 (iii); it takes a large value only when the CVC due to the AF fluctuations are considered. In NCCO, ν increases gradually as T decreases, and it starts to decrease below the maximum temperature of 120 K. The obtained behaviors of ν are semiquantitatively consistent with the experimental results [7]. Therefore, the present numerical study can explain the experimental behaviors of ν and $\Delta\rho/\rho_0$ in HTSCs both above and below T^* .

Here, we explain a theoretical reason why ν is enhanced in both LSCO and NCCO: $A_{\mathbf{k}}$ in eq. (118) can be rewritten as

$$A_{\mathbf{k}} = Q_{\mathbf{k}} L_{\mathbf{k}} (\partial \theta_{\mathbf{k}}^J / \partial k_{\parallel}) \cos(\theta_{\mathbf{k}}^J - \theta_{\mathbf{k}}^Q) + Q_{\mathbf{k}} (\partial L_{\mathbf{k}} / \partial k_{\parallel}) \sin(\theta_{\mathbf{k}}^J - \theta_{\mathbf{k}}^Q), \quad (120)$$

where $\theta_{\mathbf{k}}^J = \tan^{-1}(J_{ky}/J_{kx})$, $\theta_{\mathbf{k}}^Q = \tan^{-1}(Q_{ky}/Q_{kx})$, and $L_{\mathbf{k}} = J_{\mathbf{k}}/\gamma_{\mathbf{k}}$ is the mean free path with CVC. In the RTA, the heat current is given by $\vec{q}_{\mathbf{k}} = \epsilon \cdot \vec{v}_{\mathbf{k}}$. Since $\theta_{\mathbf{k}}^v = \theta_{\mathbf{k}}^q$, the second term is absent in the RTA. If one includes the CVC, $\vec{Q}_{\mathbf{k}}$ is not parallel to $\vec{J}_{\mathbf{k}}$ because the CVC for $\vec{q}_{\mathbf{k}}$ is usually small (i.e., $\vec{Q}_{\mathbf{k}} \sim \vec{q}_{\mathbf{k}}$) as we will discuss below [39, 37]. Therefore, we obtain $\theta_{\mathbf{k}}^J \neq \theta_{\mathbf{k}}^Q$. In this case, the second term gives rise to an

enhancement of ν if $L_{\mathbf{k}}$ is highly anisotropic around the cold spot. Figure 17 (ii) shows $L_{\mathbf{k}}$ in LSCO given by the FLEX+CVC approximation. We can see that $\partial L_{\mathbf{k}}/\partial k_{\parallel}$ takes a large value near the cold spot below $T = 0.02$. (Note that $\partial L_{\mathbf{k}}/\partial k_{\parallel} = 0$ just at point A.) This is the origin of increment in ν_{FLEX} in Fig. 23 (ii). As shown in Fig. 23 (iii), ν_{FLEX} for NCCO is much larger than ν_{FLEX} for LSCO: One reason is that the anisotropy of $L_{\mathbf{k}}^{\text{FLEX}}$ in NCCO is greater since $\xi_{\text{AF}} \gg 1$ in NCCO. Another reason is that $\gamma_{\mathbf{k}}^{-1} (\propto \nu)$ in NCCO is larger than that in LSCO. For these reasons, FLEX+CVC method can explain the huge ν observed in NCCO.

Next, we consider the increment of ν in the pseudo-gap region in LSCO using the FLEX+ T -matrix method, which is shown as $\nu_{\text{FLEX}+T}$ in Fig. 23 (ii). The CVC due to SC fluctuations (Maki-Thompson term) represents the acceleration of quasiparticles caused by the short-lived Cooper pairs. Since HTSCs are $d_{x^2-y^2}$ -wave superconductors, the CVC due to the SC fluctuations magnifies $J_{\mathbf{k}}$ except at the nodal point (point A in Fig. 14). In fact, when the Ginzburg-Landau correlation length is longer than ξ_{AF} , the total current in the FLEX+ T -matrix approximation is approximately given by [37]

$$\vec{J}_{\mathbf{k}} \approx (1 + h_{\mathbf{k}}) \frac{\vec{v}_{\mathbf{k}} + \alpha_{\mathbf{k}} \vec{v}_{\mathbf{k}^*}}{1 - \alpha_{\mathbf{k}}^2}, \quad (121)$$

$$h_{\mathbf{k}} \equiv \text{Im}\Sigma_{\mathbf{k}}^{\text{SCF}}(0)/\text{Im}\Sigma_{\mathbf{k}}^{\text{AFF}}(0), \quad (122)$$

where $a_{\mathbf{k}} = (1 - c\xi_{\text{AF}}^{-2})$ has been introduced in eq. (77). $h_{\mathbf{k}}$ represents the enhancement factor due to SC fluctuations. The anisotropy of $L_{\mathbf{k}} = |\vec{J}_{\mathbf{k}}/\gamma_{\mathbf{k}}|$ becomes considerably prominent below T^* since $\text{Im}\Sigma_{\mathbf{k}}^{\text{SCF}}(0) \propto \psi_{\mathbf{k}}^2$ increases whereas $\text{Im}\Sigma_{\mathbf{k}}^{\text{AFF}}(0)$ decreases below T^* as shown in Fig. 22 (iv). For this reason, the second term in eq. (120) takes a large value in the neighborhood of the point A, as explained in Ref. [37]. Thus, [FLEX+ T -matrix]+CVC method can explain the rapid increment in ν in LSCO below T^* .

If the AF fluctuations are absent, $\theta_{\mathbf{k}}^J = \theta_{\mathbf{k}}^Q = \theta_{\mathbf{k}}^v$ even if the CVC due to SC fluctuations are taken into account. Therefore, to explain the enhancement in ν in the pseudo-gap region, we have to include CVCs due to both the AF fluctuations and SC fluctuations. In contrast, R_{H} decreases below T^* in proportion to ξ_{AF}^2 since the second term in eq. (120) is absent if we replace $\vec{Q}_{\mathbf{k}}$ with $\vec{J}_{\mathbf{k}}$.

Finally, we explain why the heat CVC is usually small. As we have explained, the CVC represents the current of the Fermi sea that is transferred from the excited quasiparticles by the electron-electron scattering. The charge CVC can be large because of the momentum conservation law. However, the heat current $\vec{q}_{\mathbf{k}} = (\epsilon_{\mathbf{k}}^0 - \mu)\vec{v}_{\mathbf{k}}$ is not conserved even in the free dispersion model, that is, $\vec{q}_{\mathbf{k}} + \vec{q}_{\mathbf{k}'} \neq \vec{q}_{\mathbf{k}+\mathbf{q}} + \vec{q}_{\mathbf{k}'-\mathbf{q}}$ even if $\epsilon_{\mathbf{k}}^0 + \epsilon_{\mathbf{k}'}^0 = \epsilon_{\mathbf{k}+\mathbf{q}}^0 + \epsilon_{\mathbf{k}'-\mathbf{q}}^0$. For this reason, the heat CVC is small in general, and therefore the thermal conductivity κ is finite even if the Umklapp process is absent: In a 3D free dispersion model, $\kappa = (9/8)\kappa^{\text{RTA}}$ within the second-order perturbation theory with respect to U [39]. The heat CVC is also small in nearly AF metals: Since the direction of the heat CVC due to the quasiparticle at $\mathbf{k} + \mathbf{q}$ in Fig. 8 (the MT term) depends on the sign of $\epsilon_{\mathbf{k}+\mathbf{q}}^0 - \mu$, the heat CVC becomes small due to cancellation after the \mathbf{q} -summation for $|\mathbf{q} - \mathbf{Q}| \lesssim \xi_{\text{AF}}^{-1}$.

5.3. Summary of this section

In conclusion, we studied ρ , R_H , $\Delta\rho/\rho_0$, S and ν in HTSCs using the FLEX+ T -matrix approximation. The results are shown in Figs. 18 (i), 19 (i), 21 (i), and 23 (i)-(ii). We can explain that (i) R_H and S start to decrease below T^* , (ii) ρ starts to deviate from the T -linear behavior at T_0 , and it is approximately proportional to T^2 below T^* . Moreover, (iii) ν and $\Delta\rho/\rho$ further increase below T^* . Therefore, the present study gives us a unified understanding of the various anomalous transport phenomena in both below and above T^* .

This study provides strong evidence that the SC fluctuations are predominant in the pseudo-gap region. The striking increment in ν below T^* is a cooperative phenomenon between the d-wave SC fluctuations and AF fluctuations. We stress that the RTA cannot explain the enhancement of ν since the second term in eq. (120) vanishes identically in the RTA. Further, a very large Nernst signal appears also in electron-doped systems, which starts to increase in proportion to T^{-1} below $T_0 \sim 600$ K. This experimental fact is reproduced by the CVC due to the AF-fluctuations, even in the absence of SC fluctuations. In §5.2, we found that the origin of rapid increment in ν is the second term of eq. (120), which emerges only when the CVC is included. In NCCO (and CeMIn₅), ν starts to increase below T_0 because of the CVC due to strong AF fluctuations; $\xi_{AF} \gg 1$. In LSCO, on the other hand, increment in ν below T_0 is small since ξ_{AF} is of order 1; ν in LSCO starts to increase rapidly below $T^* \ll T_0$, with the aid of the strong SC fluctuations.

Here, we comment on the transport phenomena in Nd-doped LSCO, La_{1.4-x}Nd_{0.6}Sr_xCuO₄, which shows the static stripe ordered phase at $T_{st} \sim 80$ K [187]. In this compound, ρ increases whereas R_H decreases monotonically below T_{st} , which indicates that the system becomes one-dimensional due to the stripe order. This experimental fact might tempt us to consider that the stripe order is the origin of the reduction in R_H in other HTSCs in the pseudo-gap region. However, the stripe order scenario cannot explain the reduction in ρ nor increment in ν below T^* . On the other hand, the overall transport phenomena in HTSCs can be explained by considering the CVCs due to AF+SC fluctuations.

In this section, we explained that the pseudo-gap behaviors in ρ and R_H originate from the reduction of AF fluctuations, and the pseudo-gap behavior of ν reflects the increment of SC fluctuations. The pseudo-gap temperature determined by ρ , T_ρ^* , is larger than T_{RH}^* and T_ν^* determined by R_H and ν , respectively. Recently, impurity (Zn) effect on the pseudo-gap behavior in YBCO was studied [188], and found that T_ρ^* and T_{RH}^* are independent of impurities, whereas T_ν^* decreases with Zn-doping in parallel to T_c . It is an important future problem to show whether these experimental facts can be explained by the FLEX+ T -matrix approximation or not. In §7, we will show that the CVC due to fluctuations is usually sensitive to the impurities. Therefore, to reconcile this problem, we have to study the impurity effect on the CVC seriously.

It should be noted that ν takes a very large value in the vortex-liquid state above

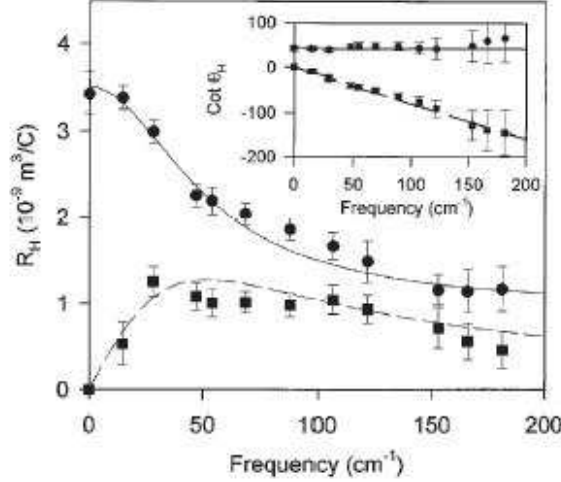


Figure 24. $R_H(\omega)$ in optimally-doped YBCO at 95 K, derived from Faraday rotation. The closed circles and squares represent experimental values of $\text{Re}R_H(\omega)$ and $\text{Im}R_H(\omega)$, respectively. [Ref. [192]]

H_{c1} in a clean 2D sample, reflecting the high mobility of the vortices. Therefore, ν is frequently used as a sensitive probe for the mixed state. Based on his observation, Ong *et al.* proposed that spontaneous vortex-antivortex pairs emerge in under-doped systems below T^* , and they govern the transport phenomena in the pseudo-gap region [180]. However, this assumption seems to contradict with the other transport coefficients; for example, the flux-flow resistance does not appear below T^* .

6. AC transport phenomena in HTSCs

In previous sections, we discussed the DC transport phenomena in nearly AF metals, and found that the CVC produces various non-Fermi-liquid-like behaviors. In principle, the AC transport phenomena can yield further useful and decisive information about the electronic status. Unfortunately, the measurements of the AC transport coefficients are not common because of the difficulty in their observations, except for the optical conductivity $\sigma_{xx}(\omega)$ measurements.

Fortunately, Drew's group has performed intensive measurements of the AC Hall coefficient $R_H(\omega) = \sigma_{xy}(\omega)/\sigma_{xx}^2(\omega)$ in YBCO [189, 190, 191, 192], BSCCO [193], LSCO [194], and PCCO [195]. They found that the ω -dependence of $R_H(\omega)$ in HTSC shows amazing non-Fermi-liquid-like behaviors, which have been a big challenge for researchers for a long time. Here, we show that this crucial experimental constraint is well satisfied by the numerical study using the FLEX+CVC method.

In the RTA, both $\sigma_{xx}(\omega)$ and $\sigma_{xy}(\omega)$ in a single-band model will follow the following "extended Drude forms":

$$\sigma_{xx}^{\text{RTA}}(\omega) = \Omega_{xx}(2\gamma_0(\omega) - iz^{-1}\omega)^{-1}, \quad (123)$$

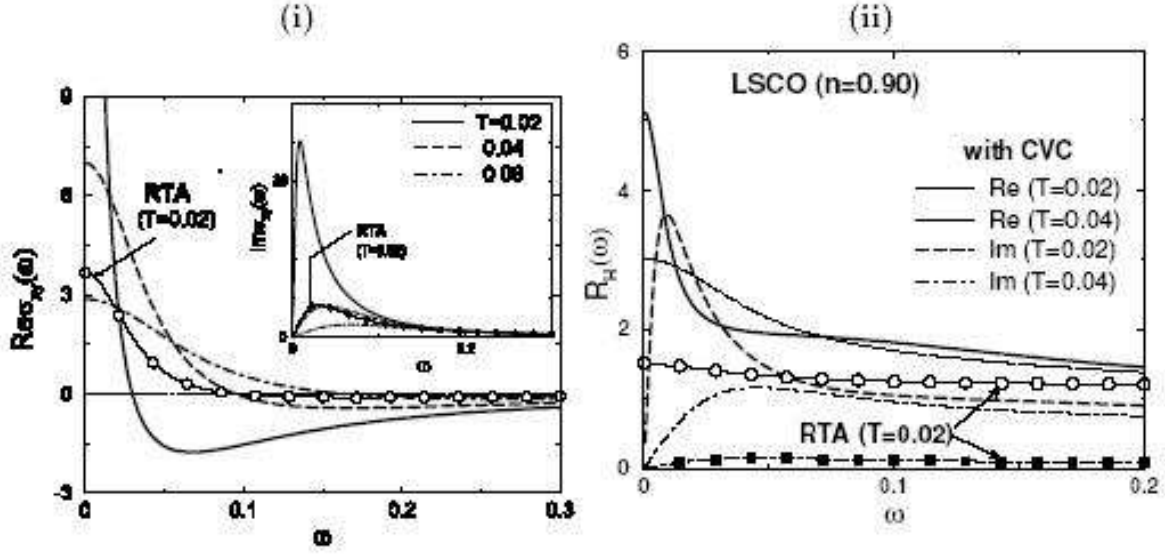


Figure 25. (i) $\sigma_{xy}(\omega)$ and (ii) $R_H(\omega)$ for LSCO ($n = 0.9$, $U = 5$) given by the FLEX+CVC method. $\omega = 0.1$ corresponds to $\sim 300\text{cm}^{-1}$. Because of the CVC, $\sigma_{xy}(\omega) \gg \sigma_{xy}^{\text{RTA}}(\omega)$ at low frequencies. [Ref. [196]]

$$\sigma_{xy}^{\text{RTA}}(\omega) = \Omega_{xy}(2\gamma_0(\omega) - iz^{-1}\omega)^{-2}, \quad (124)$$

where z^{-1} is the mass-enhancement factor and $\gamma_0(\omega)$ is the ω -dependent damping rate in the optical conductivity, which is approximately given by $\gamma_0(\omega) \approx (\gamma_{\text{cold}}(\omega/2) + \gamma_{\text{cold}}(-\omega/2))/2$ for small ω . According to the spin fluctuation theory [56], $\gamma_0(\omega) \propto \max\{\omega/2, \pi T\}$, which is observed by the optical conductivity measurements. The ω -dependence of z is important in heavy-fermion systems ($1/z \gg 1$ at $\omega = 0$), whereas it will not be so important in HTSC since $1/z$ is rather small. Expressions (123) and (124) are called the “extended Drude form”. Within the RTA, the AC-Hall coefficient is independent of ω even if the ω -dependence of z is considered:

$$R_H^{\text{RTA}}(\omega) = \Omega_{xy}/\Omega_{xx}^2 \sim 1/ne. \quad (125)$$

Very interestingly, Drew’s group has revealed that $R_H(\omega)$ in HTSC decreases drastically with ω : as shown in Fig. 24, $\text{Im}R_H(\omega)$ shows a peak at $\sim \omega_0 = 50 \text{ cm}^{-1}$ in optimally-doped YBCO [192]. Moreover, $\text{Im}R_H(\omega)$ is as large as $\text{Re}R_H(\omega)$ for $\omega \gtrsim \omega_0$, as a consequence of the Kramers-Kronig relation between $\text{Re}R_H(\omega)$ and $\text{Im}R_H(\omega)$. Such a large ω -dependence of R_H cannot be explained by the RTA, even if one assume an arbitrary (\mathbf{k}, ω) -dependence of the quasiparticle damping rate $\gamma_{\mathbf{k}}(\omega)$. Therefore, the AC-Hall effect severely constrains the theories involving the normal state of HTSCs.

Recently, we studied both $\sigma_{xx}(\omega)$ and $\sigma_{xy}(\omega)$ in HTSC using the FLEX+CVC method, by performing the analytic continuation of eqs. (51) and (53) using the Pade approximation [196, 197]. Since the ω -dependence of the CVC is correctly considered, the obtained $\sigma_{xx}(\omega)$ and $\sigma_{xy}(\omega)$ satisfy the f -sum rule very well — $\int_0^\infty \text{Re}\sigma_{xx}(\omega)d\omega = \pi e^2 \sum_{\mathbf{k}} (\partial^2 \epsilon_{\mathbf{k}}^0 / \partial k_x^2) n_{\mathbf{k}}$ and $\int_0^\infty \text{Re}\sigma_{xy}(\omega)d\omega = 0$; the relative error is less than 2.5% [196].

Note that a useful f -sum rule for the Hall angle has been derived in Ref. [198]. The obtained numerical results are shown in Fig. 25. We find that (a) $\sigma_{xx}(\omega) \approx \sigma_{xx}^{\text{RTA}}(\omega)$ follows eq. (123), by substituting $\gamma_0(\omega) = (\gamma_{\text{cold}}(\omega/2) + \gamma_{\text{cold}}(-\omega/2))/2$. Therefore, the reduction in the Drude weight in $\sigma_{xx}(\omega)$ due to the CVC is small within the FLEX+CVC method. However, we stress that the f -sum rules for both $\sigma_{xx}^{\text{RTA}}(\omega)$ and $\sigma_{xy}^{\text{RTA}}(\omega)$ do not hold since the CVC is ignored [196]. (b) $R_{\text{H}}^{\text{RTA}}(\omega)$ is a nearly real constant of the order $1/ne$ since $[\sigma_{xx}^{\text{RTA}}(\omega)]^2 \propto \sigma_{xy}^{\text{RTA}}(\omega)$ is well satisfied. (c) $\sigma_{xy}(\omega)$ obtained using the FLEX+CVC method completely deviates from the extended Drude forms in eq. (124). The effect of CVC on $\sigma_{xy}(\omega)$ is very large for the far-infrared region $\omega \lesssim 0.03$ ($\sim 100\text{cm}^{-1}$), since the CVC due to AF fluctuations is strong for $\omega \lesssim \omega_{\text{sf}} \sim T$. Therefore, $\sigma_{xy}(\omega)$ and $R_{\text{H}}(\omega)$ obtained using the FLEX+CVC method show striking ω -dependences as shown in Fig. 25. In Fig. 25 (i), the peak frequency of $\text{Im}\sigma_{xy}(\omega)$, ω_{xy} , is six times less than that of $\text{Im}\sigma_{xx}(\omega)$, ω_{xx} , which is consistent with experiments. This fact cannot be explained by using the extended Drude form.

Here, we analyze a qualitative ω -dependence of $\sigma_{xy}(\omega)$ by considering the ω -dependence of the CVC. The Bethe-Salpeter equation for $\omega \neq 0$ is given by

$$\begin{aligned} \vec{J}_{\mathbf{k}}(\epsilon; \omega) &= \vec{v}_{\mathbf{k}} + \int \frac{d\epsilon'}{4\pi i} \sum_{\mathbf{k}'\mathbf{q}} \mathcal{T}_{\mathbf{k},\mathbf{k}+\mathbf{q}}^{(0)}(\epsilon, \epsilon'; \omega) \\ &\quad \times G_{\mathbf{k}+\mathbf{q}}^R(\epsilon' + \omega/2) G_{\mathbf{k}+\mathbf{q}}^A(\epsilon' - \omega/2) \vec{J}_{\mathbf{k}+\mathbf{q}}(\epsilon'; \omega), \end{aligned} \quad (126)$$

which is equivalent to eq. (60) when $\omega = 0$. A simplified Bethe-Salpeter equation for $\omega = 0$ is given in eq. (78). Here, we extend eq. (78) to the case of $\omega \neq 0$. By noticing the relationship $G_{\mathbf{k}+\mathbf{q}}^R(\epsilon' + \omega/2) G_{\mathbf{k}+\mathbf{q}}^A(\epsilon' - \omega/2) \approx \pi \rho_{\mathbf{k}}(\epsilon') \cdot 2/(2\gamma_{\mathbf{k}} - i\omega z^{-1})$, eq. (126) is simplified for $|\omega| \ll \gamma$ as

$$\vec{J}_{\mathbf{k}}(\omega) = \vec{v}_{\mathbf{k}} + \frac{\alpha_{\mathbf{k}} \cdot 2\gamma_{\mathbf{k}}}{2\gamma_{\mathbf{k}} - i\omega z^{-1}} \vec{J}_{\mathbf{k}^*}(\omega), \quad (127)$$

where $(1 - \alpha_{\mathbf{k}})^{-1} \propto \xi_{\text{AF}}^2$. In deriving eq. (127), we assumed that the ϵ -dependence of $\chi_{\mathbf{q}}^s(\epsilon + i\delta)$ is small for $|\epsilon| < \gamma$. The solution of eq. (127) is given by

$$\vec{J}_{\mathbf{k}} = \frac{(2\gamma - i\omega z^{-1})^2}{(2\gamma - i\omega z^{-1})^2 - (\alpha_{\mathbf{k}} \cdot 2\gamma)^2} \left[\vec{v}_{\mathbf{k}} + \frac{\alpha_{\mathbf{k}} \cdot 2\gamma}{2\gamma - i\omega z^{-1}} \vec{v}_{\mathbf{k}^*} \right], \quad (128)$$

which is equivalent to eq. (79) when $\omega = 0$. Similar to the derivation of eq. (96), we get

$$\vec{J}_{\mathbf{k}} \times \frac{\partial \vec{J}_{\mathbf{k}}}{\partial k_{\parallel}} = \frac{(2\gamma - i\omega z^{-1})^2}{(2\gamma - i\omega z^{-1})^2 - (\alpha \cdot 2\gamma)^2} \cdot \vec{v}_{\mathbf{k}} \times \frac{\partial \vec{v}_{\mathbf{k}}}{\partial k_{\parallel}}. \quad (129)$$

As a result, $\sigma_{xy}(\omega)$ for $\omega \ll \gamma_0$ is approximately given by

$$\begin{aligned} \sigma_{xy}(\omega)/H_z &= e^3 \oint_{\text{FS}} \frac{dk_{\parallel}}{(2\pi)^2} \frac{1}{(2\gamma - i\omega z^{-1})^2} \left(\vec{J}_{\mathbf{k}} \times \frac{\partial \vec{J}_{\mathbf{k}}}{\partial k_{\parallel}} \right)_z \\ &\approx \frac{\Omega_{xy}}{((1 - \alpha_{\mathbf{k}})2\gamma_0 - i\omega z^{-1})((1 + \alpha_{\mathbf{k}})2\gamma_0 - i\omega z^{-1})}. \end{aligned} \quad (130)$$

If we omit the CVC (i.e., $\alpha_{\mathbf{k}} = 0$), eq. (130) is equivalent to the extended Drude form in eq. (124). According to eq. (130), the solution of $\text{Re}\sigma_{xy}(\omega_0) = 0$ is given by

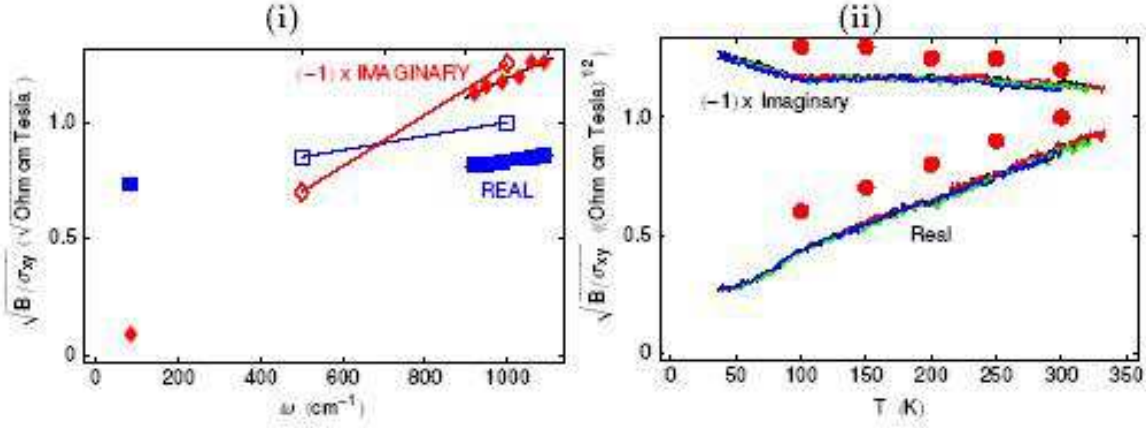


Figure 26. (i) ω -dependence of $\sqrt{B/\sigma_{xy}}$ in BSCCO at 300K. Open squares and diamonds represent real and imaginary part of theoretical result given by the FLEX+CVC method. (ii) $\sqrt{B/\sigma_{xy}}$ in optimally-doped BSCCO at 950 cm^{-1} . The solid dots represent the result of the FLEX+CVC method. [Ref. [193]]

$\omega_0 = 2\sqrt{1 - \alpha_{\mathbf{k}}^2}z\gamma$, which is much smaller than the solution obtained from the RTA; $\omega_0^{\text{RTA}} = 2z\gamma$. This analytical result can be recognized in the numerical result shown in Fig. 25. As a result, the striking ω -dependence of $R_{\text{H}}(\omega)$ in HTSCs for $|\omega| < \gamma_0$ can be explained by including the CVC.

Furthermore, the effect of CVC is still large even for the infrared region $\omega \lesssim 0.3$ ($\sim 1000\text{cm}^{-1}$), which is consistent with the experimental results. This fact requires the satisfaction of the f -sum rule, $\int_0^\infty d\omega \sigma_{xy}(\omega) = 0$, since the DC σ_{xy} is significantly enhanced. Schmadel et al. [193] observed $\sigma_{xy}(\omega)$ in optimally doped BSCCO for a wide range of ω ($\leq 0.3 \sim 1000\text{cm}^{-1}$), and found that $\sigma_{xy}(\omega)$ follows a “simple Drude form”; $\sigma_{xy} \propto (2\gamma_{xy} - iz\omega)^{-2}$, where ω -dependence of γ_{xy} is much smaller than $\gamma_0(\omega)$ and $\gamma_{xy} \ll \gamma_0(0)$. The experimental ω -dependence of $\sqrt{B/\sigma_{xy}}$ as well as theoretical result are shown in Fig. 26 (i). Moreover, Fig. 26 (ii) shows that $\text{Re}\{\sigma_{xy}^{-1/2}\} \propto \gamma_{xy}$ depends on T sensitively. Therefore, γ_{xy} is independent of ω in the infrared region. In terms of the RTA, this experimental result highly contradicts the fact that γ_0 is independent of T for $\omega \gg T$; $\gamma_0 \propto \max\{\omega, \pi T\}$. This mysterious behavior is well reproduced by the FLEX+CVC method, as indicated by the solid dots in Fig. 26 (ii). This numerical result suggests that the effect of the ω -dependence of $\gamma_0(\omega)$ on the AC-Hall conductivity, by which $\sigma_{xy}^{\text{RTA}}(\omega)$ deviates from the simple Drude form, approximately cancels with that of the CVC.

Interestingly, the Hall angle $\theta_{\text{H}}(\omega) = \sigma_{xy}(\omega)/\sigma_{xx}(\omega)$ follows an approximate simple Drude form in both YBCO [190] and LSCO [194] — $\theta_{\text{H}}(\omega) \propto (2\gamma_{\text{H}} - iz\omega)^{-1}$ with an ω -independent constant $\gamma_{\text{H}} \propto T^{-n}$ ($n = 1.5 \sim 2$). [Exactly speaking, both σ_{xy} and θ_{H} cannot follow the simple Drude forms at the same time when σ_{xx} exhibits an extended Drude form.] This experimental fact has also been theoretically reproduced [196]. Therefore, the anomalous (ω, T) -dependences of $\sigma_{xy}(\omega)$ and $R_{\text{H}}(\omega)$ in HTSCs can

be semiquantitatively explained by the FLEX+CVC method — a microscopic theory without any fitting parameters except for U . At the present stage, the FLEX+CVC method is the only theory with the capability to explain the anomalous AC and DC transport coefficients in a unified way. We briefly comment on the carrier-doping dependence of $\Omega_H \equiv -\omega/\text{Im}\{\theta_H^{-1}(\omega)\}$: The experimental value of Ω_H/H_z for optimally-doped YBCO ($n \sim 0.85$) is 0.15 [$\text{cm}^{-1}T^{-1}$] and it increases to 0.3 [$\text{cm}^{-1}T^{-1}$] in slightly under-doped YBCO and BSCCO ($n \sim 0.9$). This experimental doping dependence can be quantitatively reproduced by using the FLEX+CVC method for $n \leq 0.9$ [196]. However, this method cannot explain the large experimental value $\Omega_H/H_z \approx 0.5$ [$\text{cm}^{-1}T^{-1}$] in heavily under-doped YBCO ($T_c = 0$) [189]. This experimental fact will give us an important hint to understand the essential electronic properties in heavily under-doped HTSCs.

Recently, the infrared Hall coefficient in PCCO ($\delta = 0.12 \sim 0.18$) was measured for $\omega = 1000 \sim 3000 \text{ cm}^{-1}$ [195]. The observed ω -dependences for $\delta \leq 0.15$ cannot be explained by simple extended Drude models. They show that the experimental results can be understood by assuming a SDW gap $\Delta_{\text{SDW}} \sim 1000 \text{ cm}^{-1}$. It is an important future problem to study the role of the CVC in the infrared Hall coefficient in PCCO.

7. Impurity effects in nearly AF metals

In earlier sections, we studied the transport phenomena in nearly AF metals without randomness. By including CVCs, we succeeded in explaining the anomalous DC and AC transport phenomena in a unified way, in both hole- and the electron-doped HTSCs. However, we have neglected the impurity or disorder effects on the transport phenomena, although they are prominent in real under-doped HTSCs. In fact, the residual resistivity due to disorder increases drastically as the system approaches the half-filling [156]. Moreover, STM/STS measurements revealed that the electronic states in under-doped HTSCs are highly inhomogeneous at the nanoscale, reflecting the random potential induced by the disordered atoms outside of the CuO_2 plane [199]. These experimental facts are reproduced by assuming that the SC pairing potential is strongly influenced by the impurity potential [200, 201]

Further, the anomalous transport phenomena near the AF QCP are sensitive to randomness. For example, within the Born approximation, the CVC due to electron-electron interaction vanishes at zero temperature since only elastic scattering exists at $T = 0$. In fact, the CVC term in eq. (75) vanishes at $T = 0$ if we replace $\gamma_{\mathbf{k}+\mathbf{q}}$ with $\gamma^{\text{imp}} \neq 0$. However, the Born approximation is applicable only when the impurity potential is weak. In fact, we will show that a “strong” local impurity potential in under-doped HTSCs induces drastic and widespread changes in the electron-electron correlation around the impurity site. Thus, the impurity effect in HTSCs depends on the strength of the impurity potential. Hereafter, we study the nontrivial impurity effects in nearly AF Fermi liquids.

7.1. Hall coefficient in the presence of weak local impurities

First, we study the effect of “weak local impurities” on the transport phenomena within the Born approximation, where the quasiparticle damping rate due to impurity scattering is given by

$$\gamma^{\text{imp}} = n_{\text{imp}} I^2 \sum_{\mathbf{k}} \text{Im} G_{\mathbf{k}}(-i\delta) = \pi n_{\text{imp}} I^2 N(0), \quad (131)$$

where n_{imp} is the impurity density, I is the impurity potential, and $N(0)$ is the DOS at the chemical potential. Then, the total quasiparticle damping rate $\tilde{\gamma}_{\mathbf{k}}$ is given by

$$\tilde{\gamma}_{\mathbf{k}} = \gamma_{\mathbf{k}} + \gamma^{\text{imp}}, \quad (132)$$

where $\gamma_{\mathbf{k}}$ represents the quasiparticle damping rate due to inelastic scattering, which is given by eq. (68) in the Fermi liquid theory or by eq. (24) in the FLEX approximation. (Here, we ignored the self-energy correction given by the cross terms between U and I . This simplification is not allowed for a large I , as we will show in §7.2.) Also, the CVC due to local impurities vanishes identically within the Born approximation. Therefore, in the case of $\gamma^{\text{imp}} \neq 0$, the Bethe-Salpeter equation (75) is changed to become

$$\begin{aligned} \vec{J}_{\mathbf{k}} &= \vec{v}_{\mathbf{k}} + \sum_{\mathbf{q}} \frac{3U^2}{2} (\pi T)^2 \text{Im} \chi_{\mathbf{q}}^s(0) \frac{\rho_{\mathbf{k}+\mathbf{q}}(0)}{2\tilde{\gamma}_{\mathbf{k}+\mathbf{q}}} \vec{J}_{\mathbf{k}+\mathbf{q}} \\ &\approx \vec{v}_{\mathbf{k}} + \tilde{\alpha}_{\mathbf{k}} \vec{J}_{\mathbf{k}^*}, \end{aligned} \quad (133)$$

where $\tilde{\alpha}_{\mathbf{k}} = \alpha_{\mathbf{k}} \cdot (\gamma_{\mathbf{k}}/\tilde{\gamma}_{\mathbf{k}})$. Thus, an approximate solution of eq. (133) is

$$\vec{J}_{\mathbf{k}} = \frac{1}{1 - \tilde{\alpha}_{\mathbf{k}}^2} (\vec{v}_{\mathbf{k}} + \tilde{\alpha}_{\mathbf{k}} \vec{v}_{\mathbf{k}^*}). \quad (134)$$

In the absence of impurities, $\vec{J}_{\mathbf{k}}$ exhibits singular \mathbf{k} -dependence because $\alpha_{\mathbf{k}} \approx (1 - c/\xi_{\text{AF}}^2)$ approaches one. In the case of $\gamma_{\mathbf{k}} \sim \gamma^{\text{imp}}$, on the other hand, $\tilde{\alpha}_{\mathbf{k}} \ll \alpha_{\mathbf{k}} \lesssim 1$ and therefore $\vec{J}_{\mathbf{k}} \sim \vec{v}_{\mathbf{k}}$. As a result, the CVC is strongly suppressed by high density “weak local impurities”, when the elastic scattering is comparable to the inelastic scattering due to AF fluctuations.

In Ref. [34], we have pointed out that the enhancement of R_{H} due to the CVC is easily suppressed by the weak impurities. Figure 27 shows the impurity effects on ρ and R_{H} obtained by the FLEX+CVC method for electron-doped systems. As expected, R_{H} is suppressed by a small amount of impurities, although the induced residual resistivity is small. (Note that $\rho = 1$ corresponds to $250 \mu\Omega\text{cm}$.) As a result, R_{H} becomes positive at low temperatures in the presence of impurities, which is consistent with the experimental behavior of R_{H} in PCCO for $\delta = 0.16 \sim 0.18$ [8]. Finally, we consider the case where the impurity potential is widespread (nonlocal). In this case, the impurity potential $I(\mathbf{q})$ is momentum-dependent, and the kernel of the Bethe-Salpeter equation in eq. (133), $(3U^2/2)(\pi T)^2 \text{Im} \chi_{\mathbf{q}}^s(0)$, is replaced with $n_{\text{imp}} I^2(\mathbf{q}) + (3U^2/2)(\pi T)^2 \text{Im} \chi_{\mathbf{q}}^s(0)$. When $I(\mathbf{q})$ is large only for $\mathbf{q} \sim 0$ (forward scattering), both the residual resistivity and the reduction in R_{H} due to the impurities will be small. In HTSCs, it is considered that impurities outside of the CuO_2 plane causes the forward impurity scattering [202].

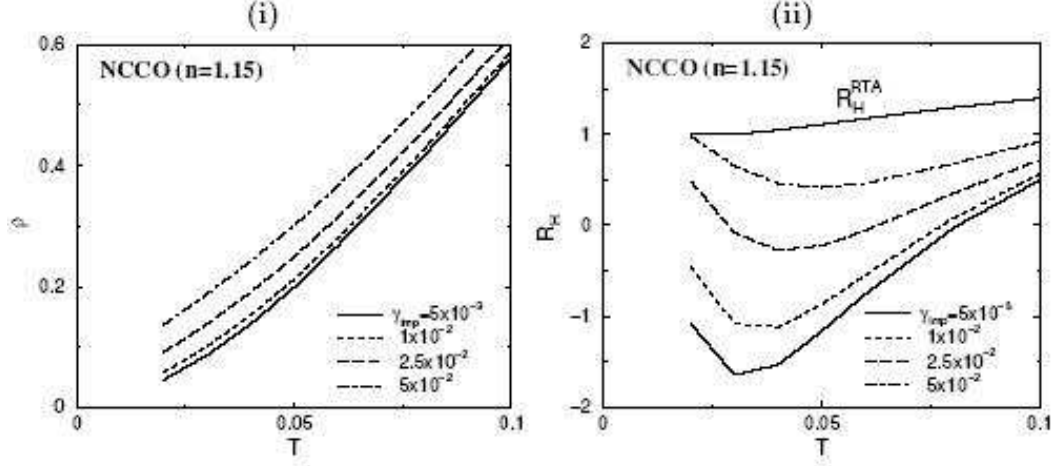


Figure 27. Theoretically obtained T -dependence of (i) ρ and (ii) R_H for NCCO in the presence of elastic scattering due to weak local impurities. In the case of $\gamma_{\text{imp}} \neq 0$, R_H becomes positive at low temperatures since the CVC is reduced by elastic scattering.

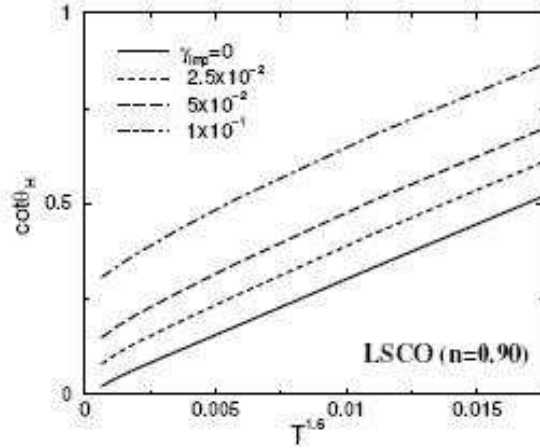


Figure 28. Obtained T -dependence of $\cot\theta_H = \rho/R_H$ for LSCO for $0.01 \leq T \leq 0.08$. $\cot\theta_H \propto T^{1.6} + c$ is realized well, and c is proportional to γ_{imp} .

Figure 28 shows the impurity effects on $\cot\theta_H = \rho/R_H$ obtained by the FLEX+CVC method for LSCO. The relationship $\cot\theta_H \propto T^{1.6} + c$ holds well, and $c \propto \gamma_{\text{imp}}$. Such a parallel shift of $\cot\theta_H$ by impurity doping is observed in various hole-doped HTSCs [169].

7.2. Effect of strong local impurities near AF QCP

Now, we discuss the effect of “strong local impurities” in HTSCs. According to a recent LDA study [203], a Zn atom introduced in the CuO_2 plane of HTSCs induces a large positive potential (less than 10eV), and the potential radius is only $\sim 1\text{\AA}$. In HTSCs,

however, Zn doping causes a nontrivial widespread change of the electronic states. In Zn-doped YBCO compounds, site-selective ^{89}Y NMR measurements revealed that both local spin susceptibility [204, 205] and staggered susceptibility [206] are prominently enhanced around the Zn site, within a radius of the AF correlation length ξ_{AF} . The same result was obtained by the ^7Li Knight shift measurement in Li-doped YBCO compounds [207], and by the ^{63}Cu NMR measurement in Zn-doped YBCO compounds [208]. Moreover, a small concentration of Zn induces a huge residual resistivity, which is significantly greater than the s -wave unitary scattering limit [156]. These nontrivial impurity effects were frequently considered as evidence for the breakdown of the Fermi liquid state in under-doped HTSCs.

Up to now, many theorists have studied this important issue. The single-impurity problem in a cluster t - J model has been studied by using the exact diagonalization method [209, 210]. When the number of holes is two, both AF correlations and electron density increase near the impurity site. This problem was also studied by using the extended Gutzwiller approximation [211]. Although these methods of calculation are founded, the upper limit of the cluster size is rather small. Moreover, these studies are restricted to $T = 0$.

In this section, we study a single-impurity problem in a large size square lattice (say 64×64) Hubbard model based on the nearly AF Fermi liquid theory [130]:

$$H = \sum_{i,j,\sigma} t_{ij} c_{i\sigma}^\dagger c_{j\sigma} + U \sum_i n_{i\uparrow} n_{i\downarrow} + I(n_{0\uparrow} + n_{0\downarrow}), \quad (135)$$

where I is the local impurity potential at site $i = 0$. It is a difficult problem since we have to consider two different types of strong interactions (U and I) on the same footing. Moreover, the absence of translational symmetry severely complicates the numerical analysis. To overcome these difficulties, we developed the GV^I method — a powerful method for calculating the electronic states in real space in the presence of impurities [130]. The GV^I method is applicable for finite temperatures since the thermal fluctuation effect is taken into account appropriately. Based on the GV^I method, we successfully explain the nontrivial impurity effects in HTSCs *in a unified way* without assuming any exotic mechanisms.

In the GV^I method, the real-space spin susceptibility $\hat{\chi}^{Is}(\omega_l)$ is given by

$$\hat{\chi}^{Is} = \hat{\Pi}^I \left(1 - U \hat{\Pi}^I \right)^{-1}, \quad (136)$$

$$\Pi^I(\mathbf{r}_i, \mathbf{r}_j; \omega_l) = -T \sum_{\epsilon_n} G^I(\mathbf{r}_i, \mathbf{r}_j; \epsilon_n + \omega_l) G^I(\mathbf{r}_j, \mathbf{r}_i; \epsilon_n). \quad (137)$$

Here, G^I is given by solving the following Dyson equation;

$$\hat{G}^I(\epsilon_n) = \hat{G}^0(\epsilon_n) + \hat{G}^0(\epsilon_n) \hat{I} \hat{G}^I(\epsilon_n), \quad (138)$$

where $(\hat{I})_{i,j} = I \delta_{i,0} \delta_{j,0}$, and \hat{G}^0 is the real-space Green function in the FLEX approximation without the impurity potential I . The solution of eq. (138) is

$$G_{i,j}^I = G_{i,j}^0 + I \frac{G_{i,0}^0 G_{0,j}^0}{1 - I G_{0,0}^0}, \quad (139)$$

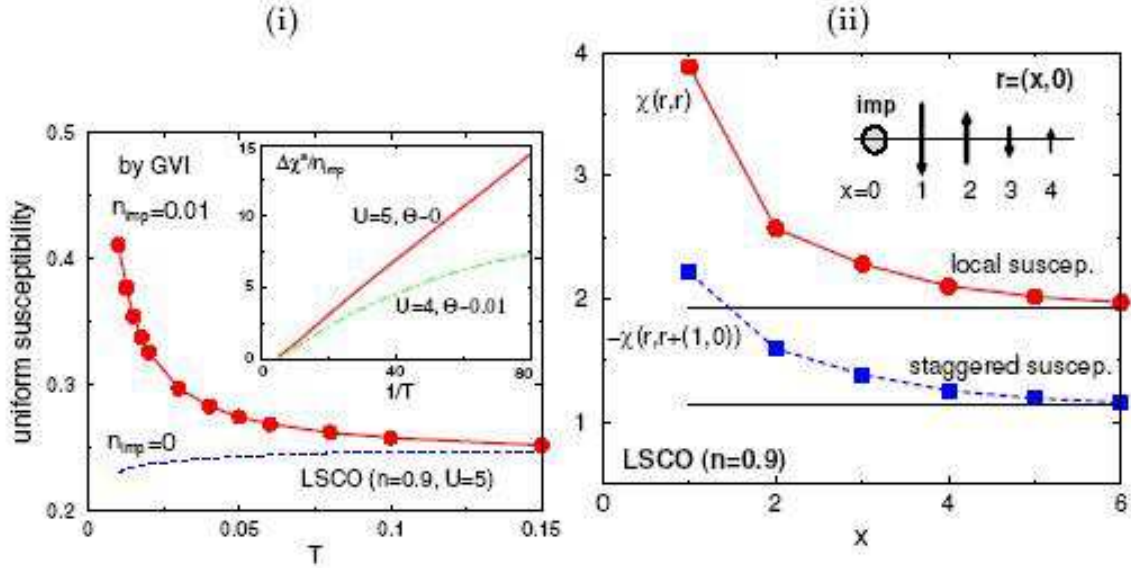


Figure 29. (i) The uniform susceptibility given by the GV^I method in the presence of impurities ($n_{\text{imp}} = 0.01$) for the impurity potential $I = \infty$. A single impurity induces a large Curie-term $\Delta\chi^s$, which is consistent with the experimental results. (ii) The local susceptibility $\chi^s(\mathbf{r}, \mathbf{r})$ and staggered one $\chi^s(\mathbf{r}, \mathbf{r} + (1, 0))$ given by the GV^I method. The inset describes the state in which both local and staggered susceptibilities are enhanced around the impurity site.

where the position of the impurity potential is $i = 0$.

In Fig. 29, we show the numerical results for spin susceptibilities, $\hat{\chi}^{Is}$, for $I = \infty$. Surprisingly, a nonmagnetic impurity induces a huge Curie-like component in the uniform susceptibility; $\Delta\chi \approx n_{\text{imp}} \cdot \mu_{\text{eff}}^2/3T$. This result explains the long-standing experimental problem [212, 213, 214]. The obtained value of μ_{eff} is $0.74\mu_B$, which is close to the experimental value $\mu_{\text{eff}} \sim 1\mu_B$ in $\text{YBa}_2\text{Cu}_3\text{O}_{6.66}$ ($T_c \approx 60K$) [212] and in LSCO ($\delta = 0.1$) [214]. We also emphasize that both the local and staggered susceptibilities get enhanced around the impurity site within a radius of about 3 ($\sim \xi_{\text{AF}}$) at $T = 0.02$. Here, we discuss the physical reason for this drastic impurity effect. In the FLEX approximation, the AF order (in the mean-field level) is suppressed by the self-energy correction (see §2), which represents the destruction of the long-range order due to thermal and quantum fluctuations. In the FLEX approximation, the reduction in the DOS due to the large quasiparticle damping rate $\gamma_{\mathbf{k}} = \text{Im}\Sigma_{\mathbf{k}}$ renormalizes the spin susceptibility. Around the impurity site, the self-energy effect due to electron-electron correlation is expected to be smaller. In fact, quantum fluctuation is reduced near the vacant site in the $s = 1/2$ Heisenberg model [215]. For this reason, in the GV^I method, the AF correlations are prominently enhanced around the impurity site due to the reduction of thermal and quantum fluctuations. The examples of the cross terms between U and I for susceptibility are shown in Fig. 30 (i). The same physics occurs in quantum spin systems with vacancies; AF spin correlations are enhanced around a vacancy, due to the reduction in quantum fluctuations [215, 216, 217, 218, 219].

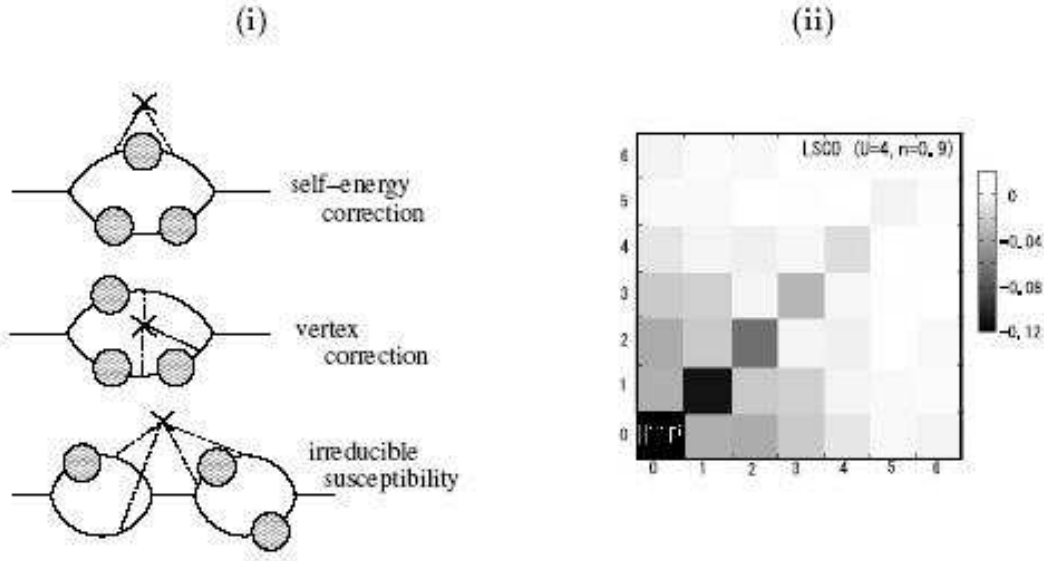


Figure 30. (i) Examples of diagrams for χ^{Is} in the presence of a single-impurity potential I in the Hubbard model. They are cross terms between I and U . The cross represents I , and the large circle with the shadow represents the self-energy given by the FLEX approximation for $I = 0$. (ii) The local DOS given by the GV^I method: it decreases around the impurity site within the radius of about 3, due to the nonlocal “effective complex impurity potential”, $\delta\Sigma(\mathbf{r}, \mathbf{r}'; \epsilon = 0)$.

Prior to the GV^I method, the single impurity problem in the Hubbard model had been studied using the RPA [220, 221, 222], assuming a nonlocal impurity potential; V_0 for the onsite and V_1 for the site adjacent to the impurity atom. The obtained result strongly depends on the value of V_1 : When $V_1 = 0$, the enhancement of susceptibility is tiny or absent although $V_1 \approx 0$ for the Zn impurity atom in the CuO_2 -plane according to the LDA study [203]. On the other hand, in the GV^I method, the considerable enhancement of the susceptibility is realized even when $V_1 = 0$ (local impurity potential case), since χ_Q is renormalized by the self-energy correction in the FLEX approximation: Then, χ_Q is easily enhanced when the self-energy effect is reduced by introducing an impurity. Therefore, we have to use the GV^I method for investigating the impurity problem in HTSCs.

Next, we discuss the transport phenomena in the presence of dilute impurities according to the GV^I method [130]. The enhanced susceptibilities due to the impurity induce the “additional self-energy correction $\delta\Sigma \equiv \Sigma^I - \Sigma^{I=0}$ ” around the impurity site. If the area of $\delta\Sigma \neq 0$ is large, a large residual resistivity will be induced by the non- s -wave scattering channels. In the GV^I method, $\delta\Sigma$ is given by

$$\delta\Sigma(\mathbf{r}_i, \mathbf{r}_j; \epsilon_n) = T \sum_l G(\mathbf{r}_i, \mathbf{r}_j; \omega_l + \epsilon_n) V^I(\mathbf{r}_i, \mathbf{r}_j; \omega_l) - \Sigma^0(\mathbf{r}_i - \mathbf{r}_j; \epsilon_n), \quad (140)$$

$$V^I(\mathbf{r}_i, \mathbf{r}_j; \omega_l) = U^2 \left(\frac{3}{2} \chi^{Is}(\mathbf{r}_i, \mathbf{r}_j; \omega_l) + \frac{1}{2} \chi^{Ic}(\mathbf{r}_i, \mathbf{r}_j; \omega_l) - \Pi^I(\mathbf{r}_i, \mathbf{r}_j; \omega_l) \right), \quad (141)$$

where Σ^0 is the self-energy given by the FLEX approximation without the impurity potential ($I = 0$). The Green function $G(\mathbf{r}_i, \mathbf{r}_j; \epsilon_n)$ is given by solving the following Dyson equation in real space:

$$\hat{G}(\epsilon_n) = \hat{G}^I(\epsilon_n) + \hat{G}^I(\epsilon_n) \delta \hat{\Sigma}(\epsilon_n) \hat{G}(\epsilon_n). \quad (142)$$

In the GV^I method, we solve eqs. (140) and (142) self-consistently. The local DOS given by the GV^I method in real space — $\rho(\mathbf{r}, \omega) = \text{Im}G(\mathbf{r}, \omega - i\delta)/\pi$ — is shown in Fig. 30 (ii). The local DOS decreases around the impurity site within the radius of approximately $3a$ (a is the lattice spacing), since the quasiparticle lifetime is very short due to the large $\text{Im}\delta\hat{\Sigma}$. We verified that the radius of $\text{Im}\delta\hat{\Sigma}$ increases as the filling number n approaches unity, in proportion to ξ_{AF} . As explained in Ref. [130], we should not solve V^I in eq. (141) self-consistently, since the feedback effect on V^I introduced by iteration is canceled by the vertex correction for V^I that is absent in the FLEX approximation.

To derive the resistivity in the presence of impurities, we have to obtain the t -matrix, $\hat{t}(\epsilon)$, which is defined as $\hat{G} = \hat{G}^0 + \hat{G}^0 \hat{t} \hat{G}^0$. The expression of $\hat{t}(\epsilon)$ in the case of $n_{\text{imp}} \ll 1$ is derived in Ref. [130]. Using the t -matrix, the quasiparticle damping rate due to the impurity is given by [40, 41]

$$\gamma_{\mathbf{k}}^{\text{imp}}(\epsilon) = \frac{n_{\text{imp}}}{N^2} \sum_l \text{Im}T_l(\epsilon - i\delta) e^{i\mathbf{k}\cdot\mathbf{r}_l}, \quad (143)$$

where $T_l(\epsilon) = \sum_m t_{m,m+l}(\epsilon)$. n_{imp} is the density of the impurities. In the case of $n_{\text{imp}} \neq 0$, the total quasiparticle damping rate is $\gamma_{\mathbf{k}}(\epsilon) = \gamma_{\mathbf{k}}^0(\epsilon) + \gamma_{\mathbf{k}}^{\text{imp}}(\epsilon)$, where $\gamma_{\mathbf{k}}^0(\epsilon) = \text{Im}\Sigma_{\mathbf{k}}^0(\epsilon - i\delta)$. The resistivity for $n_{\text{imp}} \neq 0$ is approximately given by $\rho \propto \gamma_{\text{cold}}$.

Figure 31 (i) shows \mathbf{k} -dependences of $\gamma_{\mathbf{k}}^{\text{imp}}$ ($n_{\text{imp}} = 0.05$) and $\gamma_{\mathbf{k}}^0$. We emphasize that $\gamma_{\mathbf{k}}^{\text{imp}}$ exhibits strong \mathbf{k} -dependence that is similar to the \mathbf{k} -dependence of $\gamma_{\mathbf{k}}^0$. This result suggests that the effective impurity potential $\delta\Sigma$ is nonlocal. As a result, the structure of the “hot spot” and the “cold spot”, is not smeared out by the strong non-magnetic impurities, although it will be smeared out by the weak local impurities. This finding strongly suggests that the enhancement of the Hall coefficient near the AF QCP, which is induced by the strong CVC around the cold spot [33, 32], does not decrease due to the strong impurities. Moreover, the enhancement of χ_{AF} due to n_{imp} will also enhance R_{H} . Experimentally, R_{H} for under-doped YBCO and $\text{Bi}_2\text{Sr}_{2-x}\text{La}_x\text{CuO}_{6+\delta}$ are approximately independent of the doping of Zn and other non-magnetic impurities [9, 10, 5], whereas R_{H} for LSCO decreases with Zn doping [11, 12].

Figure 31 (ii) shows the resistivity ρ for YBCO with $n_{\text{imp}} = 0.02$ for $I = 0, 4, 6$, and ∞ . The obtained impurity effect is the most prominent when $I = 6$. As T decreases, nonmagnetic impurities cause a “Kondo-like upturn” of ρ below T_x , reflecting an extremely short quasiparticle lifetime near the impurities. In other words, *the considerable residual resistivity is caused by the large scattering cross section of the*

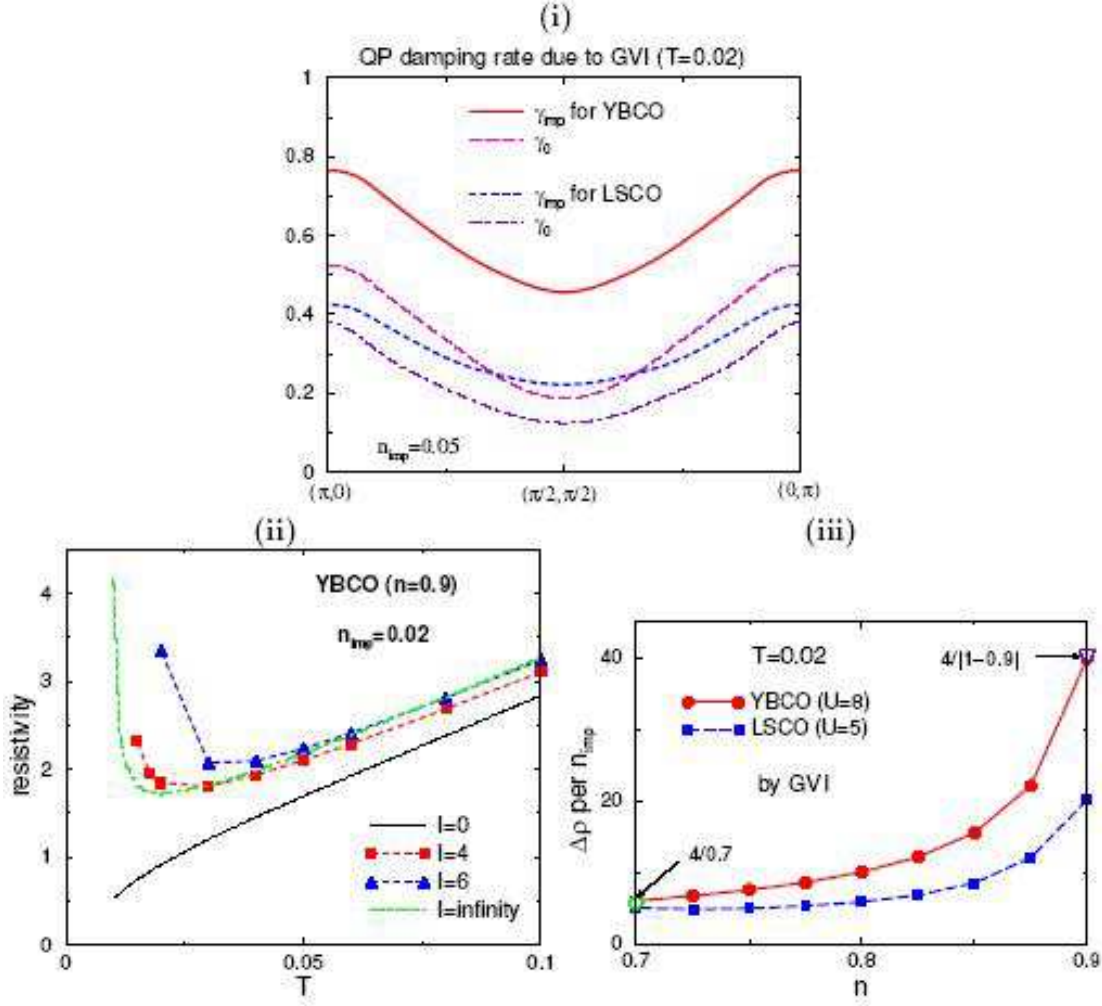


Figure 31. (i) $\gamma_{\mathbf{k}}^{\text{imp}}$ for $n_{\text{imp}} = 0.05$ and $\gamma_{\mathbf{k}}^0$ for YBCO and LSCO at $T = 0.02$. \mathbf{k} -dependent $\gamma_{\mathbf{k}}^{\text{imp}}$ obtained using the GV^I method will be verified by the ARPES measurements for Zn-doped compounds. (ii) ρ in YBCO ($n = 0.9$) for $n_{\text{imp}} = 0.02$ given by the GV^I method. At lower temperatures, an insulating behavior is observed in the close vicinity of the AF QCP. In HTSCs, $T = 0.1$ and $\rho = 1$ correspond to 400K and $250\mu\Omega\text{-cm}$, respectively. (iii) The filling dependence of $\Delta\rho \equiv \rho_{\text{imp}} - \rho_0$ per n_{imp} at $T = 0.02$ given by the GV^I method. Note that $\Delta\rho = (4n_{\text{imp}}/n) [\hbar/e^2]$ in a 2D electron-gas model due to strong local impurities.

“effective impurity potential”, $\delta\hat{\Sigma}$, as shown in Fig. 30 (ii). Note that T_x increases with n_{imp} . This amazing result strongly suggests that the insulating behavior of ρ observed in under-doped LSCO [223, 224] and NCCO [225] is caused by the residual disorder in the CuO_2 plane. As shown in Fig. 31 (iii), the parallel shift of the resistivity at finite temperatures due to impurities ($\Delta\rho$) grows drastically in the under-doped region; $\Delta\rho$ exceeds the s -wave unitary scattering limit in the 2D electron gas model, $\Delta\rho = (\hbar/e^2)(4n_{\text{imp}}/n)$. This result effectively explains experimental carrier-doping dependence of $\Delta\rho$ [156].

The enhancement of the residual resistivity is also observed near the AF QCP in

heavy-fermion systems such as CeAl₃ [226] and CeCu₅Au [227], and in the organic superconductor κ -(BEDT-TTF)₄Hg_{2.89}Br₈ [239]. In these compounds, $\Delta\rho$ quickly decreases with pressure, as the distance from the AF QCP increases. In κ -(BEDT-TTF)₄Hg_{2.89}Br₈, $\Delta\rho$ under 2 GPa is six times smaller than the value at 0.5 GPa. Such a large change in $\Delta\rho$ is difficult to be explained by the pressure dependence of the DOS. In fact, according to the t -matrix approximation, $\gamma^{\text{imp}} = (\pi I^2 N(0)/2)/(1 + (\pi IN(0)/2)^2)$. The residual resistivity in 2D free dispersion model ($\epsilon_{\mathbf{k}}^0 = \mathbf{k}^2/2m$) is $\Delta\rho = 2\pi N(0)\gamma_{\text{imp}}/e^2 n$. Therefore, $\Delta\rho$ is given by

$$\Delta\rho = \frac{\hbar}{e^2} \frac{4(\pi IN(0)/2)^2}{1 + (\pi IN(0)/2)^2} \frac{n_{\text{imp}}}{n}, \quad (144)$$

in 2D free dispersion model. Note that the renormalization factor z does not appear in the expression of $\Delta\rho$. In case of $IN(0) \gg 1$, eq. (144) gives the s -wave unitary scattering value; $\Delta\rho = (\hbar/e^2)4(n_{\text{imp}}/n)$. In case of weak impurity scattering where $IN(0) \ll 1$ (Born limit), we obtain the relation $\Delta\rho \propto I^2 N^2(0)$, which will decrease under pressure since $N(0) \propto 1/W_{\text{band}}$. However, pressure dependence of $\Delta\rho$ in κ -(BEDT-TTF)₄Hg_{2.89}Br₈ seems too strong to be explained by the Born approximation. We comment that the increment in $\Delta\rho$ due to charge fluctuations is discussed in some heavy-fermion systems [228, 229].

In summary, the present study revealed that a single impurity strongly influence the electronic states in a wide area around the impurity site near the AF QCP. Using the GV^I method, the characteristic impurity effects in under-doped HTSCs are well explained in a unified way, without assuming any exotic non-Fermi-liquid ground states. We successfully explain the nontrivial impurity effects in HTSCs *in a unified way* in terms of a spin fluctuation theory, which strongly suggests that the ground state of HTSCs is a Fermi liquid. We expect that the novel impurity effects in other metals near the AF QCP, such as heavy-fermion systems and organic metals, will be explained by the GV^I method. The validity of the GV^I method is verified in Ref. [130] based on the microscopic Fermi liquid theory.

Recently, we extended the GV^I -FLEX method to be applicable even in below T_c , and analyzed the Hubbard cluster model given by eq. (135). We found that both local and staggered susceptibilities are enhanced around the impurity site even in the SC state [230]. This result is consistent with ¹⁷O NMR measurement for YBCO with Zn impurities [231]. Interestingly, it is also reproduced by analyzing the Hubbard model together with the d -wave pairing interaction using the mean-field approximation [232]. In the normal state, on the other hand, the enhancement of the local and staggered susceptibilities cannot be explained qualitatively within the mean-field approximation or RPA [220, 221, 222]. It is an important future issue to explain the sensitive impurity effects on the SC state in HTSCs [199] based on the *repulsive Hubbard model*, using the GV^I -FLEX method.

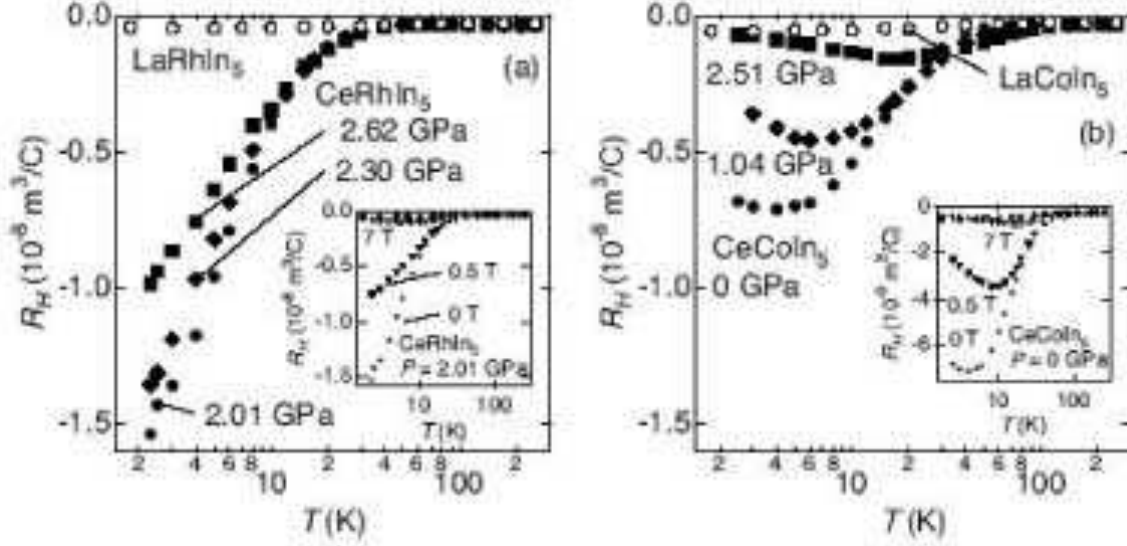


Figure 32. Temperature dependence of R_H in (a) CeRhIn_5 for $P \geq P_c = 2.01$ GPa, and in (b) CeCoIn_5 for $P \geq 0$. [Ref. [20]]

8. Anomalous transport behaviors in CeMIn_5 ($M=\text{Co}$ or Rh) and κ -(BEDT-TTF)

Thus far, we showed that the CVC due to strong AF+SC fluctuations induces various anomalous transport phenomena in HTSCs. To validate this idea, we have to study the various nearly AF systems other than HTSCs. In general, the electronic structure of heavy-fermion systems and organic metals are very sensitive to the pressure. Therefore, the distance from the AF QCP can be easily changed by applying the pressure, without introducing disorders in the compounds. This is a great advantage with respect to investigating the intrinsic electronic states near the AF QCP, free from the disorder effects. A useful theoretical review for heavy-fermion systems near the AF QCP is given in Ref. [233]. Recently, detailed measurements of the transport phenomena under pressure have been performed in the heavy-fermion superconductor CeMIn_5 ($M=\text{Co}$ or Rh) and in the organic superconductor κ -(BEDT-TTF). They exhibit striking non-Fermi-liquid-like behaviors as observed in HTSCs — eqs. (1)-(4). Hereafter, we explain the experimental and theoretical studies on the transport phenomena in these systems.

8.1. CeMIn_5 ($M=\text{Co}$ or Rh)

CeMIn_5 is a quasi 2D heavy-fermion superconductor with $T_c = 2.3\text{K}$. According to the angle-resolved measurements of thermal conductivity [102] and specific heat [105], the symmetry of the SC gap is d -wave. Figure 32 shows the temperature dependence of R_H in CeCoIn_5 and CeRhIn_5 in the limit of $H_z = 0$. In CeRhIn_5 , the critical pressure under which the AF QCP is realized is $P_c \approx 2.01\text{GPa}$. At $P = P_c$, $R_H(2.3\text{K})/R_H(300\text{K})$ reaches 50, whereas the magnitude of R_H rapidly decreases as the pressure is increased.

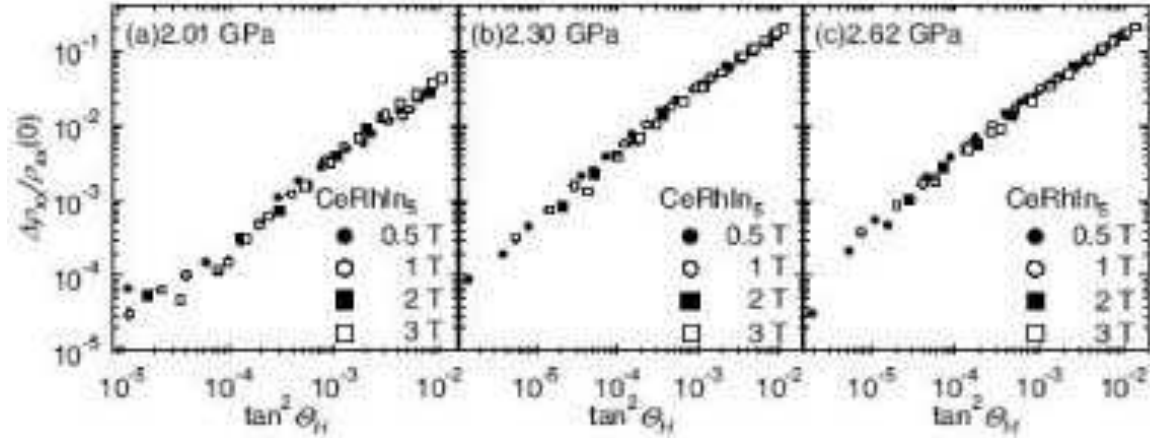


Figure 33. $\Delta\rho/\rho_0$ plotted as a function of $\tan^2 \Theta_H$ for CeRhIn_5 . [Ref. [20]]

A similar pressure dependence of R_H is observed in CeCoIn_5 , where P_c is slightly below the ambient pressure. In both these compounds, R_H is inversely proportional to T at higher temperatures. Moreover, as shown in Fig. 33, the modified Kohler's rule given in eq. (106) is well satisfied in CeRhIn_5 [20] for over four orders of magnitude. Furthermore, this is well satisfied in CeCoIn_5 [19, 20]. Therefore, both R_H and $\Delta\rho/\rho_0$ in CeMIn_5 shows anomalous behaviors which are similar to HTSCs. This experimental fact strongly suggests that the CVC due to the strong AF fluctuations is the origin of the anomalous transport phenomena.

Now, we discuss the magnetic field dependence of the transport coefficients. Interestingly, $R_H \equiv d\rho_H(H_z)/dH_z$ in CeMIn_5 near P_c is easily suppressed only by a small magnetic field, as shown in the inset of Fig. 32. At the same time, $(\Delta\rho/\rho_0)H_z^{-2}$ is also significantly suppressed. Therefore, the relationships $\sigma_{xy} \propto H_z$ and $\Delta\sigma_{xx} \propto H_z^2$ are satisfied only below ~ 0.1 Tesla near the QCP [19, 20]. These behaviors cannot be attributed to the orbital effect (i.e., the cyclotron motion of conduction electrons) since $\omega_c^* \tau^* = (eH_z/m^*c)\tau^* \gtrsim 1$ is satisfied only when $H_z \gg H_{c2} = 5$ Tesla and $T \ll 1$ K [234]. The condition $\omega_c^* \tau^* \ll 1$ is also recognized from the relationship $\Delta\rho/\rho_0 \lesssim 0.1$ for $T > 2$ K and $H < 3$ Tesla, as shown in Fig. 33.

When $\omega_c^* \tau^* \ll 1$ is satisfied, we can safely expand Nakano-Kubo formula given in eq. (42) with respect to the vector potential, as we did in §4 - 7. Then, the following relationships derived in §4

$$\rho_H \propto H_z \xi_{\text{AF}}^2, \quad (145)$$

$$\Delta\rho/\rho_0 \propto H_z^2 \xi_{\text{AF}}^4 / \rho_0^2, \quad (146)$$

are expected to be valid for CeMIn_5 . Here, the factors ξ_{AF}^2 and ξ_{AF}^4 in eqs. (145) and (146), respectively, come from the CVCs. Therefore, experimental striking non-linear behaviors of R_H and $\Delta\rho/\rho_0$ with respect to H_z should originate from the field-dependence of $\chi_Q(0) \propto \xi_{\text{AF}}^2$: The suppression of ξ_{AF} due to the magnetic field results in reducing both eqs. (145) and (146). Since the correlation length is sensitive to the

outer parameters in the vicinity of the QCP [235], the anomalous sensitivity of ρ_H and $\Delta\rho/\rho_0$ to the magnetic field in CeMIn_5 originates from the field-dependence of the CVC. Recently, ρ_H and $\Delta\rho/\rho_0$ in PCCO were measured in magnetic field up to 60 T, and it is found that both of them shows striking non-linear behaviors with respect to H_z [236]. Their behaviors will be explained by the field-dependence of the CVC.

Even if the field dependence of CVC is prominent, the modified Kohler's rule in eq. (106) should be satisfied for a wide range of the magnetic field strength, since both $\Delta\rho/\rho_0$ and $\cot^2\theta_H$ are proportional to $\xi_{\text{AF}}^4\rho^{-2}$ if the preset theory of CVC is correct. In fact, the modified Kohler's rule is well satisfied for $T = 2.5 - 30\text{K}$ and $0 < H_z \lesssim 3$ Tesla in CeRhIn_5 as shown in Fig. 33, regardless of the fact that the conventional Kohler's rule is violated only for 0.1 Tesla. This fact strongly suggests that both σ_{xy} and $\Delta\sigma_{xx}$ are enhanced by the same origin, namely, the CVC due to the AF fluctuations. Therefore, the anomalous transport phenomena in CeCoIn_5 are consistently described by the theory of CVC in nearly AF Fermi liquids.

The Nernst signal ν in CeCoIn_5 is also very anomalous [107]. Below 20K, ν starts to increase approximately in proportion to T^{-1} , exhibiting anomalously large values ($\nu \sim 1\mu\text{V}/\text{KT}$) below 4K. This behavior is very similar to that of ν in electron-doped HTSC, whose T -dependence and the magnitude are well reproduced by the CVC due to strong AF fluctuations. It reaches $\sim 0.1\mu\text{V}/\text{KT}$ in optimally-doped NCCO. Considering that ν is proportional to $\tau \propto \rho_0^{-1}$, the experimental relations $\nu_{\text{CeCoIn}_5(4\text{K})}/\nu_{\text{NCCO}(100\text{K})} \approx 1(\mu\text{V}/\text{KT})/0.1(\mu\text{V}/\text{KT}) = 10$ and $\rho_{\text{CeCoIn}_5(4\text{K})}/\rho_{\text{NCCO}(100\text{K})} \approx 5(\mu\Omega)/50(\mu\Omega) = 1/10$ are naturally understood as the quasiparticle transport phenomena. Thus, the giant Nernst signal in CeCoIn_5 is expected to be caused by the CVC due to strong AF fluctuations.

Although the spin susceptibility $\chi^s(\mathbf{q})$ in CeMIn_5 has a quasi 2D structure, the anisotropy of resistivity is only two ($\rho_c/\rho_{ab} \sim 2$) at low temperatures. In the dynamical-mean-field-theory (DMFT) [109, 110], which is believed to effectively describe the electronic properties in 3D systems, the CVC vanishes identically. Therefore, it is highly desired to confirm whether the CVC can be really significant in 3D systems or not. Recently, we performed the numerical study for 3D Hubbard model with the conduction electron spectrum is $\epsilon_{\mathbf{k}}^{3\text{D}} = \epsilon_{\mathbf{k}}^0 + 2t_z \cos k_z$, where $\epsilon_{\mathbf{k}}^0$ is given in eq. (12). The obtained ρ , R_H and ν in quasi 2D Hubbard model are shown in Fig. 34 (i)-(iii). Since the unit cell lengths in CeMIn_5 are $a_a = a_b = 4.6 \text{ \AA}$ and $a_c = 7.6 \text{ \AA}$, $\rho = 1$ and $R_H = 1$ correspond to $300 \mu\Omega\text{cm}$ and $1.0 \times 10^{-9} \text{ m}^3/\text{C}$, respectively. We find that both R_H and ν are strikingly enhanced due to the CVC even if $t_z/t_0 \sim 1$. In CeCoIn_5 , R_H starts to increase below $\sim 40\text{K}$, which corresponds to $T = 0,08$ in Fig. 34 (ii). At $T = 0.02$ ($\sim 8\text{K}$ for CeMIn_5), $R_H \sim 5$ for $t_z/t_0 = 0.8$. Then, the extrapolated value of R_H at 2K is 20.

As shown in Fig. 34 (iii), the obtained ν is drastically enhanced by the CVC, which is consistent with experiments. To derive the correct absolute value of ν , we have to take account of the fact that ν is proportional to the mass-enhancement factor $1/z$. According to the de Haas-van Alphen measurement, $1/z = m^*/m_{\text{band}} \sim 50$ in CeCoIn_5 . Since the mass-enhancement factor in the present FLEX approximation is $1/z_{\text{FLEX}} \sim 3$,

we describe the experimental mass-enhancement factor as $1/z = 1/(z_{\text{FLEX}}z^*)$, where $1/z^* = 50/3$ is the mass enhancement factor which cannot be described by the FLEX approximation in the Hubbard model. [Even in the FLEX approximation, relatively large $1/z_{\text{FLEX}} \sim 10$ is obtained in the periodic Anderson model, which is an effective model for heavy fermion systems [237]. We will comment on this fact in §9.2.] We present $\nu = \nu_{\text{FLEX}}/z^*$ in Fig. 34 (iii), where ν_{FLEX} is given by the FLEX approximation, by using the relation $k_{\text{B}}a_{\text{a}}^2/\hbar = 28 \text{ nV/KT}$. Recently, we extended the FLEX approximation to reproduce appropriate results under a finite magnetic field, and calculated the field dependence of R_{H} and ν . It was suggested that both these quantities were rapidly suppressed by the magnetic field near AF QCP, reflecting the reduction of AF fluctuations. The obtained result is in good agreement with the experimental results.

In CeCoIn₅, R_{H} exhibits a peak at $T_{\text{RH}}^* \sim 4\text{K}$ at ambient pressure, and T_{RH}^* increases with pressure [see Fig. 32]. This is different from the pseudo-gap behavior in underdoped HTSCs since T_{RH}^* in CeCoIn₅ increases as the system goes away from the AF-QCP. In particular, R_{H} of CeRhIn₅ at $P = P_{\text{c}}$ maintains its increasing trend just above T_{c} . These behaviors can be understood as the effect of the weak (local) residual disorders, as we have discussed in §7.1: as shown in Fig. 27 (ii), $|R_{\text{H}} - R_{\text{H}}^{\text{RTA}}|$ starts to decrease at lower temperatures when $\gamma_{\text{imp}} > 0$. The peak temperature T_{RH}^* increases with γ_{imp} . In CeCoIn₅, the resistivity at T_{RH}^* is $\rho(T = T_{\text{RH}}^*) \sim 6\mu\Omega \text{ cm}$ [20] for $P = 0 \sim 2.5 \text{ GPa}$. On the other hand, in CeRhIn₅ at $P = 2 \text{ GPa}$, $\rho(T \gtrsim T_{\text{c}}) \approx 10\mu\Omega \text{ cm}$ because of the large inelastic scattering. Since γ_{imp} in CeCoIn₅ and that in CeRhIn₅ are expected to be similar, $\tilde{\alpha}_{\mathbf{k}} = \alpha_{\mathbf{k}} \cdot \gamma_{\mathbf{k}}/(\gamma_{\mathbf{k}} + \gamma_{\text{imp}})$ in eq. (134) will be smaller in CeCoIn₅. That is, reduction of CVC due to impurities is more prominent in CeCoIn₅. Therefore, we can explain the different behaviors of R_{H} in CeRhIn₅ and CeCoIn₅ at low temperatures as the effect of residual disorders.

One may ascribe the temperature dependence of R_{H} in CeMIn₅ to the multiband effect. For example, a sign change in R_{H} can occur if a hole-like Fermi surface and an electron-like Fermi surface coexist and their mean free paths have different T -dependences. However, it is very difficult to explain the relation $|R_{\text{H}}| \gg 1/ne$ in a multiband model based on the RTA. In fact, in order to explain the pressure dependence of R_{H} in CeCoIn₅, one has to assume that a small Fermi surface governs the transport phenomena at 0GPa (near AF QCP), whereas a large Fermi surface should consequently govern the transport phenomena under 2.5GPa. The same drastic change in the electronic states should occur by applying a magnetic field $H \sim 1\text{Tesla}$. This unnatural assumption is not true since the other transport coefficients cannot be explained at all, as discussed in Ref. [20] in detail. In particular, the elegant modified Kohler's rule plot for CeRhIn₅ shown in Fig. 33 *for over four orders of magnitude* is strong evidence that the CVC is the origin of the anomalous transport phenomena, and the anomalous transport phenomena are mainly caused by a single large Fermi surface with heavy quasiparticles. Since the enhancements of both R_{H} and $\Delta\rho/\rho_0$ originate from a small portion of the Fermi surface (i.e., the cold spot) as shown in Fig. 19 (ii), the multiband effect is unimportant in CeMIn₅. Therefore, the modified Kohler's rule will be realized

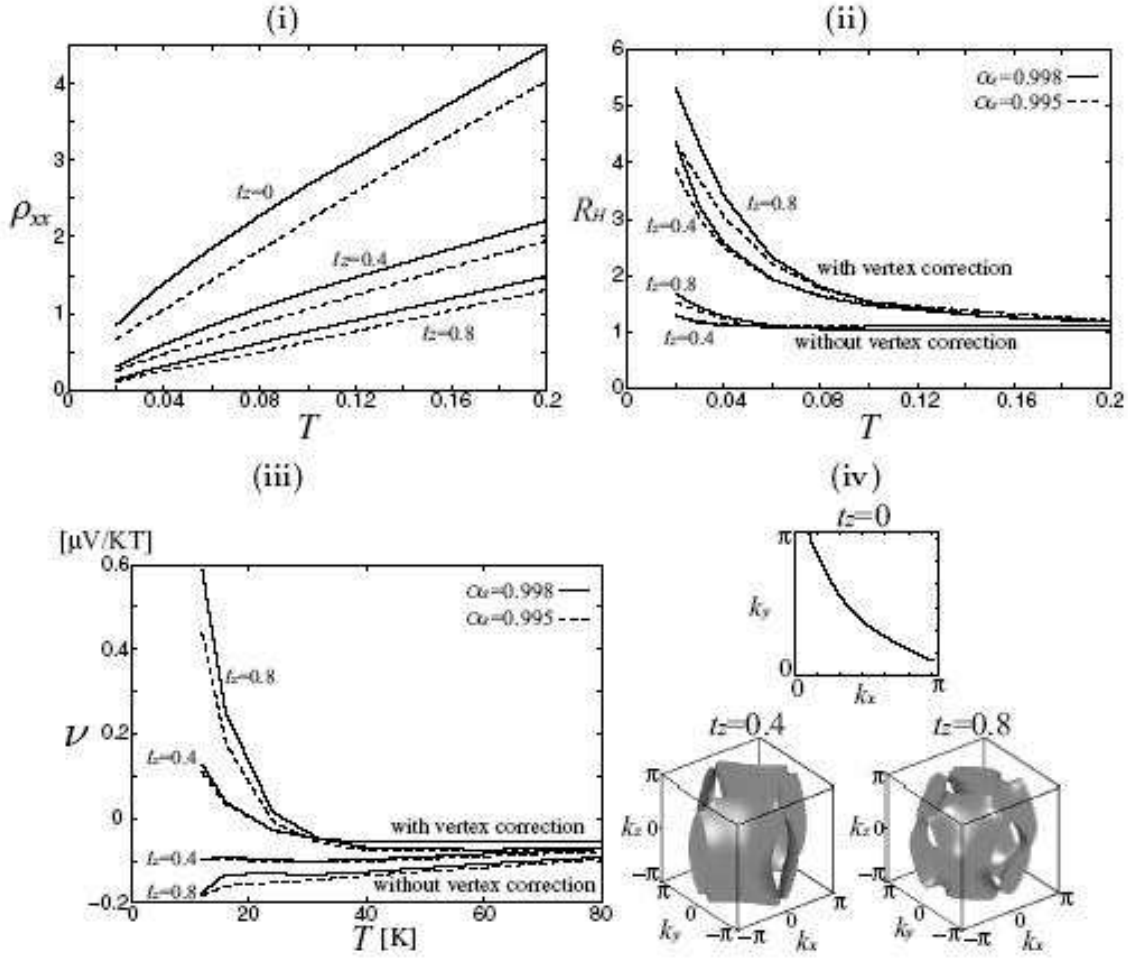


Figure 34. (i) ρ , (ii) R_H and (iii) ν for the 3D Hubbard model ($t_z = 0.4, 0.8$) given by the FLEX+CVC method. Broken lines represent the numerical results for $U = 9.4$ ($t_z = 0$), $U = 6.2$ ($t_z = 0.4$) and $U = 5.4$ ($t_z = 0.8$). In these parameters, the Stoner factors α_S is 0.995 at $T = 0.02$. Full lines represents the numerical results for U s with which $\alpha_S = 0.998$ is satisfied at $T = 0.02$. (iv) Fermi surfaces for $t_z = 0, 0.4, 0.8$. [Ref. [108]]

near the AF QCP even in multiband systems like CeMIn_5 .

In usual heavy-fermion compounds, R_H exhibits a Curie-like behavior above the coherent temperature T_0 due to the large anomalous Hall effect, which is caused by the angular momenta of the f -orbitals as we will discuss in §9.4. For $T \ll T_0$, R_H due to the AHE is proportional to ρ^2 . In heavy-fermion compounds near the AF QCP, on the other hand, both the ordinary Hall coefficient R_H^n and the anomalous Hall coefficient R_H^{AHE} can show large temperature dependences. Paschen et al. extracted R_H^n from the experimental Hall coefficient in YbRh_2Si_2 , and discussed the critical behavior of R_H^n near AF QCP, which is realized under the magnetic field [22]. In contrast, R_H in CeMIn_5 ($M = \text{Co, Rh}$) is almost constant above 50 K as shown in Fig. 32. Therefore, anomalous Hall effect in CeMIn_5 is very small, and therefore $R_H^{\text{HF}} \approx R_H^n$ as explained in detail in

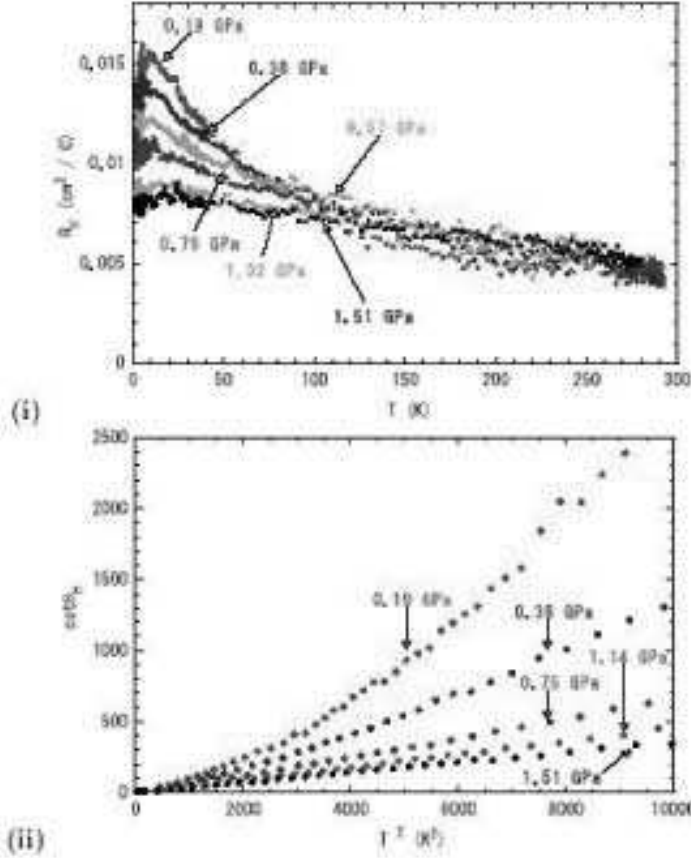


Figure 35. Temperature dependence of (i) R_H and (ii) $\cot \theta_H$ for κ -(BEDT-TTF)₂Cu(NCS)₂ under pressure. [Ref. [17]]

Ref. [19, 20]. This fact is a great advantage to study the anomalous T -dependence of the ordinary Hall effect in CeMIn_5 .

In CeCoIn_5 , novel kinds of critical behaviors are observed near $H_{c2} \sim 5$ Tesla for $T \ll 1$ K, where prominent increment in the effective mass was observed. This phenomenon is referred to as a “field-induced QCP”. One possible origin will be the field-induced SDW state that is hidden in the SC state. We will discuss this important future problem in §9.2 in more detail.

8.2. κ -(BEDT-TTF)

The measurements of R_H under pressure have been intensively performed in κ -(BEDT-TTF)₂X. Figure 35 shows the temperature dependence of R_H and $\cot \theta_H$ for $X=\text{Cu}(\text{NCS})_2$ under homogeneous pressure. Here, the AF correlations are the strongest at the lowest experimental pressure (0.19GPa). As the pressure is increased, the AF fluctuations get reduced and a conventional Fermi liquid state is realized. At the same time, R_H is reduced and exhibits a constant value. The observed R_H is independent of pressure at room temperature. Therefore, the origin of the increment in R_H below 100 K

cannot be related to deformation of the Fermi surface under pressure. Note that similar increment in R_H is observed in $X=\text{Cu}[\text{N}(\text{CN})_2]\text{Cl}$, which has a single elliptical Fermi surface [92]. Because the observed T dependences of R_H and $\cot\theta_H$ are very similar to the observations involving HTSCs and in CeMIn_5 , the CVC is expected to play a significant role in $\kappa\text{-(BEDT-TTF)}_2X$.

As discussed in §2.3, the resistivity in 2D systems in the presence of AF fluctuations is [147],

$$\rho \propto T^2 \xi_{\text{AF}}^2. \quad (147)$$

This relationship is reliable when $\omega_{\text{sf}} \gtrsim T$, which is satisfied in optimally- or over-doped HTSCs. The T -dependence of ω_{sf} is given in eq. (10). We consider eq. (147) is realized in $X=\text{Cu}(\text{NCS})_2$ since the AF fluctuations are not so prominent. Since R_H is proportional to ξ_{AF}^2 as shown in eq. (97), we obtain

$$\cot\theta_H = \rho/R_H \propto T^2. \quad (148)$$

Figure 35 (ii) shows that eq. (148) is well satisfied below 80K, except at $P = 0.19$ GPa. [The thermal contraction of the sample might modify this relationship at the lowest pressure.] The success of the scaling relationships (97), (147) and (148) is strong evidence that the enhancement of R_H in $\kappa\text{-(BEDT-TTF)}_2X$ is caused by the CVC due to AF fluctuations.

In many $\kappa\text{-(BEDT-TTF)}_2X$ compounds, the phase transition between the Mott insulating phase and the metallic (SC) phase induced by pressure is weak first order. Therefore, the AF fluctuations are not so strong even in the vicinity of the AF insulating phase. As a result, the enhancement of R_H in $\kappa\text{-(BEDT-TTF)}_2X$ is much smaller than that in CeMIn_5 . On the contrary, carrier doped (11% doping) κ -type superconductor $\kappa\text{-(BEDT-TTF)}_4\text{Hg}_{2.89}\text{Br}_8$ ($T_c = 4$ K at ambient pressure) exhibits very strong AF fluctuations, and therefore the critical pressures is expected to be slightly below 0 kbar. According to NMR measurement, $1/T_1T$ [$\propto \xi_{\text{AF}}^2$] increases with decreasing temperature above ~ 10 K, in proportion to $(T + \Theta)^{-1}$ with $\Theta = 13$ K [238]. The P - T phase diagram and transport properties of $\kappa\text{-(BEDT-TTF)}_4\text{Hg}_{2.89}\text{Br}_8$ are carefully measured by Taniguchi et al. [239]: It was found that T_c shows two-peak structure under pressure. Also, the power n in $\rho = \rho_0 + AT^n$ increases from 1 to 2 with increasing pressure, which indicates that the AF fluctuations are suppressed under the pressure.

Taniguchi et al. also measured the R_H in $\kappa\text{-(BEDT-TTF)}_4\text{Hg}_{2.89}\text{Br}_8$ under pressures, and found that R_H exhibits a Curie-Weiss temperature dependence; $R_H \propto (T - \Theta_{\text{RH}})^{-1}$ where $\Theta_{\text{RH}} < 0$ [18]. At 0.19GPa where AF fluctuations are strong, $R_H(10\text{K})/R_H(300\text{K})$ reaches 10, whereas the enhancement of R_H is totally suppressed by 1 GPa. The behavior of R_H in $\kappa\text{-(BEDT-TTF)}_4\text{Hg}_{2.89}\text{Br}_8$ is very similar to the observation in CeMIn_5 . Θ_{RH} decreases with pressure, and its extrapolated value to 0 GPa (-13 K) coincides with the Weiss temperature of $1/T_1T$ at ambient pressure. This is strong evidence that the Hall coefficient in $\kappa\text{-(BEDT-TTF)}_4\text{Hg}_{2.89}\text{Br}_8$ is proportional to ξ_{AF}^2 , due to the CVC induced by AF fluctuations. It is noteworthy that the residual resistivity $\Delta\rho$ in $\kappa\text{-(BEDT-TTF)}_4\text{Hg}_{2.89}\text{Br}_8$ drastically decreases with pressure [239]. As

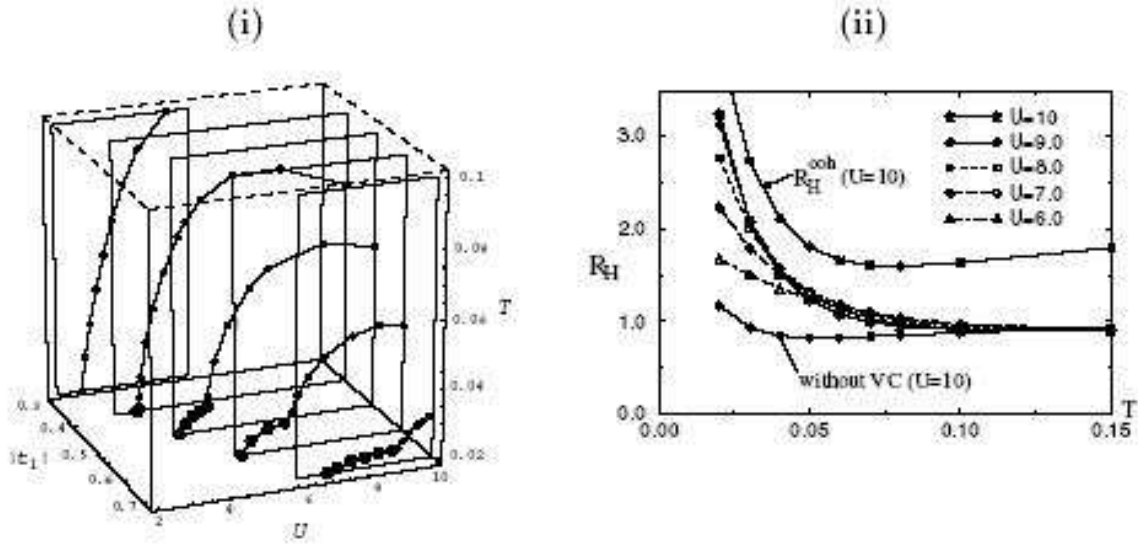


Figure 36. (i) U - T phase diagram for the anisotropic triangular lattice Hubbard model [$t_1 = 0.3 \sim 0.7$] given by the FLEX approximation. The large (small) dots represent the d -wave T_c (T_N). (ii) R_H given by the FLEX+CVC method. [Refs. [93] and [96]]

we have discussed in §7.2, the large residual resistivity near 0 GPa is expected to be given by the enlarged effective impurity potential due to the many-body effect.

Note that R_H in κ -(BEDT-TTF) $_2$ Cu[N(CN) $_2$]Br changes to be negative under high pressures and low temperatures, when the electron-electron correlation becomes very weak. The origin of this experimental fact is considered to be the lattice deformation with the long-period structure inherent in this compound [13].

Here, we analyzed the anisotropic triangular lattice Hubbard model at half-filling, which is a theoretical effective model for κ -(BEDT-TTF) $_2$ X. Figure 36 (i) shows the numerical results for the U - T phase diagram given by the FLEX approximation. Here, t_0 (> 0) and t_1 (> 0) are the nearest neighbor integrals of the triangular lattice; t_0 is for two of three axes and t_1 is for the remaining axis, respectively. In many κ -(BEDT-TTF) $_2$ X compounds, $t_1/t_0 \approx 0.7$. Then, the corresponding Fermi surface is hole-like and ellipsoidal around the Γ -point. Hereafter, we substitute $t_0 = 1 \sim 600$ K. Then, the AF ordered state appears at $T_N \lesssim 0.04 \sim 24$ K when U is as large as the bandwidth (~ 10). As U decreases, T_N decreases and the $d_{x^2-y^2}$ -wave SC appears next to the AF phase. The obtained U - T phase diagram well explains the experimental P - T phase diagram (Kanoda diagram [91]), since the increment in P corresponds to the reduction in U/W_{band} . Figure 36 (ii) also shows the T -dependence of R_H for $t_1/t_0 = 0.7$. We see that R_H increases at low temperatures due to the CVC and it becomes smaller as U decreases. At half-filling, obtained enhancement of R_H is not so large since the AF fluctuations in this model are rather weak due to the strong geometric frustration ($t_1/t_0 \sim 0.7$). Therefore, a consistent understanding of the P - T phase diagram as well as the P -dependence of R_H are achieved by using the FLEX+CVC method.

9. Discussions

9.1. Summary of the present study

In the present study, we investigated the mechanism of non-Fermi-liquid-like transport phenomena in strongly correlated Fermi liquids in the presence of strong magnetic fluctuations. This problem was first realized in the study of HTSC, which has been one of the central issues in HTSC. For example, the relaxation time approximation (RTA) for the highly anisotropic $\tau_{\mathbf{k}}$ model cannot reproduce relationships (1)-(4) at the same time, even for a narrow range of temperatures. Recent experiments have been revealed that these anomalous transport properties are not a special phenomena in HTSC, but a universal phenomena in Fermi liquids near AF QCP. We discussed two typical examples — CeMIn_5 ($M=\text{Co}$ or Rh) and $\kappa\text{-(BEDT-TTF)}_2\text{X}$. The ratio $R_{\text{H}}(2.5\text{K})/R_{\text{H}}(300\text{K})$ in CeRhIn_5 reaches ~ 50 , which is much larger than the ratio in HTSCs.

Here, we studied this long-standing problem by developing the microscopic Fermi liquid theory. In the RTA, the momentum and energy conservation laws in quasiparticles scattering are violated, as explained in §1 and §3. To overcome this defect, we take account of the CVC to satisfy the conservation laws. The total current $\vec{J}_{\mathbf{k}}$, which is responsible for the transport coefficients, is given by the summation of the quasiparticle velocity $\vec{v}_{\mathbf{k}}$ and the CVC $\Delta\vec{J}_{\mathbf{k}}$. In interacting electron systems, an excited quasiparticle induces other particle-hole excitations by collisions. The CVC represents the current due to these particle-hole excitations. Since the CVC is caused by quasiparticle interactions, it can be significant in strongly correlated Fermi liquids. However, the effects of CVC in HTSCs have not been studied in detail until recently. Since the CVC is totally ignored in the RTA, the RTA frequently yields unphysical results in strongly correlated systems.

In the presence of strong AF fluctuations, we find that **(a)** quasiparticle damping rate $\gamma_{\mathbf{k}} = 1/2\tau_{\mathbf{k}}$ becomes anisotropic, and the portion of the Fermi surface with small $\gamma_{\mathbf{k}}$ (cold spot) governs the transport phenomena [24, 25]. At the same time, **(b)** the total current $\mathbf{J}_{\mathbf{k}}$ becomes highly anisotropic due to the prominent CVC [33]. (a) and (b) should occur simultaneously since both of them are caused by the same origin; highly anisotropic incoherent scattering due to AF fluctuations. That is, both (a) and (b) are induced by the strong backward scattering between \mathbf{k} and \mathbf{k}^* ($\mathbf{k} - \mathbf{k}^* \approx \mathbf{Q}$), as shown in Fig. 4 (i). Mathematically, $\gamma_{\mathbf{k}} = \text{Im}\Sigma_{\mathbf{k}}(-i\delta)$ and the CVC are closely connected by the Ward identity near AF QCP, that is, the same vertex function $\mathcal{T}_{\mathbf{k},\mathbf{k}'}^{(0)}$ appears in eqs. (68) and (60). The facts (a) and (b) naturally explain the enhancement of R_{H} , $\Delta\rho/\rho_0$, and ν in nearly AF metals in a unified way. As shown in Fig. 14 (ii), the large curvature of the effective Fermi surface around the cold spot gives rise to the enhancement of R_{H} . In §3.4, we proved the significance of the CVC beyond the one-loop (such as the FLEX) approximation.

It is also very important to demonstrate to what extent the CVC can reproduce the aspects of anomalous transport properties based on a standard spin fluctuations theory. For this purpose, we study R_{H} , $\Delta\rho/\rho_0$, S and ν based on the FLEX (or FLEX+ T -matrix) approximation by including CVCs. The obtained results semiquantitatively

reproduce the various experimental facts in slightly under-doped HTSCs. The present study strongly suggests that *the striking deviation from the Fermi liquid behaviors (such as eqs. (1)-(4)) are ubiquitous in strongly correlated metals near the AF QCP, not specific to HTSCs.* Note that the increment in R_H is also observed in non-SC metals near AF phase, such as $V_{2-y}O_3$ [240] and $R_{2-x}Bi_xRu_2O_7$ ($R = \text{Sm or Eu}$)[241].

The main results in the present study are as follows:

- (i) Hall coefficient: Due to the CVC, $R_H \propto \xi_{AF}^2 \propto T^{-1}$. The large curvature of the effective Fermi surface around the cold spot is the origin of the enhancement of R_H . In particular, we can explain that the R_H for NCCO and PCCO are negative even above $T_N \sim 150$ K, since the curvature of the “effective Fermi surface” at point B in Fig. 14 is negative, although the curvature of the true Fermi surface is positive.
- (ii) Magnetoresistance: $\Delta\rho/\rho_0 \propto \xi_{AF}^4/\rho_0^2 \propto T^{-4}$ due to the CVC, which means that the conventional Kohler’s rule $\Delta\rho/\rho_0 \propto \rho_0^{-2}$ is violated. On the other hand, the modified Kohler’s rule $\Delta\rho/\rho_0 \propto (R_H/\rho_0)^2$ is realized since the same factor ξ_{AF}^4 appears in both sides.
- (iii) Thermoelectric power: For $T > T^*$, $|S|$ increases as T decreases since the ϵ -dependence of $\tau_{\mathbf{k}}(\epsilon)$ becomes prominent when the AF fluctuations are strong. Further, $S > 0$ ($S < 0$) in many hole-doped (electron-doped) systems.
- (iv) Nernst coefficient: Due to the CVC, ν gradually increases in NCCO below the room temperature. With regard to LSCO, a rapid increase in ν in the pseudo-gap region is well explained by the FLEX+ T -matrix approximation, due to the CVC induced by the strong AF+SC fluctuations.
- (v) AC Hall effect: The strong ω -dependence of $R_H(\omega)$ appears due to the frequency dependence of the CVC. Both T - and ω -dependences of $R_H(\omega)$ are well reproduced by the FLEX+CVC method.
- (vi) Impurity effect: The strong CVC near the AF QCP is suppressed by the *weak* local impurities. For *strong* local impurities, the residual resistivity exceeds the s -wave unitary scattering value since the local and staggered susceptibilities are strongly enhanced around the impurity sites.

Results (i)-(vi) are given by the same mechanism — the hot/cold spot structure and the singular \mathbf{k} -dependence of the total current $\vec{J}_{\mathbf{k}}$ in nearly AF metals, which is shown in Fig. 14. We emphasize that the abovementioned results are not derived from a special defect of the FLEX approximation. They are also reproduced by another spin fluctuation theory. In fact, Kanaki and Kontani [34] calculated $\vec{J}_{\mathbf{k}}$ based on the Millis-Monien-Pines model in eq. (8), by assuming a realistic set of parameters for optimally-doped YBCO. The obtained $\vec{J}_{\mathbf{k}}$ represents the characteristic \mathbf{k} -dependence in nearly AF metals as shown in Fig. 14. Moreover, we proved the significance of the CVC near AF QCP beyond the one-loop (such as the FLEX) approximation in §3.4. As a result, it is general that R_H is prominently enhanced by the CVC when the AF fluctuations are strong, independent of the types of the spin fluctuation theories.

9.2. Applicable scope of the present study and future problems

In this study, we explained that the CVC plays a significant roles in nearly AF metals, based on the microscopic Fermi liquid theory. To illustrate this theoretical idea, we performed numerical studies using the FLEX+CVC method in §4 - 7. Since the FLEX is a conserving approximation, we can perform a reliable study of the transport phenomena by including CVCs. As we discussed in §2.2, the FLEX approximation can explain characteristic electronic properties in optimally-doped HTSC. For example, the appropriate spin fluctuation $\chi_{\mathbf{q}}^s(\omega)$ and the hot/cold spot structure of quasiparticle damping rate $\gamma_{\mathbf{k}}$ are reproduced satisfactorily. Although the FLEX approximation cannot explain the “strong pseudo-gap behavior” below $T^* \sim 200$ K, the FLEX+ T -matrix approximation can reproduce various transport anomalies below T^* in slightly under-doped systems as discussed in §5. In the FLEX+ T -matrix approximation, we take account of the strong SC fluctuations that are induced by AF fluctuations. The success of the FLEX+ T -matrix method is strong evidence that SC fluctuations are the origin of strong pseudo-gap.

Here, we discuss the applicable scope of the FLEX approximation. First, we discuss the “weak pseudo-gap behavior” below $T_0 \sim 600$ K, where the DOS [242, 243, 244, 245], the Knight shift [80, 246, 247] and the uniform susceptibility [248, 249] decrease inversely with the growth of AF fluctuations. The weak pseudo-gap in the DOS is shallow and wide in energy. Although weak pseudo-gap behaviors are reproduced by the FLEX approximation, the obtained gap behaviors are too moderate. [Since the weak pseudo-gap affects transport phenomena only slightly, FLEX+CVC approximation can explain anomalous transport phenomena in HTSC.] This failure of the FLEX will originate from the fully self-consistent determination of the self-energy and the Green function. In fact, although a large weak pseudo-gap in the DOS is reproduced at the first iteration stage, it vanishes in the course of iteration. Mathematically, additional self-energy correction introduced by iteration (i.e., the feedback effect) should be canceled by the vertex correction in the self-energy that is absent in the FLEX approximation (e.g., $\gamma_{\mathbf{k}}^{(2)}$ in Fig. 15 (ii)). The same result is reported in the GW approximation: This is a first principle calculation for the self-energy, which is given by the convolution of the Green function G and the screened interaction W within the RPA. Although the descriptions of the bandwidth reduction and satellite structure in the quasiparticle spectrum are satisfactory in a partially self-consistent GW method, they are smeared out in the fully self-consistent GW due to the feedback effect by iteration [250, 251, 252].

To produce a weak pseudo-gap successfully, it is better to derive the self-energy by performing (i) fully self-consistent calculation with vertex corrections or (ii) partially (or no) self-consistent calculation. Along the lines of method (i), Schmalian and Pines calculated the self-energy with all the vertex corrections by applying a high-temperature approximation [253]. Using a similar technique, Fujimoto calculated the pseudogap phenomena due to quasistatic SC fluctuations [254]. It is noteworthy that the fourth-order-perturbation theory with respect to U well reproduces the weak pseudo-gap

since the vertex corrections for the self-energy are considered [255]. This method also reproduces the difference of T_c between YBCO and LSCO [256], and the p -wave SC state in Sr_2RuO_4 [257]. Along the lines of method (ii), Vilk and Tremblay proposed a two-particle self-consistent (TPSC) method [258], where full self-consistency is not imposed on the self-energy. The renormalization of the spin susceptibility is described by introducing the effective Coulomb interaction $U_{\text{eff}} (< U)$ that is determined so as to satisfy the sum rule for $\chi_{\mathbf{q}}^s(\omega)$. This philosophy has been applied to extend the dynamical mean field theory (DMFT) by including self-energy correction due to spin fluctuations [259, 260]. These theories can explain the weak pseudo-gap in the DOS. However, they are not suitable for the study of the transport phenomena since they are not conserving approximations. For this reason, we use the FLEX approximation in the numerical study for the transport phenomena. Since the FLEX approximation tends to underestimate the anisotropy of $\tau_{\mathbf{k}}$ due to the overestimated feedback effect, the enhancements of R_{H} and $\Delta\rho_{\text{imp}}$ given by the FLEX+CVC method might be underestimated quantitatively.

Finally, we present important future problems. Since the FLEX (or FLEX+ T -matrix) approximation is a one-loop approximation, it does not work satisfactorily in under-doped systems. However, the analysis in §3.4 have shown that the enhancement of R_{H} due to the CVC is not an artifact of the FLEX approximation, but will be universal near the AF-QCP beyond the one-loop approximation. Therefore, relations $R_{\text{H}} \propto \xi_{\text{AF}}^2$ and $\Delta\rho/\rho_0 \propto \cot^2\theta_{\text{H}}$ are expected to hold in under-doped HTSCs. It is an important challenge to perform a numerical study of the CVC using the higher-loop approximation, by taking the vertex corrections for the self-energy. Then, we will be able to judge clearly whether the striking transport anomaly in heavily under-doped systems can be understood based on the Fermi liquid theory, or the idea of non-Fermi liquid theory explained in §1.4 has to be employed.

In under-doped systems, small amount of impurities drastically changes the electronic states of the system as discussed in §7.2. Therefore, to understand transport phenomena in under-doped systems, we have to develop the theory of transport phenomena in the presence of disorder.

In §8.1, we presented a numerical study of the transport coefficients in the quasi 2D and 3D Hubbard models using the FLEX+CVC approximation, and explained the experimental results in CeMIn_5 . However, in real heavy fermion systems, the Fermi surfaces is much more complicated. As discussed in §8.1, the huge R_{H} ($\gg 1/ne$) in CeMIn_5 cannot be accounted for a simple RTA in the multiband system. However, we have to study the multiband system for a more realistic study. In fact, we recently studied the 2D and 3D periodic Anderson model, which is a two-band model for a heavy fermion system, and found that a relatively large mass-enhancement factor $z^{-1} \sim 10$ is obtained in the FLEX approximation [237]. Since ρ , R_{H} and $\Delta\rho/\rho_0$ are independent of z^{-1} , we could discuss their critical behaviors using the Hubbard model as we have explained in §8.1. Since S and ν are proportional to z^{-1} , on the other hand, we have to take account of the experimental z^{-1} if one compare the theoretical results with experimental values.

Finally, we comment on the “field-induced QCP” in CeCoIn₅ near $H_{c2} \sim 5$ Tesla, where prominent increment in the effective mass m^* was inferred experimentally. Paglione et al. [234] measured the in-plane resistivity near H_{c2} , and derived the relation $A \propto (H - H_{c2})^{-4/3}$, where A is the coefficient of the T^2 -term in the resistivity. According to the Kadowaki-Woods relation $\sqrt{A} \propto m^*$ (see eq. (164)), m^* diverges at $H = H_{c2}$. This fact strongly suggests that the field-induced QCP occurs at $H = H_{c2} = 5$ Tesla in CeCoIn₅. The prominent increment of m^* around the field-induced QCP is also confirmed by thermoelectric transport measurements (S and ν) [261]. Interestingly, a similar field-induced QCP is also realized in heavily over-doped Bi2212 ($T_c = 10$ K) [262]. Up to now, the origin of the critical behavior is unknown. One possible origin will be the (field-induced) SDW state that is hidden in the SC state. In CeCoIn₅, Tanatar et al. [263] measured the anisotropy of the resistivity near H_{c2} , and found that the in-plane resistivity (ρ_a) is linear-in- T above 4 K, whereas it decreases more quickly below 4 K. The observed T -dependence of ρ_a looks similar to the theoretical result in Fig. 34 (i). In contrast, inter-plane resistivity (ρ_c) shows a complete T -linear dependence from 25 mK to 16 K, which might suggest that the CVC is unimportant for ρ_c . Moreover, the Wiedemann-Frantz law ($\kappa/\sigma T = (\pi^2/3)(k_B/e)^2$; κ being the thermal conductivity) is strongly violated only for the inter-plane direction. This strong anisotropy in transport may be difficult to explain by the current theory. Since the transport phenomena under high magnetic field is outside of the scope of the present study, this is an important future problem of transport phenomena.

Up to now, electronic properties in strongly correlated metals under high magnetic field have not been studied sufficiently. This issue is an important future challenge. We should note that the H_{c2} -line in CeCoIn₅ is a weak first-order line for $T \ll T_{c0}$ [106]. Therefore, exactly speaking, the field-induced QCP in CeCoIn₅ cannot be a true QCP.

9.3. Fermi arc picture and transport phenomena

According to the ARPES measurements for under-doped Bi2212 [85, 264, 265, 266] and LSCO [267], the intensity of the spectrum $\rho_{\mathbf{k}}(\omega) = \text{Im}G_{\mathbf{k}}(\omega - i\delta)/\pi$ on the Fermi surface at $\omega = 0$ takes very small value around the hot spot below the pseudo-gap temperature T^* . As a result, $\rho_{\mathbf{k}}(0)$ has finite intensity only around the cold spot, which is frequently called the “Fermi arc”. The length of the Fermi arc diminishes as the temperature decreases, particularly below T^* . References [85, 264, 265] have shown that the pseudo-gap is a precursor of the SC gap. Based on this observation, T -matrix theory [87] and the FLEX+ T -matrix theory [51, 52, 88, 89] have been proposed. Moreover, recent ARPES measurements [268] suggests that the reduction in $\rho_{\mathbf{k}}(0)$ around the hot spot in the Fermi arc state is not due to a “density order”.

The temperature dependence of the Fermi arc in under-doped systems is qualitatively reproduced by the FLEX+ T -matrix approximation, where no hidden order is assumed. Figure 37 shows $\rho_{\mathbf{k}}(0)$ given by the FLEX and FLEX+ T -matrix approximations for LSCO ($n = 0.9$) at $T = 0.02 \sim 80$ K. The intensity of $\rho_{\mathbf{k}}(0)$ at around

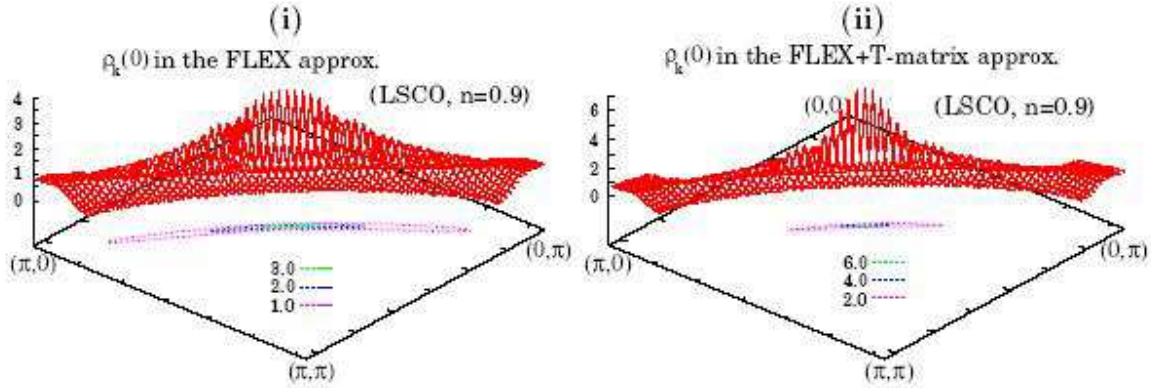


Figure 37. (i) Quasiparticle spectrum $\rho_{\mathbf{k}}(0) = \text{Im}G_{\mathbf{k}}(-i\delta)/\pi$ for LSCO at $T = 0.02$ given by the FLEX approximation. $\rho_{\mathbf{k}}(0)$ is shown only when $\rho_{\mathbf{k}}(0) > 0.1$. The contour is shown on the basal plane. (ii) $\rho_{\mathbf{k}}(0)$ given by the FLEX+ T -matrix approximation. The contour shows a “Fermi arc structure”.

$(\pi, 0)$ is suppressed in the FLEX approximation. The Fermi arc structure becomes more prominent in the FLEX+ T -matrix approximation, because the quasiparticle damping rate due to strong $d_{x^2-y^2}$ -wave SC fluctuations, which is given in eq. (115) in the FLEX+ T -matrix approximation, takes large values around $(\pi, 0)$. In §5, we explained that anomalous transport phenomena below T^* are well explained by the FLEX+ T -matrix approximation, by considering the CVC due to AF+SC fluctuations. Even above T^* , the weak pseudo-gap due to the AF fluctuations is widely observed by ARPES measurements, which reflects the hot/cold-spot structure of $\tau_{\mathbf{k}}$. Therefore, a kind of the Fermi arc structure exists even above T^* .

The Fermi arc structure is also observed in under-doped NCCO: In the ARPES measurements [70], the intensity of $\rho_{\mathbf{k}}(0)$ for a portion of the Fermi surface near the AFBZ (see Fig. 4) is strongly suppressed below $T_N \sim 150$ K by the SDW order. Below T_N , R_H is negative by reflecting the small electron-like Fermi surface around $(\pi, 0)$, which is caused by the reconstruction of the Fermi surface due to the SDW order. Surprisingly, R_H remains negative even above T_N , although SDW-induced Fermi surface reconstruction is absent. Moreover, no anomaly in R_H is observed at T_N . This highly nontrivial fact is explained by the Fermi liquid theory by considering the CVC, as shown in Fig. 19 (iv). According to the ARPES measurements [269], pseudo-gap state due to AF fluctuations is observed even above T_N . Therefore, a Fermi arc state appears to be realized in electron-doped systems.

When a distinct Fermi arc structure exists, the “effective carrier density at the Fermi level (n_{eff})” reduces in proportion to the length of the Fermi arc. Since $R_H \propto 1/en_{\text{eff}}$ in the RTA, it is sometimes claimed that the enhancement of R_H in HTSCs can be explained by the reduction in n_{eff} due to the emergence of the Fermi arc. This idea seems to be valid in heavily under-doped compounds [270]. However, this idea is not true for slightly under-doped systems since R_H starts to decrease below T^* , whereas

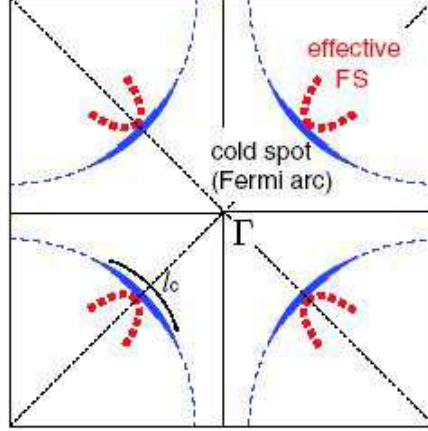


Figure 38. Schematic picture of the “Fermi arc structure” in a hole-doped system. The “effective Fermi surface (FS)” above T^* , which was explained in Fig. 14 (ii), is also described. The smallness of the effective Fermi surface is the origin of the enhancement of R_H above T^* . Below T^* , the effective Fermi surface approaches the true Fermi surface since the CVC due to AF fluctuations are reduces. Therefore, R_H decreases below T^* .

the length of the Fermi arc shrinks due to SC fluctuations. The reduction in R_H in the pseudo-gap region is explained by the reduction in the AF fluctuation, as explained in §5.1.

Here, we discuss the Hall coefficient in the presence of the “Fermi arc structure due to strong AF fluctuations”, by taking the CVC into consideration. The cases we consider correspond to the hole-doped systems above T^* , and the electron-doped systems above T_N . Figure 38 shows the Fermi arc structure due to the weak pseudo-gap formation and the “effective Fermi surface” that is defined to be perpendicular to the total current \vec{J}_k , as introduced in Fig. 14 (ii). (Note that the “effective Fermi surface” is not visible in the ARPES measurements.) Within the RTA, $\sigma_{xx}^{\text{RTA}} \propto l_c/\gamma_{\text{cold}}$ and $\sigma_{xy}^{\text{RTA}} \propto l_c/\gamma_{\text{cold}}^2$, where l_c is the length of the cold spot (Fermi arc). Therefore,

$$R_H^{\text{RTA}} \propto 1/l_c. \quad (149)$$

As we have discussed, σ_{xy} is proportional to the curvature of the effective Fermi surface at the cold spot. In the presence of strong AF fluctuations above T^* , θ_k^J rotates approximately by π around the cold spot, as shown in Fig. 38. Therefore, the curvature of the effective Fermi surface at the cold spot in Fig. 38 is proportional to $1/l_c$. As a result, due to the CVC above T^* ,

$$R_H \propto 1/l_c^2 \quad (150)$$

approximately. The large curvature of the effective Fermi surface around the cold spot is the origin of the enhancement of R_H . In conclusion, when the Fermi arc emerges, the magnitude of R_H is much larger than the value obtained by the RTA that is given in eq. (149).

We note that if the distinct Fermi arc structure due to the highly anisotropic $\tau_{\mathbf{k}}$ is realized, it should lead to a huge magnetoresistance within the RTA: in fact, $\Delta\sigma_{xx}$ diverges when the \mathbf{k} -dependence of the mean free path $l_{\mathbf{k}} = v_{\mathbf{k}}\tau_{\mathbf{k}}$ is not continuous on the Fermi surface; in this case, the second term in eq. (99) diverges as pointed out in Refs. [26]. Therefore, the modified Kohler's rule given by eq. (4) cannot be satisfied. In summary, a unified understanding of anomalous transport phenomena in HTSC cannot be achieved by the RTA even if the Fermi arc structure is taken into account.

9.4. Unconventional transport phenomena in multiorbital systems: anomalous Hall effect and grand Kadowaki-Woods relation

In previous sections, we studied single-band models, and showed that the CVC induces various striking non-Fermi-liquid-like behaviors in the presence of AF fluctuations. For example, R_H shows strong temperature dependence due to the CVC. In multiband systems, however, R_H can exhibit temperature dependence or sign change within the RTA, if a hole-like Fermi surface and an electron-like Fermi surface coexist and their relaxation times have different T -dependences. There are many such examples even in conventional metals. In this study, we did not discuss the multiband effect, since the magnitude $|R_H|$ will remain $\sim 1/ne$ in this mechanism. Thus, the multiband mechanism is impossible to explain the huge $|R_H|$ observed in various systems near the AF QCP.

However, a kind of multiorbital effect causes a huge Hall coefficient in d - and f -electron systems, which is known as the ‘‘anomalous Hall effect (AHE)’’. In the presence of the AHE, the Hall resistivity is given by

$$\rho_H = R_H^n B + R_H^a M, \quad (151)$$

where B is the magnetic field and R_H^n is the ordinary Hall coefficient. R_H^a is the anomalous Hall coefficient, which is (generally) proportional to the magnetization M . In general, R_H^n and R_H^a are even functions of B and M . In ferromagnets, the second term $R_H^a M$ takes a finite value even if $B = 0$. Study of the AHE due to multiband effect was initiated by Karplus and Luttinger [271], and by Luttinger [272]. They found that the anomalous Hall conductivity (AHC) $\sigma_{xy}^a (= R_H^a M/\rho^2)$ is independent of the resistivity ρ . This Karplus-Luttinger-term is called the ‘‘intrinsic AHE’’ because it exists even in systems without impurities. Later, Smit presented a mechanism of ‘‘extrinsic AHE’’ [273]: he found that the spin-polarized electrons are scattered asymmetrically around an impurity site in the presence of spin-orbit interaction. The AHC due to this skew-scattering mechanism is linearly proportional to ρ .

In paramagnetic heavy-fermion systems, the observed Hall coefficient is given by

$$R_H^{\text{HF}} \equiv \rho_H/B = R_H^n + R_H^{\text{AHE}}, \quad (152)$$

where $R_H^{\text{AHE}} = R_H^a \cdot \chi$ and $\chi = M/B$ is the uniform magnetic susceptibility. In heavy-fermion systems, the AHE due to the second term of eq. (152) takes large value since the uniform susceptibility $M/B = \chi$ is widely enhanced due to the strong Coulomb interaction. Due to the AHE, R_H^{HF} starts to increase with increasing temperature from

0K, and it turns to decrease after exhibiting its maximum value around the coherent temperature T_{coh} . The maximum value of $|R_H^{\text{HF}}|$ is more than one order of magnitude greater than $1/|ne| \sim 1.0 \times 10^{-9} \text{ m}^3/C$. The AHE cannot be derived from the RTA since the interband hopping of electrons is important. [In the AHE, the effect of CVC is not expected to be crucial.] Experimentally, R_H^{a} is positive in usual Ce and U based heavy-fermion systems [274, 275].

Here, we discuss the AHE in heavy-fermion systems. Bandstructure of Ce- and Yb-based heavy-fermion system is described by the following orbitally degenerate periodic Anderson model [276, 277]:

$$H = \sum_{\mathbf{k}\sigma} \epsilon_{\mathbf{k}} c_{\mathbf{k}\sigma}^\dagger c_{\mathbf{k}\sigma} + \sum_{\mathbf{k}M} E_f f_{\mathbf{k}M}^\dagger f_{\mathbf{k}M} + \sum_{\mathbf{k}M\sigma} (V_{\mathbf{k}M\sigma}^* f_{\mathbf{k}M}^\dagger c_{\mathbf{k}\sigma} + \text{h.c.}) + \frac{U}{2} \sum_{\mathbf{k}\mathbf{k}'\mathbf{q}MM'} f_{\mathbf{k}+\mathbf{q}M}^\dagger f_{\mathbf{k}'-\mathbf{q}M'}^\dagger f_{\mathbf{k}'M'} f_{\mathbf{k}M}, \quad (153)$$

where $c_{\mathbf{k}\sigma}^\dagger$ ($f_{\mathbf{k}M}^\dagger$) is the creation operator of the conduction electron (f -electron) with $\sigma = \pm 1$ ($M = J, J-1, \dots, -J$). f -orbital degeneracy is $N_f = 2J + 1$. $\epsilon_{\mathbf{k}}$ (E_f) is the spectrum for conduction electrons (f electrons). In the case of Ce-compound ($J = 5/2$), the complex c - f mixing potential is given by $V_{\mathbf{k}M\sigma} = \sigma V_0 \sqrt{4\pi/3} \sqrt{(7/2 - 2M\sigma)/7} Y_{l=3}^{M-\sigma}(\theta_k, \varphi_k)$, where $Y_{l=3}^m(\theta_k, \varphi_k)$ is the spherical harmonic function, In the case of Yb-compound ($J = 7/2$), $V_{\mathbf{k}M\sigma} = V_0 \sqrt{\pi} \sqrt{(7/2 + 2M\sigma)/7} Y_{l=3}^{M-\sigma}(\theta_k, \varphi_k)$. Note that the relation $\sum_{M=-J}^J |V_{\mathbf{k}M\sigma}|^2 = V_0^2$ holds.

The Green function for c electron is given by [276, 277]

$$G_{\mathbf{k}}^c(\omega) = \left(\omega + \mu - \epsilon_{\mathbf{k}} - \frac{(V_0)^2}{\omega + \mu - E_f - \Sigma(\omega)} \right)^{-1} \approx \left(\omega + \mu - \epsilon_{\mathbf{k}} - \frac{(V_0^*)^2}{\omega - \tilde{E}_f - i\gamma^*} \right)^{-1}, \quad (154)$$

where $V_0^* = \sqrt{z}V_0$, $\tilde{E}_f = z(E_f + \text{Re}\Sigma(0) - \mu)$, $\gamma^* = z\text{Im}\Sigma(0)$, and $z = (1 - \partial\text{Re}\Sigma(\omega)/\partial\omega)^{-1}|_{\omega=0}$ is the renormalization factor. Since the quasiparticle energy $E_{\mathbf{k}}^*$ satisfies $\text{Re}\{1/G_{\mathbf{k}}^c(E_{\mathbf{k}}^*)\} = 0$, the equation for $E_{\mathbf{k}}^*$ is given by

$$E_{\mathbf{k}}^* + \mu - \epsilon_{\mathbf{k}} - \frac{(V_0^*)^2(E_{\mathbf{k}}^* - \tilde{E}_f)}{(E_{\mathbf{k}}^* - \tilde{E}_f)^2 + (\gamma^*)^2} = 0. \quad (155)$$

Here, we derive the quasiparticle energy by analyzing eq. (155): At zero temperature where $\gamma^* = 0$, heavy quasiparticles band is formed due to c - f hybridization. Below T_{coh} , the quasiparticles band is

$$E_{\mathbf{k}\pm}^* = \frac{1}{2} \left(\epsilon_{\mathbf{k}} - \mu + \tilde{E}_f \pm \sqrt{(\epsilon_{\mathbf{k}} - \mu - \tilde{E}_f)^2 + 4(V_0^*)^2} \right), \quad (156)$$

where $E_{\mathbf{k}-}^*$ ($E_{\mathbf{k}+}^*$) represents the lower (upper) quasiparticles band. γ^* grows monotonically as temperature increases, and $|\tilde{E}_f| \sim \gamma^*$ at the coherent temperature T_{coh} . When $T \gg T_{\text{coh}}$, c - f hybridization is prohibited by $\gamma^* \gg |\tilde{E}_f|$.

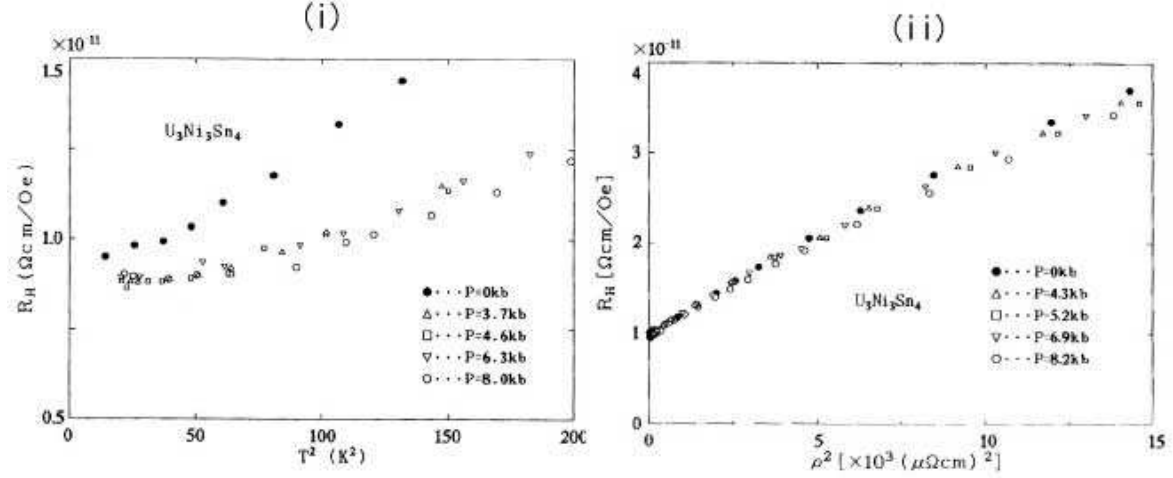


Figure 39. R_H in $U_3Ni_3Sn_4$ plotted as functions of (i) T^2 and (ii) ρ^2 . The relation $R_H^{\text{HF}} - R_H^n \propto \rho^2$ is satisfied well, as predicted by the theory of AHE [277]. [Ref. [278]]

We summarize the electronic states in heavy-fermion systems: **(i)** Below T_{coh} , Fermi liquid state with heavy quasiparticles is realized due to c - f hybridization. Mass enhancement factor z^{-1} and uniform susceptibility $\chi \propto z^{-1}$ are constant. The heavy quasiparticle bandwidth W_{HF} is approximately given by $W_{\text{HF}} \sim \min\{E_{\mathbf{k}+}^* - E_{\mathbf{k}-}^*\} \sim (V_0^*)^2/W_c \sim |\tilde{E}_f|$, where W_c is the c -electron bandwidth. **(ii)** Above T_{coh} , c - f hybridization ceases, and localized f -electrons causes Curie-Weiss susceptibility. Experimentally, the temperature of maximum resistivity T_ρ^* is larger than T_{coh} .

In paramagnetic heavy-fermion systems, the Hall coefficient takes huge values due to the AHE [274, 275, 278]. In the early stage, Coleman et al [279] and Fert and Levy [280] developed theories of extrinsic AHE: they studied the extrinsic mechanism based on the f -electron impurity Anderson models with d -orbital channels, and predicted the relation $R_H^{\text{AHE}} \propto \chi\rho$ above T_{coh} when the d -orbital phase-shift is finite.

On the other hand, Kontani and Yamada studied the intrinsic AHE due to multiband effect based on the $J = 5/2$ periodic Anderson model, which is the model in the strong limit of spin-orbit interaction [277, 281]. In this model, the anomalous velocity originates from the angular momentum of the localized f -electrons. That is, the AHE originates from the transfer of angular momentum of the f -electron to the conduction electron. Based on the linear-response theory, they derived a large intrinsic AHC: $\sigma_{xy}^a/H [1/\Omega \text{ cm Gauss}] = 5.8 \times 10^{-9} (n[\text{cm}^{-3}])^{1/3} / \tilde{E}_f [\text{K}]$ where \tilde{E}_f is the renormalized f -level measured from the Fermi energy. $|\tilde{E}_f|$ gives approximate quasiparticle bandwidth. The present study predicts that $R_H^{\text{AHE}} > 0$ (< 0) in Ce (Yb) based heavy-fermion systems since $\tilde{E}_f > 0$ (< 0). This prediction is consistent with the experimental results [274, 275]. If we substitute $\tilde{E}_f = 10\text{K}$ and $n = 10^{22}\text{cm}^{-3}$, $\sigma_{xy}^a/H = 1.3 \times 10^2 [1/\Omega \text{ cm Gauss}]$, which is a typical experimental value. The predicted temperature dependence of $R_H^{\text{AHE}} = (\sigma_{xy}^a/H)\rho^2$ is $R_H^{\text{AHE}} \propto (\gamma^{*2}/(\tilde{E}_f^2 + \gamma^{*2}))\chi$ [277].

Therefore, R_H^{AHE} shows the following cross-over behavior:

$$R_H^{\text{AHE}} \propto \chi \rho^2 [\propto \rho^2] \quad : \text{ below } T_{\text{coh}} (\gamma^* < |\tilde{E}_f|), \quad (157)$$

$$R_H^{\text{AHE}} \propto \chi [\propto 1/T] \quad : \text{ above } T_{\text{coh}} (\gamma^* > |\tilde{E}_f|). \quad (158)$$

In typical Ce-based heavy-fermion systems, $1/z \sim 100$ and $|\tilde{E}_f| \sim 10$ K. Below T_{coh} , eq. (157) is proportional to ρ^2 since χ is constant for $T < T_{\text{coh}}$. Figure 39 shows the R_H in $\text{U}_3\text{Ni}_3\text{Sn}_4$ ($\gamma = 380\text{mJ/K}^2$), where the relation $R_H^{\text{AHE}} = R_H^{\text{HF}} - R_H^n \propto \rho^2$ holds well below $\sim 0.3T_{\text{coh}} \sim 25\text{K}$. Note that the extrinsic type AHE [279, 280] and the intrinsic type AHE [277] can coexist. However, the relation $R_H^{\text{AHE}} \propto \rho^2$ suggests that the intrinsic-type AHE is dominant at least below T_{coh} . Above T_{coh} , the AHE due to interband transition is suppressed when c - f mixing is prohibited. Therefore, eq. (158) is independent of ρ . This *coherent-incoherent crossover of intrinsic AHE* was first theoretically derived in Ref. [277]. This crossover behavior is not restricted to heavy-fermions systems, but also observed in various transition ferromagnets [282].

In heavy-fermion systems near the AF QCP, R_H^n shows strong temperature dependence due to the CVC. To extract R_H^n from the observed Hall coefficient, we have to seriously consider the T -dependence of R_H^{AHE} . Very fortunately, AHE is vanishingly small in CeMIn_5 [19, 20]. Therefore, we could perform reliable analysis of the ordinary Hall effect in CeMIn_5 as discussed in §8.1, without the necessity of subtracting the AHE. Note that the AHE vanishes when the crystal-field splitting of the f -levels is much larger than T_{coh} . This may be the reason for the small AHE in CeMIn_5 .

Recently, theory of the intrinsic AHE in (ferromagnetic) d -electron systems has been developed based on realistic multiorbital tight-binding models [283, 284]. It was revealed that a large anomalous velocity emerges in general multiorbital d -electron systems because of the inter-orbital hopping. This is the origin of the large AHE in d -electron systems, which is very similar to the origin of the AHE in f -electron systems [277]. The intrinsic AHEs for Fe [286] and in SrRuO_3 [287] were also calculated based on the LDA band calculations.

Here, we present an intuitive explanation of the AHE due to the multiorbital effect [284, 288]. In a multiorbital system, a conduction electron acquires the “effective Aharonov-Bohm phase factor” due to d -atomic angular momentum with the aid of the spin-orbit interaction and the inter-orbital hoppings, which is responsible for the Hall effect. The intuitive explanation based on the tight-binding model, which is given in Fig. 40, which represents a square lattice (d_{xz}, d_{yz})-orbital tight-binding model with z -component of the spin-orbit interaction $\sum_i (l_z \cdot s_z)_i$ [284], which is a simplified model for $(\text{Ca}, \text{Sr})_2\text{RuO}_4$: This compound shows large AHE under the magnetic field [285]. Its magnitude is comparable with the large AHE in f -electron systems (such as UPt_3). In Fig. 40, $\pm t'$ represents the interorbital hopping integral between next nearest sites. Now, let us consider the motion of a down-spin electron along a triangle of half unit cell: An electron in the d_{xz} -orbital can transfer to d_{yz} -orbital and vice versa using the spin-orbit interaction $\pm \hbar \lambda l_z$, where $\langle yz | l_z | xz \rangle = -\langle xz | l_z | yz \rangle = i$. By combination of angular dependence of interorbital hopping and the spin-orbit interaction, any clockwise

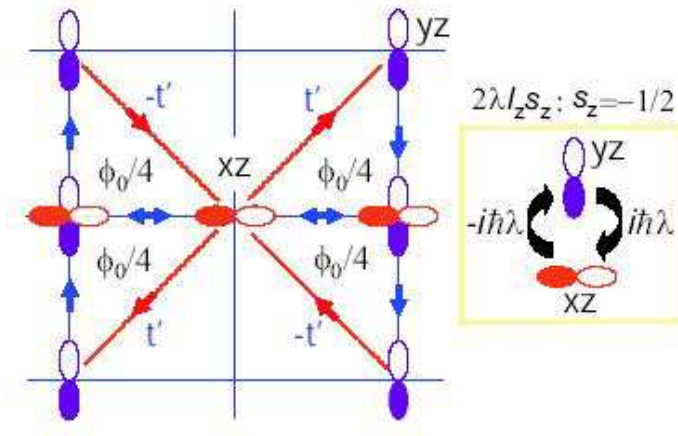


Figure 40. Effective magnetic flux for down-electrons in a square lattice (d_{xz}, d_{yz})-orbital tight-binding model with z -component of the spin-orbit interaction $\sum_i (l_z \cdot s_z)_i$. The effective magnetic flux for up-electrons is negative. Both $|xz\rangle$ and $|yz\rangle$ are given by the linear combination of $|l_z = \pm 1\rangle$. Since $\hat{l}_z^2 = 1$ in the present basis, the rotation operator $R(\theta) = e^{-i \hat{l}_z \theta} = \cos \theta - i \hat{l}_z \sin \theta$ is equal to $-i \hat{l}_z$ for $\theta = \pi/2$. Therefore, $\hat{l}_z |xz\rangle = i R(\pi/2) |xz\rangle = i |yz\rangle$ and $\hat{l}_z |yz\rangle = i R(\pi/2) |yz\rangle = -i |xz\rangle$.

(anti-clockwise) motion along any triangle path with spin-orbit interaction causes the factor $+i$ ($-i$). This factor can be interpreted as the ‘‘Aharonov-Bohm phase factor’’ $\exp(2\pi i \phi / \phi_0)$ [$\phi_0 = hc/|e|$], where $\phi = \phi_0/4$ represents the ‘‘effective magnetic flux’’ in the half unit cell. We revealed the fact that the effective magnetic flux, which is inherent in multiorbital d -electron systems, causes huge AHE in various transition metals.

In many d -electron ferromagnets, intrinsic AHE ($R_H^a \propto \rho^2$) seems to be observed experimentally. In particular, Asamitsu et al. measured AHE in various transition-metal ferromagnets, and found out a universal crossover behavior from $R_H^a \propto \rho^2$ to $R_H^a \propto \rho^n$ ($n = 0 \sim 0.5$) as the resistivity increases, around $\rho \sim 100 \mu\Omega\text{cm}$. Recent theoretical study in Ref. [284] has revealed that the experimental result is explained by the following coherent-incoherent crossover

$$R_H^a \propto \rho^2 \quad : \quad \gamma < \Delta, \quad (159)$$

$$R_H^a \propto \text{const.} \quad : \quad \gamma > \Delta, \quad (160)$$

where Δ represents the minimum bandsplitting near the Fermi level. $\Delta \gtrsim 0.1$ eV in usual transition metal ferromagnets. It is apparent that eqs. (159) and (160) correspond to eqs. (157) and (158) for heavy-fermion systems. [Note that $R_H^{\text{AHE}} = R_H^a \cdot \chi$.] Therefore, a conventional behavior $R_H^a \propto \rho^2$ is violated in high-resistivity metals since the interband particle-hole excitation, which is the origin of the AHE, is suppressed when γ is larger than bandsplitting energy Δ .

There is a simple intuitive explanation for this coherent-incoherent crossover of intrinsic AHE: When γ is sufficiently small, the intrinsic Hall conductivity is proportional to the lifetime of the interband particle-hole excitation: \hbar/Δ [271, 272, 277]. In the high-resistivity regime where $\gamma \gg \Delta$, the SHC decreases drastically with γ since the

interband excitation is suppressed when the quasiparticle lifetime \hbar/γ is shorter than \hbar/Δ . According to the above discussion, *coherent-incoherent crossover of intrinsic AHE* should be universal and is widely observed in various multiorbital p -, d -, and f -electron systems.

It is noteworthy that the large anomalous velocity also induces a sizable spin Hall effect (SHE) in paramagnetic multiorbital systems [284, 288, 289]. The SHE is the phenomena that an applied electric field induces a spin current $\vec{j}^s \equiv \vec{j}_\uparrow - \vec{j}_\downarrow$ in a transverse direction. Recently, SHE attracts great attention due to its fundamental interest and its potential application in spintronics. Karplus and Luttinger [271] showed that an applied electric field induces a spin-dependent transverse current in the presence of spin-orbit interaction. This mechanism causes the AHE in ferromagnetic metals, and the SHE in paramagnetic metals. Recently, the spin Hall conductivity (SHC) in Pt had been observed [290], and found that the SHC in Pt is 10^4 times larger than that observed in n -type semiconductors. This experiment fact has attracted considerable attention to the study of the SHE in transition metals.

Recently, we propose a new mechanism for the giant SHE originate from the d -orbital degrees of freedom, which is absent in semiconductors [288, 289, 291]. In a multiorbital system, a conduction electron acquires the “effective Aharonov-Bohm phase factor” due to d -atomic angular momentum, as explained in Fig. 40. We have studied the SHEs in Sr_2RuO_4 [288], which is the first theoretical study of the SHE in d -electron systems, in Pt [289], and in various $4d$ and $5d$ transition metals [291]. It is found that the explanation in Fig. 40 seems to capture the characteristics of SHE in d -electron systems. In contrast, the “Dirac monopole mechanism” [292] is appropriate when massless Dirac cone dispersion exists close to the Fermi level like in semiconductors. The present mechanism of SHE is also different from that in Rashba-type 2D electron-gas model due to momentum-dependent SOI [293]. Thus, giant SHE due to atomic orbital degrees of freedom is ubiquitous in various p -, d -, f -electron systems.

Finally, we discuss the multiorbital effect on the Kadowaki-Woods (KW) ratio $A\gamma^{-2}$, where A is the coefficient of the T^2 term in the resistivity, and γ is the coefficient of the T -linear term of the electric specific heat. Experimentally, the KW ratio in Ce- and U-based heavy-fermion compounds shows an approximate universal value $A\gamma^{-2} \approx 10^{-5} [\mu\Omega \text{ cm (mol}\cdot\text{K/mJ)}^2]$, which is known as the KW relation [294]. Although it was believed to be universal in heavy-fermion systems for a long time, recent experimental activities have revealed that the KW relation is strongly violated in many Yb-based compounds. Recently, the author had derived a generalized KW relation that is applicable for systems with general f -orbital degeneracy N_f for Ce- and Yb-based compounds [295] and for Sm- and Er-based compounds [296]. By considering the material dependence of N_f , the mystery of the failure of the KW relation was resolved.

Here, we analyze the KW ratio in terms of the DMFT ($d = \infty$ -limit) [109, 110], which is believed to be useful in heavy-fermion systems that is not close to the AF-QCP. By using the DMFT, we can utilize the strong-coupling Fermi liquid theory for the impurity Anderson model developed by Yamada and Yosida [297]: Using the Ward

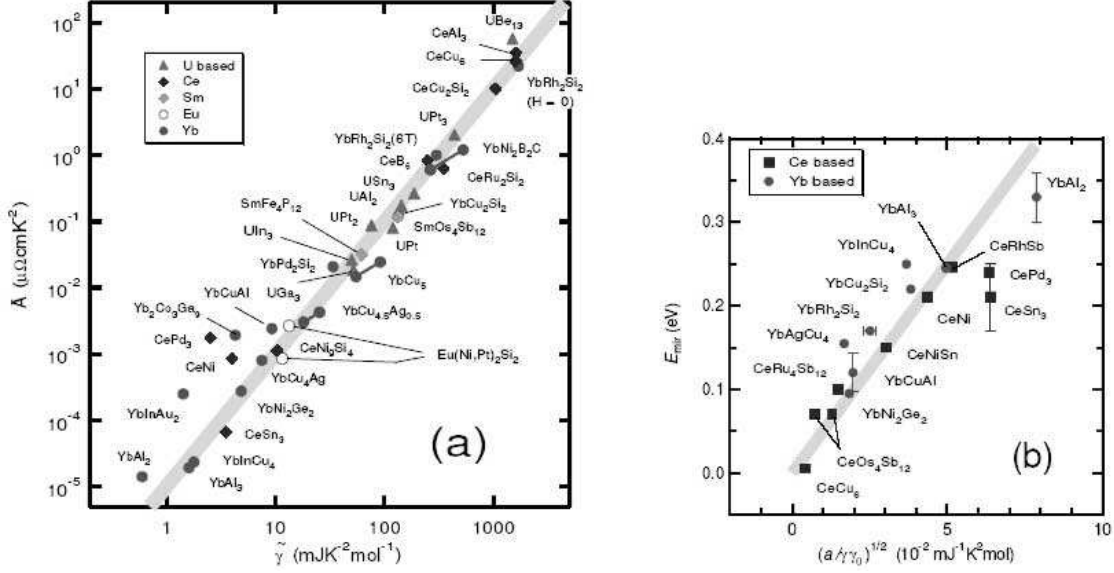


Figure 41. (a) Grand Kadowaki-Woods relation in Ref. [299], where $\tilde{A} = 2A/N_f(N_f - 1)$ and $\tilde{\gamma} = 2\gamma/N_f(N_f - 1)$. (b) A scaling relation between E_{mir} and $\sqrt{a/\gamma\gamma_0}$ [305]. E_{mir} corresponds to $2\tilde{V}$, and $\sqrt{a/\gamma\gamma_0} \propto \sqrt{zV}$ (\sqrt{a} is a constant of order $O(1)$). [Ref. [306]]

identity, they derived the exact Wilson ratio $R \equiv (\chi/\chi^0)/(\gamma/\gamma^0) = 2$ for $N_f = 2$ in the strong coupling limit, that is, $z^{-1} \gg 1$ and the f -electron charge susceptibility is zero (Kondo model limit). Here, χ^0 and γ^0 represent the non-interacting values. Using the DMFT, γ and $\text{Im}\Sigma(0)$ in the PAM (in eq. (153) is given by [295, 298]

$$\gamma = N_A k_B^2 \frac{\pi^2}{3} N_f(N_f - 1) \Gamma_{\text{loc}}(0, 0) \rho^f(0)^2, \quad (161)$$

$$\text{Im}\Sigma(0) = \frac{\pi^3 (k_B T)^2}{2} (N_f - 1) \Gamma_{\text{loc}}^2(0, 0) \rho^f(0)^3, \quad (162)$$

in the strong coupling limit. Here, $N_A = 6.02 \times 10^{23}$ is the Avogadro constant, and $\Gamma_{\text{loc}}(0, 0)$ is the local four-point vertex. $\rho^f(0)$ is the DOS for f -electron per channel; $N_f \rho^f(0)$ is the total DOS at the Fermi level. When $\epsilon_{\mathbf{k}}$ in eq. (153) is a free dispersion, the conductivity is given by

$$\sigma = \frac{e^2}{h} \frac{(3/\pi)^{1/3} n^{4/3} a^3}{N_f \rho^f(0) \cdot \text{Im}\Sigma(0)}, \quad (163)$$

where $n (= k_F^3/3\pi^2)$ is the density of quasiparticles that form the conduction band, and a is the unit cell length. According to eqs. (161)-(163), we find the scaling properties $\gamma \propto N_f(N_f - 1) \Gamma_{\text{loc}} \rho^{f^2}$ and $A \propto N_f(N_f - 1) \Gamma_{\text{loc}}^2 \rho^{f^4}$. Therefore, we obtain the “grand KW relation” that is valid for any $N_f (\geq 2)$ [295, 296, 298, 299]:

$$\begin{aligned} A\gamma^{-2} &\approx \frac{h}{e^2 k_B^2} \frac{9(3\pi)^{-1/3}}{4n^{4/3} a^3 N_A^2} \frac{1}{\frac{1}{2} N_f(N_f - 1)} \\ &\approx \frac{1 \times 10^{-5}}{\frac{1}{2} N_f(N_f - 1)} \quad [\mu\Omega \text{ cm} (\text{mol}\cdot\text{K}/\text{mJ})^2]. \end{aligned} \quad (164)$$

where we put $h/e^2 = 2.6 \times 10^4 \Omega$, $k_B = 1.38 \times 10^{-23} \text{ JK}^{-1}$, and we assumed $1/n^{4/3}a^3 \approx 4 \times 10^{-8} \text{ cm}$.

Without crystal field splitting of the f -level, $N_f = 2J + 1 = 6$ for Ce^{3+} and Sm^{3+} ions, and $N_f = 8$ for Yb^{3+} and Er^{2+} ions. Therefore, the previous KW relation turned out to be valid only when $N_f = 2$ (Kramers doublet case due to strong crystal field splitting). A similar universal relation $\lim_{T \rightarrow 0} eS/T\gamma \approx \pm 1$ (S is the Seebeck coefficient) was recently found [300, 301]. The characteristics of the electronic state in heavy-fermion systems are (i) large mass-enhancement and (ii) small charge susceptibility since the f -electron is almost localized. The grand KW relation (164) is derived only by imposing these constraints on the microscopic Fermi liquid theory. This fact illustrates a remarkable advantage of the Fermi liquid theory for the analysis of strongly correlated systems.

Figure 41 (i) shows the experimental verification of eq. (164) for various heavy-fermion compounds, where N_f in each compound was determined by the temperature dependence of χ and the inelastic neutron scattering [299]. Tsujii's study confirmed that $N_f \sim 2$ in many Ce-based compounds, where crystal-field splitting is larger than the renormalized Fermi energy W_{HF} . On the other hand, $N_f \sim 8$ in many Yb-based ones, where crystal-field splitting is smaller than W_{HF} . Torikachvili et al. also found that other Yb-based heavy-fermion systems $\text{YbT}_2\text{Zn}_{20}$ ($T = \text{Fe, Co, Ru, Rh, Os, or Ir}$) follows the grand KW relation shown in eq. (164) [302]. When N_f is larger than the number of conduction band N_c , almost unhybridized f -levels exist near the Fermi level, except when the crystal-field splitting is very large. This situation induces a huge anomalous Hall coefficient [277] as well as the large Van Vleck susceptibilities [303, 304] in Kondo insulators and in singlet SC heavy-fermion systems.

We shortly discuss the absence of the multiband effect on the KW relation: In a usual heavy-fermion compound, there are one or two (relatively) large Fermi surfaces composed of heavy quasiparticles, and several (relatively) small Fermi surfaces composed of light-quasiparticles. In the presence impurities, $AT^2 \propto \langle \gamma_{\mathbf{k}} \rangle_{\text{FS}}$ as explained in eq. (33). Therefore, heavy quasiparticles on the large Fermi surfaces give the dominant contribution to both the specific heat and the A -term. As a result, the grand-KW relation is universally realized even in multiband systems. Moreover, in many heavy-fermions, there is evidence that the heavy quasiparticles on the large Fermi surfaces give the dominant contribution to the conductivity. For example, $|R_{\text{H}}^n| \sim 1/ne$ seems to be realized in many heavy-fermions away from AF-QCPs, although $|R_{\text{H}}^n| \gg 1/ne$ should be realized when small Fermi surfaces are the most conductive.

Figure 41 (ii) shows the mid-infrared peak energies E_{mir} of the optical conductivity $\sigma(\omega)$ in various heavy-fermion systems [305]. According to the Fermi liquid theory, $E_{\text{mir}} \approx \sqrt{z}V$ is satisfied in the PAM, where V is the c - f mixing potential and $1/z = m^*/m$ is the mass enhancement factor. Okamura confirmed that the relation $E_{\text{mir}} \propto \gamma^{-1/2}$ is universally satisfied in various heavy-fermion compounds, as shown in Fig. 41 (ii). This scaling relation is well satisfied regardless of N_f . Their study established the validity of the PAM and the Fermi liquid theory in various heavy-fermion

Acknowledgments

The author would like to thank K. Yamada, K. Ueda, K. Kanki, H. Kino, S. Onari and Y. Tanaka for collaborations on the theory of the transport phenomena in strongly correlated systems. Thanks are also due to Y. Matsuda and Y. Nakajima for close discussions and collaborations on CeMIn₅ and other heavy-fermion systems. Further, I would like to thank H.D. Drew and D.C. Schmadel for the useful discussions on AC Hall effect in HTSCs. I am grateful to H. Taniguchi for the discussion on organic metals, particularly for his kind offer of providing the figures used in Fig. 35.

The work on magnetoresistance was supported by the Ministry of Education, Science, Sports, and Culture, Japan, during my stay in Augsburg University. The author was supported by a Grant-in-Aid for the Encouragement of Young Scientists under the contract Nos. 18740197, 15740198 and 13740202 from the Ministry of Education, Culture, Sports, Science, and Technology (MEXT) of Japan. This work has been also supported by Grants-in-Aid for Scientific Research in Priority Areas “Skutterudites” and “anomalous quantum material” from MEXT.

References

- [1] J. M. Ziman: *Electrons and Phonons* (Clarendon, Oxford, 1960).
- [2] J. Takeda, T. Nishikawa, and M. Sato, *Physica C* **231** (1994) 293; T. Nishikawa, J. Takeda and M. Sato, *J. Phys. Soc. Jpn.* **63** (1994) 1441.
- [3] H.Y. Hwang, B. Batlogg, H. Takagi, H.L. Kao, J. Kwo, R.J. Cava, J.J. Krajewski, and W.F. Peck, Jr.: *Phys. Rev. Lett.* **72** (1994), 2636.
- [4] Peng Xiong, Gang Xiao, and X.D. Wu: *Phys. Rev. B* **47** (1993), 5516.
- [5] T.R. Chien, Z.Z. Wang, and N.P. Ong: *Phys. Rev. Lett.* **67** (1991), 2088.
- [6] Y. Kubo, Y. Shimakawa, T. Manako, and H. Igarashi: *Phys. Rev. B* **43** (1991), 7875.
- [7] P. Fournier, X. Jiang, W. jiang, S. N. Mao, T. Venkatesan, C. J. Lobb and R. L. Greene: *Phys. Rev.* **B56** (1997) 14149.
- [8] Y. Dagan, M.M. Qazilbash, C.P. Hill, V.N. Kulkarni, and R.L. Greene, *Phys. Rev. Lett.* **92** (2004) 167001.
- [9] Y. Abe, K. Segawa and Y. Ando, *Phys. Rev. B* **60**, R15055 (1999).
- [10] Y. Hanaki, Yoichi Ando, S. Ono, J. Takeya *Phys. Rev. B* **64**, 172514 (2001).
- [11] G. Xiao, P. Xiong, and M. Z. Cieplak, *Phys. Rev. B* **46**, 8687 (1992).
- [12] A. Malinowski, Marta Z. Cieplak, S. Guha, Q. Wu, B. Kim, A. Krickser, A. Perali, K. Karpiška, M. Berkowski, C. H. Shang, and P. Lindenfeld, *Phys. Rev. B* **66**, 104512 (2002).
- [13] K. Katayama, T. Nagai, H. Taniguchi, K. Satoh, N. Tajima and R. Kato, *J. Phys. Soc. Jpn.* **76**(2007) Suppl. A, 194.
- [14] Yu. V. Sushko, N. Shirakawa, K. Murata, Y. Kubo, N.D. Kushch, E.B. Yagubskii: *Synth. Met.* **85** (1997) 1541.
- [15] H. Taniguchi, unpublished.
- [16] K. Murata, M. Ishibashi, Y. Honda, N.A. Fortune, M. Tokumoto, N. Kinoshita and H. Anzai: *Solid State Comm.* **76** (1990) 377.
- [17] H. Taniguchi, unpublished.
- [18] H. Taniguchi, unpublished.

- [19] Y. Nakajima, K. Izawa, Y. Matsuda, S. Uji, T. Terashima, H. Shishido, R. Settai, Y. Onuki and H. Kontani: *J. Phys. Soc. Jpn.* **73** (2004) 5.
- [20] Y. Nakajima, H. Shishido, H. Nakai, T. Shibauchi, K. Behnia, K. Izawa, M. Hedo, Y. Uwatoko, T. Matsumoto, R. Settai, Y. Onuki, H. Kontani, and Y. Matsuda: *J. Phys. Soc. Jpn.* **76** (2007) 027403.
- [21] T. Namiki, H. Sato, H. Sugawara, Y. Aoki, R. Settai and Y. Onuki: preprint.
- [22] S. Paschen, T. Luhmann, S. Wirth, P. Gegenwart, O. Trovarelli, C. Geibel, F. Steglich, P. Coleman, Q. Si: *Nature* **432** (2004) 881.
- [23] P.W. Anderson: *Phys. Rev. Lett.* **67** (1991) 209; P.W. Anderson, *The Theory of Superconductivity in the High-Tc Cuprates* (Princeton Series in Physics).
- [24] R. Hlubina and T. M. Rice, *Phys. Rev. B* **51**, 9253-9260 (1995).
- [25] B.P. Stojkovic and D. Pines, *Phys. Rev. B* **55**, 8576 (1997).
- [26] L.B. Ioffe and A.J. Millis: *Phys. Rev. B* **58** (1998) 11631.
- [27] Y. Yanase and K. Yamada: *J. Phys. Soc. Jpn.* **68** (1999) 548.
- [28] L. Landau: *Sov. Phys. JETP* **3** (1957) 920; *ibid* **5** (1957) 101; *ibid* **8** (1959) 70.
- [29] P. Nozières and D. Pines: *Theory of Quantum Liquids*.
- [30] P. Nozières: *Theory of Interaction Fermion Systems* (Benjamin, New York, 1964).
- [31] A.A. Abrikosov, L.P. Gor'kov and I.E. Dzyaloshinskii: *Methods of Quantum Field Theory in Statistical Physics* (Dover, New York, 1975).
- [32] H. Kontani and K. Yamada: *J. Phys. Soc. Jpn.* **74** (2005) 155.
- [33] H. Kontani, K. Kanki and K. Ueda: *Phys. Rev. B* **59** (1999) 14723.
- [34] K. Kanki and H. Kontani: *J. Phys. Soc. Jpn.* **68** (1999) 1614.
- [35] H. Kontani: *Phys. Soc. Jpn.* **70** (2001) 1873.
- [36] H. Kontani: *Phys. Soc. Jpn.* **70** (2001) 2840.
- [37] H. Kontani, *Phys. Rev. Lett.* **89** (2002) 237003.
- [38] H. Kontani: *Phys. Rev. B* **64** (2001) 054413.
- [39] H. Kontani, *Phys. Rev. B* **67** (2003) 014408.
- [40] G. M. Eliashberg : *Sov. Phys. JETP* **14** (1962), 886.
- [41] J.S. Langer: *Phys. Rev.* **120** (1960) 714.
- [42] K. Yamada and K. Yosida: *Prog. Theor. Phys.* **76** (1986) 621:
- [43] H. Kohno and K. Yamada: *Prog. Theor. Phys.* **80** (1988) 623.
- [44] H. Fukuyama, H. Ebisawa and Y. Wada: *Prog. Theor. Phys.* **42** (1969) 494.
- [45] S. Fujimoto, H. Kohno and K. Yamada, *Phys. Soc. Jpn.* **60** (1991) 2724.
- [46] H. Maebashi and H. Fukuyama: *Phys. Soc. Jpn.* **66** (1997) 3577; *ibid* **67** (1998) 242.
- [47] See, e.g., Y. Iye, in *Physical Properties of High Temperature Superconductors*, edited by D.M. Ginsberg (World Scientific, Singapore, 1992) Vol. 3.
- [48] See, e.g., K. Asayama, Y. Kitaoka, G.-q. Zheng, and K. Ishida: *Prog. NMR Spectroscopy* **28** (1996) 221.
- [49] Y. Suzumura, Y. Hasegawa and H. Fukuyama: *J. Phys. Soc. Jpn.* **57** (1988) 2768; G. Kotliar: *Phys. Rev. B* **37**, 3664 (1988).
- [50] P. A. Lee, N. Nagaosa, and X.-G. Wen, *Rev. Mod. Phys.* **78**, 17 (2006).
- [51] Y. Yanase, T. Jujo, T. Nomura, H. Ikeda, T. Hotta and K. Yamada: *Physics Report* **387** (2003) 1.
- [52] K. Yamada: *Electron Correlation in Metals* (Cambridge Univ. Press 2004).
- [53] T. Moriya, Y. Takahashi, and K. Ueda: *J. Phys. Soc. Jpn* **59** (1990) 2905, K. Ueda, T. Moriya, and Y. Takahashi: *J. Phys. Chem. Solids* **53** (1992) 1515.
- [54] T. Moriya and K. Ueda: *Adv. Physics* **49** (2000) 555.
- [55] K. Miyake and O. Narikiyo, *J. Phys. Soc. Jpn.* **63** (1994) 3821.
- [56] P. Monthoux and D. Pines: *Phys. Rev. B* **47** (1993) 6069.
- [57] N.E. Bickers and S.R. White: *Phys. Rev. B* **43** (1991) 8044.
- [58] K. Kuroki, R. Arita, and H. Aoki: *Phys. Rev. B* **60**, 9850 (1999).

- [59] H. Yoshimura and D.S. Hirashima: *J. Phys. Soc. Jpn* **73** (2004) 2057.
- [60] P. Coleman, C. Pépin, Q. Si and R. Ramazashvili: *J.Phys.: Condens. Matter* **13** (2001) R723.
- [61] S. Sachdev: *Quantum Phase Transitions*, (Cambridge University Press, Cambridge UK 1999).
- [62] A. V. Chubukov, D. Pines and J. Schmalian, *The Physics of Superconductors, Vol. 1*, ed. K.-H. Bennemann and J. B. Ketterson, (Springer, Berlin, 2002); A. Abanov, A. V. Chubukov and J. Schmalian, *Adv. Phys.* **52** (2003) 119 and references therein.
- [63] D. Manske, *Theory of Unconventional Superconductors: Cooper-Pairing Mediated By Spin Excitations* (Springer 2004, Berlin).
- [64] M. Sigrist and T. M. Rice, *J. Phys. Soc. Jpn.* **61** (1992) 4283.
- [65] D. A. Wollmann, D. J. Van Harlingen, W. C. Lee, D. M. Ginsberg and A. J. Leggett, *Phys. Rev. Lett.* **71** (1993) 2134.
- [66] C. C. Tsuei, J. R. Kirtley, C. C. Chi, L. S. Yu-Jahnes A. Gupta, T. Shaw, J. Z. Sun, and M. B. Ketchen, *Phys. Rev. Lett.* **73** (1994) 593.
- [67] S. Kashiwaya and Y. Tanaka, *Rep. Prog. Phys.* **63** (2000) 1641.
- [68] T. Hotta, *J. Phys. Soc. Jpn.* **63** (1994) 4126.
- [69] see, e.g., N. P. Ong: *Physical Properties of High Temperature Superconductors*, edited by D.M. Ginsberg (World Scientific, Singapore, 1992), Vol.2.
- [70] N.P. Armitage, D.H. Lu, C. Kim, A. Damascelli, K.M. Shen, F. Ronning, D.L. Feng, P. Bogdanov, and Z.-X. Shen: *Phys. Rev. Lett.* **87** (2001) 147003; N. P. Armitage, F. Ronning, D. H. Lu, C. Kim, A. Damascelli, K. M. Shen, D. L. Feng, H. Eisaki, Z.-X. Shen, P. K. Mang, N. Kaneko, M. Greven, Y. Onose, Y. Taguchi, and Y. Tokura: *Phys. Rev. Lett.* **88**, 257001 (2002).
- [71] J. M. Harris, Y. F. Yan, P. Mati, N. P. Ong, P. W. Anderson, T. Kimura and K. Kitazawa: *Phys. Rev. Lett.* **75** (1995) 1391.
- [72] T. Kimura, S. Miyasaka, H. Takagi, K. Tamasaku, H. Eisaki, S. Uchida, K. Kitazawa, M. Hiroi, M. Sera, and N. Kobayashi: *Phy. Rev. B* **53** (1996) 8733.
- [73] A. W. Tyler, Y. Ando, F. F. Balakirev, A. Passner, G. S. Boebinger, A. J. Schofield, A. P. Mackenzie, and O. Laborde: *Phys. Rev. B* **57** (1998) R728.
- [74] Z.A. Xu, Y. Zhang, N.P. Ong, cond-mat/9903123.
- [75] Y. Ando and T. Murayama : *Phys. Rev. B* **60** (1999) R6991.
- [76] Yasushi Abe, Yoichi Ando, J. Takeya, H. Tanabe, T. Watauchi, I. Tanaka, H. Kojima, *Phys. Rev. B* **59**, 14753 (1999).
- [77] F. F. Balakirev, I. E. Trofimov, S. Guha, M.Z. Cieplak, and P. Lindenfled, *Phys. Rev. B* **57**, R8083 (1998).
- [78] H. Yasuoka, T. Imai and T. Shimizu, *Strong Correlation and Superconductivity* (Springer-Verlag, Berlin 1989), p. 254.
- [79] W. W. Warren, R. E. Walstedt, G. F. Brennert, R. J. Cava, R. Tycko, R. F. Bell and G. Dabbagh, *Phys. Rev. Lett.* **62** (1989) 1193.
- [80] M. Takigawa, A. P. Reyes, P. C. Hammel, J. D. Thompson, R. H. Heffner Z. Fisk and K. C. Ott, *Phys. Rev. B* **43** (1991) 247.
- [81] Y. Itoh, H. Yasuoka, Y. Fujiwara, Y. Ueda, T. Machi, I. Tomeno, K. Tai, N. Koshizuka and S. Tanaka, *J. Phys. Soc. Jpn.* **61** (1992) 1287.
- [82] M. H. Julien, P. Carretta and M. Horvatić, *Phys. Rev. Lett.* **76** (1996) 4238.
- [83] H. Ding, T. Yokoya, J. C. Campuzano, T. Takahashi, M. Randeria, M. R. Norman, T. Mochiku, K. Kadowaki and J. Giapintzakis, *Nature.* **382** (1996) 51.
- [84] A. G. Loeser, Z. X. Shen, D. S. Dessau, D. S. Marshall, C. H. Park, P. Fournier and A. Kapitulnik, *Science.* **273** (1996) 325.
- [85] M. R. Norman, H. Ding, M. Randeria, J. C. Campuzano, T. Yokoya, T. Takeuchi, T. Takahashi, T. Mochiku, K. Kadowaki, P. Guptasarma and D. G. Hinks, *Nature.* **392** (1998) 157.
- [86] A. Damascelli, Z. Hussain and Z.-X. Shen, *Rev. Mod. Phys.* **75** (2003) 473.
- [87] Q. Chen, I. Kosztin, B. Jankó and K. Levin: *Phys. Rev. Lett* **81** (1998) 4708; Q. Chen, I. Kosztin, B. Janko, and K. Levin: *Phys. Rev. B* **59**, 7083 (1999); J. Maly, B. Janko, and K. Levin: *Phys.*

- Rev. B **59**, 1354 (1999).
- [88] T. Dahm, D. Manske and L. Tewordt: Europhys. Lett. **55** (2001) 93.
- [89] A. Kobayashi, A. Tsuruta, T. Matsuura and Y. Kuroda: J. Phys. Soc. Jpn. **70** (2001) 1214; A. Kobayashi, A. Tsuruta, T. Matsuura and Y. Kuroda: J. Phys. Soc. Jpn. **71** (2002) 1640; A. Kobayashi, A. Tsuruta, T. Matsuura and Y. Kuroda: J. Phys. Soc. Jpn. **68** (1999) 2506.
- [90] Y. Yanase and K. Yamada: J. Phys. Soc. Jpn. **70** (2001) 1659.
- [91] K. Kanoda: Physica C **282-287** (1997) 299.
- [92] H. Kino and H. Fukuyama: J. Phys. Soc. Jpn. **65** (1996) 2158.
- [93] H. Kino, and H. Kontani: J. Phys. Soc. Jpn. **67** 3691 (1998).
- [94] H. Kondo and T. Moriya: J. Phys. Soc. Jpn. **67** 3695 (1998).
- [95] J. Schmalian: Phys. Rev. Lett. **81** (1998) 4232.
- [96] H. Kontani and H. Kino: Phys. Rev. B **63** (2001) 134524.
- [97] C. Petrovic, P.G. Pagliuso, M.F. Hundley, R. Movshovich, J.L. Sarrao, J.D. Thompson, Z. Fisk and P. Monthoux: J. Phys. Condens. Matter **13** (2001) L337.
- [98] H. Hegger, C. Petrovic, E.G. Moshopoulou, M.F. Hundley, J.L. Sarrao, Z. Fisk, and J.D. Thompson: Phys. Rev. Lett. **84** (2000) 4986.
- [99] C. Petrovic, R. Movshovich, M. Jaime, P.G. Pagliuso, M.F. Hundley, J.L. Sarrao, Z. Fisk, and J.D. Thompson: Europhys. Lett. **53** (2001) 354.
- [100] G.-q. Zeng, K. Tanabe, T. Mito, S. Kawasaki, Y. Kitaoka, D. Aoki, Y. Haga and Y. Onuki: Phys. Rev. Lett. **86** (2001) 4664.
- [101] Y. Kawasaki, S. Kawasaki, M. Yashima, T. Mito, G.-q. Zheng, Y. Kitaoka, H. Shishido, R. Settai, Y. Haga and Y. Onuki: J. Phys. Soc. Jpn. **72** (2003) 2308.
- [102] K. Izawa, H. Yamaguchi, Y. Matsuda, H. Shishido, R. Settai and Y. Onuki: Phys. Rev. Lett. **87** (2001) 057002.
- [103] Y. Matsuda, K. Izawa and I. Vekhter, J. Phys.: Condens. Matter **18** (2006) R705.
- [104] R. Movshovich, M. Jaime, J.D. Thompson, C. Petrovic, Z. Fisk, P.G. Pagliuso and J.L. Sarrao: Phys. Rev. Lett. **86** (2001) 5152.
- [105] H. Aoki, T. Sakakibara, H. Shishido, R. Settai, Y. Onuki, P. Miranovic and K. Machida: J. Phys.: Condens. Matter **16** (2004) L13.
- [106] H.A. Radovan, N.A. Fortune, T.P. Murphy, S.T. Hannahs, E.C. Palm, S.W. Tozer and D. Hall: Nature **425** (2003) 51, A. Bianchi, R. Movshovich, C. Capan, P.G. Pagliuso, J.L. Sarrao: Phys. Rev. Lett. **91** (2003) 187004, T. Watanabe, Y. Kasahara, K. Izawa, T. Sakakibara, Y. Matsuda, C.J. van der Beek, T. Hanaguri, H. Shishido, R. Settai and Y. Onuki: Phys. Rev. B **70** (2004) 020506, K. Kakuyanagi, M. Saitoh, K. Kumagai, S. Takashima, M. Nohara, H. Takagi and Y. Matsuda: Phys. Rev. Lett. **94** (2005) 047602; Y. Matsuda and H. Shimahara, J. Phys. Soc. Jpn. **76** (2007) 051005.
- [107] R. Bel, K. Behnia, Y. Nakajima, K. Izawa, Y. Matsuda, H. Shishido, R. Settai and Y. Onuki: Phys. Rev. Lett. **92** (2004) 217002; Note that the sign of ν in CeCoIn₅ is *positive* according to the definition of the present paper [eq. (116)]. See also Ref. [261].
- [108] S. Onari, H. Kontani and Y. Tanaka: Phys. Rev. B **73** (2006).
- [109] A. Georges, G. Kotliar, W. Krauth, and M. J. Rozenberg: Rev. Mod. Phys. **68** (1996) 13.
- [110] G. Kotliar and D. Vollhardt: Physics Today **57** (2004) 53.
- [111] J. Feldman, D. Lehmann, H. Knorrer and E. Trubowitz: *Constructive Physics, ed. V. Rivasseau*, (Springer, Berlin, 1995);
- [112] T. Tohyama, Phys. Rev. B **70**, 174517 (2004).
- [113] E. Dagotto, Rev. Mod. Phys. **66**, 763 (1994).
- [114] T. Yanagisawa, S. Koike, and K. Yamaji, Phys. Rev. B **64**, 184509 (2001).
- [115] H. Yokoyama and M. Ogata, J. Phys. Soc. Jpn. **65** (1996) 3615; H. Yokoyama and M. Ogata and Y. Tanaka, J. Phys. Soc. Jpn. **75** (2006) 114706.
- [116] F.F. Assaad and M. Imada, J. Phys. Soc. Jpn. **65** (1996) 189.
- [117] R. Preuss, W. Hanke, C. Grober, and H. G. Evertz, Phys. Rev. Lett. **79**, 1122-1125 (1997)

- [118] C. M. Varma, P.B. Littlewood, S. Schmitt-Rink, E. Abrahams, and A.E. Ruckenstein, *Phys. Rev. Lett.* **63**, 1996 (1989).
- [119] C. M. Varma, *Phys. Rev. B* **55**, 14554 (1997).
- [120] A.J. Millis, H. Monien, and D. Pines: *Phys. Rev. B* **42**, 167 (1990).
- [121] V. Barzykin and D. Pines: *Phys. Rev. B* **52** (1995) 13585.
- [122] E.M. Motoyama, G. Yu, I.M. Vishik, O.P. Vajk, P.K. Mang, and M. Greven, *Nature* **445**, 186 (2007).
- [123] T. Moriya: **Spin Fluctuations in Itinerant Electron Magnetism** (Springer-Verlag, Berlin, 1985).
- [124] T. Dahm and L. Tewordt: *Phys. Rev. B* **52** (1995) 1297.
- [125] T. Takimoto and T. Moriya: *J. Phys. Soc. Jpn.* **67** (1994) 3570.
- [126] S. Koikegami, S. Fujimoto and K. Yamada, *J. Phys. Soc. Jpn.* **66** (1997) 1438.
- [127] H. Kontani and K. Ueda: *Phys. Rev. Lett.* **80** (1998) 5619.
- [128] S. Wernbter: *Phys. Rev. B* **55** (1997) R10149.
- [129] D. Manske, I. Eremin and K.H. Bennemann: *Phys. Rev. B* **67** (2003) 134520.
- [130] H. Kontani and M. Ohno: *Phys. Rev. B* **74**, 014406 (2006); H. Kontani and M. Ohno: *J. Mag. Mag. Mat.* **310** (2007) 483.
- [131] J. Yu, S. Massidda, A.J. Freeman and D.D. Koelling: *Phys. Lett. A* **122** 203.
- [132] S. Massidda, N. Hamada, J. Yu, and A.J. Freeman: *Physica C* **157** (1989) 571.
- [133] A.J. Freeman and J. Yu: *Physica B* **150** (1988) 50.
- [134] J.-H. Xu, T.J. Watson-Yang, J. Yu and A.J. Freeman: *Phys. Lett. A* **120** (1987) 489.
- [135] J.C. Campuzano, G. Jennings, M. Faiz, L. Beaulaigue, B.W. Veal, J.Z. Liu, A.P. Paulikas, K. Vandervoort, H. Claus, R.S. List, A.J. Arko and R.J. Bartlett: *Phys. Rev. Lett.* **64** (1990), 2308.
- [136] A. Ino, C. Kim, M. Nakamura, T. Yoshida, T. Mizokawa, A. Fujimori, Z.-X. Shen, T. Kakeshita, H. Eisaki, and S. Uchida, *Phys. Rev. B* **65**, 094504 (2002).
- [137] T. Tanamoto, H. Kohno, and H. Fukuyama: *J. Phys. Soc. Jpn* **61** (1992) 1886.
- [138] M. Lindroos, S. Sahrakorpi, V. Arpiainen, R.S. Markiewicz, and A. Bansil, *J. Phys. Chem. Solids* **67** (2006) 244.
- [139] G. Baym and L.P. Kadanoff: *Phys. Rev.* **124** (1961), 287.
- [140] G. Baym: *Phys. Rev.* **127** (1962), 1391.
- [141] H. Kino, H. Kontani and T. Miyazaki, *J. Phy. Soc. Jpn.* **73** (2004) 25; *ibid* **75** (2006) 104702.
- [142] S. Onari, R. Arita, K. Kuroki, and H. Aoki, *Phys. Rev. B* **68**, 024525 (2003).
- [143] C. Honerkamp and M. Salmhofer, *Phys. Rev. Lett.* **87**, 187004 (2001).
- [144] C.J. Halboth and W. Metzner, *Phys. Rev. B* **61**, 7364 (2000).
- [145] J. Kishine and K. Yonemitsu, *Int. J. Mod. Phys. B* 16, 711 (2002).
- [146] H. Kontani, unpublished.
- [147] H. Kohno and K. Yamada: *Prog. Theor. Phys.* **85**, 13 (1991).
- [148] A. Rosch, *Phys. Rev. Lett.* **82**, 4280 (1999).
- [149] M. Abdel-Jawad, M.P. Kennett, L. Balicas, A. Carrington, A.P. Mackenzie, R.H. McKenzie and N.E. Hussey: *Nature Physics* **2**, 821 (2006); M. Abdel-Jawad, J.G. Analytis, L. Balicas, A. Carrington, J.P.H. Charmant, M.M.J. French, N.E. Hussey: *Phys. Rev. Lett.* **99**, 107002 (2007).
- [150] A. Narduzzo, G. Albert, M. M. J. French, N. Mangkorntong, M. Nohara, H. Takagi, N.E. Hussey: *arXiv:0707.4601*.
- [151] K. Yamaji: *J. Phys. Soc. Jpn.* **58** (1989) 1520; R. Yagi, Y. Iye, T. Osada and S. Kagoshima, *J. Phys. Soc. Jpn.* **59**, 3069 (1990).
- [152] H. Nakano: *Int. J. Mod. Phys. B* **7** (1993) 2397.
- [153] R. Kubo: *J. Phys. Soc. Jpn.* **12** (1957) 570.
- [154] M. S. Green: *J. Chem. Phys.* **20** (1952) 1281; *ibid* **22** (1954) 398.
- [155] A. Rosch, *Ann. Phys. (Leipzig)* 15, 526 (2006).

- [156] Y. Fukuzumi, K. Mizuhashi, K. Takenaka, and S. Uchida: Phys. Rev. Lett. **76** (1996) 684.
- [157] S. D. Obertelli, J.R. Cooper and J.L. Tallon: Phys. Rev. B **46** (1992) 14928.
- [158] C. P. Popoviciu and J. L. Cohn, Phys. Rev. B **55**, 3155 (1997).
- [159] A. Yamamoto, W.-Z. Hu, and S. Tajima, Phys. Rev. B **63**, 024504 (2000).
- [160] A. Yamamoto, K. Minami, W.-Z. Hu, A. Miyakita, M. Izumi, and S. Tajima, Phys. Rev. B **65**, 104505 (2002).
- [161] T. Honma, P. H. Hor, H. H. Hsieh, and M. Tanimoto, Phys. Rev. B **70**, 214517 (2004).
- [162] T. Takemura, T. Kitajima, T. Sugaya, I. Terasaki, T. Takemura, T. Kitajima and T. Sugaya, J. Phys.: Condens. Matter **12** (2000) 6199.
- [163] G. V. Williams, R. Dupree, A. Howes, S. Kramer, H. J. Trodahl, C. U. Jung, Min-Seok Park, and Sung-Ik Lee, Phys. Rev. B **65**, 224520 (2002).
- [164] G. Hildebrand, T. J. Hagenaars, W. Hanke, S. Grabowski, and J. Schmalian, Phys. Rev. B **56**, R4317 (1997).
- [165] J. M. Luttinger: Phys. Rev. **135** (1964) A1505.
- [166] M. Jonson and G. D. Mahan: Phys. Rev. B **42** (1990) 9350; G. D. Mahan: Solid State Physics, **51** (1998) 81.
- [167] H. Kontani, K. Kanki and K. Ueda, J. Phy. Chem. Sol. **62** (2001) 83.
- [168] M. Tsuji: J. Phys. Soc. Jpn. **13** (1958) 979.
- [169] N.P. Ong: Phys. Rev. B **43** (1991) 913.
- [170] I. Tsukada and S. Ono, Phys. Rev. B **74**, 134508 (2006).
- [171] W. Kohn, Phys. Rev. **123**, 1242 (1961).
- [172] Y. Takada and T. Ando: J. Phys. Soc. Jpn. **44** (1978) 905.
- [173] K. Kanki and K. Yamada: J. Phys. Soc. Jpn. **66** (1997) 1103.
- [174] T. Okabe: J. Phys. Soc. Jpn. **67** (1998) 2792.
- [175] T. Jujo, J. Phys. Soc. Jpn. **70** (2001) 1349.
- [176] T.P. Devereaux and A.P. Kampf, Phys. Rev. B **59**, 6411 (1999).
- [177] Z. Konstantinovic, Z. Z. Li, and H. Raffy, Phys. Rev. B **62**, R11989 (2000).
- [178] E.W. Carlson, V.J. Emery, S.A. Kivelson, D. Orgad, *The Physics of Superconductors, Vol. 2*, ed. K.-H. Bennemann and J. B. Ketterson, (Springer, Berlin, 2002).
- [179] S. Tewari, H.Y. Kee, C. Nayak and S. Chakravarty, Phys. Rev. B **64**, 224516 (2001).
- [180] Z.A. Xu, N.P. Ong, Y. Wang, T. Kakeshita and Uchida: Nature **406** (2000) 486; Y. Wang, Z. A. Xu, T. Kakeshita, S. Uchida, S. Ono, Y. Ando, and N. P. Ong: Phys. Rev. B **64** (2001) 224519; Y. Wang, L. Li, and N. P. Ong, Phys. Rev. B **73**, 024510 (2006).
- [181] C.C. Capan et al.: Phys. Rev. Lett. **88** (2002) 056601.
- [182] F. Rullier-Albenque, R. Tourbot, H. Alloul, P. Lejay, D. Colson, and A. Forget, Phys. Rev. Lett. **96**, 067002 (2006).
- [183] I. Ussishkin, S. L. Sondhi, and D. A. Huse Phys. Rev. Lett. **89**, 287001 (2002).
- [184] S.-K. Yip, Phys. Rev. B **41**, 2612 (1990).
- [185] T. Nakano, M. Oda, C. Manabe, N. Momono, Y. Miura, and M. Ido, Phys. Rev. B **49**, 16000 (1994).
- [186] K. Takenaka et al.: Phys. Rev. **B50** (1994) 6534.
- [187] T. Noda, H. Eisaki and S. Uchida, Science **286** (1999) 265.
- [188] Z. A. Xu, J. Q. Shen, S. R. Zhao, Y. J. Zhang, and C. K. Ong, Phys. Rev. B **72**, 144527 (2005).
- [189] L. B. Rigal, D. C. Schmadel, H. D. Drew, B. Maierov, E. Osquiguil, J. S. Preston, R. Hughes, and G. D. Gu: Phys. Rev. Lett. **93** (2004) 137002.
- [190] M. Grayson, L. B. Rigal, D. C. Schmadel, H. D. Drew, and P.-J. Kung: Phys. Rev. Lett. **89** (2002) 037003.
- [191] J. Cerne, M. Grayson, D. C. Schmadel, G. S. Jenkins, H. D. Drew, R. Hughes, A. Dabkowski, J. S. Preston, and P.-J. Kung: Phys. Rev. Lett. **84** (2000) 3418.
- [192] S.G. Kaplan, S.Wu, H.-T.S. Lihn, H.D. Drew, Q. Li, D.B. Fenner, J.M. Phillips and S.Y. Hou: Phys. Rev. Lett. **76** (1996) 696.

- [193] D.C. Schmadel, G.S. Jenkins, J.J. Tu, G.D. Gu, H. Kontani, and H.D. Drew, *Phys. Rev. B* **75**, 140506(R) (2007).
- [194] L. Shi, D. Schmadel, H. D. Drew, I. Tsukada, and Y. Ando, *cond-mat/0510794*.
- [195] A. Zimmers, L. Shi, D. C. Schmadel, W. M. Fisher, R. L. Greene, H. D. Drew, M. Houseknecht, G. Acbas, M.-H. Kim, M.-H. Yang, J. Cerne, J. Lin, and A. Millis, *Phys. Rev. B* **76**, 064515 (2007).
- [196] H. Kontani, *J. Phys. Soc. Jpn* **75** (2006) 013703.
- [197] H. Kontani, *J. Phys. Soc. Jpn* (2007) 074707.
- [198] H. D. Drew and P. Coleman *Phys. Rev. Lett.* **78**, 1572 (1997).
- [199] K. McElroy, Jinho Lee, J. A. Slezak, D.-H. Lee, H. Eisaki, S. Uchida, and J. C. Davis, *Science* **309** (2005) 1048.
- [200] B.M. Andersen, A. Melikyan, T.S. Nunner, and P.J. Hirschfeld, *Phys. Rev. B* **74**, 060501(R) (2006).
- [201] A.C. Fang, L. Capriotti, D.J. Scalapino, S.A. Kivelson, N. Kaneko, M. Greven, and A. Kapitulnik, *Phys. Rev. Lett.* **96**, 017007 (2006).
- [202] H. Eisaki, N. Kaneko, D.L. Feng, A. Damascelli, P.K. Mang, K.M. Shen, Z.-X. Shen, and M. Greven, *Phys. Rev. B* **69**, 064512 (2004).
- [203] L.-L. Wang, P. J. Hirschfeld, and H.-P. Cheng, *Phys. Rev. B* **72** (2005) 224516.
- [204] A. V. Mahajan, H. Alloul, G. Collin, and J. F. Marucco: *Phys. Rev. Lett.* **72** (1994) 3100.
- [205] W. A. MacFarlane, J. Bobroff, H. Alloul, P. Mendels, N. Blanchard, G. Collin, and J.-F. Marucco: *Phys. Rev. Lett.* **85** (2000) 1108.
- [206] A. V. Mahajan, H. Alloul, G. Collin, J. F. Marucco, G. Collin, and J.-F. Marucco: *Eur. Phys. J. B* **13** (2000) 457.
- [207] J. Bobroff, W. A. MacFarlane, H. Alloul, P. Mendels, N. Blanchard, G. Collin, and J.-F. Marucco: *Phys. Rev. Lett.* **83** (1999) 4381.
- [208] M.-H. Julien, T. Feher, M. Horvatic, C. Berthier, O.N. Bakharev, P. Segransan, G. Collin, J.-F. Marucco: *Phys. Rev. Lett.* **84** (2000) 3422.
- [209] J. Riera and S. Koval, D. Poilblanc and F. Pantigny, *Phys. Rev. B* **54** (1996) 4771.
- [210] T. Tohyama, M. Takahashi and S. Maekawa: *Physica C* **357-360** (2001) 93.
- [211] H. Tsuchiura, Y. Tanaka, M. Ogata, and S. Kashiwaya: *Phys. Rev. B* **64** (2001) 140501(R).
- [212] P. Mendels, J. Bobroff, G. Collin, H. Alloul, M. Gabay, J.F. Marucco, N. Blanchard and B. Grenier: *Europhys. Lett.* **46** (1999) 678.
- [213] K. Ishida, Y. Kitaoka, K. Yamazoe, K. Asayama, and Y. Yamada: *Phys. Rev. Lett.* **76** (1996) 531.
- [214] R. S. Islam, J. R. Cooper, J. W. Loram, S. H. Naqib, *cond-mat/0607153*
- [215] N. Bulut, D. Hone, D.J. Scalapino, and E.Y. Loh: *Phys. Rev. Lett.* **62** (1989) 2192.
- [216] A.W. Sandvik, E. Dagotto, and D.J. Scalapino: *Phys. Rev. B* **56** (1997) 11701.
- [217] G.B. Martins, M. Laukamp, J. Riera and E. Dagotto: *Phys. Rev. Lett.* **78** (1997) 3563.
- [218] M. Laukamp et al., *Phys. Rev. B* **57** (1998) 10755. *Phys. Rev. Lett.* **96**, 017204 (2006).
- [219] Fabrizio Anfuso and Sebastian Eggert: *Phys. Rev. Lett.* **96**, 017204 (2006).
- [220] N. Bulut: *Physica C* **363** (2001) 260.
- [221] N. Bulut: *Phys. Rev. B* **61** (2000) 9051.
- [222] Y. Ohashi: *J. Phys. Soc. Jpn.* **70** (2001) 2054.
- [223] Y. Ando, G.S. Boebinger, A. Passner, T. Kimura and K. Kishio: *Phys. Rev. Lett.* **75** (1995) 4662.
- [224] G.S. Boebinger, Y. Ando, A. Passner, T. Kimura, M. Okuya, J. Shimoyama, K. Kishio, K. Tamasaku, N. Ichikawa, and S. Uchida: *Phys. Rev. Lett.* **77** (1996) 5417.
- [225] T. Sekitani, M. Naito, and N. Miura: *Phys. Rev. B* **67** (2003) 174503.
- [226] D. Jaccard and J. Sierro, *Physica B* **206-207** (1995) 625.
- [227] H. Wilhelm, S. Raymond, D. Jaccard, O. Stockert, H.v. Lohneysen and A. Rosch, *J. Phys.: Condens. Matter* **13** L329.

- [228] K. Miyake and O. Narikiyo: J. Phys. Soc. Jpn. **71** (2002) 867.
- [229] A.T. Holmes, D. Jaccard and K. Miyake, Phys. Rev. B **69**, 024508 (2004).
- [230] H. Kontani and M. Ohno, unpublished.
- [231] S. Ouazi, J. Bobroff, H. Alloul, M. Le Tacon, N. Blanchard, G. Collin, M. H. Julien, M. Horvati, and C. Berthier, Phys. Rev. Lett. **96**, 127005 (2006).
- [232] J.W. Harter, B.M. Andersen, J. Bobroff, M. Gabay and P.J. Hirshfeld, Phys. Rev. B **75** (2007) 054520.
- [233] P. Coleman, *Handbook of Magnetism and Advanced Magnetic Materials, vol. 1* (J. Wiley and Sons, 2007); cond-mat/0612006.
- [234] J. Paglione, M. A. Tanatar, D. G. Hawthorn, E. Boaknin, R. W. Hill, F. Ronning, M. Sutherland, L. Taillefer, C. Petrovic, and P. C. Canfield, Phys. Rev. Lett. **91**, 246405 (2003).
- [235] K. Sakurazawa, H. Kontani and T. Saso: J. Phys. Soc. Jpn. **74**, 271 (2004).
- [236] P. Li, F.F. Balakirev and R.L. Greene, Phys. Rev. Lett. **99**, 047003 (2007).
- [237] S. Onari, H. Kontani and Y. Tanaka: to be published in J. Phys. Soc. Jpn. **77** (2008).
- [238] K. Miyagawa and H. Taniguchi, private communication.
- [239] H. Taniguchi, T. Okuhara, T. Nagai, K. Satoh, M. Mori, Y. himizu, M. Hedo and Y. Uwatoko, J. Phys. Soc. Jpn. **76** (2007) No.11.
- [240] T.F. Rosenbaum, A. Husmann, S.A. Carter and J.M Honig: Phys. Rev. B **57** (1998) R13997.
- [241] S. Yoshii, K. Murata and M. Sato, J. phys. Soc. Jpn. **69** (2000) 17; S. Yoshii, K. Murata and M. Sato, J. Phys. Chem. Solids **62** (2001) 129.
- [242] Ch. Renner, B. Revaz, J.-Y. Genoud, K. Kadowaki and Ø. Fischer, Phys. Rev. Lett. **80** (1998) 149.
- [243] N. Miyakawa, P. Guptasarma, J. F. Zasadzinski, D. G. Hinks and K. E. Gray, Phys. Rev. Lett. **80** (1998) 157.
- [244] R. M. Dipasupil, M. Oda, N. Momono and M. Ido, J. Phys. Soc. Jpn. **71** (2002) 1535.
- [245] T. Sato, T. Yokoya, Y. Naitoh, T. Takahashi, K. Yamada and Y. Endoh, Phys. Rev. Lett. **83** (1999) 2254.
- [246] H. Alloul, T. Ohno and P. Mendels, Phys. Rev. Lett. **63** (1989) 1700.
- [247] K. Ishida, Y. Kitaoka, G.-q. Zheng and K. Asayama, J. Phys. Soc. Jpn **60** (1991) 3516.
- [248] D. C. Johnston, Phys. Rev. Lett. **62** (1989) 957.
- [249] M. Oda, H. Matsuki and M. Ido, Solid State Commun. **74** (1990) 1321.
- [250] B. Holm and F. Aryasetiawan: Phys. Rev. B **56** (1997) 12825.
- [251] B. Holm and U. von Barth: Phys. Rev. B **57** (1998) 2108.
- [252] P. Garcia-Gonzalez and R.W. Godby: Phys. Rev. B **63** (2001) 075112.
- [253] J. Schmalian, D. Pines, and B. Stojkovi, Phys. Rev. B **60**, 667 (1999); J. Schmalian, D. Pines, and B. Stojkovi, Phys. Rev. Lett. **80**, 3839 (1998).
- [254] S. Fujimoto, J. Phys. Soc. Jpn. **71** (2002) 1230.
- [255] H. Ikeda, S. Shinkai and K. Yamada, submitted to J. Phys. Soc. Jpn. (2007).
- [256] S. Shinkai, H. Ikeda and K. Yamada, J. Phys. Soc. Jpn. **74** (2005) 2592; *ibid* **75** (2006) 104712.
- [257] T. Nomura and K. Yamada: J. Phys. Soc. Jpn. **69** (2000) 3678; *ibid* **71** (2002) 1993.
- [258] M. Vilk and A.-M.S. Tremblay, J. Phys. I France **7**, 1309 (1997).
- [259] H. Kusunose, J. Phys. Soc. Jpn. **75** (2006) 054713.
- [260] T. Saso: J. Phys. Soc. Jpn. **68** (1999) 3941.
- [261] K. Izawa, K. Behnia, Y. Matsuda, H. Shishido, R. Settai, Y. Onuki, J. Flouquet, Phys. Rev. Lett. **99**, 147005 (2007).
- [262] T. Shibauchi, private communication.
- [263] M.A. Tanatar, J. Paglione, C. Petrovic, and L. Taillefer, Science **316**, 1320 (2007).
- [264] H. Ding, M. R. Norman, T. Yokoya, T. Takeuchi, M. Randeria, J. C. Campuzano, T. Takahashi, T. Mochiku, and K. Kadowaki, Phys. Rev. Lett. **78**, 2628 (1997).
- [265] M. R. Norman, M. Randeria, H. Ding, and J. C. Campuzano, Phys. Rev. B **57**, R11093 (1998).
- [266] U. Chatterjee, M. Shi, A. Kaminski, A. Kanigel, H. M. Fretwell, K. Terashima, T. Takahashi, S.

- Rosenkranz, Z. Z. Li, H. Raffy, A. Santander-Syro, K. Kadowaki, M. R. Norman, M. Randeria, and J. C. Campuzano: *Phys. Rev. Lett.* **96**, 107006 (2006).
- [267] T. Yoshida, X. J. Zhou, T. Sasagawa, W. L. Yang, P. V. Bogdanov, A. Lanzara, Z. Hussain, T. Mizokawa, A. Fujimori, H. Eisaki, Z.-X. Shen, T. Kakeshita, and S. Uchida: *Phys. Rev. Lett.* **91**, 027001 (2003).
- [268] U. Chatterjee, M. Shi, A. Kaminski, A. Kanigel, H. M. Fretwell, K. Terashima, T. Takahashi, S. Rosenkranz, Z. Z. Li, H. Raffy, A. Santander-Syro, K. Kadowaki, M. R. Norman, M. Randeria, and J. C. Campuzano, *Phys. Rev. Lett.* **95**, 107006 (2006).
- [269] H. Matsui, K. Terashima, T. Sato, T. Takahashi, S.-C. Wang, H.-B. Yang, H. Ding, T. Uefuji, and K. Yamada, *Phys. Rev. Lett.* **94**, 047005 (2005).
- [270] S. Ono, S. Komiya, and Y. Ando, *Phys. Rev. B* **75**, 024515 (2007).
- [271] R. Karplus and J. M. Luttinger: *Phys. Rev.* **95** (1954) 1154.
- [272] J. M. Luttinger: *Phys. Rev.* **112** (1958) 739.
- [273] J. Smit: *Physica* **24** (1958) 39.
- [274] Y. Ōnuki, T. Yamayoshi, I. Ukon, T. Komatsubara, A. Umezawa, W. K. Kwok, G. W. Crabtree and D. G. Hinks: *J. Phys. Soc. Jpn.* **58** (1989) 2119.
- [275] Y. Ōnuki, T. Yamayoshi, T. Omi, I. Ukon, A. Kobori and T. Komatsubara: *J. Phys. Soc. Jpn.* **58** (1989) 2126.
- [276] K. Hanzawa, K. Yosida and K. Yamada, *Prog. Theor. Phys.* **81** (1989) 960.
- [277] H. Kontani and K. Yamada: *J. Phys. Soc. Jpn.* **63** (1994) 2627.
- [278] T. Hiraoka, T. Sada, T. Takabatake and H. Fujii, *Physica B* **186-188** (1993) 7603.
- [279] P. Coleman, P. W. Anderson and T. V. Ramakrishnan: *Phys. Rev. Lett.* **55** (1985) 414.
- [280] A. Fert and P. M. Levy: *Phys. Rev. B* **36** (1987) 1907.
- [281] H. Kontani and K. Yamada: *J. Phys. Soc. Jpn.* **66** (1997) 2252.
- [282] T. Miyasato, N. Abe, T. Fujii, A. Asamitsu, S. Onoda, Y. Onose, N. Nagaosa, Y. Tokura: *cond-mat/0610324*.
- [283] M. Miyazawa, H. Kontani and K. Yamada: *J. Phys. Soc. Jpn.* **68** (1999) 1625.
- [284] H. Kontani, T. Tanaka, K. Yamada, *Phys. Rev. B* **75**, 184416 (2007).
- [285] J. Jin et al., *cond-mat/0112405*; L.M. Galvin et al., *Phys. Rev. B* **63**, 161102(R) (2001).
- [286] Y. Yao, L. Kleinman, A.H. MacDonald, J. Sinova, T. Jungwirth, D. Wang, E. Wang and Q. Niu: *Phys. Rev. Lett.* **92** (2004) 037204.
- [287] Z. Fang et al.: *Science* **302** (2003) 92.
- [288] Kontani, T. Tanaka, D.S. Hirashima, K. Yamada, and J. Inoue, *cond-mat/0702447*.
- [289] Kontani, M. Naito, D.S. Hirashima, K. Yamada, and J. Inoue, *J. Phys. Soc. Jpn.* **76** (2007) 103702.
- [290] T. Kimura, Y. Otani, T. Sato, S. Takahashi, and S. Maekawa, *Phys. Rev. Lett.* **98**, 156601 (2007).
- [291] T. Tanaka, H. Kontani, M. Naito, T. Naito, D.S. Hirashima, K. Yamada and J. Inoue, unpublished.
- [292] S. Murakami, N. Nagaosa, and S. C. Zhang, *Science* **301**, 1348 (2003).
- [293] J. Sinova et al., *Phys. Rev. Lett.* **92**, 126603 (2004).
- [294] K. Kadowaki and S.B. Woods: *Solid State Commun.* **58** (1986) 507.
- [295] H. Kontani: *J. Phys. Soc. Jpn.* **73** (2004) 515.
- [296] H. Kontani: *Physica B.* **359-361** (2005) 202.
- [297] K. Yamada: *Prog. Theor. Phys.* **53** (1975) 970; K. Yamada and K. Yosida: *Prog. Theor. Phys.* **53** (1975) 1286; K. Yamada and K. Yosida: *Prog. Theor. Phys.* **54** (1975) 316.
- [298] In Refs. [295, 296], we put $\gamma = (\pi T)^2/6 \cdot N_f \rho^f(0)$ by mistake; the correct relation is $\gamma = (\pi T)^2/3 \cdot N_f \rho^f(0)$. For this reason, eq. (161) is two times eq. (8) in ref. [295]. Since the author of ref. [295] assumed $1/n^{4/3} a^3 \approx 1 \times 10^{-8}$ cm, the grand-KW relation in ref. [295] is equal to eq. (164) in the present paper.
- [299] N. Tsujii, H. Kontani and K. Yoshimura: *Phys. Rev. Lett.* **94** (2005) 057201.
- [300] K. Behnia, D. Jaccard and J. Flouquet: *J. Phys.: Condens. Matter* **16** (2004) 5187.

- [301] K. Miyake and H. Kohno: J. Phy. Soc. Jpn. **74** (2005) 254.
- [302] M. S. Torikachvili, S. Jia, E. D. Mun, S. T. Hannahs, R. C. Black, W. K. Neils, Dinesh Martien, S. L. Bud'ko, P. C. Canfield, Proc. Natl. Acad. Sci. U. S. A. **104**, 9960 (2007).
- [303] H. Kontani and K. Yamada: J. Phys. Soc. Jpn. **65** (1996) 172.
- [304] H. Kontani and K. Yamada: J. Phys. Soc. Jpn. **66** (1997) 2232.
- [305] H. Okamura et al.:J. Phys. Soc. Jpn. **76** (2007) 023703.
- [306] H. Kontani: JPSJ Online-News and Comments [Feb. 13, 2007]